RECOVERY OF FINE COAL PARTICLES BY FLOTATION: HYDRODYNAMICS AND KINETICS

Thesis

Submitted in partial fulfillment of the requirements for the degree of

Doctor of Philosophy in Engineering

by

Fahad M K

Roll No. 126107038

Under the supervision of

Prof. Subrata Kumar Majumder

and

Prof. Pallab Ghosh

DEPARTMET OF CHEMICAL ENGINEERING

INDIAN INSTITUTE OF TECHNOLOGY GUWAHATI

GUWAHATI-781039, INDIA

JUNE 2020

RECOVERY OF FINE COAL PARTICLES BY FLOTATION: HYDRODYNAMICS AND KINETICS

FAHAD M K

DEDICATED TO MY FAMILY

INDIAN INSTITUTE OF TECHNOLOGY GUWAHATI

GUWAHATI-781039, INDIA

DEPARTMENT OF CHEMICAL ENGINEERING

CERTIFICATE

This is to certify that the thesis titled "Recovery of fine coal particles by flotation: Hydrodynamics and kinetics" submitted by Fahad M K in fulfillment of the requirement of the degree of Doctor of Philosophy in Engineering is a bonafide research work carried out by him, in the Department of Chemical Engineering, Indian Institute of Technology, Guwahati, under our guidance and supervision. The work documented in this thesis has not been submitted to any other University or Institute for the award of any degree or diploma. In my opinion, the thesis has reached the standard meeting the requirements of the Ph.D. degree as prescribed in the regulation of this institute.

Prof. S. K. Majumder
Department of Chemical Engineering
Indian Institute of Technology Guwahati
Guwahati – 781039
Assam

Prof. Pallab Ghosh
Department of Chemical Engineering
Indian Institute of Technology Guwahati
Guwahati – 781039
Assam

ACKNOWLEDGMENTS

I would like to express my gratitude to all those who have helped me in various ways in completing this research work, directly or indirectly. First and foremost, I would like to express my deep-felt gratitude to my supervisors, **Prof. Subrata Kumar Majumder** and **Prof. Pallab Ghosh** for providing me continuous inspiration and guidance throughout the entire course of this work. In addition, their philosophical guidance has built-up a momentum inside me. Their uncompromising approach to complete the experimental part, data analysis, writing papers, and thesis within the stipulated time period has helped me a lot in completing my research work. The numerous brain-storming sessions during the meetings with them were very useful in enriching my analytical power. I also remain indebted for their understanding, support, and caring during the times when I was really down and depressed due to personal problems. I also thank the Almighty for giving me a chance to work under their great stewardship.

I wish to express my respectful thanks to **Prof. Vijay S Mohalker** and **Prof. Bhishnupada Mandal** (the former heads of our department) and **Prof. Anugrah Singh** (the present head of our department) for extending all necessary facilities to carry out my research. I am also grateful to all the professors in the department for their sincere cooperation. I wish to thank all the non-teaching staff of our department for the help received from them.

I also thank my Doctoral Committee members, **Prof. Chandan Das**, **Dr. Tapas Kumar Mandal** (Department of Chemical Engineering), and **Prof S Sreedeep** (Department of Civil Engineering) for their valuable suggestions and contributions towards my research work.

I would like to thank my co-researchers and friends, Mr. Ritesh Prakash, Mr. Bharat Kumar Goshika, Mr. Soumen Mondal, Ms. Surubhi Patel, Ms. Kumari Ruby, Mr. Pongliba Sangtam, Ms. Varanasi Venkata Radha Sai Bhavana, Mr. Adhwarshu Bhattacharyya, Mr. Gaurav Singh, Mr. Babban Lal Maurya, Dr. Rajeev Parmar, and Dr. Anil Kumar Thandlam for their enormous help

and support during my research. I am also thankful to all other departmental friends, seniors, and juniors for their encouragement, support, and good wishes.

I also thank my family members, who have not only supported me with patience to complete my thesis, but also have stood by me throughout my life. I am particularly indebted to my mother, Sainaba Pangat, and my wife, Ramseena Fahad, for their constant encouragement, suggestion, patience, and motivation. The moral support of my son, Faizan Fahad M K, and my sisters, Fidha P K and Fadiya P K, has enabled me to complete this work in a peaceful and cheerful manner. They have transformed all the dreams to reality.

Date: 5th June 2020

Place: IIT Guwahati Fahad M K

CURRICULUM VITAE

Name	Fahad M K
Date of Birth	02.06.1983

A. Education qualification

Degree	**University/Institute**	**Duration**
Bachelor of Technology in Chemical Engineering	TKM College of Engineering (Kollam, Kerala)	2002 – 2006
Master of Technology in Chemical Engineering	DDIT (Nadiad, Gujarat)	2009 – 2011
Doctor of Philosophy in Chemical Engineering	Indian Institute of Technology Guwahati (Assam)	2012 – 2020

B. Technical Experience

Position	**Employer`**	**Duration**
Graduate Apprentice	Bharat Petroleum Corporation Ltd- Kochi Refinery, Kochi, Kerala	2007-2008
External Engineer	Bharat Petroleum Corporation Ltd- Kochi Refinery, Kochi, Kerala	2008-2008
Field Operation and Panel Engineer	Reliance Industries Ltd, Vadodara, Gujarat	2008-2009

C. Academic Experience

Position	Employer`	Duration
Adhoc Lecturer	National Institute of Technology. Calicut, Kerala	2011-2012

D. Awards, Scholarships, and Recognitions

1. Scholarship given by the Ministry of Human Resource Development (Government of India) for Ph.D. from December 2012 to July 2018.
2. Topper of the Class (10^{th}), Darul Uloom High School (Panakkad, Malappuram) for the Board of Public Examination (Kerala).

E. Research Papers in Journals

1. Fahad, M.K., Prakash, R., Majumder, S.K., Ghosh, P., 2019. Gas holdup in the gas–liquid–coal slurry flow in a flotation column in presence of surface-active agent. Multiphase Sci. Technol. 31, 199–214. **DOI:** 10.1615/MultScienTechn.2019029957

2. Fahad, M.K., Prakash, R., Majumder, S.K., Ghosh, P., 2019. Frictional pressure drop in a flotation column: An experimental investigation in continuous mode and its prediction by a general model. Multiphase Sci. Technol, 31, 235–254. **DOI:** 10.1615/MultScienTechn.2019031051

3. Fahad, M. K., Prakash, R., Majumder, S. K., Ghosh, P., 2020. Dispersion characteristics in a gas–liquid–coal slurry flotation column and its analysis by the velocity distribution model. J. Dispersion Sci. Technol. https://doi.org/10.1080/01932691.2020.1737105.

F. Manuscript under Review

4. Fahad, M. K., Prakash, R., Majumder, S. K., Ghosh, P., Experimental studies on frictional pressure drop in gas–liquid–coal slurry flow in a flotation column. Arabian J. Sci. Eng. Manusript ID: AJSE-D-19-02906.

5. Fahad, M. K., Bhavana. V.V.R.S., Majumder, S. K., Ghosh, P. Effect of different variables on entrainment of coal particles in the gas–liquid–coal slurry flow in a flotation column. Multiphase Sci. Technol. Manuscript ID: MST-33709.

6. Fahad, M. K., Bhavana. V.V.R.S., Majumder, S. K., Ghosh, P., Kinetics and recovery of fine coal particles by flotation: Experiments and modeling. (under preparation)

G. Conferences

- Fahad, M. K, Majumder, S.K., Ghosh, P., Beneficiation of fine particles by fine bubble-aided flotation, MPT-2017, February 1–3, Radisson Blu, Mahabalipuram, Chennai, India.
- Fahad, M. K, Majumder, S.K., Ghosh, P., Hydrodynamic studies on fine bubble-aided flotation, Reflux-2017, March 24–26, Indian Institute of Technology Guwahati, Guwahati, India.
- Fahad, M. K, Majumder, S.K., Ghosh, P., Hydrodynamic studies on fine bubble-aided flotation, Research Conclave-2017, March 16–19, Indian Institute of Technology Guwahai, Guwahati, India.

ABSTRACT

Experimental works were carried out in the batch and continuous modes in the two- and three-phase systems to examine the effects of the concentration of the ionic (i.e., cationic and anionic) and non-ionic surface-active agents, particle size, slurry concentration, superficial gas velocity, and superficial slurry velocity on the gas holdup. The gas holdup was inferred by the drift-flux model for the batch process. The drift-flux and slip velocity models were used to analyze the change in volume fraction of gas for the continuous process. Empirical correlations were developed for the batch and continuous modes. The gas holdup of the system increased profoundly with increasing superficial gas velocity, whereas it decreased with increasing slurry concentration. The effects of four different particle size on gas holdup were also analyzed. The gas holdup of the system reduced due to the solid loading, and this reduction was more pronounced at the higher slurry concentrations. The gas holdup of the system was higher in the presence of CTAB as compared to SDBS and 1-Hexanol. Particle size did not have a significant effect on gas holdup.

The frictional pressure drop characteristics in a two- and three-phase flotation column was studied in the presence of different surfactants. An in-depth investigation was carried out on the impact of the operating variables on frictional pressure drop. It was observed from the experimental results that the frictional pressure drop increased with increasing slurry concentration, average particle size, and superficial gas velocity. However, it decreased by the addition of surfactant to the system. Frictional pressure drop was lower in the presence of the cationic surfactant than the anionic and non-ionic surfactants. Also, empirical correlations were developed to predict the frictional pressure drop for batch and continuous mode operation.

The dispersion number was computed and analyzed in a three-phase counter-current flotation column. The velocity distribution model was used to analyze the axial dispersion phenomenon. The parameters of the velocity distribution model, dispersion due to bubble motion, and the velocity distribution characteristic factor were also determined under the given experimental conditions. Empirical correlations were developed to predict the dispersion number, dispersion due to bubble motion, and the velocity distribution characteristics factor. These correlations were compared with those reported in the literature. The study was carried out to understand the effects of slurry concentration, particle size, surfactant dose, and gas and slurry velocities on the

dispersion number. For the three-phase counter-current flow system, the characteristic factor of the velocity distribution decreased with increasing superficial gas velocity and surfactant concentration. However, it increased as the slurry concentration and particle size increased. The dispersion coefficient of the bubble motion increased as the superficial gas velocity and surfactant concentration increased. It also increased as the slurry concentration and particle size increased.

The bubble size and its distribution in the coal slurry were measured by image analysis. The effects of the superficial gas velocity, slurry concentration, particle size, surfactant concentration, and axial height were enunciated. The Sauter mean bubble diameter was found to vary in the range of 2.14 –5.94 mm. The Sauter mean bubble diameter increased as the superficial gas velocity, slurry concentration, axial height, particle size, and surfactant concentration increased. Correlations were developed for the Sauter mean diameter.

Experiments were conducted in a continuous flotation column to determine the degree of entrainment of the coal particles, and to examine its dependence on surfactant concentration, particle size, slurry concentration, superficial gas velocity, and superficial liquid velocity. Using Warren's model, the degree of entrainment was analyzed. An empirical correlation was developed to predict the degree of entrainment, based on a wide range of operating variables. It was observed that the cationic surfactant gave better entrainment than the anionic surfactant. The degree of entrainment of the coal particles was proportional to the superficial gas and slurry velocities. The entrainment decreased with increasing particle size but increased with increasing particle concentration.

Experiments were carried out to interpret the effects of different operating variables in the presence of cationic and anionic surfactants on the recovery of fine coal particles in the flotation column. The kinetics of the cumulative recovery was determined. The flotation rate constant and induction time were analyzed based on the recovery efficiency, incorporating the stability, attachment, and collision efficiencies of the particles with the bubbles. Generalized correlations for the rate constant and the induction time were also developed based on the experimental results. The correlations were made by the multiple regression analysis of the experimental data.

CONTENTS

PAGE NO.

FIGURES

TABLES

CHAPTER 1: BACKGROUND AND FORMULATION OF WORK

1.1. Introduction

Flotation is the method for separating minerals from gangue by the differences in their hydrophobicity, or it is a process for selectively separating hydrophobic materials from hydrophilic. Flotation column is a multiphase contacting device where the liquid is in a continuous phase while the gas and solid are in the dispersed phase. Inside the flotation column, mixing, dispersion, and transportation of materials take place due to the movement of gas bubbles in the continuous liquid phase. Fine particle separation is widely encountered in mineral industries. A large number of valuable minerals are thrown away as fines and ultrafines because of inadequate technology to process them economically. The separation of fine particles is a challenging problem in raw material processing units (Rousseau, 1987). It is the most significant beneficiation method in this regard. However, when considering finer size ranges, flotation faces problems, because the bubble-particle collision probability decreases with decreasing particle size (Weber and Paddock, 1983). Hydrophobicity differences between valuable minerals and waste gangue are increased by adding surfactants and wetting agents. The selective separation of the minerals makes processing complex ores economically viable. It is used for the separation of a large range of carbonates, sulfides, and oxides before further refinement, in which particles are removed selectively from the suspension by attachment to the rising bubble. The main operating parameters are feed rate, air rate, frother dosage, collector dosage, wash water rate, and tailing rate. The controlled variables are froth depth, interface level, gas hold up, percentage solids in concentration and pulp density of slurry.

The concentrate grade and recovery determine the metallurgical performance after the flotation. The recovery can be estimated from a material balance. Accordingly, automatic control and optimization of flotation columns need to be performed using process variables with a strong influence on the metallurgical performance. It is the most efficient, most sensitive, most complicated, most challenging, and least understood mineral processing operation today. It is essential in the area of mineral beneficiation because of low energy requirements, high removal efficiency, reasonable capital investment, and comparatively low levels of maintenance and operational requirements. Also, there is the possibility in many instances of recovery, and re-use, not only of the separated substances but also of the somewhat costly surfactants. Nearly one billion of ore is treated by this process annually in the world. The basic concept of the flotation process looks relatively simple, but the fundamental principles related to the performance of mineral processing by the flotation technique are quite complex. So the influence of separation process technology on the profitability is strong in the mineral industries (Rousseau, 1987). In this regard, flotation is the most common method to separate the valuable components. Flotation is beneficial not only to mineral separation but also to a large variety of chemical species such as molecules, ions, microorganisms, oil droplets, etc. by this method. It can be separated either from one another or concentrated from a solution (Al-Shamrani et al., 2002; Gaudin et al., 1960; Matis and Mavros, 1991).

1.2. Principle of flotation

Froth flotation begins by commination, crushing, and grinding, which is used to increase the surface area of the ore for subsequent processing and break the rocks into the desired mineral and gangue in a process known as liberation, which then has to be separated from the desired ore. The

ore is converted into a fine powder and mixed with water to form a slurry. The desired mineral is rendered hydrophobic by the addition of a surfactant or collector. The particular chemical depends on which ore is processed. The slurry of hydrophobic and hydrophilic particles is then introduced to a water bath, which is aerated, creating bubbles. The hydrophobic particles attach to the air bubbles, which rise to the surface, forming a froth. The froth is removed, and the concentrate is further refined. To be used on a given ore slurry, the collectors are chosen based upon their selective wetting of the particles to be separated. A good collector will adsorb, physically or chemically, with one of the types of particles. This provides the thermodynamic requirement for the particles to bind to the surface of a bubble. The wetting activity of a surfactant on a particle can be quantified by measuring the contact angles that the liquid/bubble interface makes with it. Another important measure for attachment of bubbles to particles is induction time. The induction time is the time required for the particle and bubble to rupture the thin film separating the particle and bubble. This rupture is achieved by the surface forces between the particle and bubble.

The principle for the bubble-particle attachment is very complex and consists of three steps, collision, attachment, and detachment. The collision is affected by the velocity of the bubble and the size of the bubble. The collision tube corresponds to the region in which a particle will collide with the bubble, with the perimeter of the collision tube corresponding to the grazing trajectory. The attachment of the particle to the bubble is controlled by the induction time of the particle and bubble. The particle and bubble need to bind, and this occurs if the time in which the particle and bubble are in contact with each other is larger than the required induction time. This induction time is affected by the fluid viscosity, particle and bubble size, and the forces between the particle and bubbles. The detachment of a particle and bubble occurs when the shear and gravitational forces exceed the force exerted by the surface tension. These forces are complex and vary within the cell.

High shear will be experienced close to the impeller of a mechanical flotation cell and mostly gravitational force in the collection and cleaning zone of a flotation column. Significant issues of entrainment of fine particles occur as these particles experience low collision efficiencies as well as sliming and degradation of the particle surfaces.

Coarse particles show a low recovery of the valuable mineral due to the little liberation and high detachment efficiencies. Chemical compounds, which cause a reaction in combination with another substance, called reagent. Reagents that possess unlike poles (both polar and non-polar) called heteropolar. Frothers (heteropolar surface-active) are organic reagents, which can absorb on the air–water interface. When the reagent is exposed to water, the water dipoles react with the polar groups and hydrate them, but not with the non-polar groups, and the non-polar groups are forced into the air phase. During the absorption of heteropolar molecules of frothers, polar groups are oriented towards the water and non-polar groups towards the air. Frothers can adsorb on the air-water interface due to their surface-active property and thus reduce the surface tension, which stabilizes the air bubble (Wills, 2006).

1.3. Hydrophobicity and hydrophilicity

The basis of froth flotation is the difference in the wettabilities of different minerals. Particles, which are easily wettable by water, are termed hydrophilic, and those who are water-repellent, are termed hydrophobic. If a mixture of hydrophobic and hydrophilic particles are suspended in water, and the air is bubbled through the suspension, then the hydrophobic particles will tend to attach to the air bubbles and float to the surface. The froth layer that forms on the surface will then be heavily loaded with the hydrophobic mineral and can be removed as a separated product. The hydrophilic particles will have much less tendency to attach to the air bubbles, and so they will remain in

suspension and be flushed away. Particles can be either naturally hydrophobic, or the hydrophobicity can be induced by chemical treatments. Usually, hydrophobic materials include hydrocarbons and nonpolar solids such as elemental sulfur. Coal is an excellent example of a naturally hydrophobic material because it is mostly composed of hydrocarbons. Chemical treatments to render the surface of a particle hydrophobic involve coating the surface with a monolayer of non-polar oil.

1.4. Flotation reagents

These are the chemicals that maintain the correct froth characteristics and also make the particles hydrophobic. Many different reagents are involved in the froth flotation process, and the selection of reagents depends on the specific mineral mixtures being treated. Surfactants are the surface-active agents, which absorb on the mineral surface and change its characteristics.

1.4.1. Collectors

Collectors are the chemical reagents, which selectively adsorb on the mineral surface and make it hydrophobic. They form a monolayer of non-polar hydrophobic hydrocarbons on the mineral surface. Collectors increase the contact angle between the air bubble and the mineral particle so that the bubbles will adhere to the mineral surface. The selection of the correct collector is a critical factor for an effective separation by froth flotation. Collectors are generally classified depending upon their ionic charge, i.e., nonionic, anionic, and cationic. The nonionic collectors are pure hydrocarbon oils, while the anionic and cationic collectors consist of a polar part that selectively attaches to the mineral surfaces, and the non-polar part projects out into the solution and makes the surface hydrophobic. The process in which collectors are chemically bonded to the mineral

surface is called chemisorption. The process in which collectors are bonded to the mineral surface by physical forces is called physical adsorption. An excess concentration of the collector develops a multilayer on the mineral surface, which reduces the hydrophobicity and hence restricts the recovery of valuable minerals. Examples of industrially-used amphoteric collectors are cetyl amino acetic acid, n-lauryl-ρ-amino propionic acid, n-myristyl taurine, n-lauryl-β aminobutyric acid, n-lauryl-β iminodipropionic acid, sodium hydroxylethyldodecylamino acetate, and sodium cetylamino diacetate.

Excess concentration of surfactant or collector forms the aggregates called *micelles*. The bulk concentration of the surfactant at which the micelles form is known as critical micelle concentration (CMC). If we continuously increase the concentration of surfactant or collector in water then there will be a decrease in the surface tension of water up to the CMC; above that, the surface tension of water will become roughly constant, because the activity of surfactant remains constant above the CMC (Fuerstenau and Han, 2003).

1.4.1.1. Type of collectors

1.4.1.1.1. Ionizing collectors

These are complex molecules, which are asymmetric, and are heteropolar as well. They have a longer hydrocarbon chain length and possess a powerful water repulsion capability. They ionize in water. There are two types of ionizing collectors, i.e., anionic and cationic collectors.

1.4.1.1.1.1. Anionic collectors

The anionic collector is a negatively-charged ion, which makes the mineral water repellent. It can be a weak acid or an acid salt that ionizes in water. It has a negatively-charged end that will attach

to the mineral surfaces and a hydrocarbon chain that extends out into the liquid. e.g., carboxylic, sulfates, sulphonates, xanthates, sodium oleate.

1.4.1.1.1.2. Cationic collectors

The cationic collector uses a positively-charged amine group to attach to mineral surfaces. Since the amine group has a positive charge, it can connect to negatively-charged mineral surfaces. Cationic collectors, therefore, have the opposite effect of the anionic collectors, which attach to positively-charged surfaces. Cationic collectors are mainly used for flotation of silicates and certain rare-metal oxides, and the separation of potassium chloride (sylvite) from sodium chloride (halite).

The cationic collector is a positively charged ion, which makes the mineral water repellent. In a cationic collector, the polar group is cation-based, e.g., pentavalent nitrogen. The cationic collector is very sensitive to the pH of the working medium. It is very much sensitive in slightly acidic solution and insensitive in strongly alkaline and acid media. It is water repellent based on the pentavalent nitrogen e.g., amine, tri-n-amyl amine, amyl amine hydrochloride, tetramethyl ammonium chloride, aniline, benzylamine, diphenylamine, pyridine, quinoline hydrochloride, piperidine hydrochloride, and ether amine (Bulatovic, 2007).

1.4.1.1.2. Non-ionizing collectors

These are the collectors, which have an affinity for surfaces that are already partially hydrophobic. They selectively adsorb on these surfaces and increase hydrophobicity (e.g., hydrocarbon oils, kerosene, and fuel oil used in coal recovery). The non-ionizing collector is a non-polar liquid hydrocarbon, which does not dissociate in water. It is practically insoluble in water and makes

minerals water repellent by adsorbing on their surface in the form of a thin film. It is assumed that the adsorption of the non-ionic collector on the mineral surface takes place by adhesion. The common origin of the non-ionic collector is either crude oil or coal. The non-ionic collector does not have a fixed chemical composition due to the different properties of crude oil or coal (since they are obtained from various sources). Some industrially used non-ionic collectors are kerosene, transformer oil, and synthetic hydrocarbon oil (Bulatovic, 2007).

1.4.2. Frother

Frothers are used to stabilize air bubbles so that they will remain well-dispersed in the slurry, and will form a stable froth layer that can be removed before the bubbles burst. Frother helps in the formation of stable bubbles in the pulp phase and enhances the flotation kinetics. Frothers are heteropolar organic surface-active reagents, which have the potential to adsorb on the air-water interface and reduce the surface tension, therefore stabilizing the air bubble. The amount of froth generated in the flotation column is known as *froth power*, which depends on the type of frother and the collector used. Generally, the froth power increases when the number of carbon atoms in the hydrocarbon chain is up to seven, and start to decrease beyond 8-carbon atom compound, e.g., alcohols, particularly Methyl Isobutyl Carbinol (MIBC) and any number of water-soluble polymers based on propylene oxide such as polypropylene glycols. Cresols and pine oils are also used as frothers (Bulatovic, 2007).

1.4.3. Regulators

Regulators control the interaction of collectors between discrete minerals. Separation of particular mineral increases because the selectivity of the collector on a specific mineral can be increased or

decreased by the regulator. It extensively modifies the action of collectors by enhancing or reducing its water-repellent effect on the mineral surface. There are three kinds of regulators, i.e., activators, depressants, and pH regulators.

1.4.3.1. Activators

Activators are specific compounds that make it possible for the collectors to adsorb onto surfaces that they could not usually attach. A classic example of an activator is copper sulfate, which acts as an activator for sphalerite (ZnS) flotation with xanthate collectors. Some of the minerals do not adsorb collectors on their surface, and therefore, they do not float. Activators are widely used to activate the adsorption of the collectors on the mineral surface.

1.4.3.2. Depressants

The depressants have the opposite effect of the activators, i.e., they prevent the collectors from adsorbing onto particular mineral surfaces. They are used to increase selectivity by preventing one mineral from floating while allowing another mineral to float without any obstruction. For example, cyanide (CN^-) is used in the flotation of sulfide minerals, especially pyrite (FeS_2). Lime is used either as CaO or $Ca(OH)_2$. When it dissolves, it creates the calcium ions, which can adsorb onto the mineral surfaces. In combination with its strong alkaline nature, this makes it particularly useful in manipulating sulfide flotation. A large number of organic compounds are useful as flotation depressants. They are soluble polymers (such as starch), which selectively coat mineral surfaces and prevent collectors from attaching. Some of the examples of depressants are carboxymethyl cellulose (polymeric, less hazardous than inorganic depressants), phosphate, calcium, aluminum salt, sodium silicate, chromates, hydrophilic alkanol amine (silica controls

oxide mineral flotation), polyacrylamide-based polymers (depression of iron sulfides in base metals sulfide flotation**,** chitosan starch, carboxymethyl celluloses, lignosulphonates, and guar gum (Herrera-Urbina, 2003)).

1.4.3.3. pH regulators

The simplest modifiers are pH-control chemicals. The surface chemistry of most minerals is affected by the pH. In general, the surface of the minerals develops a positive charge under acidic conditions, and a negative charge is developed under alkaline conditions. Since each mineral changes from negatively-charged to positively-charged at some particular pH, it is possible to manipulate the attraction of collectors to their surfaces by pH adjustment. There are also other more complex effects due to pH that change how a particular collector adsorbs on the mineral surfaces. Sulfhydryl collectors, such as xanthate ions, compete with the OH^- ions to adsorb on mineral surfaces. Therefore, adsorption is a function of pH. This makes it possible for the sulfhydryl collectors to separate specific minerals progressively. The pH at which the xanthate ion wins the competition with OH^- ions depends both on the concentration of xanthate in the solution, and on the specific sulfide mineral present.

1.4.3.3.1. Acids

The acids, which give the most considerable pH change at the lowest cost, are generally used. Sulfuric acid is the most popular. A pivotal point to consider is that the anion of the acid can potentially have effects of its own, apart from lowering the pH. There are some cases where acids other than sulfuric acid are more useful.

1.4.3.3.2. Alkalis

Like acids, the most popular alkalis are those which are cheapest. The lowest-cost alkali is lime [i.e., CaO or $Ca(OH)_2$]. However, the calcium ion often interacts with the mineral surfaces to change their flotation behavior. In some cases, the calcium ions have beneficial effects, while in other cases, they change the flotation in undesirable ways. It may, therefore, be necessary to use sodium-based alkalis such as NaOH or Na_2CO_3, because the sodium cation generally does not have any significant effect on the particle surface chemistry.

1.5. Types of flotation and their application

1.5.1. Dissolved-air flotation

In this process, the air is dissolved and saturated with water under high pressure. It is then released by using the pressure-reducing valve, which causes the generation of microbubbles. Generally, the air is used, but gases like methane, carbon dioxide, and nitrogen also have been used in some applications**.** Different sizes of microbubbles are generated by varying the pressure and nozzle diameter (Kim et al., 2015). Some of the important applications are separation of nickel, zinc, ferric and copper ions from dilute aqueous solutions (Lazaridis et al., 1992), separation of zinc from hydroxide precipitate (Qi and Aldrich, 2002), separation of feldspar from feldspathic slime and iron-containing minerals in batch mode (Karagüzel, 2010), and separations of mercury, arsenic and selenium ions from gold cyanide leach solutions (Tassel et al., 1997; Tessele et al., 1998).

1.5.2. Induced- or dispersed-air flotation

In this method, bubbles are generated by the mechanical mixing of gas and liquid. High-speed rotating impellers, diffusers, agitators, and air injection systems are using for mechanical mixing. Some applications are wastewater treatment for removing oil or solid [the range of bubble size is about 700 – 1500 μm (Rubio et al., 2002)], industrial wastewater treatment [e.g., oil from the refinery, natural gas processing plant, and petrochemical and chemical plant (El-Kayar et al., 1993)].

1.5.3. Electro-flotation

An electric field is established between electrodes due to the conductivity of the liquid if liquid waste is placed between the electrodes. On electrolysis of water, hydrogen and oxygen bubbles are generated on electrodes. Essential variables, which affect the bubble diameter, number of bubbles, and current density are pH, type of electrolyte (e.g., NaCl, NaOH, and HCl), and retention time. In this process, ions or solid particles, which are suspended or dissolved in the liquid phase, float by attaching to the fine bubbles, which rise in the flotation column due to buoyancy. Hydrogen and oxygen bubble generate on cathode and anode electrode, respectively. Some of the important applications are the separation of emulsified paraffin from water (Mohammed, 2007) and the separation of wastewater from washing soil (Mota et al., 2015). This method is efficient for the removal of 97% of Pb, Ba, and Zn metals (Mota et al., 2015). (Matis et al., 1993) have given an extensive review of the various flotation techniques, which may be useful for further explanation of the various methods.

1.5.4. Column flotation

Column flotation is highly used in the mineral processing industry. The success of column flotation depends on the hydrophilic and hydrophobic nature of minerals, or in their activated form by using reagents. Bubbles are generated at the bottom of the column. The hydrophobic mineral particles get attached to the bubbles, and they rise up along with the bubble. Gas hold up, bubble generation method, bubble size distribution, bubble rise velocity, bubble–particle interaction, entrainment, frictional pressure drop, and drag coefficient are the significant parameters in the degree of particle separation in the flotation column. Wastes from asbestos, polymer, paper industries, electroplating, vegetables, poultry processing, oil industries, food, dairy, textile fiber, rubber, and dye are commonly processed by column flotation using suitable collectors.

However the studies regarding the hydrodynamics, holdup characteristics, mixing characteristics, bubble size distribution and specific interfacial area the flotation kinetics and the particle entrainment in the flotation column are scanty. Therefore, a precise knowledge of the hydrodynamic, mixing characteristics, bubble size distribution, entrainment charatcteristics and flotation finetice of the coal particles in a flotation column, would be of considerable interest based on the present study.

1.6. The importance of the hydrodynamic studies

1.6.1. Gas holdup

The gas holdup is important for the scale-up process in two-phase and three-phase bubble columns. A higher gas holdup may result in higher efficiency of the transport processes. It is also used for the estimation of the interfacial area, which directs the particle recovery by flotation. The desired recovery has a great dependence on the determination of gas holdup and flow regime (Kantarci et al., 2005). An increase in gas holdup increases the gas-liquid interfacial area, which increases the

rate of transport and hence increases the yield of the process. The gas holdup in a flotation column depends on superficial gas and liquid velocities, liquid and solid phase properties, column geometry, operating temperature and pressure, and the design of gas sparger (Kantarci et al., 2005). The gas holdup in the flotation column depends on the number of bubbles, average bubble size, and rise velocity of the bubbles (Joshi et al., 1998). Small bubbles yield high gas holdup (Kantarci et al., 2005). Several models are available to interpret the gas holdup characteristics in a multiphase contactor. In this regard, the slip velocity and drift flux model are mostly used. The drift flux model is generally applied to analyze the overall holdup of the gas in a vertical column. This model considers the effect of non-uniform flow and concentration distribution across the duct as well as the effect of local relative velocity between the phases. To analyze the gas holdup data by drift flux model the average gas velocity is plotted against the gas-liquid mixture velocity, which is given by the equation as, $\frac{u_{sg}}{\varepsilon_g} = C_o\left(u_{sg} + u_{sl}\right) + u_d$ where C_o is the velocity distribution coefficient, and u_d is the gas phase drift velocity, which are obtained by experiment. The distribution coefficient accounts for the interaction of the velocity and gas holdup distributions. u_d accounts for the effect of local relative velocity between bubbles and liquid. This analysis of gas holdup is important to assess the flow patterns of the fluid flow in the column. The more details about it with experimental observation is given in the chapter 2. In the present study, an attempt has also been made to analyze the experimental gas holdup data of the present system by Slip-velocity model proposed by Behringer (1936). A correlation in terms of various physical, geometric and operating parameters of the present system has also been developed to analyze the gas holdup.

1.6.2. Pressure drop

The pressure drop in the flotation column determines the requirement of flow energy for the transportation of fluids in the multiphase system. The pressure drop provides the information on the pattern of energy dissipation, which helps in modeling and assessment of the performance of the system. High pressure-drop results when the flow rate is high and the viscosity is high. The details of the frictional mpressure drop and its analysis is given in Chapter 3.

1.6.3. Mixing characteristics

Mixing of gas, liquid, and solid inside the flotation column is a significant parameter since it affects the bubble–particle collision and detachment process. The high intensity of mixing is required to bring the solid particles in contact with the gas bubbles. The geometry of the column, operating conditions, and physicochemical properties of the fluid have important roles in the mixing process. Therefore, the study of mixing is necessary for the optimization and design of the flotation column (Gharai and Venugopal, 2016). Mixing characteristics inside the flotation column governs the particle suspension, fine bubble generation, and dispersion so that the collision between the gas bubbles and the particles takes place. Mixing in the flotation column due to pulp recirculation and dispersion results from turbulence caused by bubble motion and feed slurry. Liquid circulation in the flotation column governs the rate of mixing and degree of particle recovery. Mixing inside the flotation column is estimated by the dispersion number, which is related to the Peclet number. The analysis of residence time distribution with model is described in details in chapter 4

1.7. Importance of entrainment and flotation kinetics

1.7.1. Entrainment characteristics

Entrainment is the root cause that hampers the performance of the flotation column. Entrainment of gangue material into the froth concentrates dilutes the desired material and decreases the grade of the concentrate and hence improves the selectivity and performance of the column. The froth height above the level of pulp significantly affects the performance of the flotation column (Smith and Warren, 1989). The more details abot the entrainment cjharacteristics is given in chapter 5.

1.7.2. Analysis of flotation by kinetic and non-kinetic models

Flotation kinetics determines the variation of rate of change of froth overflow product with time and recognizes the variables that affect the flotation kinetics (Fuerstenau, 1962). The removal rate of particles or probability of collection of solid particles on gas bubbles in the pulp phase in the flotation column is a function of the probability of collision, probability of adhesion, and the probability of detachment. According to (Yoon and Luttrell, 1989), the rate constant of the flotation process is directly proportional to the probability of collection of particle and surface area of the rising bubble. The rate constant signifies the ability of the species to float. The rate constant will help to develop kinetic and non-kinetic models of recovery. Knowledge of mathematical modeling is important since it predicts the metallurgical behavior of the flotation column. The mathematical model helps design, control, and optimization of the flotation column. The analysis of the present experimental data is given in more details in chapter 7.

1.8. Formulation of the research work

1.8.1. Scope of the research work

The study of hydrodynamics characteristics is important to analyze the process efficiency of a flotation system. The hydrodynamic study is an important aspect that helps to understand the

performance, control, modeling, design, and optimization of the equipment. Many researchers have studied the hydrodynamic characteristics of circular and rectangular flotation columns for mineral beneficiation. Flotation technique is the major industrial operation used in mineral beneficiation, wastewater treatment, oil separation, and several other separation processes. However, it is still very complex to understand complete hydrodynamic behavior. There is a lack of study in the separation of coal by flotation, and comparison of efficiency of the process with different surfactants; particle entrainment characteristics by the bubble movement in the column flotation technique; particle attachment and detachment behaviour during flotation based on the different flow pattern regimes, and how gas holdup significantly plays a role in the recovery of the particle in a flotation column.

1.8.2. Objectives of the work

As per the scope of the work, the present study is conducted as per the following objectives:

- Study the holdup characteristics of gas and its analysis in the presence of a surface-active agent in batch and continuous modes
- Study the frictional pressure drop characteristics and its analysis in the presence of a surface-active agent in batch and continuous modes
- Study the mixing characteristics of phases and its analysis in the presence of a surface-active agent in a flotation column
- Study the effects of different variables on the entrainment of coal particles in the flotation column.
- Study the efficiency of recovery of fine coal particles by flotation and its analysis by kinetics model.

CHAPTER 2: GAS HOLDUP CHARACTERISTICS

This chapter analyzed the gas holdup characteristics is in batch mode and also in continuous mode operation. An experimental investigation was carried out to study the effects of particle size, slurry concentration, superficial gas velocity, superficial slurry velocity, surfactant concentration, and type of surfactant on the gas holdup. The gas holdup was analyzed by the drift flux model for the batch process. The drift–flux and slip velocity models were used to analyze the gas holdup for the continuous process. An empirical correlation was also established for both batch and continuous processes.

2.1. Introduction and literature

The gas holdup is an essential parameter in the chemical and petroleum industries for coal gasification and catalytic synthesis of hydrocarbon. It has an indispensable role in mineral beneficiation and chemical and biochemical processes. The process for the liquefaction of coal involves preheating slurry consisting of coal particles in a fluidized slurry bubble column reactor (Ghani et al., 2011). Flotation is widely used as physical separation process such as for mineral processing (Chakraborty et al., 2009; Xing et al., 2018), wastewater treatment (Gharai and Venugopal, 2016; Khuntia et al., 2012), oil-water separation in the petroleum industry (Li et al., 2016), coal particle upgradation (Li et al., 2016; Xing et al., 2017), plastic recycling (Wang et al., 2015b) and de-inking of paper pulp (Labidi et al., 2007). Due to its high separation efficiency and cost-effectiveness, this process is most appropriate (Tao, 2004). For analyzing the efficiency of the flotation system, the gas holdup is one of the crucial hydrodynamic characteristics. For proper design, operation, scale-up, and modelling of the flotation system, it is used. A fluidized bed is

widely used as a multiphase reactor in petrochemical, chemical, and biochemical process industries, and mineral processing (Kunii and Levenspiel, 1991). In the case of coal flotation, the gas passes through the reactor in the form of bubbles supplying hydrogen to the slurry where the liquefaction reactions take place. The gas phase, as a dispersed phase of bubbles, stays in the reactor, and occupies a fraction of the volume of the reactor. The amount of the gas bubbles, i.e., the gas holdup in the reactor, determines the residence time of the slurry phase and the degree of slurry mixing and mass transfer (Prakash and Majumder, 2017). An increase in the gas holdup would increase the gas–liquid interfacial area, which would increase the rate of transport and hence increase the yield of the process (Prakash et al., 2018b). The gas holdup in the reactor is controlled by the superficial gas and liquid velocities, liquid and solid phase properties, column geometry, working pressure and temperature, and the design of gas sparger (Ishkintana and Bennington, 2010; Kantarci et al., 2005). The presence of particle suspension leads to the decrease in the gas holdup with slurry concentration (Banisi et al., 1995a; Bhunia et al., 2017; Mena et al., 2005). The addition of surfactant to the liquid phase reduces the radial variation of the gas holdup, and this reduction increases with the increasing dose of surfactant (Tavera et al., 2001).

The volume fraction of gas in a multiphase unit depends on many factors, such as the feeding device, properties of the gas and the liquid, pressure, temperature, unit size, as well as the superficial gas velocity (Tavera et al., 2001). A low gas velocity tends to give a homogeneous bubble flow. In contrast, a high gas velocity leads to a heterogeneous bubble flow or a churn-turbulent flow in which the rising bubbles have either a broad size distribution or irregular distorted shapes due to frequent bubble coalescence and/or breakup (Anastasiou et al., 2013). (Bhunia et al., 2014) reported that the effects of slurry concentration, solid type, superficial liquid and gas velocities, and gas holdup in the presence of coal and sphalerite slurry mixture on the axial pressure

drop. They reported an axial pressure drop decreases with increasing superficial gas velocity because of the increasing gas holdup of the system. Results from the experiments also indicated that the sphalerite slurry system containing particles (specific gravity: 3.16) had a higher pressure drop than the coal particles (specific gravity: 1.6). In three-phase reactors, all of those factors would change more or less along with the progress of coal processing and, in turn, affect the gas holdup in a complex manner. The surface-active agents can enhance the gas holdup under control of mass transfer in a bubble bed. However, a minimal number of data are available in the literature on the gas holdup in the presence of surface active agents. There is a lack of research on a gas holdup in flotation columns despite broad applications of the flotation systems. No reliable method is available for assessing the gas holdup in the slurry systems and characterizing the fluid flow.

2.2. Experimentation

2.2.1. Experimental setup

The diagrammatic representation of the experimental setup is depicted in Figure 2.1. All experiments were conducted at standard temperature and pressure. The superficial gas velocity range is $0.007 \leq u_{sg} \leq 0.035$ m/s, and the superficial liquid velocity range is $0.007 \leq u_{slr} \leq 0.035$ m/s. The slurry concentration range was $1.5 \leq c_{slr} \leq 10.89$ kg/m^3. The experimental setup consisted of a cylindrical column made of Plexiglas (height = 0.91 m and diameter = 0.055 m), spherical gas sparger (inner diameter = 0.051 m), liquid rotameter, gas rotameter, manometers, compressor, and slurry pump.

The pore diameter of the gas distributor (i.e., sparger) was 35 μm as mentioned by the manufacturer (make: Flamingo Filters Pvt. Ltd, India). The rotameter was calibrated, and its accuracy was ± 2%

deviation of the full range (0 – 5 l/min). The locations of the pressure taps were 0.05 and 0.55 m from the base of the column within the homogeneous regime. Air was supplied through a compressor (make: Friends Air Compressors, India). The gas flow rate was measured by the pre-calibrated rotameter, and the flow was controlled by a needle valve. For every experiment, the initial liquid level was kept at 0.58 m.

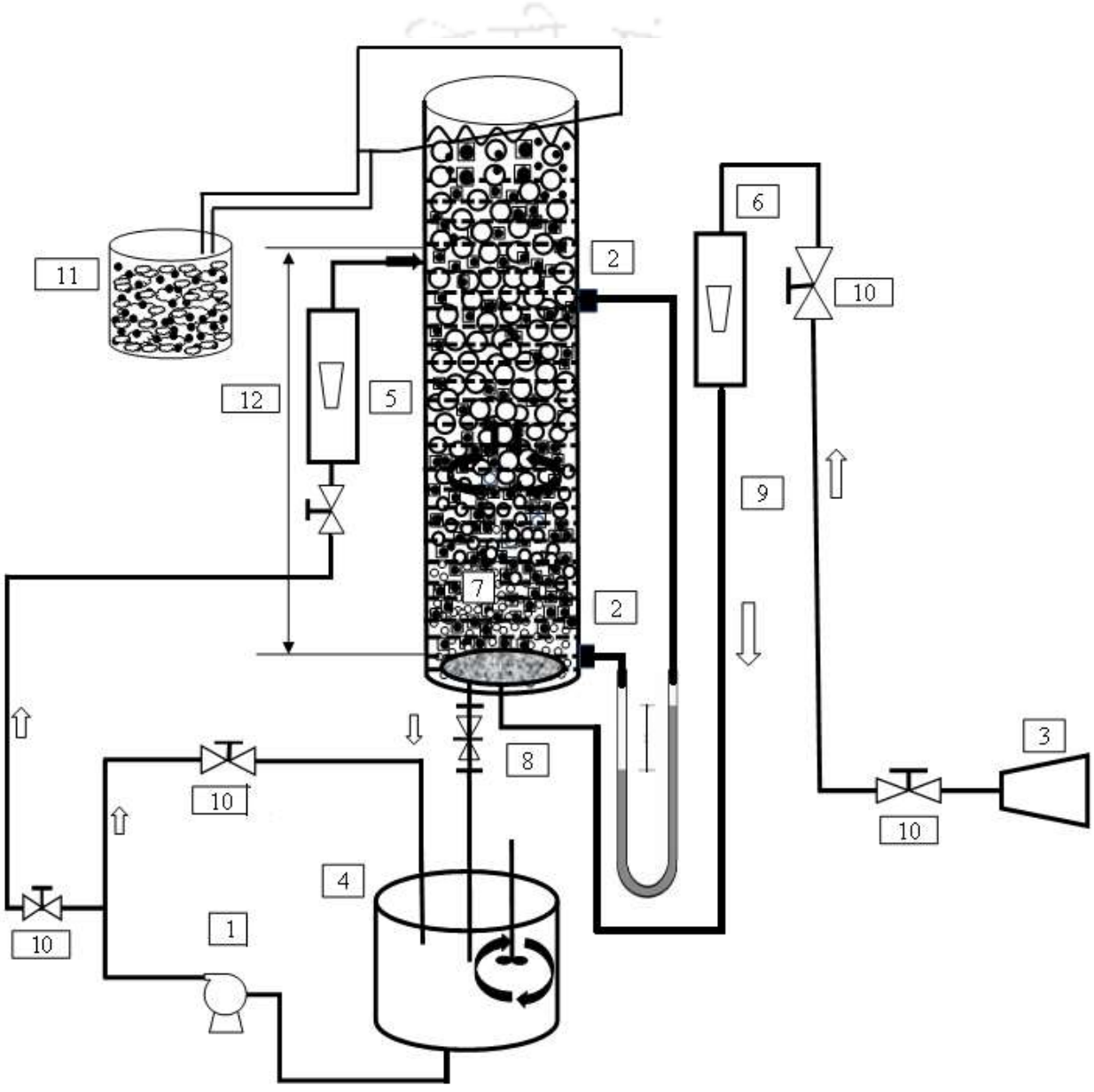

Figure 2.1: Schematic representation of the experimental setup: 1. pump, 2. flotation column, 3. compressor, 4. storage tank, 5. liquid rotameter, 6. gas rotameter, 7. spherical sparger, 8. solenoid valve, 9. manometer, 10. globe valve, 11. froth collecting drum, and 12. collection zone of the flotation column.

2.2.2. Materials and experimental procedure

The surface tension, viscosity, and slurry density were estimated by the tensiometer (make: Kyowa Interface Science, model: DY-300, Japan), interfacial rheometer (make: Anton Paar, model: Physica MCR-301, Austria), and specific gravity bottle, respectively.

Three different surfactants [i.e., sodium dodecylbenzene sulfonate (SDBS), 1-Hexanol, and cetrimonium bromide (CTAB)] were used as surface-active agents. All the surfactants were purchased from Merck (India). Tap water was used for the experiment. The coal samples were collected from the mines (Meghalaya, India). They were crushed using a Jaw crusher (make: Malik Engineering Work, model: MEC-262, India) followed by a roll crusher (make: K. C. Engineers, India). The density of the coal was 1400 kg/m^3, as calculated by the gas pycnometer. Three different particle size ranges were screened after crushing, i.e., < 150, 150 – 300, 300 – 425, and 425– 600 μm. The diameter of the particles was measured by a particle size analyzer (make: Malvern Instruments Ltd, model: Master Sizer 2000, UK). The average size of the particles was 63.22, 235.61, 404.97, and 507.67 μm, respectively. The slurry concentration range is 3.63 – 10.89 kg/m^3 for batch mode and 1.5 – 10.89 kg/m^3 for continuous mode. The continuous mode refers here the flow of slurry and gas countercurrently. The slurry flows downward direction wheras air

flows upward direction. A typical result of particle size distribution $\left(d_p = 63.22\ \mu\text{m}\right)$ is shown in Figure 2.2a.

The gas holdup was determined by the bed expansion technique. The difference in mixture (gas-liquid-solid-surfactant) height after the aeration and clear slurry height before the aeration was taken by a digital camera (make: Nikon, model: Coolpix P520). The digital camera was placed at a distance of 0.25 m from the column wall. A halogen lamp (500 Watts) was kept beside the column to capture a good quality image. Black paper was also placed to the backside of the column to obtain the enhanced quality of the free surface. The level difference was obtained from the captured images, and the final level difference was taken by averaging data points from five different images. As per this method, the average gas holdup (by the volume of the system) can be expressed as per Vadlakonda and Mangadoddy, (2018). The shape of the coal particles was analyzed by a field emission scanning electron microscope (FESEM) (make: Zeiss., Germany; model: Sigma). A typical image of particle shape for $d_p = 235.61\ \mu\text{m}$ is shown in Figure 2.2b.

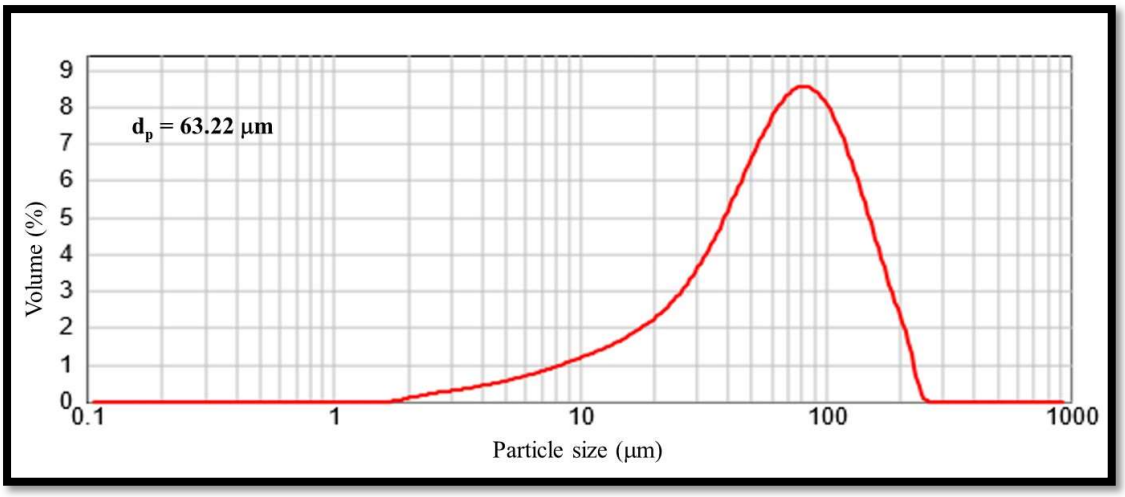

Figure 2.2a. Particle size distribution of coal (d_p= 63.22 µm).

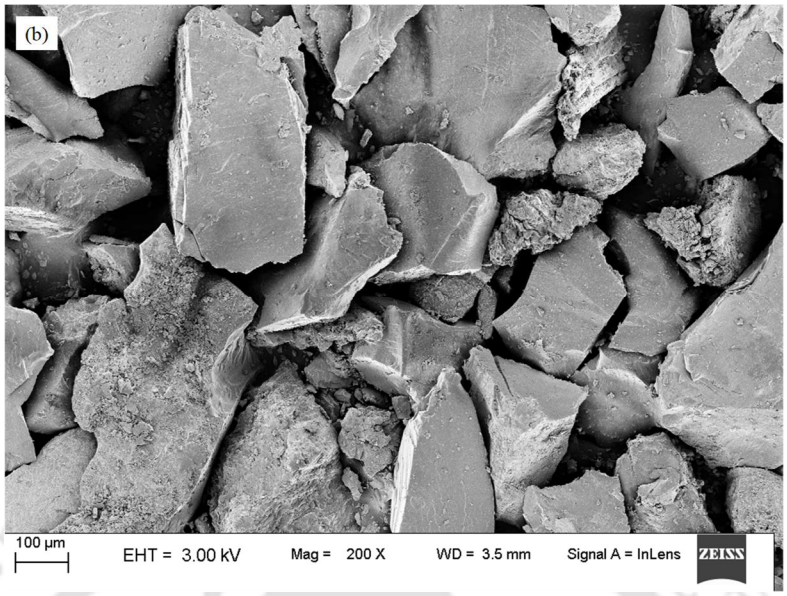

Figure 2.2b: A micrograph showing the particle shape and size analysis obtained by FESEM $\left(d_p = 235.61\ \mu\text{m}\right)$ at 200× magnification.

The fraction of the gas occupied by the air bubbles in the entire volume of the column is the average gas holdup (ε_g). In the current work, the gas holdup is estimated by the bed expansion technique. Two types of readings are essential to measuring the gas holdup: one is the gas-liquid mixture height after gas sparging is done at the steady-state, and the other is the clear slurry mixture height after stoppage of gas sparging at steady state. The average gas holdup of the system can be expressed as (Prakash et al., 2018a; Vadlakonda and Mangadoddy, 2018).

$$\varepsilon_g = 1 - \left(\frac{h_l}{h_m}\right) \tag{2.1}$$

Where h_m and h_l are the gas-liquid-solid height after gas sparging and clear slurry height, respectively. Gas holdup measurement by bed expansion technique is widely acceptable for laboratory flotation column and pilot column (Vadlakonda and Mangadoddy, 2018). Physical

properties of the fluids and also surface tension of the aqueous surfactant solution used in batch mode are shown in Table 2.1 and Table 2.2, respectively. Physical properties of the fluids and surface tension of the aqueous surfactant solution used in the continuous mode are shown in Table 2.3 and Table 2.4, respectively.

Table 2.1: Physical properties of the system in the batch mode measured at 298 ± 1 K.

Slurry concentration (kg/m^3)	Surfactant concentration (g/m^3)	Viscosity (mPa s)			Density (kg/m^3)		
		SDBS	CTAB	1-Hexanol	SDBS	CTAB	1-Hexanol
3.63	3	1.085	1.073	1.092	1000.12	1000.16	1000.13
	6	1.140	1.132	1.135	1000.15	1000.19	1000.17
	10	1.232	1.221	1.211	1000.26	1000.35	1000.31
7.26	3	1.091	1.083	1.095	1001.21	1001.32	1001.08
	6	1.131	1.155	1.151	1001.35	1001.41	1001.32
	10	1.248	1.251	1.243	1001.61	1001.74	1001.64
10.89	3	1.098	1.092	1.098	1002.33	1002.09	1002.41
	6	1.169	1.163	1.166	1002.52	1002.32	1002.52
	10	1.271	1.274	1.267	1002.81	1002.72	1002.65

Table 2.2: Surface tensions of the aqueous surfactant solutions in the batch mode measured at 298 ± 1 K.

	Surface tension (N/m)

Surfactant concentration (g/m^3)	SDBS	CTAB	1-Hexanol
3	0.048	0.041	0.061
6	0.043	0.037	0.060
10	0.039	0.035	0.059

Table 2.3: Physical properties of the three-phase system in the continuous mode measured at 298 ± 1 K.

Slurry concentration (kg/m^3)	Surfactant concentration (g/m^3)	Viscosity × 10^3 (kg/ms)			Density (kg/m^3)		
		SDBS	CTAB	1-Hexanol	SDBS	CTAB	1-Hexanol
1.5	10	1.235	1.248	1.255	1002.21	1002.44	1002.35
	30	1.304	1.362	1.308	1002.42	1002.68	1002.57
	50	1.408	1.481	1.413	1002.78	1002.95	1002.83
3.63	10	1.248	1.256	1.262	1004.26	1004.35	1004.31
	30	1.312	1.371	1.315	1004.42	1004.58	1004.49

	50	1.416	1.492	1.422	1004.67	1004.87	1004.73
7.26	10	1.259	1.265	1.267	1005.41	1005.16	1005.37
	30	1.321	1.377	1.334	1005.65	1005.34	1005.55
	50	1.425	1.496	1.438	1005.82	1005.71	1005.78
10.89	10	1.277	1.286	1.274	1006.48	1006.19	1006.25
	30	1.353	1.393	1.351	1006.67	1006.37	1006.47
	50	1.470	1.498	1.463	1006.91	1006.84	1006.61

Table 2.4: Surface tension of the slurry in the continuous mode measured at 298 ± 1 K.

Surfactant concentration (ppm)	Surface tension (N/m)		
	SDBS	CTAB	1-HEXANOL
10	0.039	0.035	0.059
30	0.033	0.031	0.053
50	0.030	0.029	0.048

2.3. Theoretical background

2.3.1. Theory of the drift-flux model

(Zuber and Findlay, 1965) presented the drift-flux model, which is based on the presence of local slip. Drift–flux theory is broadly used to analyze the average gas holdup in the flotation column. It contemplates the volumetric flux of the gas resultant to a surface which is movable with a mean velocity of dispersion (Gandhi et al., 1999). This model is used to analyze the non-homogeneous distribution of the gas phase in the column. It considers the variation of the volume fraction of phase distribution in the radial direction, the relative velocity of the phases, and the influence of non-uniform flow. In a bubbling fluidized system, the bubbles rise locally relative to the liquid due to the density difference between the phases. The gas-phase may accumulate in the slower or faster region of the flow resulting in variation in the overall gas holdup. It considers the interstitial gas velocity u_{sg}/ε_g among the phases, the consequence of radial non-homogeneity of gas distribution, and superficial gas velocity. For a batch mode, the drift-flux model is represented by

$$\frac{u_{sg}}{\varepsilon_g} = C_o\left(u_{sg}\right) + u_d \tag{2.2}$$

This model is based on the actual gas velocity u_{sg}/ε_g and for a continuous system, it can be expressed as

$$\frac{u_{sg}}{\varepsilon_g} = C_o\left(u_{sg} + u_{slr}\right) + u_d \tag{2.3}$$

Where u_{slr} is the superficial slurry velocity, u_d is the weighted average drift velocity, and C_o is the distribution parameter, u_{sg} is the superficial gas velocity. The distribution parameter in the

drift–flux surmises the interaction of phases, velocity distribution, and the gas holdup in the flotation column (Kumar et al., 2013). (Clark and Flemmer, 1985) have reported from their experimental result that the C_0 was 0.95 for the low gas holdup < 0.2 and were 1.2 for a system of having a gas holdup > 0.2. (Clark et al., 1990) and (Zuber and Findlay, 1965) demonstrated the C_0 values range 1.2-1.5 for a heterogeneous regime. More details about the basic of the drift flux model is given by Bahramian and Elyasi (2020). In the present study, the parameter C_0 and the u_d were estimated based on the experimental data of gas holdup and fitting the equation (2.3) with the experimental data of gas holdup (by calculating $u_{sg}/\varepsilon g$) at different operating conditions.

For a given superficial gas (or liquid) velocity, thesuperficial liquid (or gas) velocity was chosen and corresponding gas volume fraction was measured. Then, u_{sg}/ε_g versus $u_{sg} + u_{sl}$ was plotted to produce a straight line with slope of C_0 and vertical intercept of u_d. A typical plot of the u_{sg}/ε_g versus $u_{sg} + u_{sl}$ is shown in Figure 2.3.

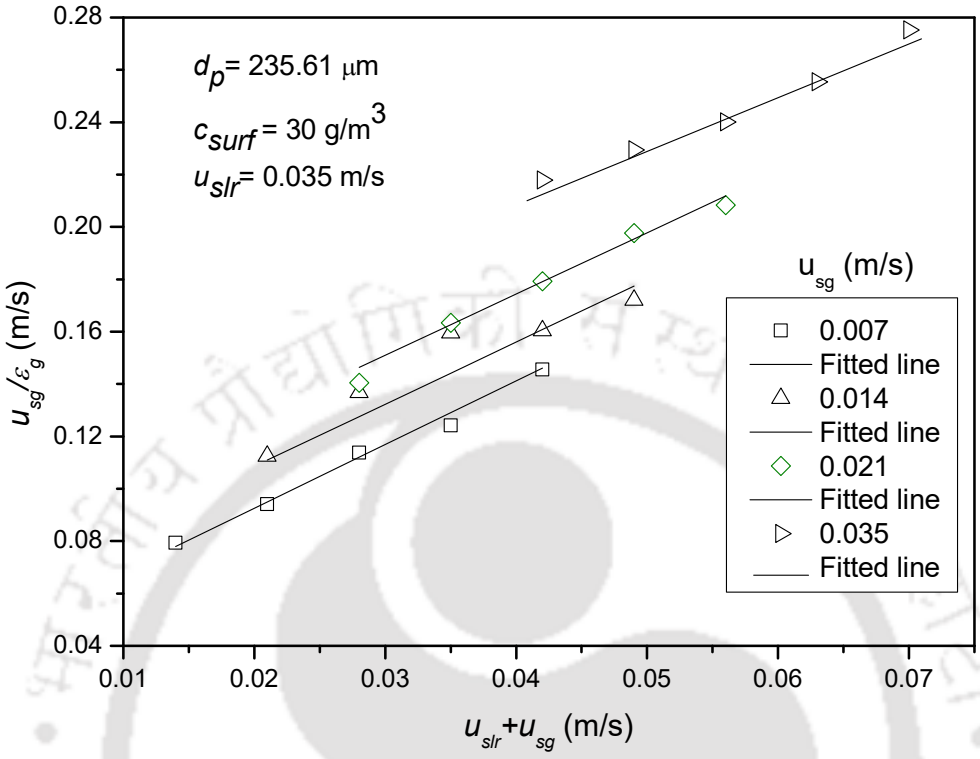

Figure 2.3: A typical plot of the u_{sg}/ε_g versus $u_{sg} + u_{sl}$ to estimate the u_d and C_o.

2.3.2. Theory of the slip velocity model

The slip velocity model was first introduced by Behringer (1952). The slip velocity of bubbles relative to surrounding liquid is defined as

$$u_s = \pm\left[u_g - u_l\right] = \pm\left[\frac{u_{sg}}{\varepsilon_g} - \frac{u_{slr}}{1-\varepsilon_g}\right] \tag{2.4}$$

Here, the negative sign indicates the inverse flow system. The bubble phase holdup data correlated as a function of u_l, and u_g. Lapidus and Elgin, (1957) reported that in the churn turbulent flow regime, the indications of bubble interaction characterize the slip velocity within the column. The

relationship is often used to find out the slip velocity that justifies the interaction between bubbles within the column as a function of the gas holdup, which can be expressed as

$$u_s = u_b f\left(\varepsilon_g\right) \tag{2.5}$$

where u_b is the bubble terminal rise velocity, and $f\left(\varepsilon_g\right)$ displays the result of the interaction of adjacent bubbles within the column. The slip velocity can be expressed as

$$u_s = u_b\left(1-\varepsilon_g\right)^n \tag{2.6}$$

2.4. Uncertainty analysis of the experimental data

Each experiment is repeated for five times. The mean of the continual experiment is measured by

$$\bar{x} = \frac{1}{N}\sum_{i=1}^{N} x_i \tag{2.7}$$

where N is the total number of parameters and x_i is the i^{th} component of parameters. The error analysis is calculated based on the percentage relative uncertainties U_r of the continual experiments and standard uncertainties U. The standard uncertainty of the average value is estimated as

$$U = \frac{STDEV}{\sqrt{N}} \tag{2.8}$$

Relative uncertainty is calculated as

$$U_r = \frac{U}{\bar{x}} \times 100\ \% \tag{2.9}$$

The standard deviation can be expressed as

$$STDEV = \sqrt{\frac{\sum_{i=1}^{N} \left(x_i - \bar{x}\right)^2}{N-1}} \tag{2.10}$$

Uncertainty analysis of experimental data for batch mode and continuous mode shows in Table 2.5 and Table 2.6, respectively.

Table 2.5: Uncertainty analysis of the experimental data for the batch mode.

Parameter	Mean, $\bar{x}$ (–)	STDEV (–)	U (–)	U_r (%)
ε_g (two-phase)	5.72×10^{-2} – 2.41×10^{-1}	8.82×10^{-3} – 7.13×10^{-2}	4.41×10^{-3} – 3.56×10^{-3}	1.48 –7.72
ε_g (three-phase)	4.45×10^{-2} – 2.24×10^{-1}	7.12×10^{-3} – 6.40×10^{-3}	3.56×10^{-3} – 3.20×10^{-3}	1.43– 7.99
u_{sg}	6.87×10^{-3} – 3.32×10^{-2}	9.39×10^{-5} – 1.18×10^{-3}	4.69×10^{-5} – 5.88×10^{-4}	6.84×10^{-1} –1.77

Table 2.6: Uncertainty analysis of the experimental data for the continuous mode.

Variables	Mean, $\bar{x}$ (–)	STDEV (–)	U (–)	U_r (%)

ε_g (two-phase)	9.98×10^{-2} – 3.11×10^{-1}	6.96×10^{-3} – 1.1×10^{-2}	3.48×10^{-3} – 5.48×10^{-3}	1.76 – 3.49
ε_g (three-phase)	7.84×10^{-2} – 2.67×10^{-1}	1.99×10^{-3}– 5.68×10^{-3}	9.94×10^{-4}– 2.84×10^{-3}	1.06 – 1.27
u_{sg}	6.94×10^{-3} – 3.48×10^{-2}	4.27×10^{-4} – 5.72×10^{-4}	2.13×10^{-4}– 2.86×10^{-4}	8.21×10^{-1} – 3.08
u_{slr}	7.12×10^{-3} – 3.52×10^{-2}	3.23×10^{-4} – 1.06×10^{-3}	1.61×10^{-4}– 5.28×10^{-4}	1.50 – 2.26

2.5. Results and discussion

2.5.1. Effect of different variables on gas holdup in the batch and continuous modes

2.5.1.1. Effect of superficial gas velocity and slurry concentration on gas holdup

The effect of slurry concentration $\left(d_p = 235.61\ \mu\text{m}\right)$ and superficial gas velocity on gas holdup in the presence of SDBS $\left(c_{surf} = 6\ \text{g/m}^3\right)$ in batch mode is shown in Figure 2.4. It is noticed that the gas holdup decreased with increasing slurry concentration, and it increased with the rising superficial gas velocity.

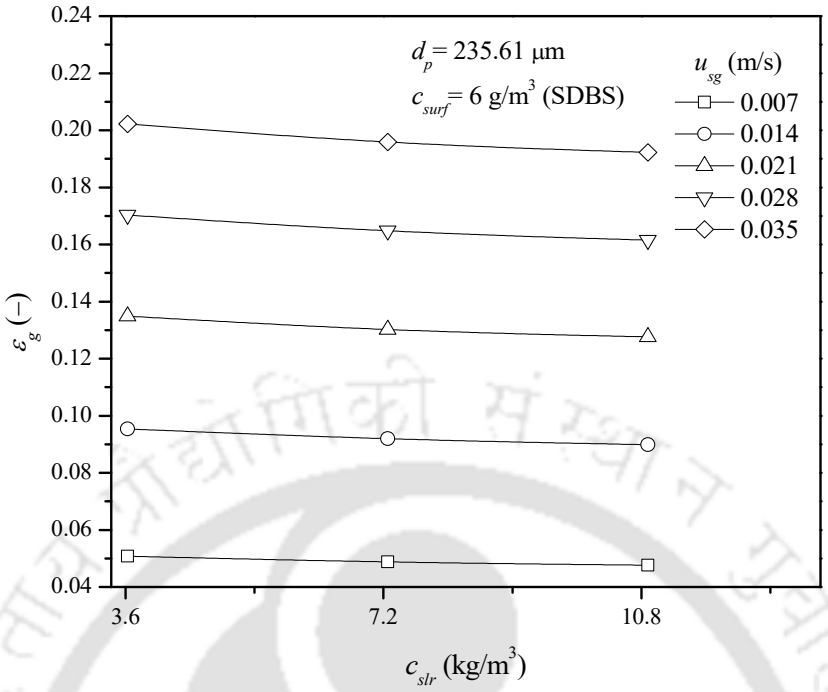

Figure 2.4: Effect of superficial gas velocity and slurry concentration on gas holdup in the batch mode.

The range of variation of the gas holdup was 4.7 to 20.2% at different slurry concentrations and superficial gas velocities. At the slurry concentration of 3.63 kg/m^3 and a minimum superficial gas velocity of 0.007 m/s, the gas holdup was 5.08%. At the maximum superficial gas velocity of 0.035 m/s, the gas holdup was 20.2%. With the increase in slurry concentration from 3.63 to 10.89 kg/m^3 (at 0.007 m/s superficial gas velocity), the reduction in gas holdup was 6.18%, and this reduction decreased with increasing superficial gas velocity. The decline in gas holdup was 6.18, 5.81, 5.41, 5.18, and 4.92% at the superficial gas velocity range of 0.007 to 0.035 m/s. It is clearly observed that at the lowest superficial gas velocity, the reduction in gas holdup was maximum, and this reduction decreased with the rise in superficial gas velocity.

The consequence of slurry concentration is more important at the lower gas velocity. The addition of particles increased the viscosity of the system. Therefore, it formed large bubbles, which had higher rising velocities. Larger bubbles have less residence time in the flotation column, and consequently, a low gas holdup is obtained (Fan et al., 2014). According to Banisi et al. (1995a), the bubble wake becomes stable due to the increased slurry viscosity, which successively increases the bubble rise velocity and reduces the gas holdup.

Effects of slurry concentrations (i.e., 1.5, 3.63, 7.26, and 10.89 kg/m^3) on gas holdup at different superficial gas velocities (i.e., 0.007 – 0.035 m/s) at fixed particle size (i.e., 235.61 μm), surfactant concentration (i.e., 30 g/m^3), and superficial slurry velocity (i.e., 0.035 m/s) in continuous mode are shown in Figure 2.5. It is perceived that the gas holdup of the system decreases with an increase in the slurry concentration while it increases with an increase in the superficial gas velocity. The increase in the gas holdup is due to the increase in the volume of the gas with an increase in the superficial gas velocity. As the volume of the gas increases, the number of gas bubbles also increases, consequently the gas holdup enhances. The decrease in the gas holdup with an increase in the slurry concentration is because of the increase in the apparent slurry viscosity and slurry density of the system (Ojima et al., 2015; Rabha et al., 2013a, 2013b; Sarhan et al., 2018a). The increase in the slurry viscosity of the system increases the rate of bubble coalescence (Prakash et al., 2019), which in turn forms the larger bubbles, hence affect the gas holdup of the system. The rising velocity of the larger gas bubbles is higher as compared to the smaller bubble size, as a result of this, the residence time of the larger bubbles becomes smaller. The smaller residence time of the bubbles in any system characterizes the lower gas holdup. A similar trend of a decrease in a gas holdup with an increase in the slurry concentration is also reported by many researchers (Banisi

et al., 1995b, 1995a; De Swart et al., 1996; Fan et al., 1999; Jianping and Shonglin, 1998; Kato et al., 1972; Kelkar et al., 1984; Koide et al., 1984; Lu et al., 1995; Ojima et al., 2015; Rabha et al., 2013a, 2013b; Reese et al., 1996; Sarhan et al., 2018a). Nevertheless, some contrary result of an increase in the gas holdup with an increase in the slurry concentration is also reported by(Fan et al., 2007; Jamialahmadi and Müller-Steinhagen, 1991). For instance, (Kara et al., 1982) reported an increase in the gas holdup in the presence of particles with their size less than 600 μm. Moreover, these contradictions of gas holdup results are because of different techniques for measurement of system holdup, and furthermore, the particle size, degree of wettability, and particle concentration are not considered equal. It is noticed that gas holdup increase from 0.25 to 5.04 % for a slurry concentration of 1.5 kg/m^3 and 0.1 to 4% for a slurry concentration of 10.89 kg/m^3 at 0.007 m/s and 0.035 m/s superficial gas velocities respectively. The decrease in the gas holdups from 60 to 20.63% when the slurry concentration increases from 1.5 to 10.89 kg/m^3 within a range of superficial gas velocity of 0.007 to 0.035 m/s. Therefore, from the current observation, it can be concluded that the effect of particle concentration is dominant at minimum superficial gas velocity.

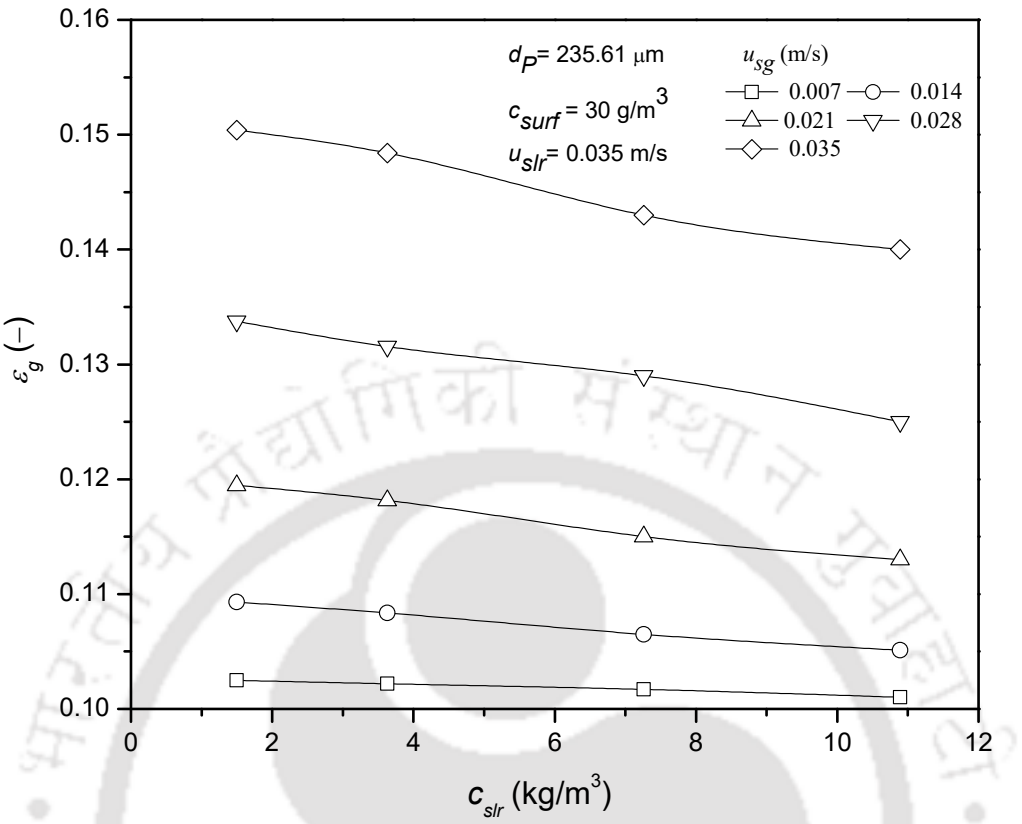

Figure 2.5. Effect of slurry concentration and superficial gas velocity on gas holdup in the continuous mode.

2.5.1.2. Effect of superficial slurry velocity on gas holdup

Variation of the gas holdup at different superficial slurry velocity at constant particle size (i.e., 235.61 μm), slurry concentration (i.e., 7.26 kg/m^3), and SDBS surfactant concentration (i.e., 30 g/m^3) in continuous mode is shown in Figure 2.6. It is noticed that the gas holdup of the flotation column reduces significantly with an increase in the superficial slurry velocity. This decrease in the gas holdup is due to the rise in the bubble coalescence rate, which generates the larger bubble size, consequently, reduces the bubble residence time in the flotation column. A contradictory result of an increase in the gas holdup with a rise in the liquid velocity is reported by many

researchers (Biń et al., 2001; Jin et al., 2010; Otake et al., 1981). Several investigators reported that gas holdup is independent of the effect of liquid velocity either in co-current or counter-current operation mode because of lower liquid velocity in comparison to bubble rise velocity (Akita and Yoshida, 1973; Rollbusch et al., 2015; Shah et al., 1982; Shawaqfeh, 2003; Voigt et al., 1980).

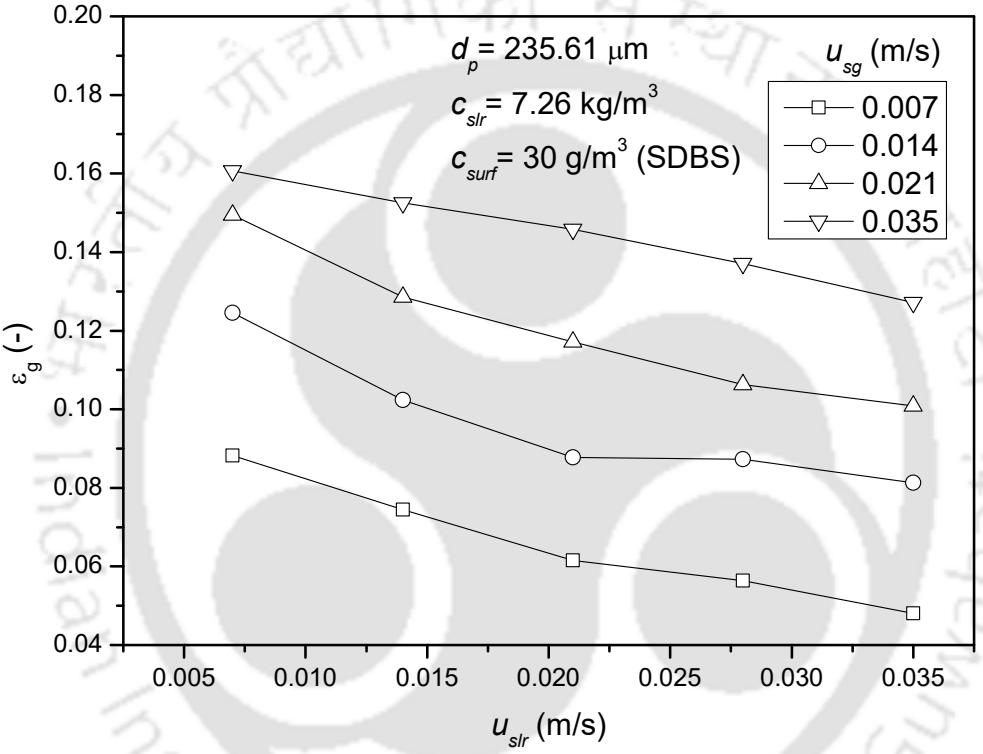

Figure 2.6: Effect of superficial slurry velocity on gas holdup in the continuous mode.

The decrease or increase in the gas holdup is because of acceleration or deceleration of the gas bubble by the liquid motion (Leonard et al., 2015; Rollbusch et al., 2015; Shawaqfeh, 2003). At a superficial slurry velocity (i.e., 0.007 m/s), the gas holdup is about 2.70%, whereas, at a superficial slurry velocity 0.035 m/s, the gas holdup is 0.21%, a significant reduction of approximately 92.26% is observed at minimum 0.007 m/s superficial gas velocity. The gas holdup reduces from

15.78 to 4.66% at the maximum superficial gas velocity at the same variation of superficial slurry velocity. Here, it can be concluded that the effect of slurry velocity on gas holdup at lower superficial is more effective as compared to the higher superficial gas velocity.

2.5.1.3. Effect of particle size on gas holdup

The effect of particle size on gas holdup at the slurry concentration of 7.26 kg/m^3 and surfactant (i.e., 1-Hexanol) concentration of 3 g/m^3 in batch mode is shown in Figure 2.7. It is seen that the gas holdup increased with increasing particle size. With the reduction in the bubble and particle size, the entrainment efficiency of the particle to the bubble improves (Bhunia et al., 2017; Khare and Joshi, 1990; Lee and Lee, 2002). With a further continuous reduction in the particle and bubble size, the probability of attachment of particles to the surface of the bubble reaches a critical value, after which it begins to decrease (Dobby and Finch, 1986; Yoon, 1993).

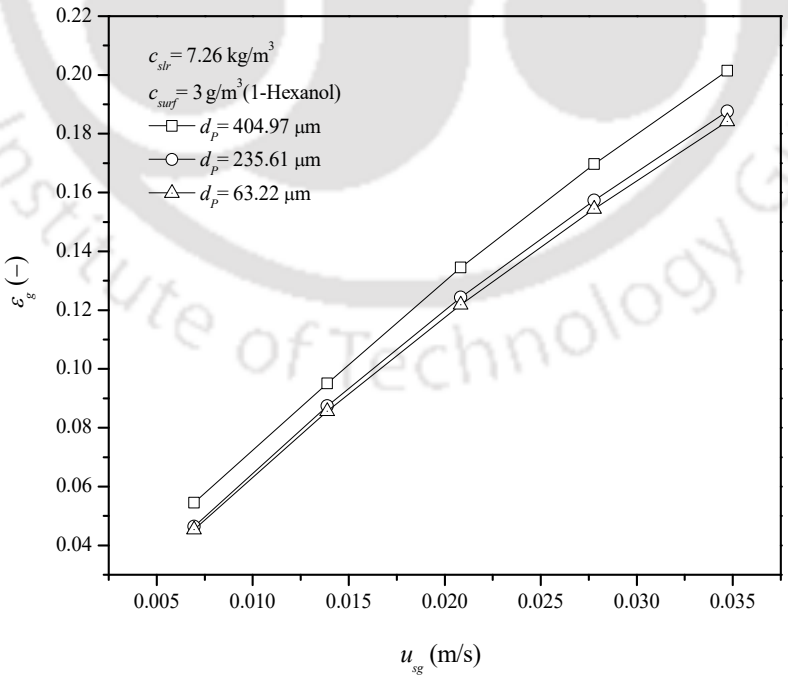

Figure 2.7: Effect of particle size on gas holdup in the batch mode.

At the fixed quantity of the particle, if the particle size is reduced, the net result is in the increase in the number of the particles. The increased particle number results in an increased slurry viscosity because of attractive particle interaction (Senapati et al., 2009; Zhou et al., 1993). In the presence of the smaller particles, the particles tend to pack together, which in turn enhances the particle-fluid and particle-particle interaction, hence the system viscosity increases. The increase in the system viscosity promotes the bubble coalesce and starts forming the larger gas bubbles (Prakash et al., 2019). The rule of the thumb says that the magnitude of the buoyancy force will be higher on the larger bubbles. Consequently, larger bubbles exhibit more significant rising velocity (Manjrekar and Dudukovic, 2015); hence the gas holdup reduces. The increased viscosity of the system also results in the dissimilarity in the increasing velocity of different size bubbles. The differences in the increasing velocity of the bubbles also responsible for bubble coalescence causes a reduction in gas holdup (Yoshida et al., 2013). A similar trend of higher gas holdup in the presence of larger particle size is also reported by (Prakash et al., 2018a). Some of the researchers reported a reduction in the bubble size by increasing the particle size (Ojima et al., 2015; Sarhan et al., 2016). The presence of the larger particle size may cause bubble breakup.

It can be observed that the gas holdups at the particle diameters of 63.22 and 235.61 μm were more or less the same. The difference between the gas holdups was less than 2.2% at all superficial gas velocities. For particle diameters 63.22 and 404.97 μm, the difference in gas holdup is in the range of 16.69-8.56% at superficial gas velocity range of 0.007-0.035 m/s, respectively. It is observed that for the particle diameters 63.22 and 404.97 μm, the difference between gas holdups decreased with increasing superficial gas velocity. This difference was maximum at the lowest gas velocity and minimum at the highest gas velocity. As particle size in the flotation column plays a critical

part in the investigation of hydrodynamic characteristics. The gas holdup in the flotation column is also affected by the different particle size in the slurry. The effect of different particle size (i.e., 63.22, 235.61, 404.97, and 507.67 μm) on gas holdup at a fixed slurry velocity (i.e., 0.021 m/s), slurry concentration (i.e.,7.26 kg/m^3), and 1-hexanol surfactant concentration (i.e., 10 g/m^3), in continuous mode is depicted in the Figure 2.8. It is noticed that the gas holdup of the flotation system gradually decreasing with an increase in the particle size. A similar kind of trend is also reported by (Kato et al., 1972), (Kara et al., 1982), and (Sada et al., 1986).

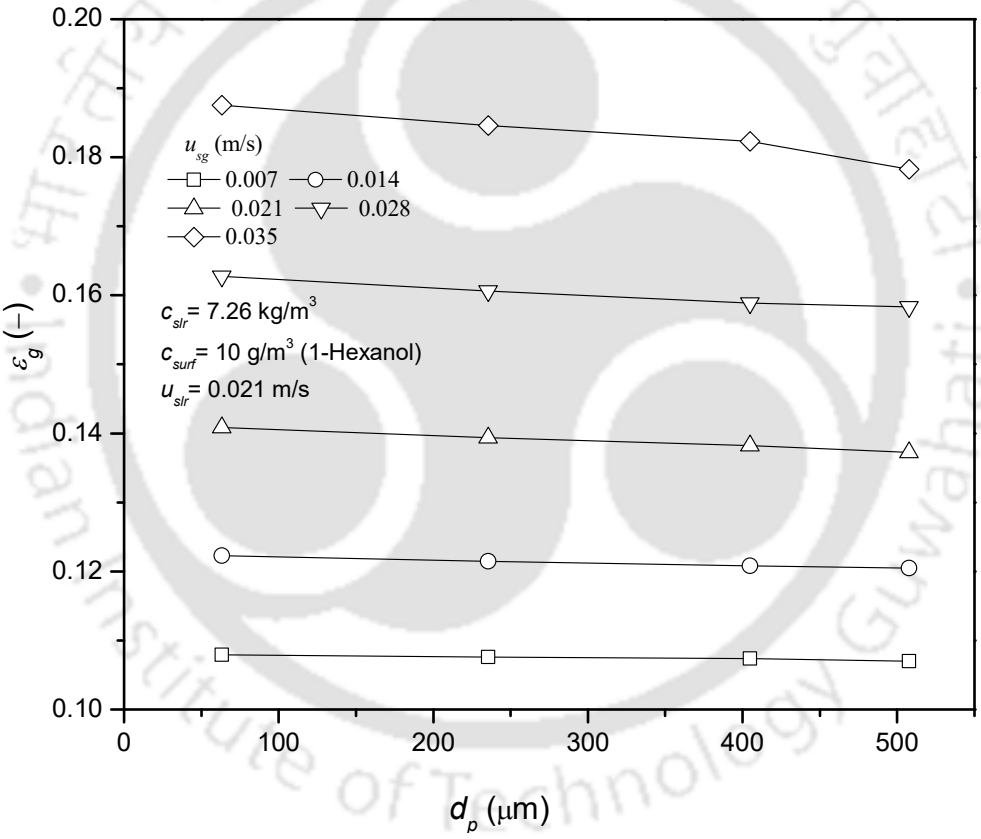

Figure 2.8: Effect of particle size on gas holdup in the continuous mode.

Some of the researchers reported that the apparent slurry viscosity is higher in presence smaller size particles because of significant particle interaction (Kara et al., 1982; Kawatra and Eisele, 1988; Sada et al., 1986; Senapati et al., 2009; Zhou et al., 1993). However, particle interaction may

depend on the type of particle. By considering the particle interaction effect, the gas holdup should be lower at the smaller particle size; however, in this present experimental result, contradictory results have been found. It is noticed that the decrease in the gas holdups were approximately 7.08 to 6.01% when particle size varied from 63.22 to 404.97 μm. It is found that the reduction in a gas holdup is more at lower superficial gas velocity, and this reduction in gas holdup decreases with an increase in the superficial gas velocity. It can be concluded that the influence of particle size is more dominant in lower superficial gas velocity.

2.5.1.4. Effects of different surfactants on gas holdup

In this work, three different surfactants, i.e., CTAB (cationic), SDBS (anionic), and 1-Hexanol (non-ionic) were used to study the gas holdup in the presence of solid at particular surfactant, particle size, and slurry concentrations.

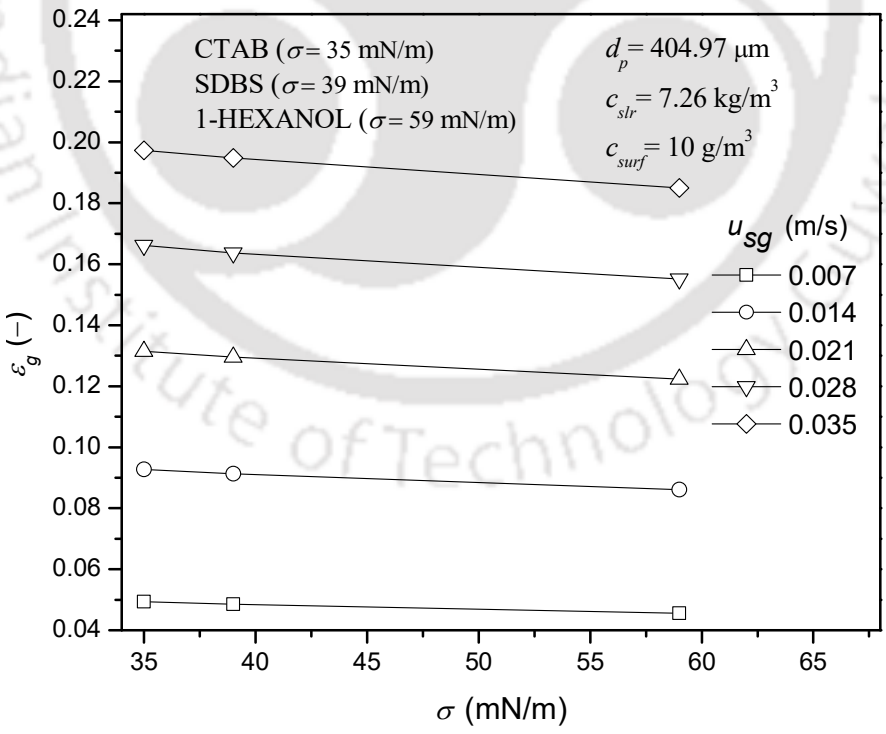

Figure 2.9: Effect of different surfactants on gas holdup in the batch mode.

It is reported that the gas holdup of the system increases as the bubble size decreases (Dobby et al., 1988). The effect of surfactant type on gas holdup in batch mode is shown in Figure 2.9. It is noted that the gas holdup was higher in the presence of the cationic (CTAB) surfactant than the anionic (i.e., SDBS) and non-ionic surfactants (i.e., 1-Hexanol). The maximum and minimum gas holdups were 19.7% (for CTAB) and 4.5% (for 1-Hexanol) at $u_{sg} = 0.035$ m/s and $u_{sg} = 0.007$ m/s respectively. At each superficial gas velocity, the difference in gas holdup between the CTAB and SDBS solutions was less than 1.71%, and the same between the SDBS and 1-Hexanol solutions was less than 6.07%. A comparison of the gas holdups in the CTAB and 1-Hexanol solutions shows that the minimum difference was 6.27% at $u_{sg} = 0.035$ m/s and the maximum was 7.68% at $u_{sg} = 0.007$ m/s. In all surfactant solutions, it was noticed that the variation was maximum at minimum superficial gas velocity and vice versa. (Parmar and Majumder, 2016)have suggested the importance of a bubble charge on the attachment of particle on it during flotation. Bubbles can have a positive or negative charge based on the type of surfactant adsorbed on their surfaces. They can attract oppositely-charged particles and entrain them. The charge of a particle can be adjusted by using suitable collectors and by controlling the pH. The addition of a surfactant diminishes the surface tension of the liquid, which in turn generates a large number of bubbles (Parmar and Majumder, 2016; Prakash et al., 2019, 2018a). The surfactant also increases the stability of the gas bubbles, which increases the gas holdup. It also hinders th.32e coalescence of bubbles, increases the coalescence time, and helps to produce smaller bubbles (Duerr-Auster et al., 2009; Ghosh, 2004; Yang and Maa, 1984).

The effect of three different surfactants, namely, CTAB, SDBS, and 1-Hexanol on gas holdup at a fixed slurry concentration (7.26 kg/m^3) and particle size (404.97 μm) at a different superficial gas

velocity in continuous mode is revealed in the Figure 2.10. The comparison of the gas holdup in different surfactants is performed at a constant surfactant dose and superficial liquid velocity of 50 g/m^3 and 0.007 m/s, respectively. It can be noticed that the gas holdup in the presence of CTAB and SDBS surfactant is more or less the same. This is due to the very little solution surface tension difference after the addition of both the surfactant. The difference in the gas holdup is less than 1% for each superficial gas velocity in the presence of the CTAB and SDBS surfactant.

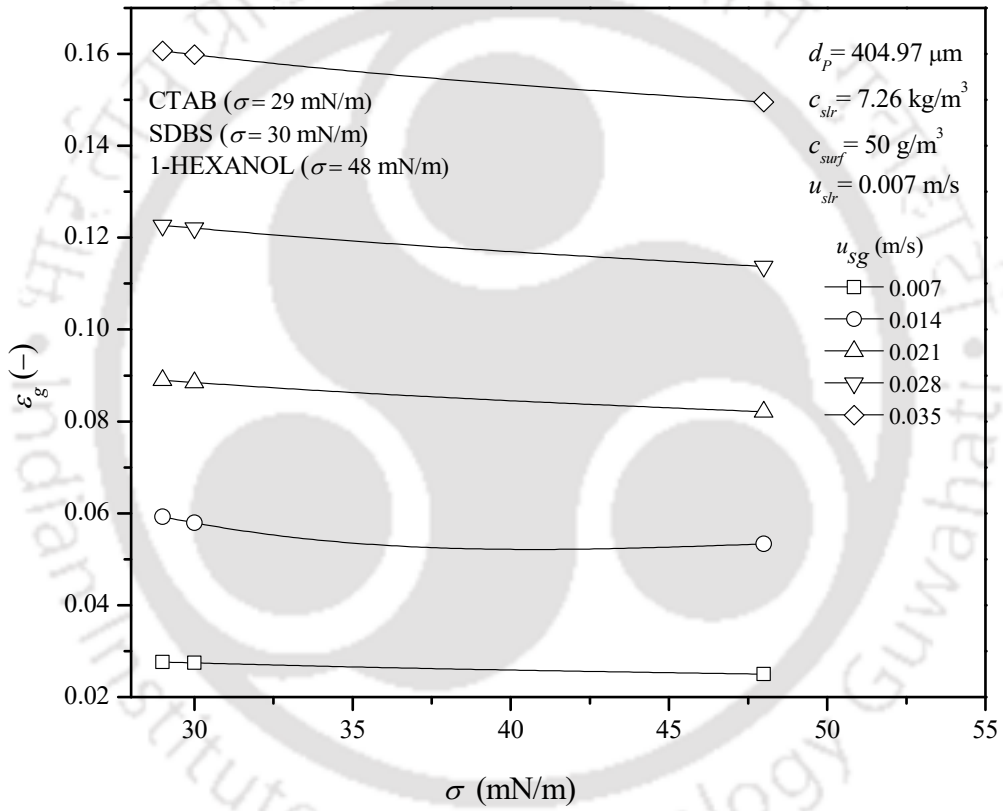

Figure 2.10: Effect of the type of surfactant on gas holdup in the continuous mode.

The solution surface tensions in CTAB and SDBS are 29 mN/m and 30 mN/m. As it was discussed in the earlier section that reduced surface tension of the liquid leads to produce the smaller bubble, which in turn enhances the gas holdup of the system. Therefore, it is noted that the solution surface tension in the presence of 1-Hexanol is about 48 mN/m, which is higher than both of other

surfactants (CTAB and SDBS); therefore, the gas holdup reduces sharply. The reduction in gas holdup (in the presence of 1-Hexanol) is approximately in the range of 6.94 – 9.55%.

2.5.1.5. Effect of solid loading on gas holdup

The effect of solid on gas holdup in the presence of CTAB (at 10 g/m^3) in batch mode is shown in Figure 2.11. It is noticed that the gas holdup was higher in the absence of the particles as compared to their presence. The bubble coalescence induced by the presence of solid particles produces larger bubbles with faster rising velocity. Hence, the gas holdup decreases.

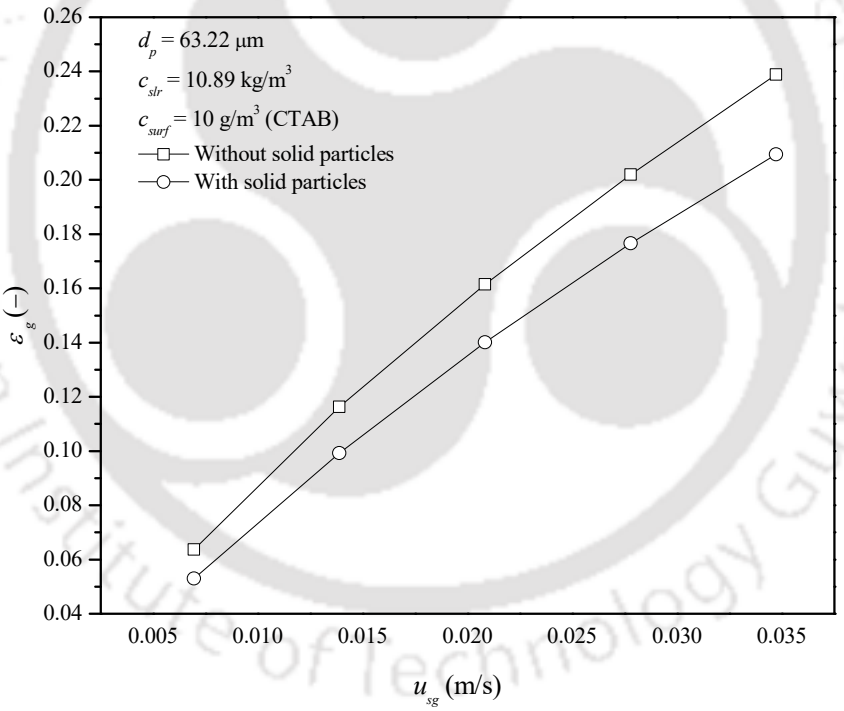

Figure 2.11: Effect of solid loading on gas holdup in the batch mode.

The addition of a surfactant stabilizes the bubbles and reduces the rate of bubble breakup. The addition of solid particles increases the viscosity of the system, which causes an increase in the coalescence behavior of the bubbles; therefore, the gas holdup reduces. Solid-induced-bubble

coalescence behavior is reduced in the presence of the surfactant (Banisi et al., 1995a). The minimum gas holdup was found to be 5.2% in the presence of particles, whereas the maximum was 23.8% in the absence of particles at 0.007 and 0.035 m/s gas velocities, respectively. The gas holdup of the system decreased from 6.36 to 5.29% when the solid concentration was increased from 0 to 10.89 kg/m^3 at 0.007 m/s superficial gas velocity. The gas holdup of the system decreased from 23.89 to 20.89% for the same solid concentration range at 0.035 m/s superficial gas velocity. Therefore, it can be concluded that the effect of the solid particles was strong at the minimum gas velocity, and this effect dwindled with increasing gas velocity.

It is observed that gas holdup is higher in the two-phase system as compared to the three-phase system at all superficial gas velocity. In Figure 2.12, it is noticed that the gas holdup of the flotation system decreases with an increase in the slurry concentration, the same argument of a decrease in the gas holdup in the presence of particles can be applied here to explain the reason of lower gas holdups in the three-phase system in comparison to the two-phase system. The difference in the gas holdup between two-phase and three-phase is higher at maximum superficial gas velocity, and this difference gradually decreases with a decrease in the superficial gas velocity. The gas holdup is approximately 33.83, 29.83, 27.37, 25.57, and 24.14% higher in the two-phase system as compared to the three-phase system at 0.007, 0.014, 0.021, 0.028, and 0.035 m/s superficial gas velocity respectively.

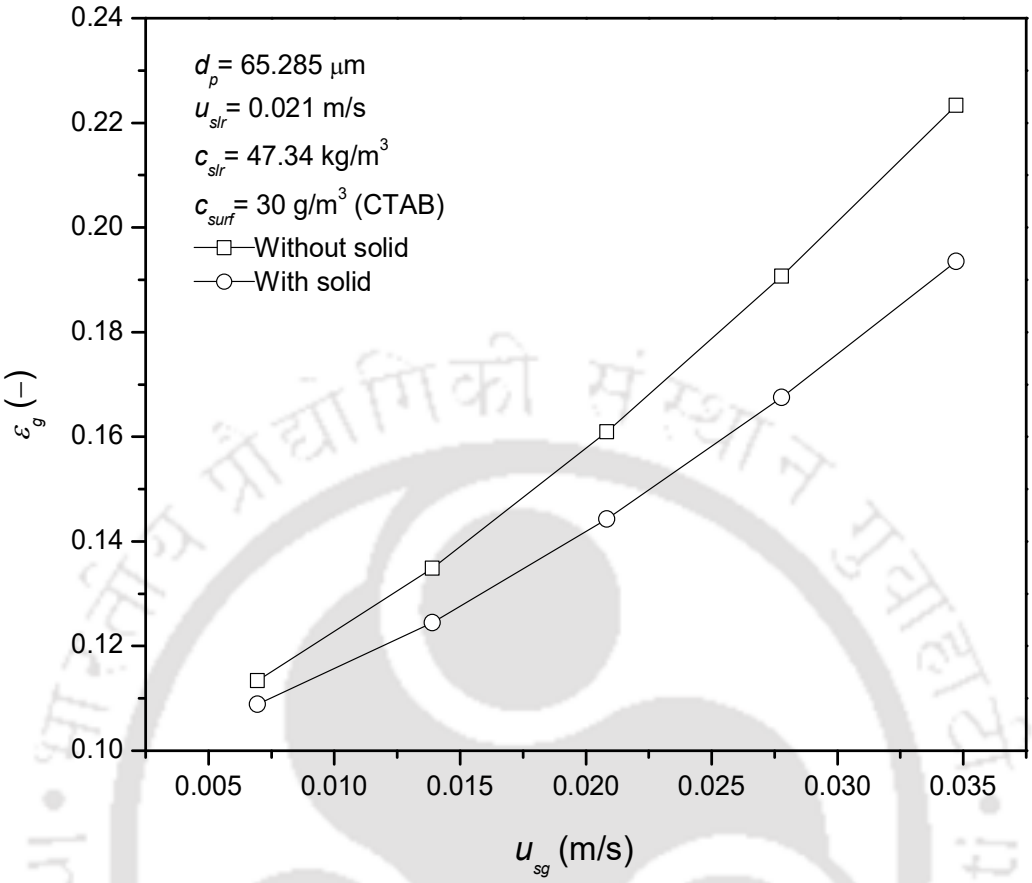

Figure 2.12: Effect of solid loading on gas holdup in the continuous mode.

2.5.2. Evaluation of gas holdup with the drift-flux model in the batch mode

The gas holdup was analyzed for the two-phase system by the drift flux model with the operating variables, i.e., superficial gas velocity u_{sg}, column diameter d_c, surface tension σ, liquid density ρ_l, and liquid viscosity μ_l, the acceleration due to gravity g. In the present experimental conditions, the range of the distribution parameter C_o is found to be 2.27– 2.89 for the two-phase system. For the two-phase system, applying the Buckingham's Pi theorem of dimensional analysis

and performing regression analysis, the distribution parameter can be predicted by the following correlation,

$$C_o = 2.78\,\mathrm{Re}_l^{0.046}\ \mathrm{Fr}_l^{0.041}\ \mathrm{We}_l^{-0.064} \tag{2.11}$$

Where is Re_l Reynolds number $\rho_l u_{sg} d_c / \mu_l$, Fr_l is Froude number $u_{sg} / \sqrt{g d_c}$, We_l is the Weber number $\rho_l u_{sg}^2 d_c / \sigma$. The standard error and correlation coefficient of the Eq. (2.11) were found to be 0.0061 and 0.9062, respectively. The correlation is valid within the range of variables : $310.10 \le \mathrm{Re}_l \le 1780.06 ; 9.46\times10^{-3} \le \mathrm{Fr}_l \le 47.29\times10^{-3} ; 4.35\times10^{-2} \le \mathrm{We}_l \le 1.89$. An empirical correlation for drift velocity for the two-phase system was developed based on the present experimental data. This correlation is as follows:

$$\frac{u_d}{u_{sg}} = 1.21\,\mathrm{Re}_l^{-0.011}\,\mathrm{Fr}_l^{-0.534}\,\mathrm{We}_l^{-0.228} \tag{2.12}$$

The standard error and the correlation coefficient for Eq. (2.12) were found to be 0.0027 and 0.9999, respectively. The correlation is valid within the range of variables : $299.19 \le \mathrm{Re}_l \le 1785.07 ;\ 9.46\times10^{-3} \le \mathrm{Fr}_l \le 47.29\times10^{-3} ; 4.35\times10^{-2} \le \mathrm{We}_l \le 1.89$.

The gas holdup is assessed by the drift-flux model for a three-phase system, with the variables such as superficial gas velocity u_{sg} , column diameter d_c , slurry density ρ_{slr} , particle diameter d_p , surface tension σ , apparent slurry viscosity μ_{slr} , the acceleration due to gravity g . For a three-phase system, C_o is found to be 2.28–2.93 for the three-phase system, and the distribution parameter C_o , and u_d can be represented as the function of the dimensionless groups as

$$C_o, u_d = f\left(u_{sg}, d_c, d_p, \sigma, \rho_{slr}, \mu_{slr}, g\right) \tag{2.13}$$

An empirical correlation for C_0 the three-phase system was developed based on the present experimental data. This correlation is as follows:

$$C_o = 36\,\mathrm{Re}_{slr}^{-0.273}\,\mathrm{Fr}_{slr}^{0.236}\,\mathrm{We}_{slr}^{0.018}\left(\frac{d_p}{d_c}\right)^{0.029} \tag{2.14}$$

Where Re_{slr} is Reynolds number $\rho_{slr} u_{sg} d_c / \mu_{slr}$, Fr_{slr} is Froude number $u_{sg} / \sqrt{g d_c}$, We_{slr} is the Weber number $\rho_{slr} u_{sg}^2 d_c / \sigma$. The standard error and the correlation coefficient while using Equation (2.14) were found to be 0.0094 and 0.9362, respectively. The correlation is valid within the range of variables: $303.50 \le \mathrm{Re}_{slr} \le 1764.32$; $9.46\times10^{-3} \le \mathrm{Fr}_{slr} \le 47.29\times10^{-3}$; $4.35\times10^{-2} \le \mathrm{We}_{slr} \le 1.90$; $1.19\times10^{-3} \le d_p/d_c \le 9.23\times10^{-3}$. The correlation for weighted mean drift velocity u_d can be represented as

$$\frac{u_d}{u_{sg}} = 1.638\,\mathrm{Re}_{slr}^{-0.286}\,\mathrm{Fr}_{slr}^{-0.681}\,\mathrm{We}_{slr}^{-0.016}\left(\frac{d_p}{d_c}\right)^{0.129} \tag{2.15}$$

The standard error and the correlation coefficient while using Equation (2.15) were found to be 0.0639 and 0.9939, respectively. The correlation is valid within the range of variables: $295.16 \le \mathrm{Re}_{slr} \le 1769.29$; $9.45\times10^{-3} \le \mathrm{Fr}_{slr} \le 47.29\times10^{-3}$; $5.53\times10^{-2} \le \mathrm{We}_{slr} \le 1.90$; $1.15\times10^{-3} \le d_p/d_c \le 7.36\times10^{-3}$. The parity of distribution parameter and mean drift velocity for the three-phase system in batch mode is shown in Figures 2.13 and 2.14, respectively.

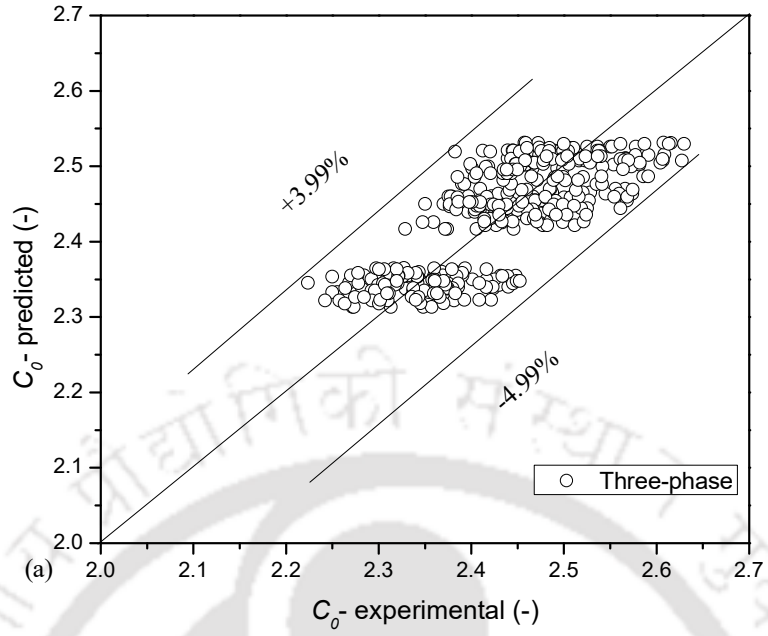

Figure 2.13: Parity of distribution parameter for the three-phase system in the batch mode.

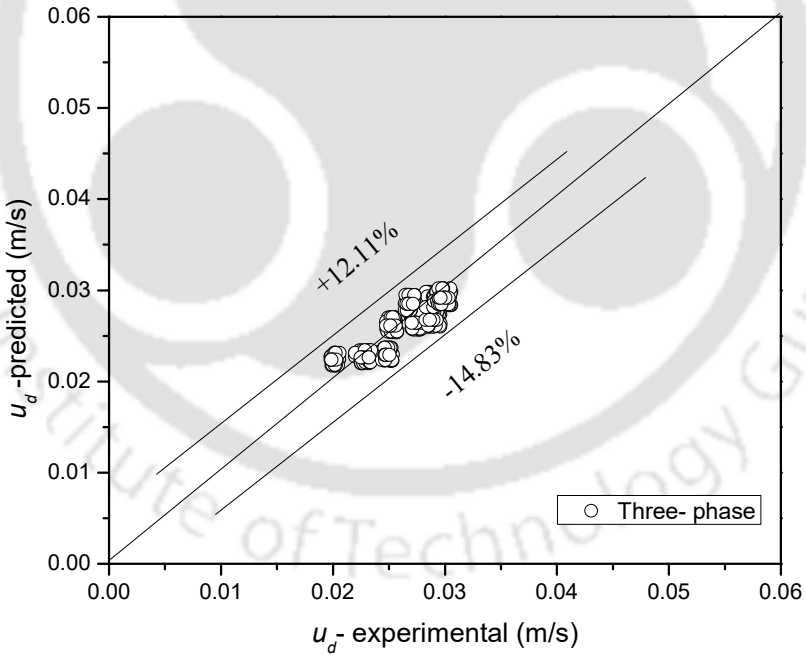

Figure 2.14: Parity of drift velocity for the three-phase system in the batch mode.

2.5.3. Evaluation of gas holdup with the drift-flux model in the continuous mode

The gas holdup is assessed by the drift-flux model for a two-phase system based on the operating variables such as superficial gas velocity u_{sg}, superficial liquid velocity u_{sl}, column diameter d_c, liquid density ρ_l, surface tension σ, liquid viscosity μ_l, the acceleration due to gravity g. The distribution parameter C_o and the weighted mean drift velocity u_d can be expressed as the function of the following variables

$$C_o, u_d = f\left(u_{sg}, u_{sl}, d_c, \sigma, \rho_l, \mu_l, g\right) \tag{2.16}$$

The distribution parameter C_0 can be predicted by the following correlation by dimensional and multiple regression analysis.

$$C_o = 1.71\,\mathrm{Re}_l^{0.009}\,\mathrm{Fr}_l^{0.136}\,\mathrm{We}_l^{-0.082}\left(\frac{u_{sl}}{u_{sg}}\right)^{-0.022} \tag{2.17}$$

The standard error and correlation coefficient of Eq. (2.17) are 0.0096 and 0.9315, respectively. The correlation is valid within the range of variables: $8.67\times10^{2} \le \mathrm{Re}_l \le 37.86\times10^{2}$, $2.84\times10^{-2} \le \mathrm{Fr}_l \le 11.35\times10^{-2}$, $40.47\times10^{-2} \le \mathrm{We}_l \le 13.18$, $14.29\times10^{-2} \le u_{sl}/u_{sg} \le 71.43\times10^{-2}$.

The weighted mean drift velocity parameter u_d can be predicted by the following correlation by the same procedure.

$$\frac{u_d}{u_{sg}} = 8.63\times10^{-1}\,\mathrm{Re}_l^{-0.009}\,\mathrm{Fr}_l^{-0.484}\,\mathrm{We}_l^{-0.253}\left(\frac{u_{sl}}{u_{sg}}\right)^{0.005} \tag{2.18}$$

The standard error and correlation coefficient of the Eq. (2.18) were found to be 0.0029 and 0.9999,

respectively. The correlation is valid within the range of variables: $7.70\times10^{2} \le \mathrm{Re}_{l} \le 36.88\times10^{2}$, $2.837\times10^{-2} \le \mathrm{Fr}_{l} \le 11.35\times10^{-2}$, $40.64\times10^{-2} \le \mathrm{We}_{l} \le 13.26$, $14.286\times10^{-2} \le u_{sl}/u_{sg} \le 71.43\times10^{-2}$.

The gas holdup is assessed by the drift-flux model for a three-phase system, with the variables such as superficial gas velocity u_{sg}, superficial liquid velocity u_{slr}, column diameter d_c, slurry density ρ_{slr}, particle diameter d_p, surface tension σ, apparent slurry viscosity μ_{slr}, the acceleration due to gravity g. For a three-phase system, the distribution parameter C_o . and weighted mean drift velocity parameter u_d is expressed as a function of the following variables

$$C_o, u_d = f\left(u_{sg}, u_{sl}, d_c, d_p, \sigma, \rho_{slr}, \mu_{slr}, g\right) \tag{2.19}$$

After applying the Buckingham's Pi theorem of dimensional analysis, the distribution parameter can be represented as the function of the succeeding dimensionless groups, which can be expressed as

$$C_o = 3.62\,\mathrm{Re}_{slr}^{-0.119}\,\mathrm{Fr}_{slr}^{0.088}\mathrm{We}_{slr}^{0.014}\left(\frac{d_p}{d_c}\right)^{0.009}\left(\frac{u_{sl}}{u_{sg}}\right)^{-0.003} \tag{2.20}$$

The standard error and correlation coefficient of Eq. (2.20) are found to be and 0.0039 and 0.9362, respectively. The correlation is valid within the range of variables: $7.54\times10^{2} \le \mathrm{Re}_{slr} \le 36.20\times10^{2}$, $2.84\times10^{-2} \le \mathrm{Fr}_{slr} \le 11.35\times10^{-2}$, $40.71\times10^{-2} \le \mathrm{We}_{slr} \le 13.41$, $1.19\times10^{-3} \le d_p/d_c \le 9.23\times10^{-3}$, $14.29\times10^{-2} \le u_{sl}/u_{sg} \le 71.43\times10^{-2}$.

Similarly, an empirical correlation for drift velocity for the three-phase system can be expressed as

$$\frac{u_d}{u_{sg}} = 12.94\ \mathrm{Re}_{slr}^{-0.268}\mathrm{Fr}_{slr}^{-0.33}\mathrm{We}_{slr}^{-0.201}\left(\frac{d_p}{d_c}\right)^{0.019}\left(\frac{u_{sl}}{u_{sg}}\right)^{0.0013} \tag{2.21}$$

The standard error and correlation coefficient of the Eq. (2.21) are 0.0243 and 0.9982, respectively. The correlation is valid within the range of variables: $6.69\times10^{2} \le \mathrm{Re}_{slr} \le 35.26\times10^{2}$, $2.83\times10^{-2} \le \mathrm{Fr}_{slr} \le 11.35\times10^{-2}$, $40.86\times10^{-2} \le \mathrm{We}_{slr} \le 13.48$, $1.15\times10^{-3} \le d_p/d_c \le 7.36\times10^{-3}$, $14.29\times10^{-2} \le u_{sl}/u_{sg} \le 71.43\times10^{-2}$.

2.5.4. Evaluation of gas holdup with the slip velocity model in the continuous mode

The gas holdup is analyzed by a slip velocity model for a two-phase system with operating variables superficial gas velocity u_{sg}, superficial liquid velocity u_{sl}, column diameter d_c, surface tension σ, liquid density ρ_l, liquid viscosity μ_l, and the acceleration due to gravity g. The parameter u_b, n can be expressed as the function of the following variables

$$u_b, n = f\left(u_{sg}, u_{sl}, d_c, \sigma, \rho_l, \mu_l, g\right) \tag{2.22}$$

An empirical correlation for the parameter u_b for the two-phase system can be expressed as

$$\frac{u_b}{u_{sg}} = 28.80\ \mathrm{Re}_{l}^{-0.011}\mathrm{Fr}_{l}^{0.144}\mathrm{We}_{l}^{-0.236}\left(\frac{u_{sl}}{u_{sg}}\right)^{0.643} \tag{2.23}$$

The standard error and correlation coefficient of the Eq. (2.23) were found to be 0.046 and 0.9905, respectively. The correlation is valid within the range of variables:

$7.70\times10^{2} \le \mathrm{Re}_l \le 36.88\times10^{2}, 2.84\times10^{-2} \le \mathrm{Fr}_l \le 11.35\times10^{-2}, 40.63\times10^{-2} \le \mathrm{We}_l \le 13.26,$

$14.29\times10^{-2} \le u_{sl}/u_{sg} \le 71.43\times10^{-2}.$

An empirical correlation for the parameter n for the two-phase system can be expressed as

$$n = 2.88\times10^{2}\ \mathrm{Re}_l^{0.046}\mathrm{Fr}_l^{1.75}\mathrm{We}_l^{-0.377}\left(\frac{u_{sl}}{u_{sg}}\right)^{1.045} \tag{2.24}$$

The standard error and correlation coefficient of the Eq. (2.24) were found to be 0.0049 and 0.9998, respectively. The correlation is valid within the range of variables:

$1.28\times10^{3} \le \mathrm{Re}_l \le 3.69\times10^{3}, 4.73\times10^{-2} \le \mathrm{Fr}_l \le 11.35\times10^{-2}, 1.71 \le \mathrm{We}_l \le 13.26,$

$0.30 \le u_{sl}/u_{sg} \le 0.71.$

The Gas holdup is analyzed by a slip velocity model for a three-phase system, also with operating variables such as superficial gas velocity u_{sg}, superficial liquid velocity u_{slr}, column diameter d_c, slurry density ρ_{slr}, particle diameter d_p, apparent slurry viscosity μ_{slr}, surface tension σ, acceleration due to gravity g. The parameter u_b, n can be expressed as the function of the following variables

$$u_b, n = f\left(u_{sg}, u_{slr}, d_c, d_p, \sigma, \rho_{slr}, \mu_{slr}, g\right) \tag{2.25}$$

An empirical correlation for the parameter u_b for the three-phase system can be expressed as

$$\frac{u_b}{u_{sg}} = 53.10 \mathrm{Re}_{slr}^{0.25} \mathrm{Fr}_{slr}^{-0.232} \mathrm{We}_{slr}^{-0.186} \left(\frac{d_p}{d_c}\right)^{0.018} \left(\frac{u_{sl}}{u_{sg}}\right)^{0.632} \quad (2.26)$$

The standard error and correlation coefficient of the Eq. (2.26) were found to be 0.0529 and 0.9871, respectively. The correlation is valid within the range of variables: $6.69\times10^{2} \le \mathrm{Re}_{slr} \le 35.26\times10^{2}$, $2.84\times10^{-2} \le \mathrm{Fr}_{slr} \le 11.35\times10^{-2}$, $40.86\times10^{-2} \le \mathrm{We}_{slr} \le 13.48$, $11.49\times10^{-4} \le d_p/d_c \le 73.63\times10^{-4}$, $14.29\times10^{-2} \le u_{sl}/u_{sg} \le 71.43\times10^{-2}$.

An empirical correlation for the parameter *n* for the three-phase system can be expressed as

$$n = 9.04\times10^{4}\, \mathrm{Re}_{slr}^{-0.438}\, \mathrm{Fr}_{slr}^{2.29} \mathrm{We}_{slr}^{-0.367} \left(\frac{d_p}{d_c}\right)^{0.022} \left(\frac{u_{sl}}{u_{sg}}\right)^{1.15} \quad (2.27)$$

The standard error and correlation coefficient of the Eq. (2.27) were found to be 0.0826 and 0.9939, respectively. The correlation is valid within the range of variables: $6.69\times10^{2} \le \mathrm{Re}_{slr} \le 35.26\times10^{2}$, $2.84\times10^{-2} \le \mathrm{Fr}_{slr} \le 11.35\times10^{-2}$, $40.86\times10^{-2} \le \mathrm{We}_{l} \le 13.48$, $11.49\times10^{-4} \le d_p/d_c \le 73.63\times10^{-4}$, $14.29\times10^{-2} \le u_{sl}/u_{sg} \le 71.43\times10^{-2}$.

2.5.5. Development of empirical correlations for gas holdup in the two- and three-phase systems for the batch mode operation

The gas holdup of the fluidized bed system for the two-phase system depends on several operating variables as per the present experimental conditions, which can be expressed as

$$\varepsilon_g = f\left(u_{sg},\, d_c,\, \sigma,\, \rho_l,\, \mu_l,\, g\right) \quad (2.28)$$

Dimensional analysis followed by multiple linear regression of experimental data yields the following correlation for the two-phase system:

$$\varepsilon_g = 0.636\,\mathrm{Re}_l^{0.007}\,\mathrm{Fr}_l^{0.379}\,\mathrm{We}_l^{0.222} \tag{2.29}$$

The standard error and correlation coefficient were 0.0141 and 0.9996, respectively. The correlation is valid within the range of variables: $310.10 \le \mathrm{Re}_l \le 1780.06$; $9.46\times10^{-3} \le \mathrm{Fr}_l \le 47.29\times10^{-3}$; $4.35\times10^{-2} \le \mathrm{We}_l \le 1.89$. A comparison of the experimental gas holdup and the values predicted by Equation (2.29) is shown in Figure 2.15.

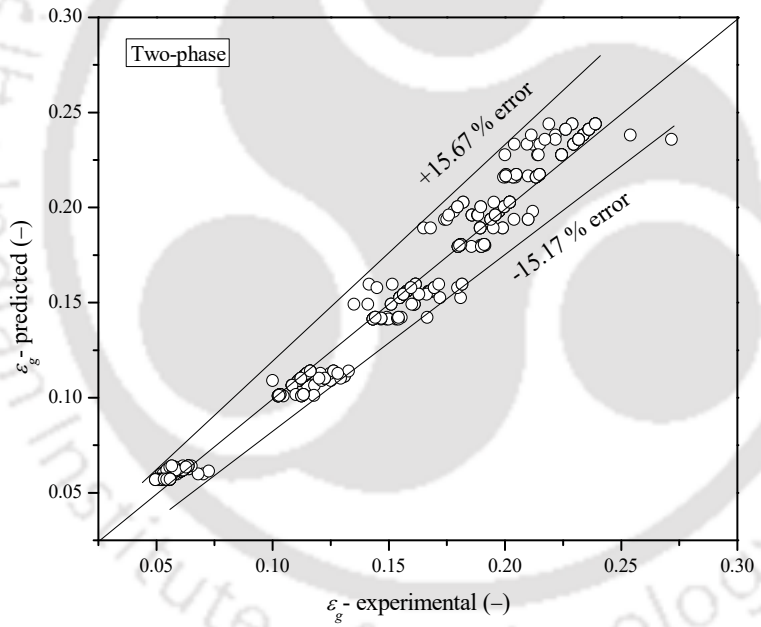

Figure 2.15: Comparison of experimental and predicted gas holdup of the two-phase system in the batch mode.

The gas holdup of the fluidized bed system for the three-phase system depends on several operating variables as per the present experimental conditions, which can be expressed as

$$\varepsilon_g = f\left(u_{sg},\, d_c,\, d_p,\, \sigma,\, \rho_{slr},\, \mu_{slr},\, g\right) \tag{2.30}$$

The correlation for predicting the gas holdup for the three-phase system is given by

$$\varepsilon_g = 1.74\times10^{-4}\,\mathrm{Re}_{slr}^{0.933}\;\mathrm{Fr}_{slr}^{-0.315}\;\mathrm{We}_{slr}^{0.12}\left(\frac{d_p}{d_c}\right)^{-0.047} \tag{2.31}$$

The standard error and the correlation coefficient were found to be 0.0208 and 0.9990, respectively. The correlation is valid within the range of variables: $303.50 \le \mathrm{Re}_{slr} \le 1764.32$; $9.46\times10^{-3} \le \mathrm{Fr}_{slr} \le 47.29\times10^{-3}$; $4.35\times10^{-2} \le \mathrm{We}_{slr} \le 1.90$; $1.19\times10^{-3} \le d_p/d_c \le 9.22\times10^{-3}$. The parity plot of the experimental and predicted gas holdups is shown in Figure 2.16.

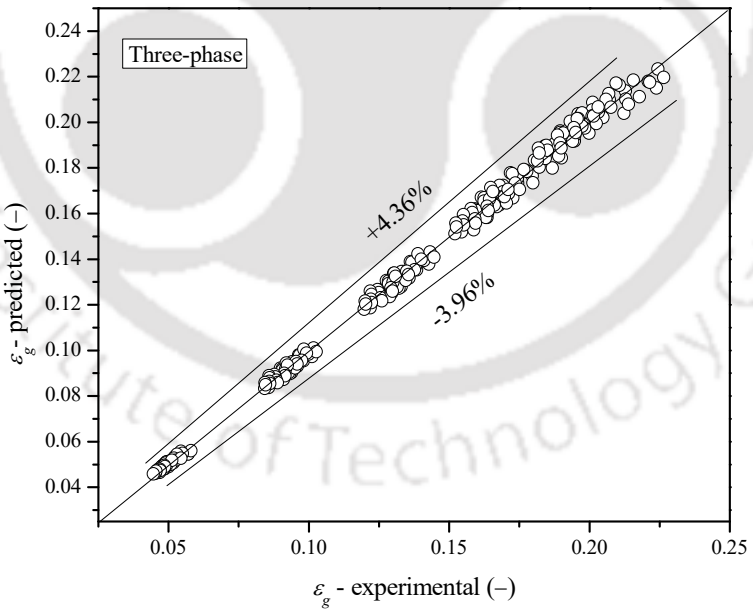

Figure 2.16: Comparison of experimental and predicted gas holdup of the three-phase system in the batch mode.

2.5.6. Development of the general empirical correlation for gas holdup in the continuous mode operation

The gas holdup for a two-phase system is observed to be depended on superficial gas velocity u_{sg}, superficial liquid velocity u_{sl}, column diameter d_c, liquid density ρ_l, liquid viscosity μ_l, surface tension σ, and acceleration due to gravity g which can be expressed as

$$\varepsilon_g = f\left(u_{sg}, \mathrm{u}_{sl}, d_c, \sigma, \rho_l, \mu_l, g\right) \tag{2.32}$$

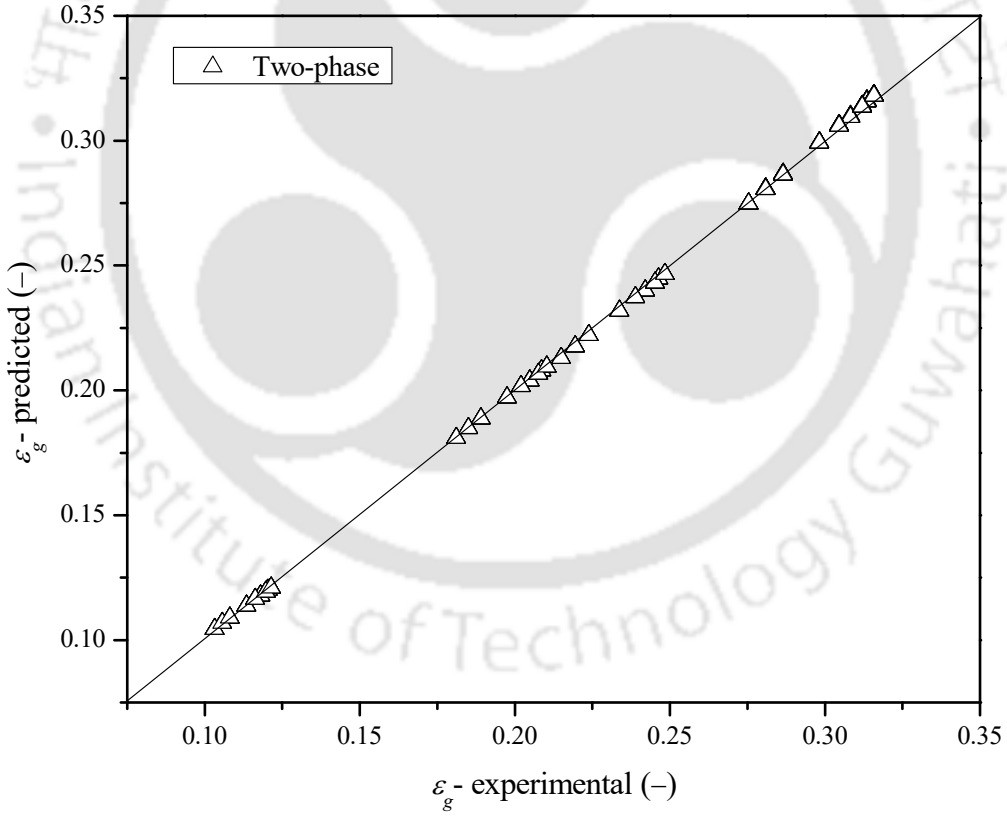

Figure. 2.17: Comparison of experimental and predicted gas holdup of the two-phase system in the continuous mode.

The following correlation for predicting the gas holdup is developed by multiple linear regression analysis with the experimental data

$$\varepsilon_g = 3.03\times10^{-1}\,\mathrm{Re}_l^{0.012}\,\mathrm{Fr}_l^{0.469}\mathrm{We}_l^{0.207}\left(\frac{u_{sl}}{u_{sg}}\right)^{-0.499} \tag{2.33}$$

The standard error and correlation coefficient of Eq. (2.33) are 0.0057 and 0.9999, respectively. The correlation is valid within the range of variables: $1.45\times10^3 \le \mathrm{Re}_l \le 3.79\times10^3$, $4.73\times10^{-2} \le \mathrm{Fr}_l \le 11.35\times10^{-2}$, $1.12 \le \mathrm{We}_l \le 13.18$, $0.2 \le u_{sl}/u_{sg} \le 0.6$. Parity plot of experimental gas holdup and predicted gas holdup obtained for a two-phase system by using Eq. (2.33) is shown in Figure 2.17.

The gas holdup of the three-phase system can also be expressed as

$$\varepsilon_g = f\left(u_{sg}, u_{sl}, d_c, d_p, \sigma, \rho_{slr}, \mu_{slr}, g\right) \tag{2.34}$$

The following correlation is developed for the three-phase system by applying multiple linear regression analyses with experimental data with the correlation coefficient and standard error of 0.9993 and 0.0121, respectively.

$$\varepsilon_g = 3.08\times10^{-3}\,\mathrm{Re}_{slr}^{0.521}\,\mathrm{Fr}_{slr}^{0.184}\mathrm{We}_{slr}^{0.116}\left(\frac{d_p}{d_c}\right)^{-0.015}\left(\frac{u_{sl}}{u_{sg}}\right)^{-0.523} \tag{2.35}$$

The correlation is valid within the range of variables: $1.26\times10^3 \le \mathrm{Re}_{slr} \le 3.62\times10^3$, $4.73\times10^{-2} \le \mathrm{Fr}_{slr} \le 11.35\times10^{-2}$, $1.13 \le \mathrm{We}_{slr} \le 13.41$, $11.87\times10^{-4} \le d_p/d_c \le 92.30\times10^{-4}$, $0.2 \le u_{sl}/u_{sg} \le 0.6$.

Parity plot of experimental gas holdup and predicted gas holdup obtained by using Eq. (2.35) is shown in Figure 2.18.

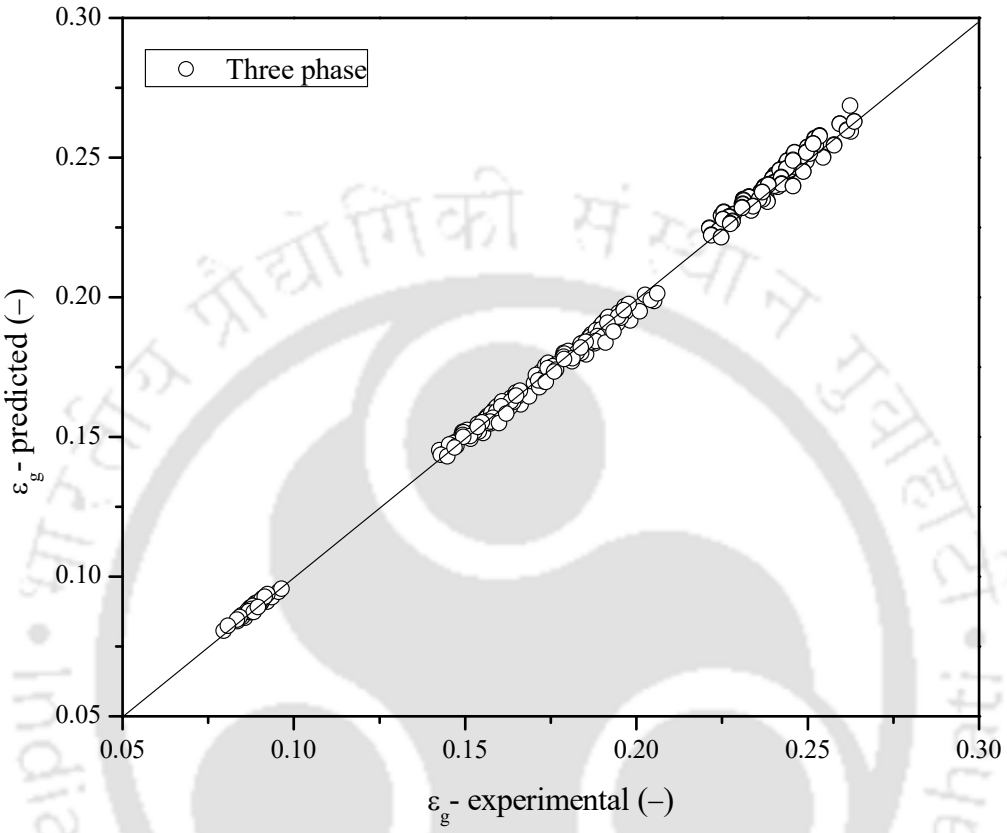

Figure. 2.18: Comparison of experimental gas holdup and predicted gas holdup for three phase system in the continuous mode.

2.6. Conclusions

The gas holdup in a laboratory flotation column in the two and three-phase system is studied. The in-depth investigation of the influence of superficial gas velocity, superficial liquid velocity, particle concentration, particle size, surfactant concentration, surfactant type on the gas holdup is done. The gas holdup of the system was reduced due to the solid loading, and this reduction was more pronounced at the higher slurry concentrations. The addition of particles decreased the gas

holdup at all gas flow rates and slurry concentrations. Solids decreased the gas holdup at all superficial gas velocities as a result of increased bubble coalescence, which increased the bubble size, and hence the bubble rise velocity through the slurry. The gas holdup of the system was higher in the presence of CTAB as compared to SDBS and 1-Hexanol. Particle size did not have a significant effect on gas holdup. Nonetheless, a slight increase in gas holdup was observed in the presence of larger particles. It is concluded that the gas holdup of the system increased profoundly with an increase in superficial gas velocity, whereas it decreases by the rise in the slurry concentration. The effects of four different particle sizes (63.22, 235.61, 404.97, and 507.67 μm) on gas holdup are also analyzed. It is noticed that the gas holdup of the flotation system is gradually decreasing with an increase in particle size due to a reduction in the apparent slurry viscosity. The reason for the decrease in the apparent slurry viscosity was the decrease in the particle interaction. It is also seen that gas holdup reduces significantly with an increase in the superficial slurry velocity. This decrease in the gas holdup is due to a rise in the bubble coalescence rate, which generates the larger bubble size, consequently, reduces the bubble residence time in the flotation column. The comparison of the gas holdup in different surfactant is also performed. It was noticed that the gas holdup was lower in the presence of 1-Hexanol; however, in the case of CTAB and SDBS surfactant solution, it was more or less the same. The gas holdup of the flotation system is analyzed with the drift-flux and slip velocity model. The generalized correlation model is also proposed to interpret the gas holdup in the two and three-phase systems. All developed correlations are suited to interpret the experimental values well within the error range of ± 20%. The present analysis will be helpful to enhance the process efficiency and scale-up the flotation systems in industrial applications.

CHAPTER 3 : PRESSURE DROP CHARACTERISTICS

This chapter reports the effect of operating variables such as particle size, slurry concentration, superficial gas velocity, superficial slurry velocity, surfactant concentration, and surfactant type on the frictional pressure drop in a flotation column in batch mode and continuous mode. Dimensionless correlations have been developed to predict the frictional pressure drop in the laboratory flotation column in different conditions.

3.1. Introduction and literature

Flotation processes are widely used as physical separation processes in mineral processing (Chakraborty et al., 2009; Xing et al., 2018), oil-water separation in the petroleum industry (Li et al., 2016), wastewater treatment (Gharai and Venugopal, 2016; Khuntia et al., 2012), coal particle up-gradation (Li et al., 2016; Xing et al., 2017), de-inking of paper pulp (Labidi et al., 2007), and plastic recycling (Wang et al., 2015b). The flotation process is most suitable due to its high separation efficiency and cost-effectiveness (Tao, 2004). Flotation column reports better efficiency in comparison to a mechanical flotation cell, mainly with fine particles (Honaker and Mohanty, 1996). The performance of the flotation column is dependent on hydrodynamic characteristics.

Frictional pressure drop plays an important role in the determination of column performance. Pressure drop is one of the essential hydrodynamic characteristics for analyzing the efficiency of the flotation system. The knowledge of hydrodynamic characteristics helps to assess the proper design, operation, scale-up, and modeling of the flotation system (Prakash et al., 2018b).

Pressure drop analysis in any multiphase contacting system provides the pattern of energy dissipation (Majumder, 2016). The necessity of flow energy requirement is decided by the pressure drop in the flotation system. It is necessary to understand the different factors, which cause the frictional pressure drop. Changes in the flow direction, friction in the column, turbulence caused by the mixing of phases, surface roughness, viscosity, and fluid velocity are some of the prime factors, which are responsible for pressure drop in the flotation system (Prakash et al., 2018b). In the past, many authors attempted to investigate the frictional pressure drop. As per (Prakash et al., 2018a), the frictional pressure drop in a three-phase system is a sum of three individual frictional forces namely (i) friction between fluid and particle, (ii) particle and column wall, and (iii) fluid and wall. They concluded that fluid-wall frictional forces are dominant in comparison to fluid-particle and particle-column wall.

The pressure drop decides the necessity of flow energy requirement in the flotation system. In a vertical column with a uniform cross-section, the measured pressure drop is known as the *total pressure drop*. It is the summation of hydrostatic, accelerative, and frictional pressure drops. Among the three different pressure drops, measurement of the frictional pressure drop is complicated, due to its dependence on flow regime, column orientation, and wall roughness. Many researchers have attempted to predict the frictional pressure drop in the Newtonian and non-Newtonian systems in vertical and horizontal two-phase flows (Lee and Lee, 2002; Majumder et al., 2011; Pouplin et al., 2011; Xu et al., 2012). However, these researchers have focused on the frictional pressure drop, mainly in the two-phase systems. A few studies on frictional pressure drop in three-phase systems have been reported by (Bhunia et al., 2014) and (Shukla et al., 2010). Bhunia et al. (2014) reported the effects of slurry concentration, solid type, superficial gas and liquid velocities, and gas holdup in the presence of coal and sphalerite slurry mixture on axial

pressure drop. They reported a decrease in axial pressure drop with increasing superficial gas velocity due to the increase in the gas holdup of the system.

Experimental results also showed that the slurry system containing sphalerite particles (specific gravity: 3.16) had a higher pressure drop than the coal particles (specific gravity: 1.6). The frictional pressure drop in the flotation system can be contributed by the frictions between fluid and wall, particle and wall, and fluid and particle. The frictional forces at the column wall and gas-liquid interface contribute to the pressure drop. In a flotation system, the presence of a large number of smaller bubbles causes significant frictional losses. Hence friction at the wall can be neglected (Bhole and Joshi, 2008). A reduction in frictional pressure drop was observed with increasing superficial gas velocity, whereas the frictional pressure increased with increasing slurry velocity. The decrease in frictional pressure drop with increasing gas velocity was due to the increase in the coalescence of bubbles, which resulted in larger bubbles. An increase in the slurry velocity resulted in intense mixing of the phases, which enhanced the particle mobility. Fine particles caused more frictional pressure drop than the coarse particles due to their higher mobility. Another reason for the high frictional pressure drop associated with the fine particles is their greater tendency to form clusters and adhere to the wall.

The frictional pressure loss occurring at the gas–liquid interface in a packed bed of bubbles is smaller due to the partial mobility of the interface. (Shukla et al., 2010) investigated the effects of various process variables such as gas and liquid velocity, surfactant concentration, and slurry concentration on frictional pressure drop. They have reported a negligible change in the frictional pressure drop for their experimental conditions. Some of the researchers also reported the impact of bubbles and void fraction on the pressure drop reduction in the upward flow (Nouri et al., 2013).

Despite the broad applications of the flotation systems, there is a lack of studies on frictional pressure drop in flotation columns. There is a lack of availability of reliable technique for accurately assessing the frictional pressure drop in the flotation systems. Most of the literature reported the evaluation of frictional pressure drop in the two-phase flow in a co-current flow arrangement. Only a few researchers have reported the assessment of frictional pressure drop in a flotation system for a limited range of experimental conditions. A few of literature shows the in-depth investigation of various operating parameters (i.e., superficial slurry and gas velocity), physical properties of slurry (i.e., surface tension, apparent slurry viscosity), and type of surfactant (i.e., cationic, anionic, non-ionic) on the frictional pressure drop. Therefore, the present study aims to analyze the effects of superficial gas velocity, superficial slurry velocity, particle size slurry concentration, surfactant concentration, and type of surfactant on the average gas holdup and frictional pressure drop in the flotation column. There is a lack of availability of frictional pressure drop correlations for the counter-current three-phase system. Therefore, a generalized empirical correlation is also proposed for the prediction of the frictional pressure drop as a function of surface tension, particle size, slurry concentration, geometric variables, effective slurry viscosity, and superficial gas velocity in the flotation column.

3.2. Experimentation

3.2.1. Experimental setup

The diagrammatic representation of the experimental setup for frictional pressure drop is shown in Figure 2.1, section 2.2.1, in chapter 2, and the details and information about the different parts of the set up are also already discussed there in section 2.2.1.

3.2.2. Materials and experimental procedure

3.2.2.1. Materials

The details and specification of the surfactants and the information about the coal particle crushing and size analyzing are already discussed in section 2.2.2 in chapter 2. A typical particle size distribution is shown in Figure 2.2. The surface tension and conductivity of the water used for the experiment were 0.070 N/m and 156.70 μS/m, respectively.

3.2.2.2. Experimental procedure

All the experimental works were conducted at standard temperature and pressure. The particle concentration range was $1.5 \leq c_{slr} \leq 10.89$ kg/m^3, the superficial gas velocity range was $0.007 \leq u_{sg} \leq 0.035$ m/s, and the superficial slurry velocity range was $0.007 \leq u_{slr} \leq 0.035$ m/s. The details and information about the measurement of density, surface tension, and viscosity measurement were already discussed in section 2.2.2. The physical properties of the fluids used in the experiments and the surface tensions of the surfactant solutions for batch and continuous mode are shown in section 2.2.2, Tables 2.1, Table 2.2, Table 2.3, and Table 2.4, respectively. The pressure taps were kept at 0.05 and 0.55 m from the base of the column within the homogeneous regime. For every set of experiments, the initial liquid level was kept at 0.58 m.

3.3. Theoretical background

3.3.1. Frictional pressure drop

In a vertical multiphase system, the total pressure drop (ΔP_T) is the sum of the hydrostatic pressure drop (ΔP_h), pressure drop due to friction (ΔP_f), and pressure drop due to acceleration (ΔP_a). The total pressure drop is given by

$$\Delta P_T = \Delta P_f + \Delta P_h + \Delta P_a \tag{3.1}$$

According to (Hughmark and Pressburg, 1961), the pressure drop due to acceleration in a vertical system of uniform cross-sectional is very small as compared to the total pressure drop. Therefore, it can be neglected and the Equation (3.1) reduces to

$$\Delta P_T \approx \Delta P_h + \Delta P_f \tag{3.2}$$

The hydrostatic pressure drop can be expressed as

$$\Delta P_h = \rho_m g \Delta H \tag{3.3}$$

where the three-phase mixture density (ρ_m) can be calculated from the following equation:

$$\rho_m = \varepsilon_g \rho_g + \varepsilon_l \rho_l + \varepsilon_s \rho_s \tag{3.4}$$

After putting Equation (3.4) into Equation (3.3), the pressure drop due to hydrostatic pressure can be expressed as

$$\Delta P_h = \left(\varepsilon_g \rho_g + \varepsilon_l \rho_l + \varepsilon_s \rho_s\right) g \Delta H \tag{3.5}$$

Where, ε_g, ε_l, and ε_s are the holdups of the gas, liquid, and solid, and ρ_g, ρ_l, and ρ_s are their respective densities. ΔH is the distance between the two successive pressure ports. Putting

Equation (3.5) into Equation (3.2) and after rearrangement, the pressure drop due to the friction can be expressed as

$$\Delta P_f = \Delta P_T - \left(\varepsilon_g \rho_g + \varepsilon_l \rho_l + \varepsilon_s \rho_s\right) g \Delta H \tag{3.6}$$

For a single-phase system, the Fanning's friction factor is related to the frictional pressure drop as

$$\Delta P_{f,sp} = \frac{2 f_{sp} \rho_{sp} u_{sg}^2 \Delta H}{\varepsilon_g^2 d_c} \tag{3.7}$$

Similarly, the frictional pressure drop for the three-phase system can be represented as

$$\Delta P_{f,tp} = \frac{2 f_{tp} \rho_{tp} u_{sg}^2 \Delta H}{\varepsilon_g^2 d_c} \tag{3.8}$$

The friction factor in the countercurrent laminar flow condition can be expressed by (Majumder, 2016)

$$f_{tp} = \frac{16}{\mathrm{Re}_r}, \quad \text{for} \quad \mathrm{Re}_r \le 2100 \tag{3.9}$$

The friction factor for the transition region could be represented as (Desouky and E1-Emam, 1981)

$$f_{tp} = 0.125\left(0.0112 + \mathrm{Re}_r^{-0.3185}\right) \text{ valid for } 2100 \le \mathrm{Re}_r \le 4000 \tag{3.10}$$

For turbulent flow condition friction factor for the three-phase system is given by Blasius equation

$$f_{tp} = \frac{0.079}{\mathrm{Re}_r^{0.25}} \quad \text{for} \quad \mathrm{Re}_r \ge 4000 \tag{3.11}$$

Where Re_r is the gas Reynolds number based on the relative velocity of gas and slurry, which can be expressed as

$$\mathrm{Re}_r = \frac{\rho_m u_r d_c}{\varepsilon_g \mu_m} \tag{3.12}$$

where $u_r = \left(u_{sg}/\varepsilon_g\right) + \left(u_{sl}/\left(1-\varepsilon_g\right)\right)$ and μ_m is the mixture viscosity, which is given as (Majumder, 2016)

$$\mu_m = \frac{\mu_g \mu_{slr}}{\mu_g + X^{1.4}\left(\mu_{slr} - \mu_g\right)} \tag{3.13}$$

where X is the Martinelli parameter and μ_{slr} is the slurry apparent viscosity. Which can be expressed as (Majumder, 2019)

$$X = \left[\left(\Delta P_f/\Delta z\right)_{slr} \Big/ \left(\Delta P_f/\Delta z\right)_g\right]^{0.5} \tag{3.14}$$

$$\mu_{slr} = \mu_l\left(1 + 2.5\phi_s + 10.5\phi_s^2 + 0.00273e^{(16.6\phi_s)}\right) \tag{3.15}$$

where ϕ_s is the particle volume fraction in the slurry.

3.4. Uncertainty analysis

The theory regarding the uncertainty analysis is already discussed in section 2.4.

Table 3.1: Uncertainty analysis of the experimental data for the batch mode.

Parameter	Mean, $\overline{x}$ (–)	STDEV (–)	U (–)	U_r (%)
ΔP_f (two-phase)	3.47–21.70	0.17–0.56	8.29×10^{-3}–0.28	1.29–2.39
ΔP_f (three-phase)	3.96–28.50	0.20–0.30	9.83×10^{-3}–0.15	0.35–3.79
u_{sg}	6.87×10^{-3} – 3.32×10^{-2}	9.39×10^{-5} – 1.18×10^{-3}	4.69×10^{-5} – 5.88×10^{-4}	0.68–1.77

Table 3.2: Uncertainty analysis of the experimental data for the continuous mode.

Variables	Mean, $\overline{x}$ (–)	STDEV (–)	U (–)	U_r (%)
ΔP_f (two-phase)	16.43 – 110.30	9.13×10^{-2}– 1.01×10^{-1}	4.56×10^{-2}– 5.04×10^{-2}	4.57×10^{-2} – 2.78×10^{-1}
ΔP_f (three-phase)	22.77 – 168.51	9.06×10^{-2}– 1.13×10^{-1}	4.53×10^{-2}– 5.66×10^{-2}	2.69×10^{-2} – 2.49×10^{-1}
u_{sg}	6.94×10^{-3}– 3.48×10^{-2}	4.27×10^{-4}– 5.72×10^{-4}	2.13×10^{-4}– 2.86×10^{-4}	8.21×10^{-1}– 3.08
u_{sl}	7.12×10^{-3} -3.52×10^{-2}	3.23×10^{-4}– 1.06×10^{-3}	1.61×10^{-4}– 5.28×10^{-4}	1.50–2.26

3.5. Results and discussions

3.5.1. Effect of different variables on frictional pressure drop in the batch and continuous modes

3.5.1.1. Effect of superficial gas velocity and slurry concentration on frictional pressure drop

The variation of frictional pressure drop with the change in slurry concentration and superficial gas velocity at constant particle diameter $\left(\text{i.e., } d_p = 235.61\ \mu\text{m}\right)$ and SDBS concentration (i.e., 6 g/m^3) in batch mode is shown in Figure 3.1.

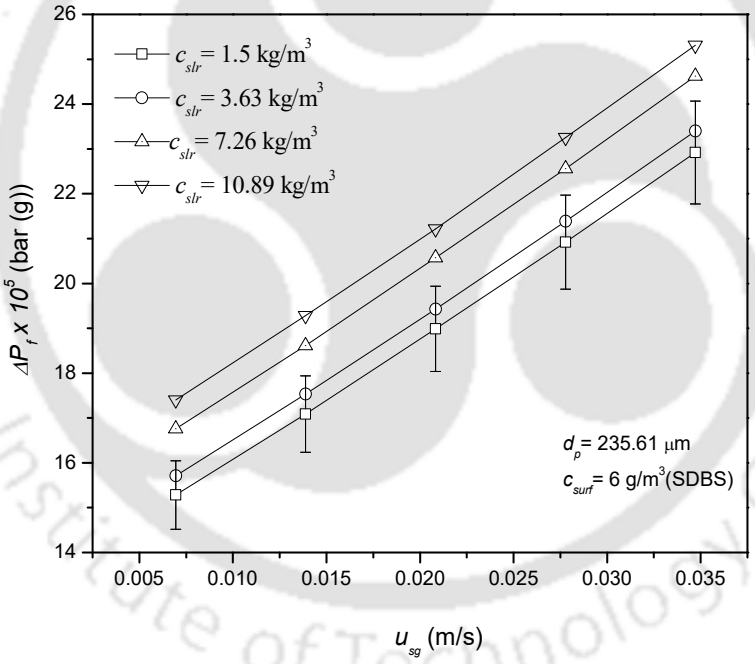

Figure 3.1: Effect of superficial gas velocity and slurry concentration on frictional pressure drop in the batch mode.

It was noticed that the frictional pressure drop increased with increasing superficial gas velocity and slurry concentration. The increase in the frictional pressure drop with superficial gas velocity

may be due to the rise in the number of gas bubbles, which increased the gas holdup in the flotation column and hence increased the actual liquid velocity. The increase in the slurry concentration increased the effective viscosity of the system, which led to an increase in the frictional pressure drop of the system. The minimum and maximum frictional pressure drops were 15.28 Pa $\left(\text{for } c_{slr} = 1.5 \text{ kg/m}^3\right)$ and 25.32 Pa $\left(\text{for } c_{slr} = 10.89 \text{ kg/m}^3\right)$ at the superficial gas velocities of 0.007 and 0.035 m/s, respectively. The frictional pressure drop increased with solid loading. The frictional pressure drop increased from 22.92 to 25.32 Pa (i.e., 10.47% increment) when the solid content increased from 1.5 to 10.89 kg/m^3 at the maximum superficial gas velocity of 0.035 m/s. The frictional pressure drop changed from 15.28 to 17.40 Pa (i.e., 13.87% increment) for the change in the solid content in the same range at the minimum superficial gas velocity of 0.007 m/s. The frictional pressure drop increments were about 49.99, 48.92, 46.92, and 45.49% when the superficial gas velocity was increased from 0.007 to 0.035 m/s at the fixed slurry concentrations of 1.5, 3.63, 7.26, and 10.89 kg/m^3, respectively. A comparison between the frictional pressure drops at 3.63, and 7.26 kg/m^3 slurry concentrations show that the minimum difference was 5.26% at 0.035 m/s, and the maximum difference was 6.69% at 0.007 m/s.

Similarly comparing at 7.26 and 10.89 kg/m^3, it was 2.80 and 3.80% at the same superficial gas velocity. It was observed that the difference in frictional pressure drop was highest at the minimum superficial gas velocity, and this difference decreased with increasing superficial gas velocity. The highest and lowest increase in the frictional pressure drop was about 13.87% and 10.47% at the minimum and maximum superficial gas velocities (i.e., 0.007 and 0.035 m/s) when the particle concentration was increased from 1.5 to 10.89 kg/m^3. Therefore, it can be concluded that the effect of slurry concentration was more predominant at the minimum superficial gas velocity.

Effect of range of superficial gas velocity (0.007 – 0.035 m/s) and range slurry concentration (1.5 – 10.89 kg/m^3) on the frictional pressure in the presence of fixed particle size (235.61 μm), slurry velocity (0.021 m/s), and surfactant concentration (SDBS, 30 g/m^3) in the continuous mode are shown in the Fig. 3.2.

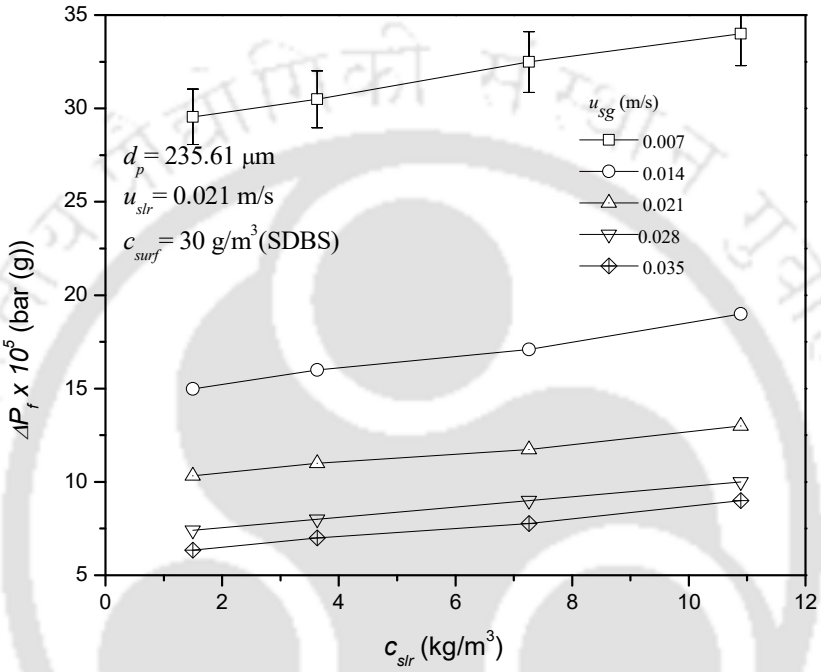

Figure 3.2: Effect of superficial gas velocity and slurry concentration on frictional pressure drop in the continuous mode.

It is perceived that the frictional pressure drop is decreasing with an increase in the superficial gas velocity. However, it is increasing with an increase in slurry concentration. In a counter-current flow arrangement, downflow slurry exerted a higher drag on the rising bubbles leads to produce a circulation of bubble-slurry aggregate in the wall region. The circulation of the bubble-slurry mixture generates turbulence and increases the total pressure drop of the system. The formation of a large number of bubbles increases the turbulence in the column, which leads to an increase the

total pressure drop in the column. On the other hand, the increase in the superficial gas velocity causes a reduction in the mixture density. Consequently, hydrostatic pressure decreases. Finally, the frictional pressure drop is increased. It was also noticed that the frictional pressure drop is more in the presence of higher slurry concentration as related to the lower slurry concentration. The reason for more frictional pressure drop in the presence of higher slurry concentration is an increase in the apparent slurry viscosity. As the slurry apparent viscosity increase, the friction between the fluid and the wall increase, hence the frictional pressure drop.

The viscosity of the flowing fluid is an important factor behind the intensification of the frictional pressure drop (Ganat and Hrairi, 2018). In general, the frictional pressure drop is caused by a change in the potential and kinetic energy of the fluid because of friction between the flowing fluid and the column wall (Besarati et al., 2015; Ganat and Hrairi, 2018). A similar trend of reduction in frictional pressure drop is also reported by (Pal et al., 1980). In the bubbly flow regime, some other researchers also reported that the reduction in the frictional pressure drop with an increase in the superficial gas velocity (Duangprasert et al., 2008; Ghajar and Bhagwat, 2013). The reduction in the frictional pressure drop is approximately 78.56% $\left(c_{slr} = 1.5 \text{ kg/m}^3\right)$, 77.05% $\left(c_{slr} = 3.63 \text{ kg/m}^3\right)$, 76.09%$\left(c_{slr} = 7.26 \text{ kg/m}^3\right)$, and 73.53% $\left(c_{slr} = 3.63 \text{ kg/m}^3\right)$ when the superficial gas velocity is varied from 0.007 to 0.035 m/s. Similarly, the increase in the frictional pressure drop is approximately 15.05, 26.82, 25.89, 34.94, and 42.04% when the slurry concentration varied from the 1.5 to 10.89 kg/m^3 at the 0.007, 0.014, 0.021, 0.028, and 0.035 m/s superficial gas velocity, respectively. From the present experimental finding, it can be concluded that the superficial gas velocity more dominantly affects the frictional pressure drop as compared to the slurry concentration.

3.5.1.3. Effect of superficial slurry velocity on frictional pressure drop

Effect of superficial slurry velocity on frictional pressure drop at a constant slurry concentration (i.e., 3.63 kg/m^3) in the presence of SDBS surfactant (i.e., 30 g/m^3) in continuous mode is reported in Fig. 3.3.

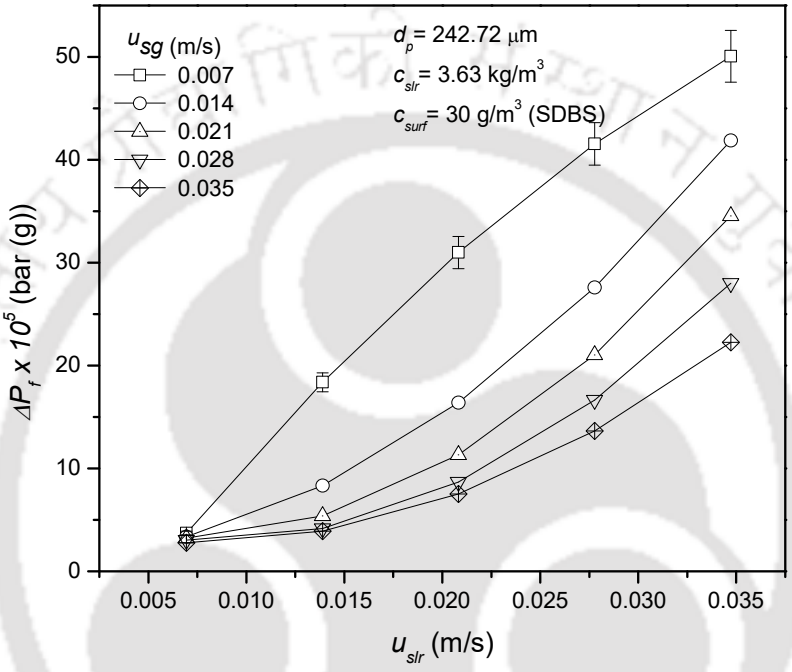

Figure 3.3: Effect of superficial slurry velocity on frictional pressure drop in the continuous mode.

It is noticed that the frictional pressure drop is significantly increased with an increase in the superficial slurry velocity for all superficial gas velocities. As the superficial slurry velocity increases, it causes an increase in the bubble coalescence rate, which in turn produces a larger gas bubble. The larger gas bubble possesses higher rising velocity (Götz et al., 2016) and also responsible for the increase in the phase circulation velocity (Wilkinson et al., 1993). The increase in the phase circulation velocity causes an increase in the slurry momentum; therefore, the frictional pressure drop increases. According to (Joshi and Sharma, 1979), the value of circulation

velocity depends on the holdup characteristics, superficial gas velocity, and slip velocity of the phases. It is noticed that the difference in frictional pressure drop at the minimum superficial slurry velocity (0.007 m/s) is not significant, however with an increase in the slurry velocity (0.007 – 0.035 m/s) this difference augments. The maximum and minimum frictional pressure drop noticed to be 27.87 $\left(u_{sg} = 0.035 \text{ m/s}\right)$, and 500.61 Pa $\left(u_{sg} = 0.007 \text{ m/s}\right)$ at the 0.007 m/s and 0.035 m/s superficial slurry velocity, respectively.

3.5.1.4. Effect of particle size on frictional pressure drop

The effect of particle size (i.e., 63.22, 235.61, 404.97, and 507.67 μm) on frictional pressure drop at the constant concentrations of the slurry (i.e., 7.26 kg/m^3) and 1-Hexanol (i.e., 3 g/m^3) in batch mode are shown in Figure 3.4. It was observed that the frictional pressure drop increased with the particle size at all superficial gas velocities.

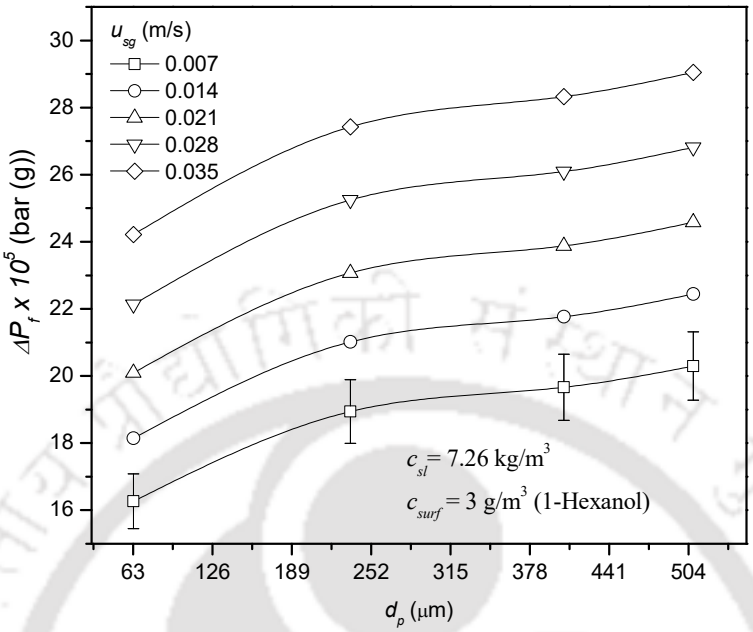

Figure 3.4: Effect of particle size on frictional pressure drop in the batch mode.

The frictional pressure drop increment was about 24.77% when the particle diameter increased from 63.22 to 507.67 μm at the minimum superficial gas velocity (i.e., 0.007 m/s). This increment was reduced to 19.94% at the maximum superficial gas velocity of 0.035 m/s. The rate of increase in frictional pressure drop at the lower gas velocity was more than that at higher gas velocity. For the higher superficial gas velocity, two opposite effects were observed on frictional pressure drop, i.e., rise in the bubble population as well as in the rate of coalescence of the bubbles. An increase in the bubble population was responsible for the increase in the frictional pressure drop, which is caused by the rise in the actual liquid velocity in the column (Mandal et al., 2004). The increase in the rate of coalescence of the bubbles increases the frictional pressure drop because the coalescence of bubbles formed larger bubbles, and consequently the liquid holdup was increased. Due to the prevalence of the first effect, the frictional pressure drop increased with superficial gas velocity,

but the rate of increment was lower than that at the lower gas superficial gas velocity. At 63.22, 235.61, 404.97, 507.67 μm particle diameters, the maximum changes in the frictional pressure drop were 48.88, 44.81, 44.01, and 43.10% within the minimum and maximum superficial gas velocities. At the maximum particle size, the increment in frictional pressure drop was lowest. A comparison shows that the maximum and minimum increases of the frictional pressure drop at 235.61 and 404.97 μm are 3.83% and 3.26% at the maximum and minimum superficial gas velocities, respectively. The maximum and the minimum differences (i.e., 24.77 and 19.94%) were observed at the particle diameters of 63.22 and 507.67 μm, respectively when the superficial gas velocity was changed from the minimum to maximum. The increase in frictional pressure drop was more between the particle diameters of 63.22 and 235.61 μm, as compared to that for the particle diameter greater than 235.61 μm. After the change in particle diameter from 235.61 to 404.97 μm the change in frictional pressure drop is below 3.83%. Therefore, it can be concluded that the effect of particle size on frictional pressure drop was more significant for the smaller particles than the larger ones.

The effect of four different particle sizes 63.22, 235.61, 404.97, and 507.67 μm at a fixed slurry concentration (i.e., 7.26 kg/m^3) in the presence of 1- Hexanol (i.e., 10 g/m^3) surfactant in continuous mode is shown in Fig. 3.5.

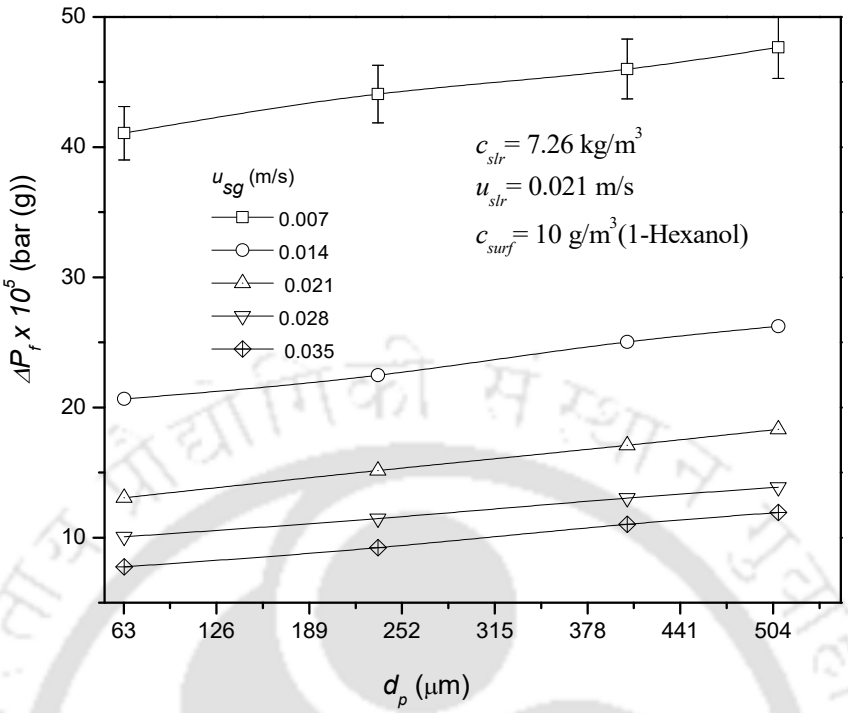

Figure 3.5: Effect of particle size on frictional pressure drop in the continuous mode.

It is observed that the frictional pressure drop is increasing with an increase in the particle diameter for all superficial gas velocity. As the particle size in the slurry increases, the friction between the flowing fluid and the column wall also increases, hence the frictional pressure in case of the presence of the larger particle sizes is more as compared to the smaller particle size. According to Besagni and Inzoli (2017) lift fore pushes the larger bubble size to the center of the column, which rises fast, which causes a rise in the phase circulation velocity; therefore, the momentum of the slurry increase. This increased momentum of the slurry is also one of the prime causes of the increase in the frictional pressure drop. A converse result of an increased frictional pressure drop noticed by decreasing the size of fine particles in the range of 4.85 – 52.26 μm (Prakash et al., 2018a). They explained that the apparent viscosity of the system is higher in the presence of the smaller particle size (Ojima et al., 2015; Rabha et al., 2013a, 2013b; Sarhan et al., 2016), because

of the attractive particle interaction (Kawatra and Eisele, 1988; Senapati et al., 2009; Shukla et al., 2008; Yoshida et al., 2013; Zhou et al., 1993). Therefore, the increased viscosity is responsible for the increase in the bubble coalescence rate, consequently larger bubbles produce. The increase in the frictional pressure drop is approximately 16.04, 26.99, 40.34, 37.84, and 53.66% of the variation of particle size from 63.22 to 404.97 μm in different superficial gas velocity of 0.007, 0.014, 0.021, 0.028, and 0.035 m/s respectively. The highest increment (53.66%) in the superficial gas velocity occurs at the superficial gas velocity of 0.035 m/s, whereas the lowest increment (16.04%) is at 0.007 m/s superficial gas velocity. It can be deduced from the present result that at a lower superficial gas velocity the effect of particle size on the frictional pressure drop reduces, whereas at the higher superficial gas velocity the effect of the particle size is dominant.

3.5.1.6. Effect of surfactant concentration on frictional pressure drop

The effect of SDBS concentration (i.e., 1, 3, 6, 10, and 12 g/m^3) on frictional pressure drop at a fixed particle diameter (i.e., 235.61 μm) and slurry concentration (i.e., 10.89 kg/m^3) in batch mode is shown in Figure 3.6. It was observed that the frictional pressure drop decreased with increasing concentration of the surfactant in the slurry. Similar trends have been reported by (Parmar and Majumder, 2014; Prakash et al., 2018a).

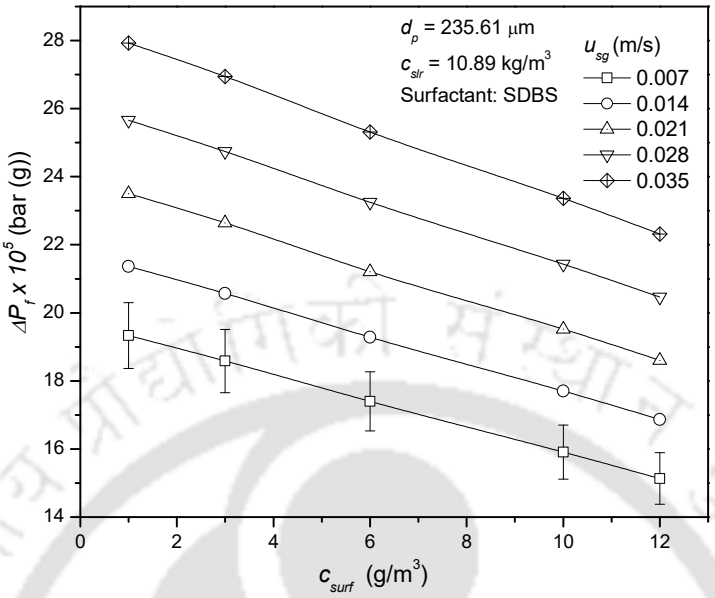

Figure 3.6: Effect of surfactant concentration on frictional pressure drop in the batch mode.

This decrease in the frictional pressure drop was due to the generation of a large number of small bubbles as a result of the reduction in surface tension, which reduced the liquid holdup in the column, hence the momentum decreases. As the momentum of the slurry decreases, the total pressure drop of the system also decreases. Therefore the frictional pressure drop falls. The frictional pressure drop was reduced from 19.34 to 15.13 Pa (i.e., 21.77% reduction) when the surfactant concentration increased from 1 to 12 g/m^3 at the superficial gas velocity of 0.007 m/s. The frictional pressure drop decreased from 27.93 to 22.31 Pa, which was 20.12% less for the variation of surfactant concentration in the same range at the superficial gas velocity of 0.035 m/s. At the superficial gas velocity of 0.007 m/s, the maximum reduction in frictional pressure drop was 6.38 and 8.56% when the surfactant concentration was increased from 3 to 6 g/m^3 and 6 to 10 g/m^3, respectively. It was observed that the reduction in frictional pressure drop was highest at the minimal superficial gas velocity, and this difference reduces with a further rise in superficial gas

velocity. The frictional pressure drop increment was about 44.63% when the superficial gas velocity varied from 0.007 to 0.035 m/s at a fixed surfactant concentration of 3 g/m^3.

Similarly, this increment was 44.42, 45.49, 46.85, and 47.46% at the surfactant concentration of 1, 6, 10, and 12 g/m^3 at the same range of variation of superficial gas velocity. It is found that an increase in the frictional pressure drop with superficial gas velocity is increasing with the rise in the surfactant concentration. The significant decrease in the surface tension of the slurry enables to form a considerable number of small bubbles with air flow rate. It is noticed that the reduction in surface tension reduces the frictional pressure drop of the system.

Effect of surfactant (SDBS) concentration at a fixed superficial liquid velocity (i.e., 0.035 m/s) and slurry concentration (i.e., 10.89 kg/m^3) in continuous mode is reported in Fig. 3.7.

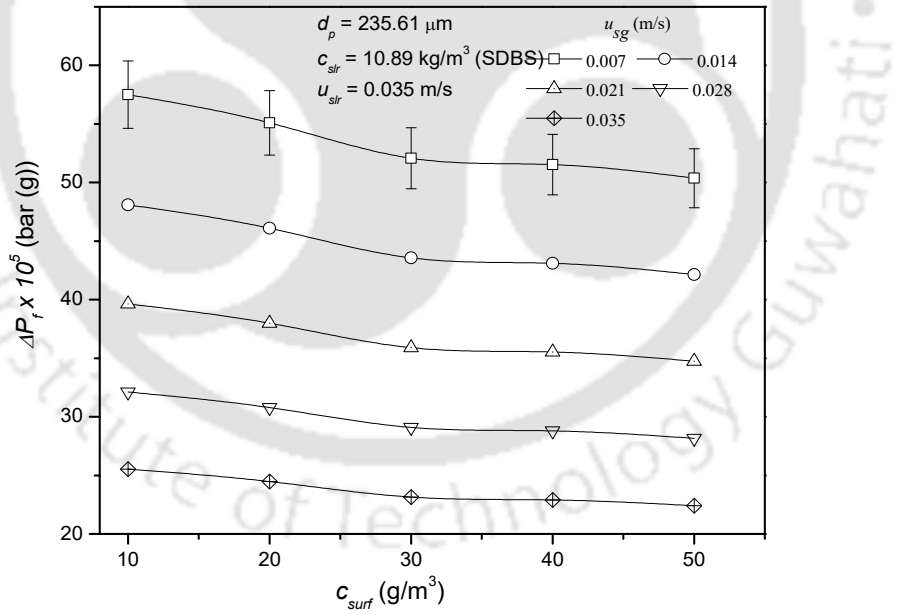

Figure 3.7: Effect of surfactant concentration on frictional pressure drop in the continuous mode.

It is noticed that frictional pressure drops are decreasing with an increase in the surfactant concentration. The addition of surfactant to the liquid reduces the surface tension of the liquid, which in turn produces a large number of tiny bubbles. Due to the further increment in the surfactant concentration, a massive amount of smaller gas bubbles produced, which reduces both the total pressure drop as well as hydrostatic pressure, consequently, frictional pressure drop reduces. Frictional pressure drop reported in the present system is mainly considered to be primarily due to the liquid-wall friction. The surfactant solution is well known to enhance the bubble stability as well reduces its size. After the addition of a surfactant in the liquid, the number of tiny bubbles in the system increases, which reduces the direct interaction of the liquid with the column wall and also reduces the interfacial shear stress between the bubble and liquid. Hence the system frictional pressure drop reduces. It was discussed earlier that larger bubbles are responsible for higher circulation velocity, which in turn increases the circulation velocity, therefore the slurry momentum increases, which increases the frictional pressure drop. In the presence of high surfactant concentration, the bubble sizes are smaller and do not cause much circulation of slurry and therefore tend to reduce the frictional pressure drop. The reduction in the frictional pressure drop is approximately 9.44% when the surfactant concentration changes from 10 to 30 g/m^3 and about 3.29% due to the further increment in the surfactant concentration to 50 g/m^3 at a minimum superficial gas velocity of 0.007 m/s. The difference in frictional pressure drop is more significant as the surfactant concentration varies from 10 to 30 g/m^3 whereas this difference reduces to 3.29% when the surfactant concentration further increases from 30 to 50 g/m^3.

3.5.1.8. Effect of surfactant type on frictional pressure drop

The effect of different surfactant type (i.e., SDBS, CTAB, and 1-Hexanol) on frictional pressure drop at the particular slurry concentration (i.e., 7.26 kg/m^3) and surfactant concentration (i.e., 10 g/m^3) in batch mode is shown in Figure 3.8.

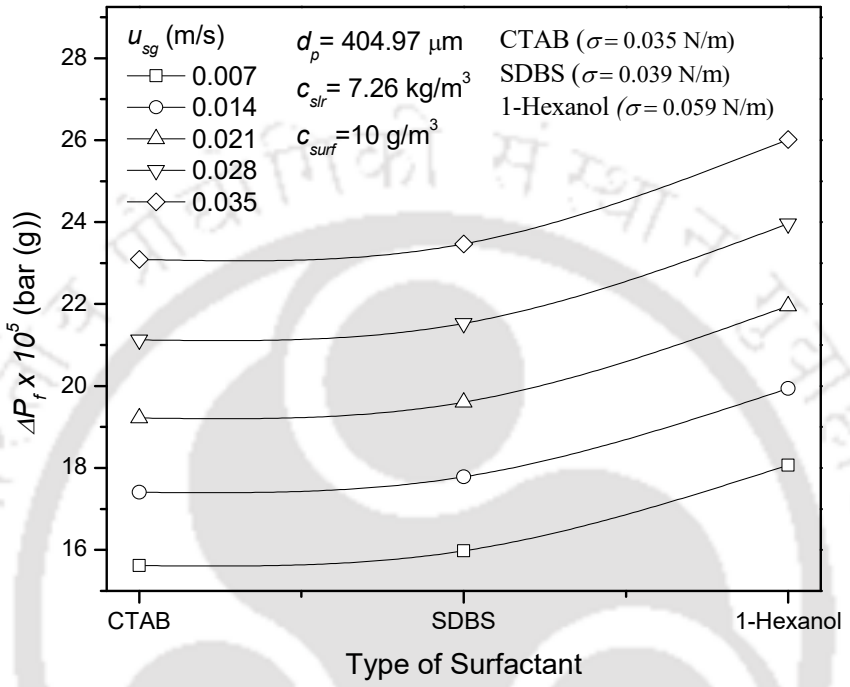

Figure 3.8: Effect of surfactant type on the frictional pressure drop in the batch mode.

The frictional pressure drop of the CTAB surfactant solution is lower than the SDBS and 1-Hexanol surfactant solution. The solution having lower surface tension can able to produce a vast amount of tiny bubbles than the higher surface tension solution. The presence of an immense amount of small bubbles will reduce the circulation velocity as well as the momentum of the slurry in the system. Therefore, the frictional pressure drop reduces. The decrease in frictional pressure drop in the CTAB surfactant solution as compared to SDBS is less than 2.33% at all superficial gas velocities. The minimum reduction in frictional pressure drop of 1.63% was noticed at the superficial gas velocity of 0.035 m/s. Comparing the frictional pressure drop of the SDBS surfactant solution with a 1-Hexanol surfactant solution, it was observed that the reduction in

frictional pressure drop was 13.08% at minimum superficial gas velocity and 10.86% at maximum superficial gas velocity. The frictional pressure drop decrease is about 15.72% when the surface tension of the solution decreases from 0.059 (i.e., 1-Hexanol) to 0.035 N/m (i.e., CTAB) at a fixed superficial gas velocity of 0.007 m/s.

Similarly, reduction in frictional pressure drop is found to be 12.68% at the same range of change in surface tension of the solution at the superficial gas velocity of 0.035 m/s. The frictional pressure drop increase was about 47.86% when the superficial gas velocity varied from 0.007 to 0.035 m/s for the CTAB solution. Similarly, this increment was 46.86 and 43.98% at SDBS and 1-Hexanol surfactant at the same range of superficial gas velocity, respectively. The decrease in frictional pressure drop at lower surface tension solution compared to higher surface tension solution is highest at the minimum superficial gas velocity, and it is found to decrease with rising in the superficial gas velocity.

The effect of three different surfactants, namely SDBS $\left(\sigma = 0.030 \text{ N/m}\right)$, CTAB $\left(\sigma = 0.029 \text{ N/m}\right)$, and 1-Hexanol $\left(\sigma = 0.048 \text{ N/m}\right)$ at a constant concentration $\left(c_{surf} = 50 \text{ g/m}^3\right)$ in the presence of slurry $\left(c_{slr} = 7.26 \text{ kg/m}^3\right)$ in continuous mode, is shown in Fig. 3.9.

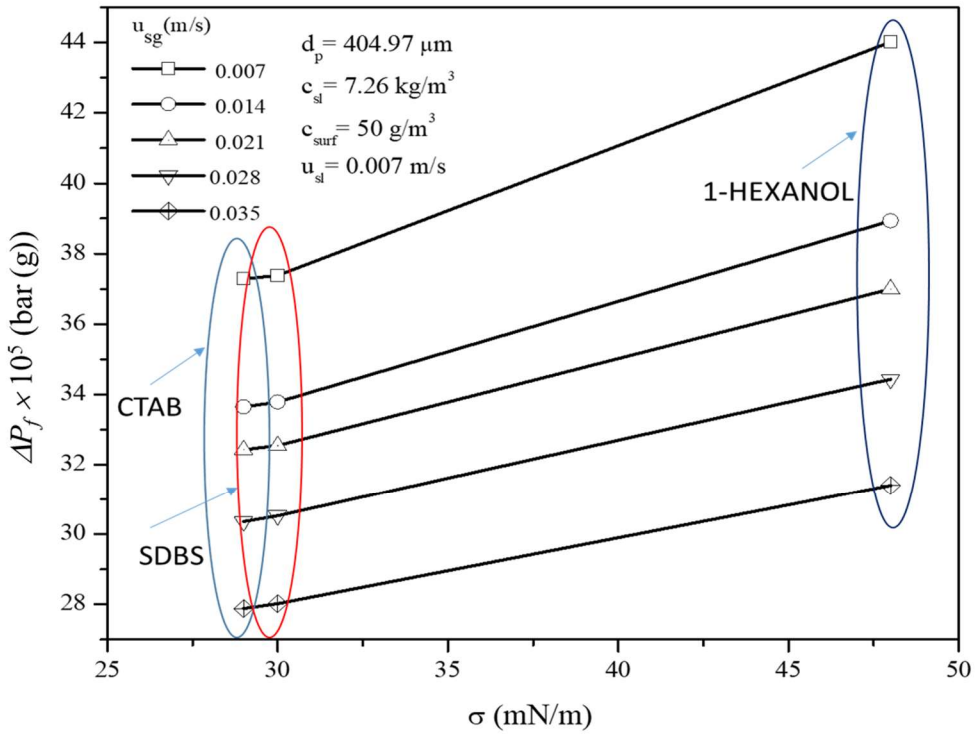

Figure 3.9: Effect of surfactant type on the frictional pressure drop in the continuous mode.

It is noticed that the frictional pressure drop in the presence of 1-Hexanol is higher as compared to the CTAB and SDBS surfactant. It was because the surface tension reduction capability of 1-Hexanol surfactant was smaller than the other two surfactants. Frictional pressure drop in the presence of CTAB and SDBS is slightly differed because of approximately the same surface tension of the liquid in the three-phase, as reported in Table 2.4. As we have discussed in the previous figure (Fig. 3.8), the higher the surface reduction capacity of the liquid, the higher is the production of large numbers of the tiny bubbles and lowers the total frictional as well as hydrostatic pressure. The difference in the frictional pressure drop in the presence of SDBS and CTAB is approximately less than 0.5% for all superficial gas velocities. The reduction in frictional pressure

drop is about 25.20% (i.e., CTAB), 25.04% (i.e., SDBS), and 28.65% (i.e., 1-Hexanol) when the superficial gas velocity increases from 0.007 m/s to 0.035 m/s. The decrease in frictional pressure drop is about 18.07, 15.72, 14.12, 13.42, and 12.62% at superficial gas velocity of 0.007, 0.014, 0.021, 0.028, and 0.035 m/s respectively. It can be noticed that the influence of surfactant addition is more effective on the frictional pressure drop at lower superficial gas velocity, and it decreases with an increase in the superficial gas velocity.

3.5.1.10. Effect of loading of solids on frictional pressure drop

According to the earlier discussion, the presence of a particle increases the viscosity of the system. Therefore, the total pressure drop increases. As a result, the frictional pressure drop increases. The effect of presence and absence of particle on frictional pressure drop at fixed particle diameter $\left(i.e.,\ d_p = 63.22\ \mu\text{m}\right)$, slurry concentration $\left(i.e.,\ c_{slr} = 10.89\ \text{kg/m}^3\right)$, and surfactant concentration $\left(i.e.,\ c_{surf} = 10\ \text{g/m}^3\right)$ in batch mode is shown in Figure 3.10. It is found that the frictional pressure drop is higher in the presence of particle compared to frictional pressure drop in the absence of particle at all superficial gas velocities consider in the present work. The addition of particle causes to increase the viscosity of the system, hence the frictional pressure drop increases. The frictional pressure drop increment is about 65.23 and 50.71% in the presence and absence of the particle, respectively, when the superficial gas velocity varied from 0.007 to 0.035 m/s. It can be noticed that the increase in frictional pressure drop with an increase in superficial gas velocity is more in the presence of particle than that in the absence of the particle. The frictional pressure drop increases from 10.11 to 13.73 Pa (i.e., 35.79% increment) after the addition of particles at 0.007 m/s superficial gas velocity. It is found that an increase in frictional pressure

drop after particle addition at minimum superficial gas velocity is highest, and this increase in frictional pressure drop is reduced with a rise in the superficial gas velocity from minimum to maximum.

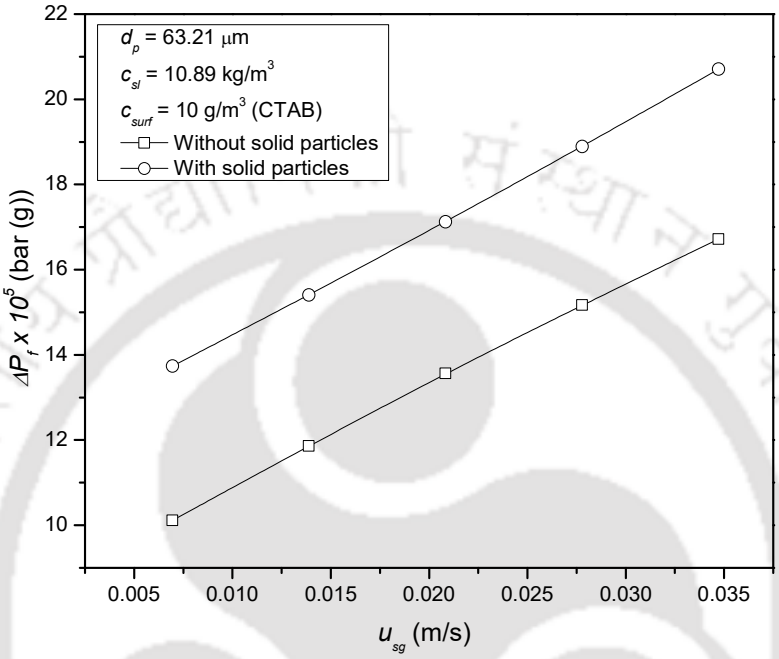

Figure 3.10: Effect of loading of solids on frictional pressure drop in the batch mode.

Fig. 3.11 reflects the effect of the presence and absence of the solid particles on the frictional pressure drop in the presence of CTAB surfactant $\left(c_{surf} = 30 \text{ g/m}^3\right)$ in continuous mode in a flotation column. It is observed that the frictional pressure drop in the three-phase system is significantly higher as compared to the two-phase system. (Prakash et al., 2018a) reported the frictional pressure drop in a slurry system is mainly due to the friction between the fluid-particle, particle-wall, and fluid-wall. Generally, a prime contribution of frictional pressure drop is considered to be due to the friction between the fluid-wall, but in the presence of a three-phase system additional two frictional forces, namely fluid-particle and particle-wall included.

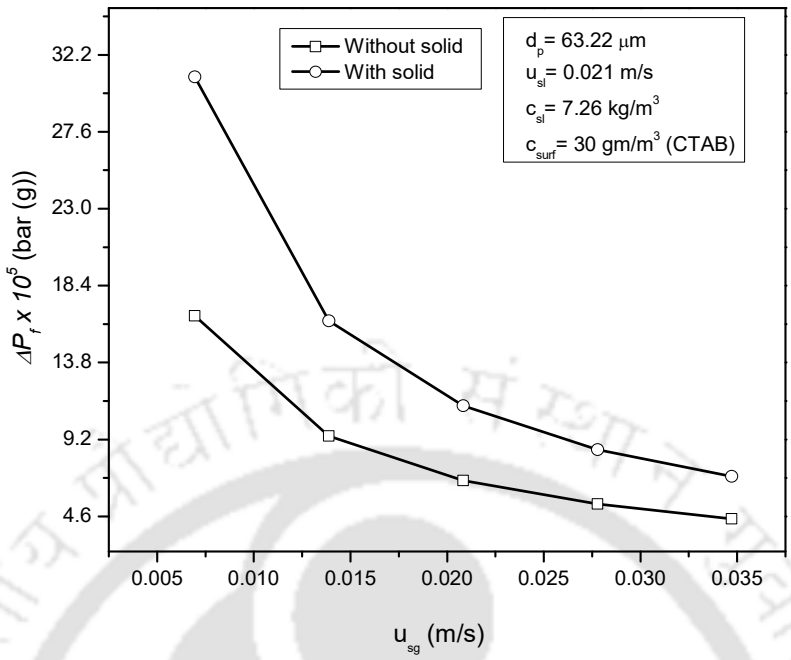

Figure 3.11: Effect of frictional pressure drops on loading of solid particles.

Due to the addition of two extra frictional forces, the frictional pressure drop in the three-phase system is more as compared to the two-phase system. The addition of a particle also increases the slurry viscosity, which tends to form the larger bubble, consequently the circulation velocity of the phases increases. This increased circulation velocity enhances the momentum of the slurry, hence the frictional pressure drop increases. At minimum superficial gas velocity (0.007 m/s), the frictional pressure drop is about 165.85 Pa (without particle) and 308.82 Pa (with particle), a profound increase of approximately 86.20%. The difference in frictional pressure drop is reducing as the superficial gas velocity increases up to 0.035 m/s. At maximum superficial gas velocity (0.035 m/s), the difference in frictional pressure drop in the system with and without particle is about 57.49%. The minimum frictional pressure drop is noticed to be 44.44 Pa (in the absence of particle) at the 0.035 m/s superficial gas velocity.

3.5.2. Development of empirical correlation for frictional pressure drop in the batch mode

Frictional pressure drop per unit length is found to be dependent on superficial gas velocity u_{sg}, column diameter d_c, particle diameter d_p, surface tension σ, slurry density ρ_l, apparent slurry viscosity μ_l, and acceleration due to gravity g.

The pressure drop per unit length $\Delta P_f / L$ for a two-phase system can be expressed as the function of all these variables as

$$\frac{\Delta P_f}{L} = f\left(u_{sg}, d_c, \sigma, \rho_l, \mu_l, g\right) \tag{3.16}$$

Applying Buckingham's Pi-theorem of dimensional followed by multiple linear regression analysis, a general correlation for the two-phase system was developed to predict the frictional pressure drop is given as

$$\frac{d_c\left(\Delta P_f / L\right)}{u_{sg}^2 \rho_l} = \frac{E_u d_c}{L} = 3.624\times10^{-5}\ \mathrm{Re}_l^{0.739}\ \mathrm{Fr}_l^{-1.692}\ \mathrm{We}_l^{-0.405} \tag{3.17}$$

Where Re_l is the Reynolds number $\rho_l u_{sg} d_c / \mu_l$, Fr_l is the Froude number $u_{sg} / \sqrt{g d_c}$, We_l is the Weber number $\rho_l u_{sg}^2 d_c / \sigma$. The standard error and correlation coefficient of the Equation (3.17) are 0.0188 and 0.9998, respectively. The correlation is valid within the range of variables: $310.10 \le \mathrm{Re}_l \le 1780.06$; $9.46\times10^{-3} \le \mathrm{Fr}_l \le 47.29\times10^{-3}$; $4.35\times10^{-2} \le We_l \le 1.89$. The parity plot of experimental frictional pressure drops and *predicted frictional pressure* drops calculated by Equation (3.17) is shown in Figure 3.12.

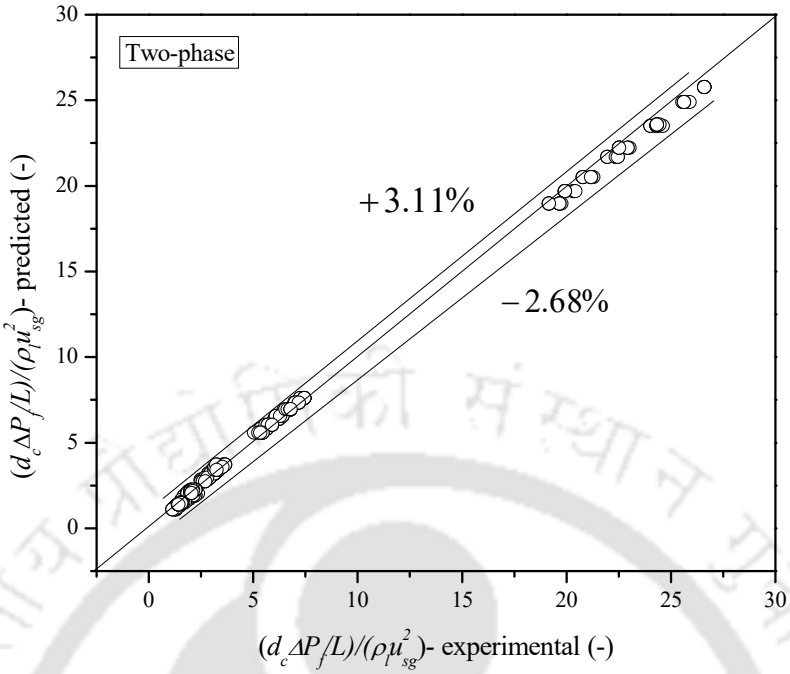

Figure 3.12: The parity of experimental and predicted frictional pressure drop for the two-phase system in the batch mode.

The pressure drop per unit length $\Delta P_f / L$ for a three-phase system can be expressed as the function of all these variables as

$$\frac{\Delta P_f}{L} = f\left(u_{sg}, d_c, d_p, \sigma, \rho_{slr}, \mu_{slr}, g\right) \tag{3.18}$$

Similarly, for the three-phase system, a correlation is developed for the prediction of frictional pressure drop, which can be represented as

$$\frac{d_c\left(\Delta P_f / L\right)}{u_{sg}^2 \rho_{slr}} = \frac{E_u d_c}{L} = 93.1 \mathrm{Re}_{slr}^{-0.916}\ \mathrm{Fr}_{slr}^{0.44}\ \mathrm{We}_{slr}^{-0.224}\ \left(\frac{d_p}{d_c}\right)^{0.087} \tag{3.19}$$

where Re_{slr} is the Reynolds number $\rho_{slr} u_{sg} d_c / \mu_{slr}$, Fr_{slr} is the Froude number $u_{sg} / \sqrt{g d_c}$ and We_{slr} is the Weber number $\rho_{slr} u_{sg}^2 d_c / \sigma$. The standard error and correlation coefficient of Equation (3.19) were found to be 0.0396 and 0.9992, respectively. The correlation is valid within the range of variables: $303.50 \le \mathrm{Re}_{slr} \le 1764.32$; $9.46\times10^{-3} \le Fr_{slr} \le 47.29\times10^{-3}$; $4.35\times10^{-2} \le \mathrm{We}_{slr} \le 1.90$; $1.19\times10^{-3} \le d_p / d_c \le 9.22\times10^{-3}$. The parity of the empirical correlation proposed for the interpretation of frictional pressure drop and experimental values is shown in Figure 3.13.

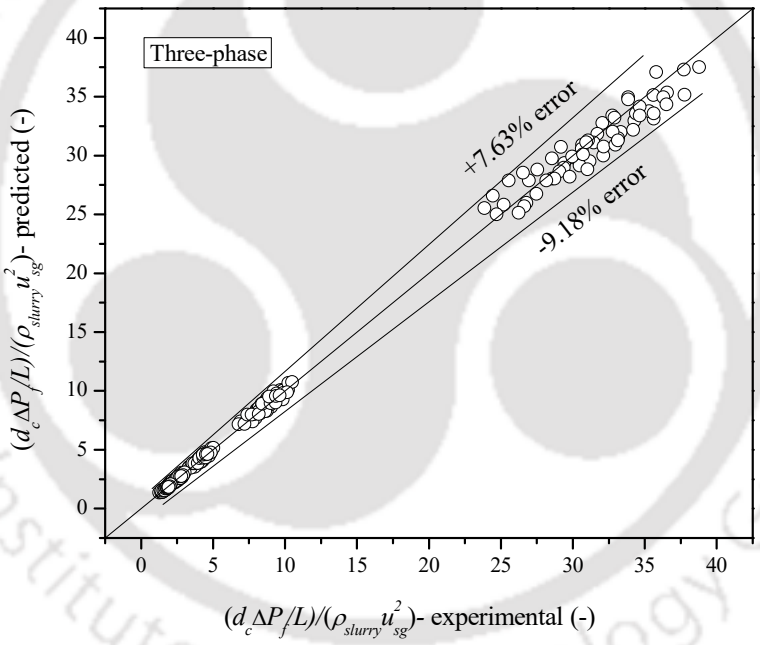

Figure 3.13: The parity of experimental and predicted frictional pressure drop for the three-phase system in the batch mode.

3.5.3. Development of empirical correlation for frictional pressure drop in the continuous mode

Theoretically, interpretation of the frictional pressure drop is not possible due to a lack of quantitative information about the wall friction, momentum exchange among the phases, and the shear at the phase interface (Friedel, 1978). Therefore, a significant effort has taken to generate an empirical correlation by dimensional analysis to interpret the frictional pressure drop as a function of the quantifiable variables. Frictional pressure drop per unit length for the two-phase system is found to be dependent on superficial gas velocity u_{sg}, superficial liquid velocity u_{sl}, liquid viscosity μ_l, liquid density ρ_l, column diameter d_c, particle diameter d_p, surface tension σ, and acceleration due to gravity g. The pressure drop per unit length $\Delta P/L$ can be expressed as the function of all these parameters.

$$\left(\frac{\Delta P_f}{L}\right)_{two-phase} = f\left(u_{sg}, u_{sl}, d_c, d_p, \sigma, \rho_l, \mu_l, g\right) \tag{3.20}$$

There fore, for the two-phase system, the developed correlation for prediction of frictional pressure drop is

$$\left(\frac{d_c\left(\Delta P/L\right)}{u_{sg}^2 \rho_l}\right)_{two-phase} = \frac{E_u d_c}{L} = 9.63\times10^{-4}\,\mathrm{Re}_l^{0.515}\,\mathrm{Fr}_l^{-1.458}\,\mathrm{We}_l^{-0.425}\left(\frac{u_{sl}}{u_{sg}}\right)^{0.457} \tag{3.21}$$

The standard error and correlation coefficient of the Eq. (3.21) are 0.0611 and 0.9969, respectively. The correlation is valid within the range of variables: $8.67\times10^2 \le \mathrm{Re}_l \le 37.86\times10^2$; $2.84\times10^{-2} \le \mathrm{Fr}_l \le 11.35\times10^{-2}$; $40.47\times10^{-2} \le \mathrm{We}_l \le 13.18\times10^{-2}$;

$0.14 \le u_{sl}/u_{sg} \le 0.5$. The parity plot of experimental frictional pressure drops and predicted frictional pressure drop (from Eq. 3.21) for a two-phase system is shown in Fig. 3.14.

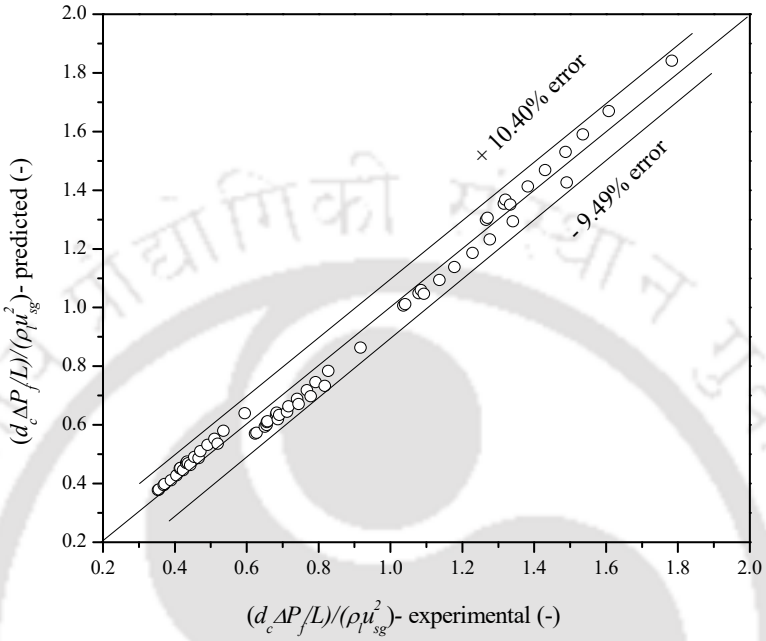

Figure 3.14: The parity of experimental and predicted frictional pressure drop for the two-phase system in the batch mode.

Similarly, frictional pressure drop per unit length for a three-phase system is found to be dependent on superficial gas velocity u_{sg}, superficial slurry velocity u_{slr}, apparent slurry viscosity μ_{slr}, slurry density ρ_{slr}, column diameter d_c, particle diameter d_p, surface tension σ, and acceleration due to gravity g. The pressure drop per unit length $\Delta P_f / L$ can be expressed as the function of all these parameters.

$$\left(\frac{\Delta P_f}{L}\right)_{three-phase} = f\left(u_{sg}, u_{slr}, d_c, d_p, \sigma, \rho_{slr}, \mu_{slr}, g\right) \tag{3.22}$$

By using the Buckingham's Pi technique of dimensional evaluation, developed general correlation which can predict the frictional pressure drop will be represented as

$$\left(\frac{d_c\left(\Delta P/L\right)}{u_{sg}^2\rho_{slr}}\right)_{three-phase} = 7.76\times10^{-1}\,\mathrm{Re}_{slr}^{-0.233}\,\mathrm{Fr}_{slr}^{-1.093}\mathrm{We}_{slr}^{-0.238}\left(\frac{d_p}{d_c}\right)^{0.031}\left(\frac{u_{sl}}{u_{sg}}\right)^{0.491} \quad (3.23)$$

The standard error and correlation coefficient of Eq. (3.23) were found to be 0.0497 and 0.9979, respectively. The correlation is valid within the range of variables: $7.54\times10^{2} \le \mathrm{Re}_{slr} \le 36.20\times10^{2}$; $2.84\times10^{-2} \le \mathrm{Fr}_{slr} \le 11.35\times10^{-2}$; $40.86\times10^{-2} \le \mathrm{We}_{slr} \le 13.41\times10^{-2}$; $14.29\times10^{-2} \le u_{sl}/u_{sg} \le 0.5$; $1.18\times10^{-3} \le d_p/d_c \le 9.23\times10^{-3}$. The parity plot of experimental frictional pressure drops and predicted frictional pressure (Eq. 3.23) drop for the three-phase system is given in Fig. 3.15.

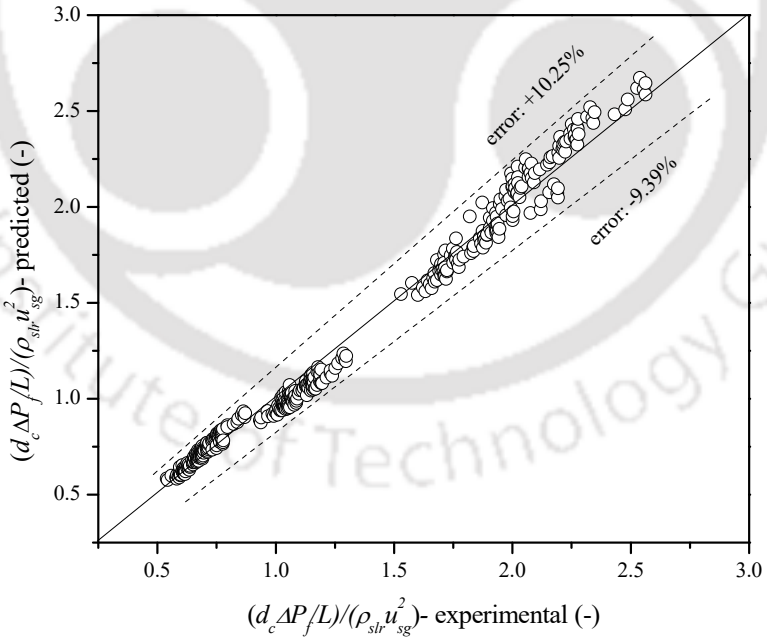

Figure 3.15: The parity of experimental and predicted frictional pressure drop in the three-phase system in the continuous mode.

3.6. Conclusion

Effects of slurry concentration, surfactant concentration, gas flow rate, particle size, and surfactant type on frictional pressure drop in the batch mode were studied. From the current study, it can be concluded that the frictional pressure drop of the system increases with an increase in the superficial gas velocity, slurry concentration, and average particle size. The frictional pressure drop is higher in the three-phase system compared to the two-phase system. The addition of surfactant to the liquid reduces the frictional pressure drop, and this reduction is more towards the increase of the surfactant concentration. In the presence of CTAB surfactant, the frictional pressure drop was smaller compared to SDBS and 1-Hexanol surfactant. The friction factor is observed to decrease with an increase in the gas Reynolds number. An empirical correlation is produced to interpret the experimental frictional pressure drop in the two and three-phase systems. The present study may be useful to understand the hydrodynamic characteristics of the laboratory flotation column, which may be used for industrial applications. The same increased with increasing slurry concentration, superficial gas velocity, and average particle size. The addition of surfactant to the liquid phase reduced the frictional pressure drop. The same was lower in the presence of cetyltrimethylammonium bromide than sodium dodecylbenzene sulfonate and 1-Hexanol.

Frictional pressure drops in a laboratory flotation column in the two and three-phase systems are studied in the continuous mode flotation column. The in-depth investigation of the influence of superficial gas velocity, superficial slurry velocity, slurry concentration, particle size, surfactant concentration, surfactant type on the frictional pressure drop is analyzed. It is found that in frictional pressure drop decreases with an increase in the superficial gas velocity while it increases with an increase in the slurry concentration and superficial slurry velocity. The increase in particle size leads to an increase the frictional pressure drop. The highest increment in frictional pressure

drop (53.66%) occurs at the superficial gas velocity of 0.035 m/s. However, the lowest increase (16.04%) is at 0.007 m/s superficial gas velocity when the particle size varies from 63.22 to 404.97 μm. The frictional pressure drop in the three-phase systems is decreasing with increases in the surfactant concentration. Frictional pressure drop reported in the present system is mainly considered to be primarily due to the liquid-wall friction and phase circulation velocity. It is concluded that the larger bubbles are responsible for higher circulation velocity, which in turn increases the slurry momentum, hence the frictional pressure drop increases. In the presence of high surfactant concentration, the bubble sizes are smaller and do not cause much circulation of slurry and, therefore, tend to reduce the frictional pressure drop. The frictional pressure drop in the presence of 1-Hexanol is higher as compared to the CTAB and SDBS surfactant, which is because of the fact that the surface tension decreasing capability of 1-Hexanol surfactant is smaller than other two surfactants. It is also concluded that the frictional pressure drop in the flotation column is lower in the case of two-phase in comparison to the three-phase system. The addition of particles to the system led to an increase in the frictional pressure drop. The correlation model is also proposed to interpret the frictional pressure drop in the two and three-phase systems. All developed correlations are suitable to interpret the experimental values well within the error range of ± 20%. The present analysis will be helpful to enhance the process efficiency and scale-up the flotation systems at the industrial scale.

CHAPTER 4 : MIXING CHARACTERISTICS

This chapter reports the experimental analysis of the dispersion characteristics in a three-phase counter-current flotation column. The residence time distribution (RTD) technique was used to estimate the dispersion number based on the axial dispersion model. The velocity distribution model was applied to analyze the dispersion due to bubble motion, and the velocity distribution characteristic factor. The parameters in the velocity distribution model, dispersion due to bubble motion, and velocity distribution characteristic factor were also determined based on the experimental conditions. An empirical correlation was developed to predict the dispersion number, dispersion due to bubble motion, and the velocity distribution characteristics factor.

4.1. Introduction and literature

Flotation columns are widely used in the mineral industries (Hassanzadeh and Karakas, 2017; Sarhan et al., 2018b, 2017a; Tian et al., 2018; Xia et al., 2017a), wastewater treatment (Li et al., 2016; Sarhan et al., 2016), plastic recycling (Wang et al., 2015b), removal of heavy metals (Li et al., 2016), ink removal (Labidi et al., 2007; Li et al., 2016; Sarhan et al., 2016; Vashisth et al., 2011), and recycling of organic compounds (Li et al., 2016). The flotation column is advantageous over other flotation devices in terms of low power consumption (due to the absence of rotating parts), low capital investment, large aerated space, ease of controlling the air flowrate and dispersion, and low floor area requirement (Massinaei et al., 2019; Rubinstein, 1994; Wills and Finch, 2015). The bubble generation technique and usage of wash water distinguish the flotation column from other conventional flotation machines. In a flotation column, bubbles are generally

generated from the sparger, which is located at the bottom of the column, and the bubble–particle interaction takes place counter-currently. The knowledge of hydrodynamic characteristics is relevant because it helps in the proper design, scale-up, control, and modeling of the column (Prakash et al., 2018b). Flow regime, gas holdup, bubble size distribution, frictional pressure drop, and mixing characteristics are some of the important hydrodynamic parameters, which affect the performance of the flotation systems. Recently, (Fahad et al., 2019) have reported hydrodynamic studies on gas holdup in a flotation column at different slurry concentrations and particle size. Due to the complex flow behavior, the performance of the flotation column is affected by the flow characteristics of the process (Jena et al., 2008). The analysis of the mixing of the material in the column is required to assess the dynamic behavior of the flotation process (Massinaei et al., 2007). Numerous researchers have conducted experiments on the mixing characteristics in the flotation column (Bhunia et al., 2018; Massinaei et al., 2007; Tokoro and Okano, 2001; Yianatos et al., 2005). Most of these studies have reported the effect of different variables, such as the impact of slurry flow rate, gas flow rate, and the internals in the two-phase system (Farzanegan et al., 2017).

The flotation column is more effective than the conventional flotation cell for fine coal recovery, due to the presence of smaller bubbles, a quiescent environment that enhances the probabilities of the bubble–particle collision, attachment of particles to the gas bubble, and ease of procurement of the froth washing system (Mankosa et al., 1992). Flotation columns have been successfully adopted worldwide for the recovery of fine coal particles in the coal preparation unit (Bhunia et al., 2018; Massinaei et al., 2019; Xia et al., 2017b). The mixing is important in the flotation processes because it is required for suspending the fine particles, generating fine bubbles, and promoting the probability of bubble–particle collision and attachment (Yianatos et al., 2005). Thus, the mixing in the flotation column is primarily due to the convective slurry circulation and

dispersion due to the turbulence caused by the bubble motion. Knowledge of the mixing characteristics helps to scale-up the flotation column (Yianatos et al., 2005).

The residence time distribution (RTD) provides a way to express the mixing characteristics (Lelinski et al., 2002). The axial dispersion model (ADM) has been frequently used to analyze column performance, design, and scale-up (Tokoro and Okano, 2001; Yianatos et al., 2005). Axial dispersion in the multiphase system reflects the degree of back mixing and molecular diffusion of fluid particles in the axial direction (Bahadori, 2012). The RTD technique provides the probability density function, which gives an idea of the time spent by an element inside the column. Variation in the RTD occurs due to the complex interaction between the phases (i.e., gas, liquid, and solid), and it affects the metallurgical performance of the flotation systems (Yianatos et al., 2015). The ADM can be used for interpreting the hydrodynamics behavior in the laboratory- or pilot-scale flotation columns because it is suitable for dispersion numbers below 0.2. However, it cannot be used for large-scale flotation columns due to the high values of the dispersion number (i.e., in the range of 0.3 – 2.7) (Massinaei et al., 2007). The tanks-in-series model can also characterize the flow behavior in a flotation column. For small-diameter columns, the axial dispersion model or the tanks-in-series model can be applied, but for the large diameter columns (> 1.50 m), the tanks-in-series model is more suitable (Mills et al., 1992). The mixing behavior in a flotation column is greatly influenced by the gas flow rate and column diameter (Cruz, 1997). Several researchers have claimed that the axial particle mixing is the same as axial fluid mixing in the case of the fine and low-density particles in the three-phase system (Finch and Dobby, 1990; Yianatos and Bergh, 1992). (Massinaei et al., 2007) have measured the mean residence time for liquid, and they observed that the liquid phase of the slurry closely exhibited the behavior of the solid particles. (Bhunia et al., 2018) have studied the mixing characteristics in a three-phase (i.e., air–water–coal)

counter-current flotation column. They found that the dispersion number varied between 0.30 and 0.60, and the mean residence time was 45 s. They attempted to fit the experimental RTD with different boundary conditions (i.e., open–open and closed–closed) and by various methods. The closed–closed boundary condition fitted their experimental data well, and the same was used to determine the dispersion number. The dispersion characteristics have been studied extensively by many researchers to fulfill industrial needs (Kato, 1972; Muroyama et al., 1978; Vail et al., 1968). They have reported that the dispersion characteristics depend directly on the heat and mass transfer phenomena. In a bed of larger particles, the axial dispersion coefficient slightly decreased with increasing gas velocity, whereas, for beds with smaller particles, a reverse phenomenon was observed.

According to (Kato et al., 1972), the axial dispersion coefficient is directly proportional to the diameter of the column. (Kato et al., 1985) suggested a correlation between the dispersion coefficient and the Peclet number. (Kang and Kim, 1986) represented the axial and radial dispersion coefficients in two- and three-dimensional liquid flows by the theory of isotropic turbulence. It was observed that the dispersion coefficient increases with increasing gas velocity and particle size and reaches a maximum value at a given liquid velocity. Several authors have studied the effects of the physical properties, and liquid and gas velocities on the dispersion coefficient. (Kim et al., 1992) observed that the axial dispersion coefficient increased with increasing liquid and gas velocities and the size of the column, but decreased with increasing particle size. (Kara et al., 1982) observed that the axial dispersion coefficient was highly dependent on the gas and slurry velocities, and the particle size, but it was independent of the particle concentration. For the two-phase system, the dispersion coefficient increased with increasing superficial gas velocity and decreased with the liquid velocity. They could not accurately analyze

the effect of particle size on the dispersion coefficient due to the large scatter in their data. Based on their correlation, a lower dispersion coefficient value was observed with larger particle sizes. (Mills et al., 1992) reported that the dispersion coefficient increased exponentially as the particle size increased. (Cao et al., 2008) observed that the sparger design had a significant effect on the Peclet number at lower solid loadings and gas velocities less than 0.025 m/s.

In contrast to the two-phase semi-batch operation, fewer studies have been devoted to the mixing characteristics in the three-phase counter-current mode, mainly due to challenges in measuring the degree of axial slurry dispersion. Therefore, the present study focuses mainly on the dispersion characteristics and their variation with slurry concentration, particle size, slurry and gas velocities, and surfactant dose in a counter-current flotation column. The present work attempts to bring together the influence of all critical variables that significantly influence the mixing characteristics in the counter-current flow. In this work, the velocity distribution model has been applied to interpret the dispersion coefficient of bubble motion and the characteristic factor of velocity distribution. Also, correlations are proposed to explain the axial dispersion coefficient, dispersion coefficient of bubble motion, and the characteristic factor of velocity distribution.

4.2. Experimentation

4.2.1. Experimental setup and procedure

All the experimental works were conducted at standard temperature and pressure. A schematic diagram of the experimental setup is shown in Figure 4.1 (a). An image of the spherical sparger is shown in Figure 4.1 (b). The details and information about the different components of the experimental set up are already discussed in section 2.2.1 in the chapter 2. The experiments were

performed in the particle concentration and superficial gas and slurry velocities range of $1.5 \leq c_{slr} \leq 10.89$ kg/m^3, $0.007 \leq u_{sg} \leq 0.021$, and $0.007 \leq u_{slr} \leq 0.021$ m/s, respectively.

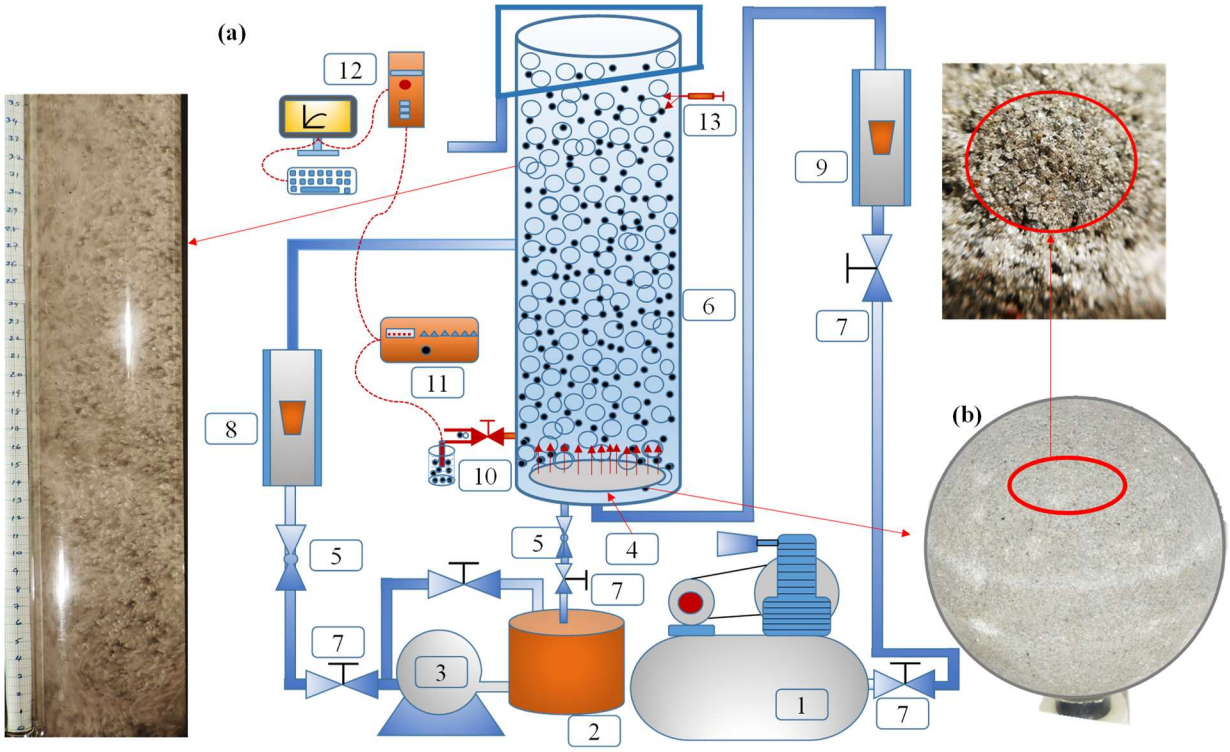

Figure 4.1: (a) A schematic diagram of the experimental setup: 1. air compressor, 2. storage tank, 3. pump, 4. spherical sparger, 5. solenoid valve, 6. flotation column, 7. control valve, 8. liquid rotameter, 9. gas rotameter, 10. conductivity probe, 11. conductivity meter, 12. computer, 13. syringe, and (b) an image of the spherical sparger.

The details about the extraction, crushing, and size analysis of the coal is already discussed in section 2.2.2. For each experiment, 9 liters of the slurry was prepared in the slurry tank. The slurry was the mixture of water, particle, and surfactant and mixed with the stirrer for at least 30 minutes for proper mixing. Slurry is fed to the flotation column at the height of 0.73 m from the base of the

column. For every set of experiments, the gas–slurry mixture level was maintained at the height of 0.60 m by adjusting the valve installed in the slurry outlet pipe, as shown in Figure 4.1 (a).

The liquid-phase residence time distribution (RTD) was determined by a tracer injection method. In order to characterize the dispersion characteristics, sodium chloride (NaCl) was used as the tracer. The amount of tracer used was less than 1% (w/v) (Levenspiel, 1972; Reith et al., 1968). For each experimental run, about 0.01 kg of a 58.44 kg/m^3 NaCl solution was used for the injection. When a continuous steady-state operation was attained, the tracer was injected at the topmost position of the column (i.e., at the height of 0.91 m from the basement of the column). The tracer injection was done quickly and smoothly by a high pressure loaded syringe, and samples were collected at every 3 s interval from the bottom of the column at the height of 0.05 m from the basement. The conductivity of the collected samples was measured with the help of a conductivity meter. The fraction of the gas occupied in the entire volume of the column is termed as the gas holdup $\left(\varepsilon_g\right)$. It was measured by the bed expansion technique, and it is already discussed in section 2.2.2.

4.2.2. Materials and physical properties of the system

The cationic surfactant, cetyltrimethylammonium bromide (CTAB) (99% purity) was purchased from Loba Chemie (India). The measurement techniques of slurry desnsity, slurry viscosity, and surface tension are discussed in section 2.2.2. The physical properties and the surface tensions of the three-phase system are given in Tables 1 and 2, respectively.

Table 4.1: Physical properties of the three-phase system at 298 ± 1 K.

Slurry concentration (kg/m^3)	Surfactant (CTAB) concentration (g/m^3)	Viscosity (mPa s)	Density (kg/m^3)
1.5	10	1.248	1002.44
	30	1.362	1002.68
	50	1.481	1002.95
3.63	10	1.256	1004.35
	30	1.371	1004.58
	50	1.492	1004.87
7.26	10	1.265	1005.16
	30	1.377	1005.34
	50	1.496	1005.71
10.89	10	1.286	1006.19
	30	1.393	1006.37
	50	1.498	1006.84

Table 4.2: Surface tension of the slurry measured at 298 ± 1 K in the presence of CTAB.

Surfactant concentration (g/m^3)	Surface tension (N/m)
10	0.035
20	0.033
30	0.031

40	0.030
50	0.029

4.2.3. Calibration of the conductivity meter

A digital conductivity meter (make: VSI Electronics Pvt. Ltd., India; model: VSI-04 ATC Deluxe) was used to measure the conductivity of the samples. The range of this conductivity meter was 0 – 999 mS/m. For the calibration of the conductivity meter, the conductivity probe was cleaned by using Millipore water. Then different solutions of NaCl were prepared in tap water with concentrations ranging from 0 to 0.05 g/m^3.

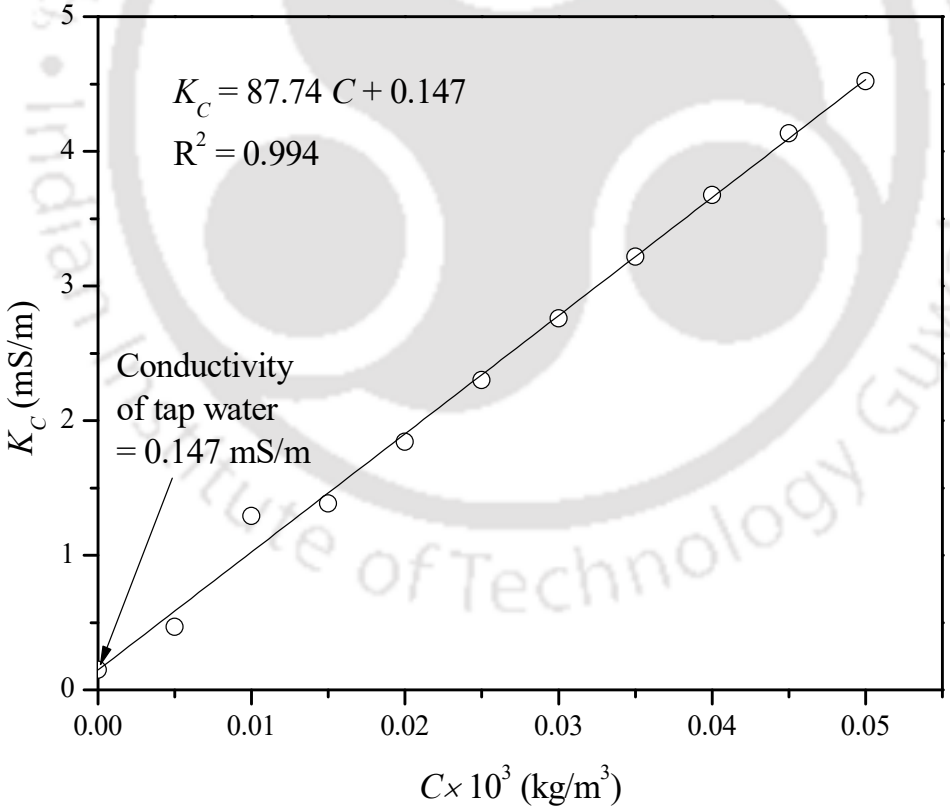

Figure 4.2: Calibration plot of the conductivity meter.

The conductivity probe was dipped in the sample solutions, and the readings from the conductivity meter were recorded. A graph of conductivity (K_C) with concentration (C) was plotted, as shown in Fig. 4.2. The data were fitted by a least-squares straight line. The correlation can be represented as

$$K_C = 87.74C + 0.147 \tag{4.1}$$

4.3. Phase mixing theories and modeling

The most crucial factor affecting the performance of the flotation column is phase mixing (Manish and Majumder, 2009). Therefore, for determining the efficiency of a flotation column, sufficient knowledge on mixing quality is required. Many researchers have applied the ADM to analyze the axial dispersion coefficient. The assumptions underlying the ADM are: (i) the slurry velocity distribution throughout the column is uniform, (ii) bulk flow exists only in the axial direction, (iii) the tracer is symmetrically distributed in the axial direction, and (iv) the liquid phase dispersion exists in the axial direction only.

The ADM was developed by (Finch and Dobby, 1990) to calculate the vessel dispersion number and explain the mixing condition in the industrial and laboratory columns. It was used to describe the axial liquid mixing in the columns. Diffusion and convection are the key phenomena considered in this model. The dimensionless form of the ADM is expressed as

$$\frac{\partial C_\theta(z,\theta)}{\partial \theta} = N_d \frac{\partial^2 C_\theta(z,\theta)}{\partial z^2} - \frac{\partial C_\theta(z,\theta)}{\partial z} \tag{4.2}$$

where $C_\theta = C/C_0$, $\theta = t/\tau$, and $z = x/L$

$$N_d = \frac{1}{\mathrm{Pe}} \tag{4.3}$$

$$\mathrm{Pe} = \frac{u_{slr} z}{\left(1-\varepsilon_g\right) E_z} \tag{4.4}$$

A minimal value of the Peclet number (i.e., $\mathrm{Pe} \to 0$) represents complete mixing, whereas a very large value of the same (i.e., $\mathrm{Pe} \to \infty$) reflects the plug flow behavior. For a closed vessel in which the tracer is injected in the pulse mode at $z = 0$, the initial and boundary conditions are as follows (Xu et al., 1991):

$$\text{At } \theta = 0,\ C_\theta(\mathrm{z}, 0) = 0, \text{ for all } z,\ \ 0 < z < 1 \tag{4.5}$$

$$\text{At } z = 0,\ N_d \frac{\partial C_\theta(0,\theta)}{\partial z} = C_\theta(0,\theta) - \delta(\theta) \tag{4.6}$$

$$\text{At } z = 1,\ \frac{\partial C_\theta(1,\theta)}{\partial z} = 0 \tag{4.7}$$

where $\delta(\theta)$ is the Dirac delta function, which represents the pulse tracer input. The different solutions of Eq. (4.2) for closed–closed boundary conditions are given by Eqs. (4.8–4.10).

$$C_\theta = \exp\left\{\frac{1}{2N_d}\left(1-\frac{\theta}{2}\right)\right\} \sum_{n=1}^{\infty} \left\{ \frac{\delta_n\left(\mathrm{Pe}\ \mathrm{Sin}\delta_n + 2\delta_n \cos\delta_n\right)}{\delta_n^2 + \left(\mathrm{Pe}/2\right)^2 + \mathrm{Pe}} \exp\left(\frac{-\delta_n^2 \theta}{\mathrm{Pe}}\right) \right\} \tag{4.8}$$

$$C_\theta = 4N_d \exp\left(\frac{1}{2N_d}\right) \sum_{n=1}^{\infty} \left\{ \frac{2(-1)^{n+1} \delta_n^2 N_d}{4\delta_n^2 N_d^2 + 4N_d + 1} \exp\left(\frac{-1 + 4\delta_n^2 N_d^2}{4N_d}\theta\right) \right\} \tag{4.9}$$

$$C_\theta = 4N_d \exp\left(\frac{1}{2N_d}\right)\sum_{n=1}^{\infty}\left\{\frac{\delta_n\left(2\delta_n N_d^2\cos\delta_n + N_d\sin\delta_n\right)}{4\delta_n^2 N_d^2 + 4N_d + 1}\exp\left(\frac{-1+4\delta_n^2 N_d^2}{4N_d}\theta\right)\right\} \tag{4.10}$$

where δ_n represents the n^{th} positive root of the transcendental equations [Eqs. (4.8), (4.9), and (4.10)]. It is given by

$$\cot\delta_n = \frac{\delta_n}{\mathrm{Pe}} - \frac{\mathrm{Pe}}{4\delta_n} \tag{4.11}$$

The Peclet number and residence time can be determined by the method of moments, described by (Levenspiel, 1972). As per this method, the mean and the variance of the RTD curve are related to the mean residence time and Peclet number as follows:

$$\sigma_\theta^2 = \frac{\sigma^2}{t_m^2} = \frac{8}{\mathrm{Pe}^2} + \frac{2}{\mathrm{Pe}} \tag{4.12}$$

where σ_θ^2 and σ^2 are the normalized variance and variance, respectively. The variance and the mean residence time can be calculated from the time-dependent experimental data of tracer as follows:

$$\sigma^2 = \frac{\sum t_i^2 C_i \Delta t_i}{\sum C_i \Delta t_i} - t_m^2 \tag{4.13}$$

$$t_m = \frac{\sum t_i C_i \Delta t_i}{\sum C_i \Delta t_i} \tag{4.14}$$

4.4. Uncertainty analysis of the experimental data

The theories related to uncertainty analysis is already discussed in section 2.4. The Uncertainty analysis of experimental data is reported in Table 4.3.

Table 4.3: Uncertainty analysis of the experimental data.

Variables	Mean, $\bar{x}$ (–)	STDEV (–)	U (–)	U_r (%)
N_d	$1.71 \times 10^{-2} - 2.49 \times 10^{-1}$	$1.36 \times 10^{-3} - 1.08 \times 10^{-2}$	$6.81 \times 10^{-4} - 5.38 \times 10^{-3}$	2.16 – 4.00
u_{sg}	0.0072 – 0.0215	$5.72 \times 10^{-4} - 1.29 \times 10^{-3}$	$2.86 \times 10^{-4} - 4.56 \times 10^{-4}$	2.12 – 3.97
u_{slr}	0.0073 – 0.0207	$7.77 \times 10^{-4} - 1.32 \times 10^{-3}$	$3.88 \times 10^{-4} - 6.60 \times 10^{-4}$	3.19 – 5.36

4.5. Results and discussions

The RTD for the three-phase system was analyzed by the axial dispersion model. It was observed that the variables such as gas and slurry flow rates, slurry concentration, particle size, and surfactant concentration affected the mixing intensity in the column. Their effects are discussed in the following sections

4.5.1. Effect of different variables on the RTD

4.5.1.1. Effect of superficial gas and slurry velocities on the RTD

The variations of C/C_0 with t/τ at different superficial gas velocities at a constant superficial slurry velocity (i.e., 0.007 m/s), particle size (i.e., 273.13 μm), slurry concentration (i.e., 3.63 kg/m^3), and surfactant concentration (i.e., 10 g/m^3) are shown in Fig. 4.3 (a). The tracer particle concentration was initially zero in the sample collected. After injection, the tracer particle dispersed in the column and underwent mixing. As it kept moving downwards, it underwent more mixing. Due to this phenomenon, a few moments were taken up by the particles to reach the sample

collection port. For the superficial gas velocities of 0.007, 0.014, and 0.021 m/s, the mean time (τ) was found to be 46.01, 47.54, and 48.21 s, respectively. There was an increase in the flow fluctuation and internal fluid circulation when the gas flow rate was higher, which increased the mean time of the tracer in the column.

The variations in C/C_0 with the superficial slurry velocity at a constant superficial gas velocity (i.e., 0.021 m/s), particle size (i.e., 273.13 µm), slurry concentration (i.e., 3.63 kg/m^3) and surfactant concentration (i.e., 10 g/m^3) are shown in Fig. 4.3 (b). It can be observed that the peak was maximum at the superficial slurry velocity of 0.007 m/s, and it was a minimum at 0.021 m/s. The maximum and minimum peaks reflect higher and lower mean residence times of the tracer particles in the column. The mean time (τ) was found to be 48.21, 47.29 and 46.87 s for 0.007, 0.014, and 0.021 m/s superficial slurry velocities. As the slurry velocity was increased, the three-phase mixture dissipated more energy resulting in more circulation, which enhanced the dispersion in the liquid. This ultimately reduced the mean time of the tracer particles and resulted in more tracer in the outlet.

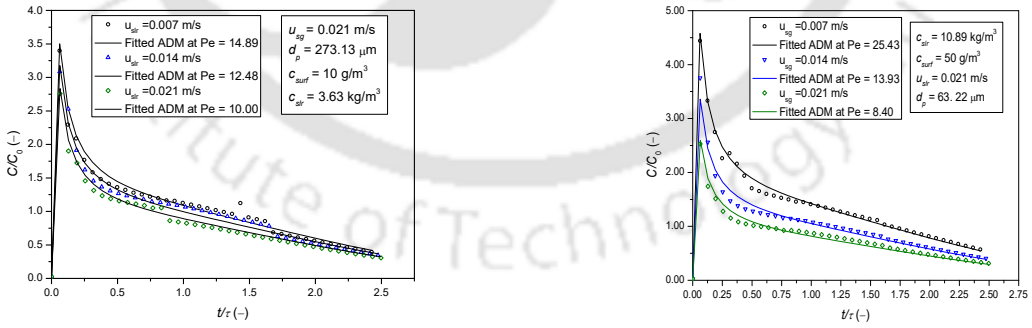

Figure. 4.3: The RTD curve depicting the effects of superficial (a) slurry velocity and (b) gas velocity.

4.5.2. Effect of different variables on the dispersion number

4.5.2.1. Effect of slurry and superficial gas velocities on the dispersion number

Figure 4.4 shows the variation of the dispersion number with the slurry and superficial gas velocities. It is observed that the dispersion number increased with increasing both slurry and gas velocities. There was a significant deviation from the plug flow as the gas flow rate increased due to the turbulence in the column. This caused the dispersion number to decrease. More intense turbulence in the column resulted when the velocity of the slurry or gas was increased, which increased the extent of mixing in the solid–liquid–gas mixture, and led to an increase in the dispersion number. Moreover, as the gas holdup increased with increasing gas velocity, more bubbles were produced, which led to more significant interactions and promotes bubble breakup because of the bubble-eddy collision rate (Sarhan et al., 2018c). This increased the dispersion number. With the increase in the gas holdup, the area in the column available for slurry flow decreased, which led to the variation in the actual velocity of the slurry $\left[u_a = u_{slr} / \left(1 - \varepsilon_g\right)\right]$. This led to more circulation of the fluid and formed a circulation cell inside the flotation column. The velocity of the fluid element increased with increasing superficial gas velocity since the flowing gas bubbles accelerated the liquid elements in the upward direction. This led to an increase in the mixing of the slurry in the column. In the present experiments, the dispersion coefficient showed more variation at the higher superficial gas velocities. An increase in the flow rate of the slurry increased the fluctuations of the particles in the column (Lim et al., 2011), which increased the mixing of the phases and increased the dispersion number. Similar trends have been reported by other researchers (Eissa and Schugerl, 1975; Gondo et al., 1973; Liang et al., 1996; Muhsin, 2008; Ohki and Inoue, 1970; Rubio et al., 2004).

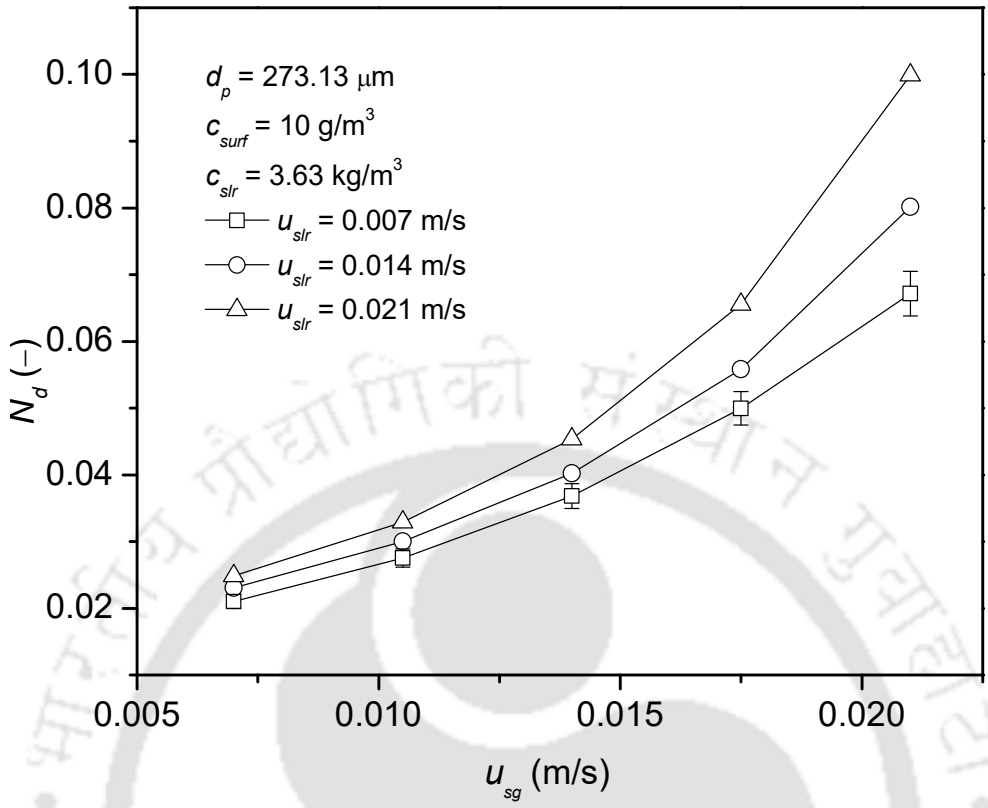

Figure 4.4: Effects of slurry and superficial gas velocities on the dispersion number.

4.5.2.2. Effect of slurry concentration on the dispersion number

The effect of variation in the slurry concentration (i.e., 1.50 – 10.89 kg/m^3) on the dispersion number at different superficial gas velocities (i.e., 0.007 – 0.021 m/s) at a fixed particle size $\left(\text{i.e., } d_p = 273.13 \text{ μm}\right)$, surfactant concentration $\left(\text{i.e., } c_{surf} = 10 \text{ g/m}^3\right)$, and slurry velocity $\left(\text{i.e., } u_{slr} = 0.007 \text{ m/s}\right)$ is shown in Fig. 4.5. The dispersion number decreased with increasing slurry concentration. The increase in the particle concentration led to an increase in the viscosity of the mixture (Sarhan et al., 2018d), which in turn reduced the momentum transfer and the rising velocity of the gas bubbles. This retards the bubble-bubble interaction, consequently the rate of bubble coalescence. The bubble coalescence takes place when they are able to overcome the

resistance that exists in the liquid film that separates them. The probability of coalescence of bubbles increases when the resistance in the liquid film is reduced (Sarhan et al., 2018a). This leads to prevailing bubble size distribution consists of small to mostly medium-size bubbles. Smaller bubbles have small wakes and carry less fluid while rising, however in the case of larger bubbles can carry more fluids behind the wakes and bubble breakup is frequent (Rubio et al., 2004) . During the upward rising of the gas bubble in the column forms a wake around the bubble, which replaces the fluid close to the bubble. This results in dispersion in the slurry phase due to transport of the slurry from one location to another behind the path of the gas bubble. Bubble transport in the fluid also stimulates eddy currents behind it, which form a local turbulence condition. This case is true for churn-turbulent flow conditions (Deckwer, 1992). (Kim et al., 1992) reported a slight reduction in dispersion coefficient with increasing the continuous phase viscosity (1 – 72.5 mPa.s). A negative effect of continuous phase viscosity is reported by (Hikita and Kikukawa, 1974) and elucidated that the dispersion coefficient is inversely proportional to the viscosity. Similar kind of trends has been reported by other researchers (Kelkar et al., 1984; Kim and Kim, 1983; Krishna et al., 2000; Liang et al., 1996; Parmar and Majumder, 2015). The dispersion number decreased by 2.73, 5.50, and 7.04% at 0.007, 0.014, and 0.021 m/s superficial gas velocities, respectively. As observed, the reduction in dispersion number as slurry concentration increases from 1.50 to 10.89 kg/m^3 is not significant because of little enhancement in the slurry viscosity (from 1.248 to 1.286 mPa.s). The increase in viscosity is about 3.04%. Therefore, it may be concluded that the increase in the slurry concentration did not have a significant impact on the dispersion number under the present experimental conditions.

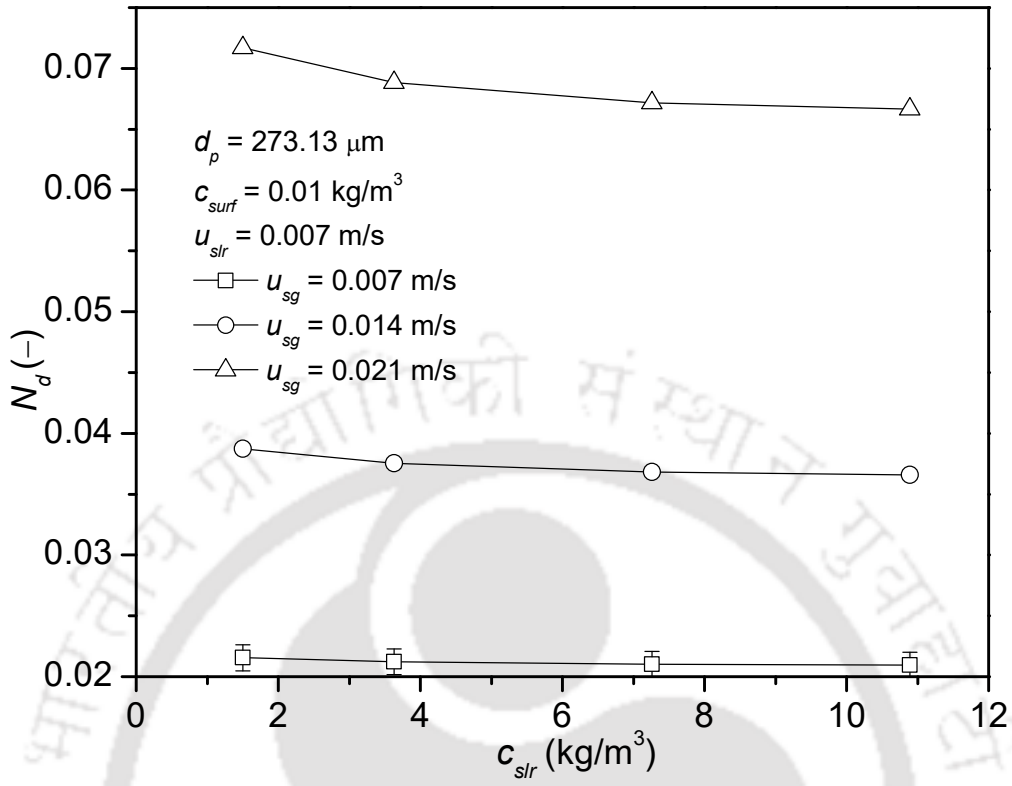

Figure 4.5: Effect of slurry concentration on the dispersion number.

4.5.2.3. Effect of particle size on the dispersion number

Particle size is one of the important variables which should be considered during the study of the hydrodynamic characteristics of the flotation column. Slurry dispersion in the flotation column is because of slurry circulation, eddy formation, and turbulence due to entrapment of slurry behind the rising gas bubbles (Degaleesan et al., 1997). It is the quantitative contribution of the back mixing that occurs in fluids in the flotation column. The effect of particle size on the dispersion number at different superficial gas velocities and constant slurry concentration, surfactant concentration, and slurry velocity (i.e., 0.021 m/s) are reported in Fig. 4.6. The dispersion number was found to decrease with an increase in the particle size. This is attributed to the considerable impact of slurry property and bubble-particle interaction on fluid flow behavior. (Uribe-Salas et

al., 2008) performed an experiment using silica particles and reported that the rising velocity of bubble-particle aggregate retards as their diameter reduces. Furthermore, the viscosity of the slurry is higher in smaller particles in comparison to that of the larger particle size due to the attractive particle interaction (Prakash et al., 2018a; Senapati et al., 2009). The increased slurry viscosity would retard the bubble rising velocity, bubble-bubble interaction, consequently decreases the momentum of the fluid and turbulence in the column. The lower apparent viscosity of the system in the presence of smaller particles. A few researchers have reported an insignificant impact of the particle size on the axial dispersion coefficient (Kelkar et al., 1984). However, other investigators have reported a reduction in the axial dispersion coefficient with increasing particle size (Kim et al., 1992).

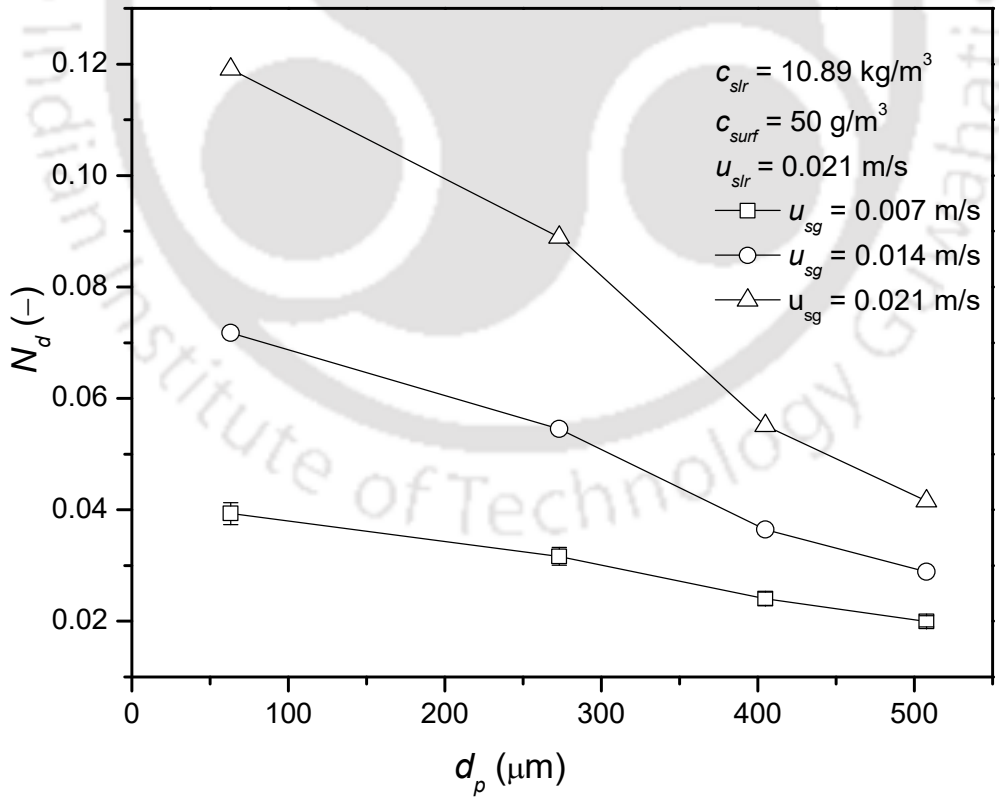

Figure 4.6: Effect of particle size on the dispersion number.

4.5.2.4. Effect of surfactant concentration on the dispersion number

The effect of five different surfactant concentrations at different superficial gas velocities for fixed particle size, slurry concentration, and slurry velocity is shown in Fig. 4.7. The dispersion number was found to increase with increasing surfactant concentration. As the surfactant concentration in the slurry increased, the surface tension of the slurry decreased. The reduced surface tension of slurry creates a smaller bubble size, increases the stability of the gas bubble, and retards the bubble coalescence rate.

The surface tension of the slurry decreased from 0.035 to 0.029 N/m when the surfactant concentration increased from 10 to 50 g/m^3. The present results corroborate the results reported earlier (Parmar and Majumder, 2015).

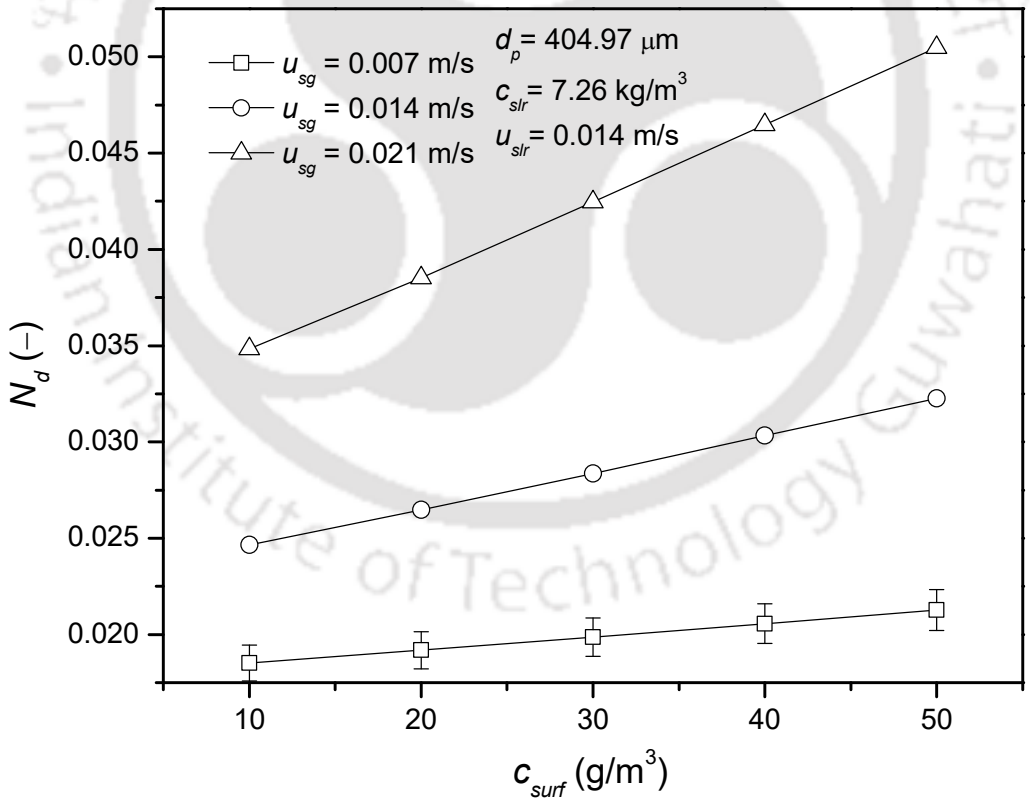

Figure 4.7: Effect of surfactant concentration on the dispersion number.

4.5.3. Prediction of dispersion number by the correlation model

No correlation has been developed so far, which depicts the cumulative impact of different variables on the axial dispersion coefficient (E_z) or the dispersion number (N_d) in counter-current operation. The present result was compared with the other systems studied earlier, e.g., two-phase semi-batch and three-phase packed bed systems. The present experimental results at $d_p = 63.22\ \mu m$, $c_{slr} = 3.63\ kg/m^3$, $c_{surf} = 30\ g/m^3$ (CTAB), $u_{slr} = 0.007\ m/s$, and $u_{sg} = 0.007 - 0.021\ m/s$ were compared with the correlations of (Kang and Kim, 1986; Lim et al., 2011; Muroyama et al., 1978; Shawaqfeh, 2003; Towell, 1972), as shown in Fig. 9a. It is found that the correlation of (Towell, 1972) and (Shawaqfeh, 2003) overpredicted, whereas the correlation of (Kang and Kim, 1986) underpredicted the axial dispersion coefficient. However, some of the present experimental data are close to the correlations suggested by (Muroyama et al., 1978) and (Lim et al., 2011).

Since most of the correlations reported in the literature are in terms of the axial dispersion coefficient (E_z), the same has been used for the comparison with our data. The comparison (shown in Fig. 4.8 (a) reflects that the correlations available in the literature are unable to predict the present experimental results accurately. The reason for this deviation lies in the different experimental conditions. Therefore, it was necessary to develop an empirical correlation valid for the present experimental conditions. The important variables which influence the dispersion number are superficial slurry velocity (u_{slr}), superficial gas velocity (u_{sg}), column diameter (d_c), particle diameter (d_p), apparent slurry viscosity (μ_{slr}), slurry density (ρ_{slr}), surface tension (σ), and acceleration due to gravity (g). The parameter, N_d, is expressed as a function of the following variables:

$$N_d = f\left(u_{slr}, u_{sg}, d_c, d_p, \mu_{slr}, \rho_{slr}, \sigma, g\right) \tag{4.15}$$

Using Buckingham's Pi technique and multiple linear regression analysis, the following correlation was developed based on the experimental results:

$$N_d = 3.78\times10^{3}\left(\frac{u_{slr}}{u_{sg}}\right)^{0.013}\left(\frac{d_p}{d_c}\right)^{-0.321} \mathrm{We}_{slr}^{0.522}\,\mathrm{Re}_{slr}^{-1.24}\,\mathrm{Fr}_{slr}^{1.219} \tag{4.16}$$

Where We_{slr} is the Weber number $\left(\equiv \rho_{slr}u_{sg}^2 d_c/\sigma\right)$, Re_{slr} is the Reynolds number $\left(\equiv \rho_{slr}u_{sg}d_c/\mu_{slr}\right)$, and Fr_{slr} is the Froude number $(=u_{sg}/\sqrt{gd_c})$. The standard error and correlation coefficient for Eq. (4.16) are 0.0771 and 0.9915, respectively. The percentage error of the correlation is ±15.47. This correlation is valid for the following ranges: $0.33 \le \left(u_{slr}/u_{sg}\right) \le 3.0$, $1.15\times10^{-3} \le \left(d_p/d_c\right) \le 7.36\times10^{-3}$, $7.62\times10^{-2} \le \mathrm{We}_{slr} \le 83.09\times10^{-2}$, $251.23 \le \mathrm{Re}_{slr} \le 908.14$, and $9.46\times10^{-3} \le \mathrm{Fr}_{slr} \le 28.38\times10^{-3}$. The parity of the experimental data and the values predicted by the correlation [i.e., Eq. (4.16)] is shown in Fig. 4.8 (b). The correlation is not valid for $u_{slr}, u_{sg} = 0$.

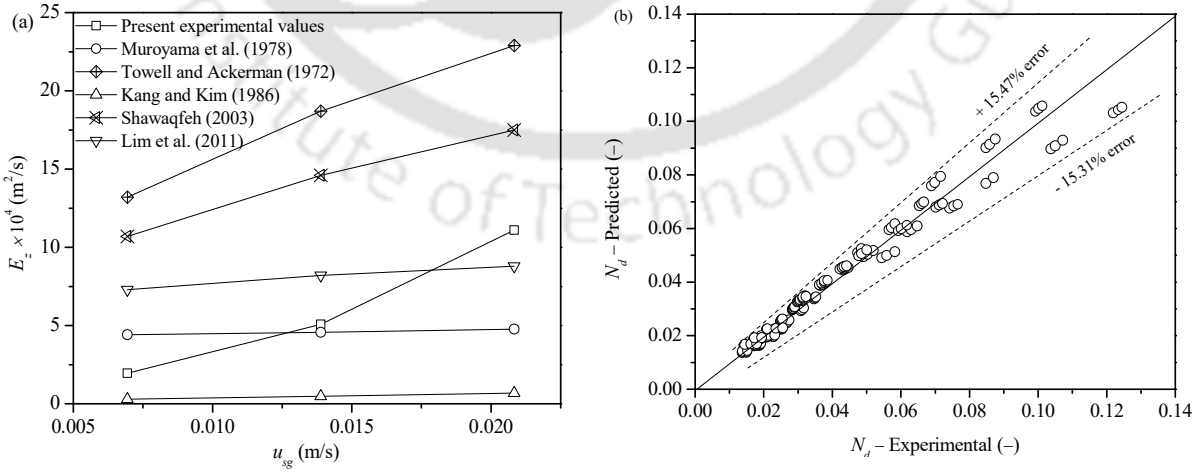

Figure 4.8: (a) Comparison of the experimental values of the axial dispersion coefficient with the correlations reported in the literature and (b) parity of the experimental data and those computed from Eq. (21).

4.5.4. Analysis of dispersion by the velocity distribution model

The axial dispersion coefficient (E_z) of fluid flow through a pipe can be determined by the equation given by (Taylor, 1953), and (Aris. R., 1956) based on the method of moment,

$$E_z = \frac{d_c^2 u_0^2}{kD_T} + D_T \tag{4.17}$$

where D_T and u_0 represent the molecular diffusivity and maximum velocity at the axis of the column, respectively. The constant, k, represents a characteristic factor, which depends on the velocity distribution in the system. The model presented by Eq. (4.17) has been applied to study and analyze the dispersion coefficient for the present solid–liquid–gas three-phase system. It is assumed that the flow in the column is homogenous and there is continuous mixing of liquid and solid with uniform distribution of the gas bubbles. Based on these assumptions and by replacing D_T with the dispersion coefficient of bubble motion, D_b, Eq. (4.17) is expressed as

$$E_z = \frac{d_c^2 u_0^2}{kD_b} + D_b \tag{4.18}$$

For a counter-current system, the interstitial liquid velocity (u_0) can be expressed as

$$u_0 = 2\frac{u_{slr}}{\left(1-\varepsilon_g\right)} \tag{4.19}$$

Substituting u_0 from Eq. (4.19) into Eq. (4.18) we get

$$E_z = \frac{4d_c^2 u_{slr}^2}{\left(1-\varepsilon_g\right)^2 kD_b} + D_b \tag{4.20}$$

The dispersion coefficient of bubble motion $\left(D_b\right)$ and velocity characteristic factor $\left(k\right)$ are estimated by fitting Eq. (4.20) to the experimental data on E_z.

4.5.4.1. Influence of different variables on the dispersion coefficient of bubble motion (D_b) and the characteristics factor of velocity distribution (k)

The influence of different variables such as slurry and superficial gas velocities, particle concentration, particle size, and surfactant concentration on the dispersion coefficient of bubble motion $\left(D_b\right)$ and the characteristics factor of velocity distribution $\left(k\right)$ is shown in Fig. 4.9. The superficial gas velocity profoundly influences fluid mixing. Hitherto, it has been noticed that turbulence and liquid circulation are the prime reasons for the mixing phenomena (Wilkinson et al., 1993). Figure 4.9 (a) shows the influence of superficial gas velocity on D_b and k for constant particle size, surfactant concentration, and slurry concentration. It is observed that D_b increased while k decreased as the superficial gas velocity increased. The phase circulation in the column took place in counter-current mode, with the bubbles flowing upward through the center of the column. This pushed the flowing slurry near the column wall downward, creating a circulation of the phases. The increase in the superficial gas velocity at a fixed slurry velocity led to the increase in the rising velocity of the gas bubbles, which caused an enhancement in the turbulence throughout the column. Therefore, D_b increased while k decreased. Our results corroborate the

trend reported by the previous workers (Kawase and Moo-Young, 1986; Yang and Fan, 2003). As per the present analysis, D_b depends on the superficial gas velocity $\left(u_{sg}\right)$ as $D_b \propto u_{sg}^{1.463}$.

The variation of D_b and k with the slurry concentration at a constant particle size, surfactant concentration, superficial gas velocity, and slurry velocity is shown in Fig. 4.9 (b). It is observed that an increase in the slurry concentration significantly increased k (i.e., by 35.14%) but decreased D_b (i.e., by 42.06 %). As the slurry concentration increased, the slurry viscosity also increased (Sarhan et al., 2020, 2017b), which resulted in a reduction in the extent of mixing of the gas-liquid-solid system. Also, the circulation of the phases was reduced due to the increase in the viscosity. Therefore, D_b reduced while k increased. According to (Lim et al., 2011), an increase in the slurry concentration reduces the particle mobility due to more friction losses between the particle and the liquid, which ultimately reduces the dispersion. Our findings on the influence of slurry concentration on D_b and k are in accordance with the previous findings (Sivaiah and Majumder, 2013a, 2013b).

In the flotation process, the particle size plays an important role during the recovery of the desired particle. Particle size may also impact the probabilities of the bubble–particle collision, bubble–particle attachment, and bubble–particle detachment, which ultimately controls the performance of the flotation system. As per the literature, the flotation technique is suitable for processing the particle size range 10 – 500 μm (Fornasiero and Filippov, 2017). Four different average particle sizes (i.e., 63.22, 273.13, 404.97, and 507.67 μm) were chosen to assess their impact on D_b and k, as shown in Fig. 4.9 (c). As expected, it was found that D_b and k were

significantly influenced by the presence of the larger particles in the flotation column. With an increase in the particle size, D_b decreased, whereas *k* increased.

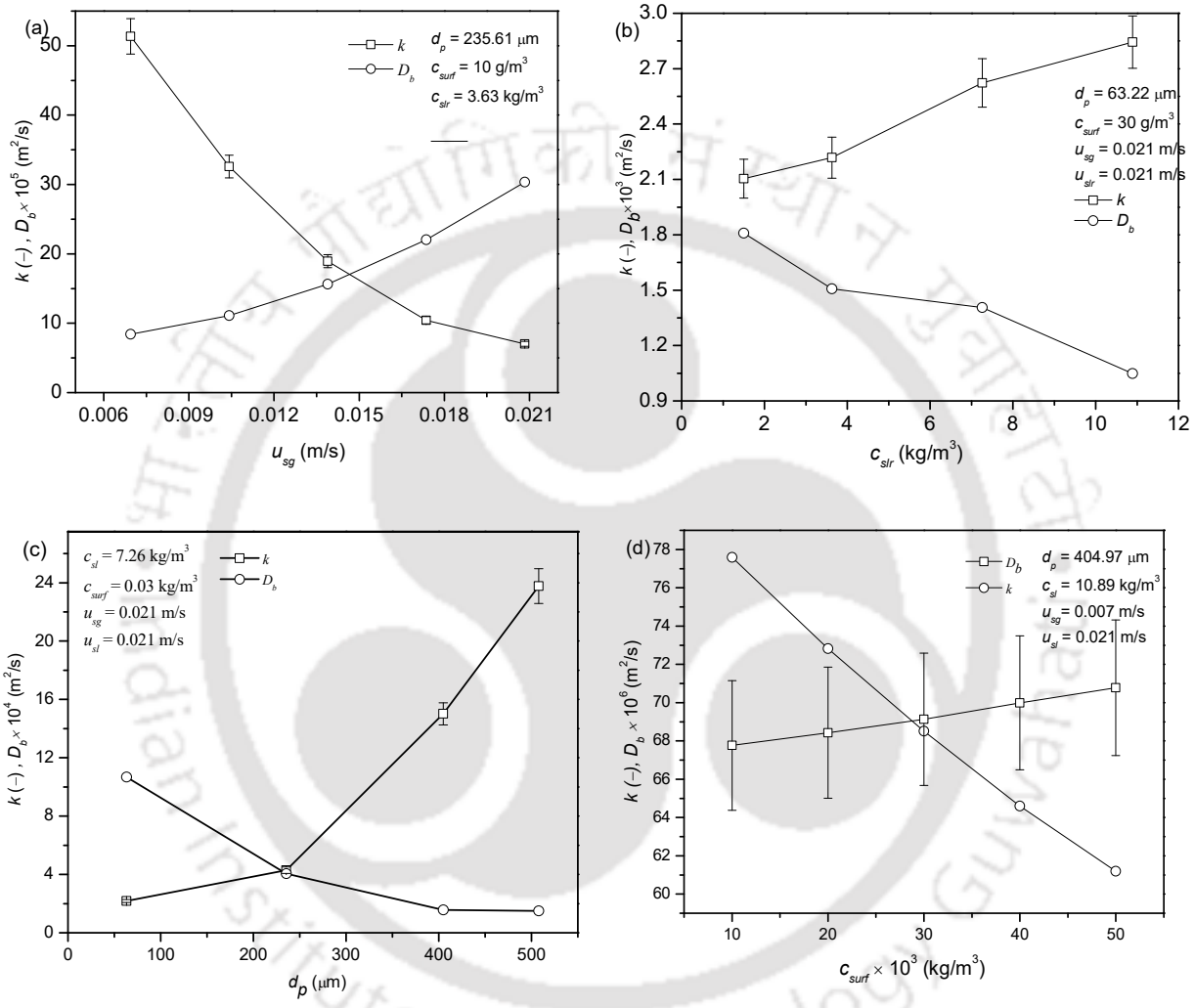

Figure 4.9: Variation of D_b and *k* with (a) superficial gas velocity, (b) particle concentration, (c) particle size, and (d) surfactant concentration.

As per our knowledge, no work has been reported on the impact of particle size on D_b and *k*. However, a few works have been reported analyzing the effect of slurry concentration on D_b and *k* (Sivaiah and Majumder, 2013a, 2013b). Based on the present data, D_b and *k* varied with the

particle diameter $\left(d_p\right)$ as $D_b \propto d_p^{-0.620}$ and $k \propto d_p^{0.983}$. The surface tension of the slurry plays a significant role in the generation of fine bubbles and the mixing of the phases in the flotation column. Figure 4.9 (d) reports the variation of D_b and k with the surface tension of the slurry. Five different concentrations of the surfactant (i.e., 10, 20, 30, 40, and 50 g/m^3) were chosen to assess the influence of slurry surface tension on D_b and k. It was observed that D_b increased whereas k decreased as the surfactant concentration increased. The addition of surfactant to the slurry significantly reduced the surface tension, which in turn produced a large number of tiny gas bubbles. As the number of gas bubbles increased, the randomness and turbulence also increased, which resulted in an enhancement of D_b. Small gas bubbles carried more liquid behind their wakes, which further increased the back-mixing of the phases (Rice et al., 1981).

4.5.4.2. Interpretation of the diffusion coefficient of bubble motion $\left(D_b\right)$ and the characteristics factor of the velocity distribution $\left(k\right)$

The values of D_b and k were compared with the values reported in the literature for other systems (e.g., two-phase semi-batch, three-phase semi-batch, and three-phase packed bed column). The comparison is shown in Fig. 4.10 (a). The values of D_b were compared with those reported by (Baird and Rice, 1975; Deckwer et al., 1974; Hikita and Kikukawa, 1974; Kato and Nishiwaki, 1971; Kawase and Moo-Young, 1986; Yang and Fan, 2003). It is observed that the present values are lower than those reported in the literature. This may be due to the different flow arrangements, column dimension, physical properties of the system, and the range of gas and liquid flow rates. The experimental values of k, under various experimental conditions, were also compared with

those reported by (Baird and Rice, 1975; Joshi, 1980; Reith et al., 1968; Towell, 1972). The comparison is shown in Fig. 4.10 (b). It is observed that the values of *k* widely differed from the literature values. This may be due to the range of the superficial gas and slurry velocities in the present experiment.

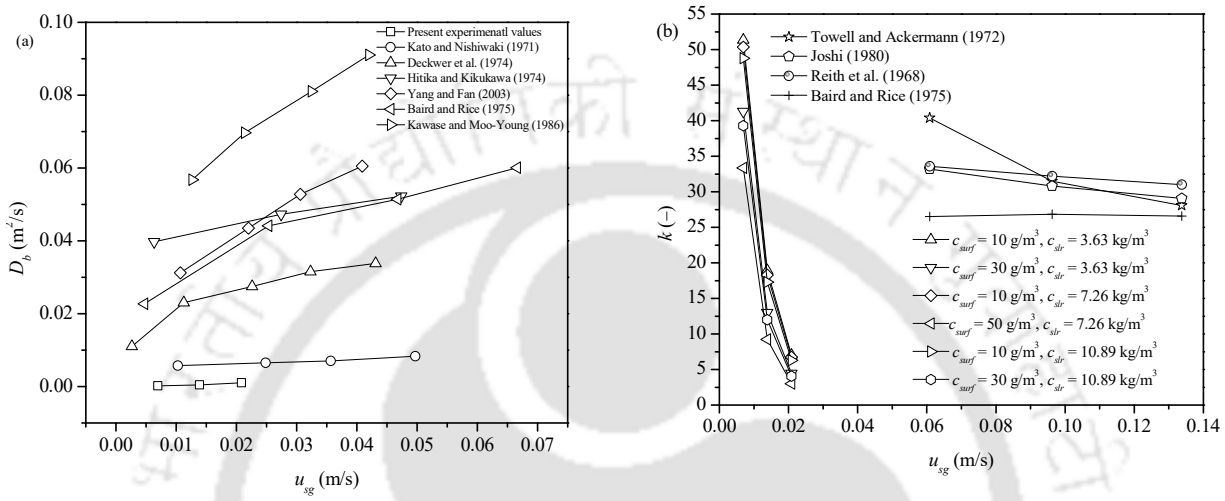

Figure 4.10: Comparison of the experimental values of (a) D_b and (b) *k* with those reported in the literature.

Based on the present experimental data, a new empirical correlation was developed for D_b as follows.

$$\left(\frac{D_b}{u_{slr}.d_c}\right)=4.69\times10^{-2}\left(\frac{u_{sg}}{u_{slr}}\right)^{1.463}\left(\frac{d_p}{d_c}\right)^{-0.620}\mathrm{We}_{slr}^{1.452}\,\mathrm{Re}_{slr}^{-0.942}\,\mathrm{Fr}_{slr}^{-1.502} \tag{4.21}$$

where We_{slr} is the Weber number $\left(\equiv\rho_{slr}u_{slr}^2d_c/\sigma\right)$, Re_{slr} is the Reynolds number $\left(\equiv d_cu_{slr}\rho_{slr}/\mu_{slr}\right)$, and Fr_{slr} is the Froude number $\left(\equiv u_{slr}/\sqrt{gd_c}\right)$. The standard error and the correlation coefficient for the fit are 0.1044 and 0.9947, respectively. This correlation is valid for the following ranges: $0.333\le u_{sg}/u_{slr}\le3.0$, $1.15\times10^{-3}\le d_p/d_c\le7.36\times10^{-3}$,

$7.62\times10^{-2} \le \mathrm{We}_{slr} \le 83.09\times10^{-2}$, $251.23 \le \mathrm{Re}_{slr} \le 908.14$, and $9.46\times10^{-3} \le \mathrm{Fr}_{slr} \le 28.37\times10^{-3}$. The percentage error of the correlation given by Eq. (4.21) is ±16.87. The parity of the experimental data and $D_b/(u_{slr}d_c)$ calculated from Eq. (4.21) is shown in Fig. 4. 11 (a).

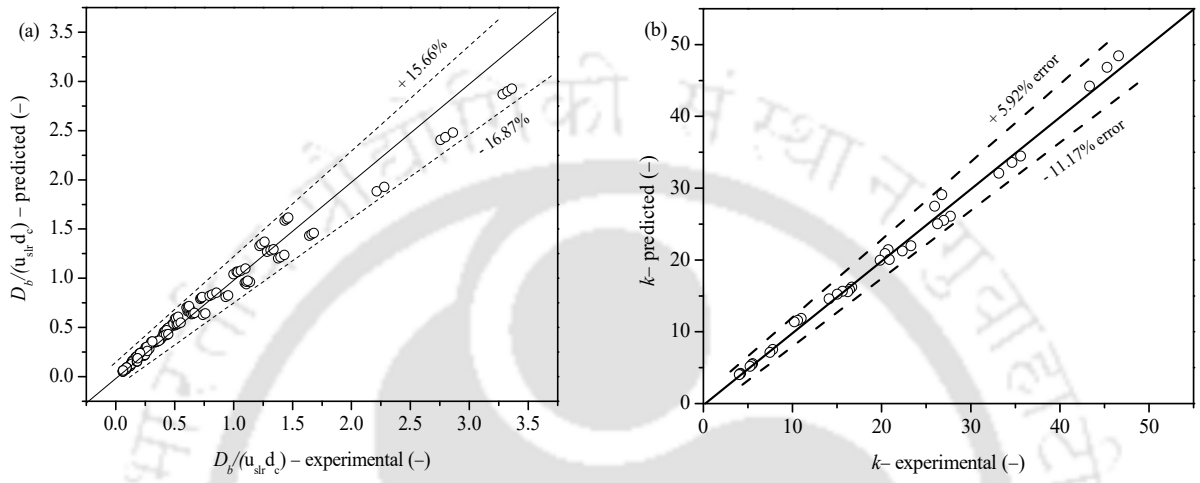

Figure 4.11: Parity of the experimental values of (a) D_b and (b) k with those calculated from Eqs. (4.21) and (4.22).

A correlation was developed to predict k, which is given by

$$k = 6.42\times10^{-9}\left(\frac{u_{sg}}{u_{slr}}\right)^{-1.949}\left(\frac{d_p}{d_c}\right)^{0.983}\mathrm{We}_{slr}^{-0.966}\,\mathrm{Re}_{slr}^{2.541}\,\mathrm{Fr}_{slr}^{-2.558} \qquad (4.22)$$

The standard error and the correlation coefficient of the fit are 0.0460 and 0.9981, respectively. This correlation is valid for the following ranges: $0.333 \le u_{sg}/u_{slr} \le 3.0$, $1.15\times10^{-3} \le d_p/d_c \le 7.36\times10^{-3}$, $7.62\times10^{-2} \le \mathrm{We}_{slr} \le 83.09\times10^{-2}$, $251.23 \le \mathrm{Re}_{slr} \le 908.14$, and $9.46\times10^{-3} \le \mathrm{Fr}_{slr} \le 28.38\times10^{-3}$. The percentage error of the correlation given by Eq. (4.22) is ±

11.17. The parity of the experimental data and the values of k calculated from Eq. (4.22) is shown in Fig. 4.11 (b).

4.6. Conclusion

The present work reports the dispersion characteristics of the slurry phase in the counter-current flotation column. The study shows that the dispersion number is a strong function of slurry concentration, particle size, surfactant dose, and gas and slurry velocities. The residence time distribution (RTD) technique was used to estimate the dispersion number based on the axial dispersion model. The velocity distribution model was successfully applied to analyze the dispersion due to bubble motion and the velocity distribution characteristic factor. The dispersion number was found to increase with increasing gas and slurry velocities. The prime cause was increased turbulence and interaction between the phases in the column. An increase in the slurry concentration caused a little reduction in the dispersion number. It was due to the rise in the apparent viscosity of the system. The increase in the particle size significantly reduced the dispersion number. For three-phase counter-current flow systems, the characteristic factor of the velocity distribution decreased with increasing superficial gas velocity and surfactant concentration. In contrast, it increased as the slurry concentration and particle size increases. The dispersion coefficient of the bubble motion increased as the superficial gas velocity and surfactant concentration increased, while it decreases with an increase in slurry concentration and particle size. A correlation was developed for the prediction of dispersion number in terms of dimensionless groups, which was in good agreement with the experimental results. This work will be helpful for improving the transport efficiency of flotation systems.

CHAPTER 5: ENTRAINMENT CHARACTERISTICS

In this chapter, experiments were conducted in a continuous flotation column to determine the degree of entrainment of coal particles and examine its dependence on surfactant concentration, type of surfactant, particle size, superficial gas velocity, slurry concentration, and superficial liquid velocity. The degree of entrainment was analyzed using Warren's model. An empirical correlation was developed, based on a wide range of operating variables, to predict the degree of entrainment. The size of the bubble, required for the model analysis, was experimentally measured by a photographic method under different operating conditions. Based on the experimental data, a general correlation was developed, which was used to calculate the bubble diameter.

5.1. Introduction and literature

The degree of entrainment is an important parameter in the processing of minerals and in various chemical industries, which is often hypothesized to be a function of particle size. The entrainment of coal particles refers to the mechanical recovery of the coal particles suspended in water using froth flotation. Entrainment is the transport process by which fine particles, suspended in liquid, are entrained by bubbles, generated by a frothing agent, in a flotation column. This technology is mainly used in the processing of the ores with a large proportion of fine gangue particles (Fuerstenau, 1980; Kirjavainen, 1996). Flotation is also widely used in wastewater treatment, paper de-inking, and mineral beneficiation. From the theoretical viewpoint, froth flotation may be considered as a sequence of two operations, i.e., reaction and separation (Matis, K.A, 1994). The reaction primarily occurs in the pulp zone. A particle–bubble aggregate, which is less dense than

the medium, moves upward against gravity to the froth zone, while the hydrophilic particles reach the tails (Yianatos et al., 2009). The effective separation occurs at the pulp–froth interface when the froth is transported to the concentrate launder.

The entrainment process can be explained using three theories. The *boundary layer theory* for entrainment suggests that the bubble lamina (i.e., a thin hydrodynamic layer of water covering the bubble) of froth is used to transport the mineral particles to the froth phase (Bascur and Herbst, 1982; Gaudin, 1957; Hemmings, 1981; Moys, 1978). The *bubble wake theory* (Smith, 1984; Yianatos et al., 1988) provides the concept of particles, rising along with the water, with the energy gained from the wake of an ascending bubble. Both theories fail due to the mass of mineral particles transported. Hence, (Smith and Warren, 1989) proposed another theory, known as the *bubble swarm theory*, to describe the mechanism of transport. According to this theory, the bubble travels upward and gets stocked up below the froth–pulp region. In the region, some of the water along with the suspended mineral particles fall back, while the others are pushed upward due to the buoyant force of the bubble swarm.

Various principal factors affect the entrainment of particles. (Jowett, 1966) was the first scientist to recognize the water current as a significant factor for the entrainment of mineral particles. (Johnson, 1972) was able to establish a direct correlation between the recovery of mineral particles and the recovery of water in the concentrate, and the degree of entrainment. Surfactant, as a frother, is an important factor that affects the transport of the particles directly by entrainment. It is used to generate the froth that carries the particles to the concentrate region. The surfactant also determines the characteristics of the bubbles. The concentration of particles in the feed is also a determining factor for the degree of entrainment (Yianatos et al., 2009). For a large-scale flotation

cell, the particle concentration in the pulp is an important factor that influences the entrainment significantly. The amount of particle recovered through entrainment is larger for a perfectly dispersed feed. Particle density is also an important factor, which affects the entrainment degree. The degree of entrainment increases with decreasing particle density (Bisshop, 1974).

The particles with lower density tend to move with water due to their less tendency for sedimentation. Entrainment to the concentrate increases as the particles become finer. If the particles are coarser, the drainage will occur significantly and reduce the entrainment (Runge, 2010). According to (Zheng et al., 2006), the amount of gas flow has a mixed effect on the recovery by entrainment. The number of particles taken from the pulp phase to the froth phase increases, the extent of drainage of water. The liquid flow rate is directly proportional to the number of particles carried to the froth section from the pulp phase. It also provides additional energy to carry the particles by entrainment. (Neethling and Cilliers, 2002) described a froth simulator (i.e., UMIST FrothSim) to assess the degree of entrainment. Their model is able to explain entrainment and collection of gangue by flotation. (Szatkowski, 1987) investigated the gangue distribution in the froth and studied the effects of the ash content in the froth in coal flotation with variation in the bubble size, air flow rate, and mineral concentration. (Zheng et al., 2006) reported about the effect of the operating parameters such as froth height and air flow rate on the degree of entrainment. (Yianatos et al., 2009) reported the efficacy of the recovery of solids and liquids by entrainment through direct measurement of the fraction of liquid and solid concentration in the flotation cell. (Wang et al., 2015a) assessed the effects of parameters such as impeller speed, gas flow rate, and froth height on the degree of entrainment. Based on the experimental data,

(Johnson, 1972) established a correlation between the recovery of particles by entrainment and water recovery to the concentrate. (Melo and Laskowski, 2007) investigated the effect of the

frother on the degree of entrainment. They reported that frother had a significant effect on the froth structure, which changed the entrainment. Rheological effects on entrainment were explained by (Shabalala et al., 2011). They reported that a variation in viscosity influenced the turbulence, which had a significant effect on the extent of solids entering the froth. (Laplante et al., 1989) proposed a non-linear relationship between particle size and degree of entrainment. They also proposed a relation between the degree of entrainment and water recovery for coarse and ultra-fine particles. The study of (Wang et al., 2015a) suggests that particle density and particle size have significant effects on the degree of entrainment. (Ata, 2001) focused on the interface that separated the gangue from the mineral particles, which significantly changed the degree of entrainment.

This work investigates the entrainment of coal particles in a continuous flotation column at regular time intervals to determine its dependence on the type of surfactant, surfactant concentration, slurry concentration, particle size, and gas and slurry velocities. The size of the bubble was experimentally determined by a photographic method under different operating conditions. Based on the present experimental data, a general correlation was developed, which was used to calculate the bubble diameter. Using Warren's model, the degree of entrainment was analyzed. A general correlation for the degree of entrainment was also developed.

5.2. Experimentation

5.2.1. Experimental setup

Fig. 5.1 (a) represents the schematic diagram of the experimental setup for entrainment characteristics. The details and specification of components of the experimental set up is already discussed in section 2.2.1.

Figure 5.1: (a) Diagrammatic representation of the experimental setup: 1. air compressor, 2. storage tank, 3. pump, 4. spherical sparger, 5. solenoid valve, 6. flotation column, 7. control valve, 8. liquid rotameter, 9. gas rotameter, 10. collecting hood, 11. collecting beaker, and (b) a photo of the spherical sparger. (This figure is withhold because of copyright)

5.2.2. Materials and experimental procedure

The anionic surfactant sodium dodecyl benzene sulfonate (SDBS) (> 99 % purity) and the cationic surfactant, N-cetyl-N,N,N-trimethylammonium bromide (CTAB) (99% purity), were bought from Sigma Aldrich (Germany), and Loba Chemie (India) respectively, which were used as surface-active agents. The extraction, crushing, and size analysis of coal particle was discussed in section 2.2.2 in the chapter 2.

All the experimental works were carried out at standard conditions of temperature and pressure. The span of superficial gas velocity and superficial slurry velocity were $0.021 \leq u_{sg} \leq 0.063$ m/s, and $0.007 \leq u_{slr} \leq 0.021$ m/s, respectively. Five surfactant concentrations i.e., 25, 50, 75, 100, and 150 g/m^3 were considered in the present work. The measurement techniques of slurry density, slurry viscosity, and surface tension are already discussed in section 2.2.2.

The physical properties of the materials used in the experiments and the surface tensions values of the aqueous surfactant solutions are given in Tables 5.1 and Table 5.2, respectively.

Table 5.1: Physical properties of the system at 298 ± 1 K.

Surfactant	Surfactant concentration (g/m^3)	Slurry concentration (kg/m^3)	Viscosity (mPa s)	Density (kg/m^3)
CTAB	25	5.56	1.347	1004.94
CTAB	50	5.56	1.494	1005.29
CTAB	100	5.56	1.786	1005.94
SDBS	100	5.56	1.619	1005.73
SDBS	100	8.33	1.621	1006.33
SDBS	100	11.11	1.702	1007.47

Table 5.2: Surface tensions of the aqueous surfactant solutions at 298 ± 1 K.

Surfactant	Surfactant concentration (g/m^3)	Slurry concentration (kg/m^3)	Surface tension (N/m)
CTAB	25	5.56	0.0312
CTAB	50	5.56	0.0290
CTAB	100	5.56	0.0162
SDBS	100	5.56	0.0208
SDBS	100	8.33	0.0208
SDBS	100	11.11	0.0208

The flotation column was thoroughly cleaned and washed with tap water. For all the experiments, tap water was used. Coal particles were added to the solution tank. The tank was filled with 9 dm^3 of water. The slurry was introduced at the height of 0.73 m from the base of the column. Froth generated in the column was collected at 0.174 (i.e., bottom section), 0.373 (i.e., middle section), and 0.547 m (i.e., top section) heights from the bottom at a regular interval of 10 s. Each set of experiments was done for 60 s. The samples were dried in an oven (make: Sonuu, India; model: Digitel) at 383 K for ~24 h. The analysis was done for several parameters such as superficial gas velocity, particle size, superficial slurry velocity, surfactant concentration, and slurry concentration using two surfactants (i.e., CTAB and SDBS).

5.3. Principle of degree of entrainment

5.3.1. Method of Warren

The method of Warren (Warren, 1985) involves a number of batch flotation tests keeping the flotation time the same for all but with variable froth height and froth removal rate to change water recovery. It was observed that there was a linear relationship between the mineral and water recovered for each system. These characteristics show the linear correlation between the true flotation and entrainment as

$$R_c = R_{TF} + e_P R_w \tag{5.1}$$

and

$$R_G = e_G R_w \tag{5.2}$$

where R_c and R_G are the cumulative mass recoveries of the valuable and gangue particles, respectively at a particular time *t*, R_{TF} is the intercept of the extrapolated line on the recovery axis

(i.e., recovery by true flotation), e_p and e_G are the degrees of entrainment for the valuable and gangue particles, respectively, and R_W is the cumulative mass of the water recovered.

5.4. Estimation of bubble size and its distribution

The photographic technique will be used to measure bubble size. This is the simplest method to determine the bubble size. The snap of bubbles in motion was captured by the high-speed camera (Make: Sony Cybershot, Model: DSC-H300, 20.1 MP). A halogen lamp was placed on the opposite side of the camera to have a clear vision for capturing the images. The captured digital images were intensified and enlarged by an image processing software (Digimizer, version 4.2) through which the boundaries of the bubbles were distinguished. The mean of the bubble size was defined by the Sauter-mean bubble diameter, i.e.

$$d_{b,32} = \frac{\sum_{i=1}^{n} n_i d_{bi}^3}{\sum_{i=1}^{n} n_i d_{bi}^2} \tag{5.3}$$

where n_i is the number of bubbles of diameter d_{bi}. The two-dimensional shape of the bubbles was assumed as a spheroid. Hence, their minimum and maximum axes were analyzed by the image analysis software (Polli et al., 2002).

5.5. Results and Discussions

5.5.1. Effect of gas velocity on the entrainment of coal particles

The effect of superficial gas velocity on the entrainment of coal particles at a constant slurry concentration (i.e., 5.56 kg/m^3), surfactant concentration (i.e., 100 g/m^3), superficial slurry velocity (i.e., 0.021 m/s), and particles size (i.e., 235.61 μm) in the presence of SDBS is shown in Fig. 5.2. The degree of entrainment increased with increasing gas velocity.

Figure 5.2: Effect of gas velocity on the entrainment of coal particles: (a) top, (b) middle, and (c) bottom sections. (This figure is withhold because of copyright)

More particles were carried from the pulp phase to the froth phase as the gas velocity was increased. According to (Wang et al., 2015), the change in the gas flow rate changes the drainage of particles suspended in the froth, at a given height. The rise in the gas flow rate enhances the rise velocity of the froth, which decreases the retention time. (Zheng et al., 2006) reported that the increase in gas flow rate increased the number of particles and water in the froth phase, which could affect the drainage of the particles. (Kursun, 2017) reported that an increase in gas velocity increased the amount of water carried away along with the suspended particles. So the increase in the gas flow rate increased the degree of entrainment of the particles. The degree of entrainment at the top section, middle section, and the bottom section at different superficial gas velocities are given in Table 5.3.

Table 5.3. Degree of entrainment at different superficial gas velocities at 298 ± 1 K.

Location	Degree of entrainment (e_G)		
	$u_{sg} = 0.021$ m/s	$u_{sg} = 0.042$ m/s	$u_{sg} = 0.063$ m/s
Top section	0.584	0.793	0.826
Middle section	0.570	0.653	0.718
Bottom section	0.502	0.620	0.708

5.5.2. Effect of superficial slurry velocity on the entrainment of coal particles

The effect of superficial slurry velocity on entrainment of coal particles at a constant slurry concentration (i.e., 5.56 kg/m^3), surfactant concentration (i.e., 100 g/m^3), superficial gas velocity (i.e., 0.063 m/s), and particle size (i.e., 235.61 μm) in the presence of SDBS is shown in Fig. 5.3

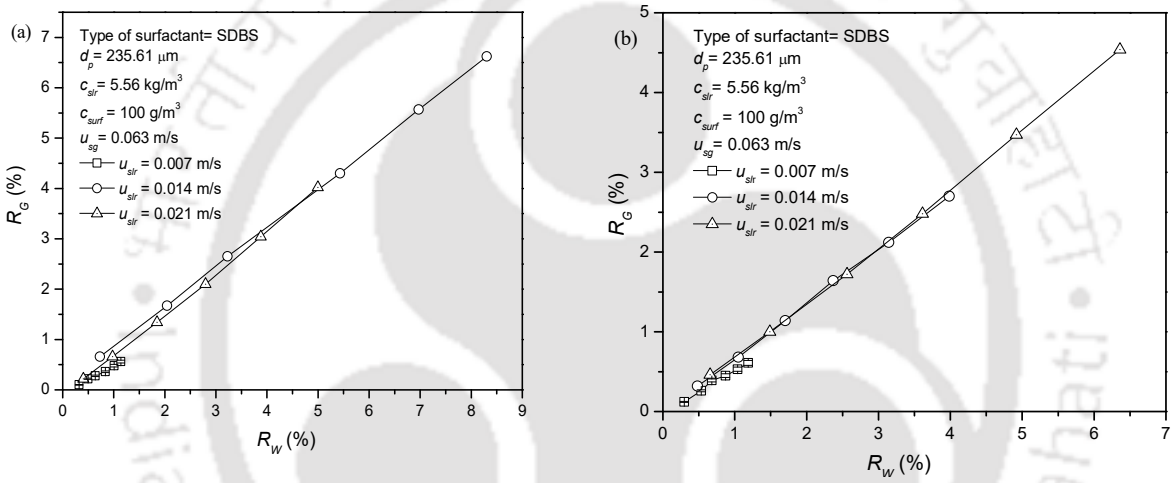

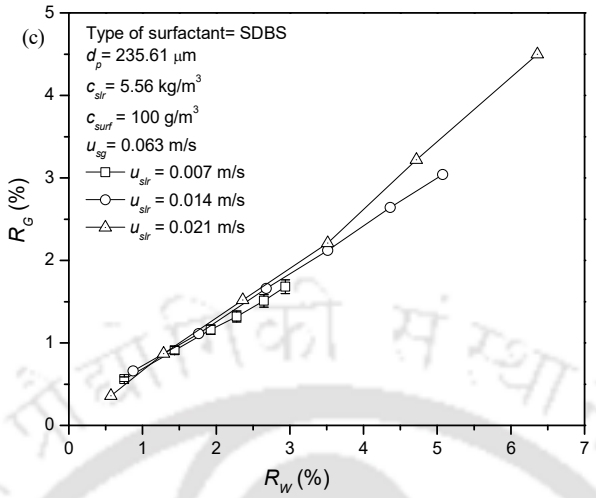

Figure 5.3: Effect of slurry velocity on the entrainment of coal particles: (a) top, (b) middle, and (c) bottom sections.

Based on these results, it is concluded that the degree of entrainment increased with increasing slurry velocity. The degree of entrainment at different superficial slurry velocities are shown in Table 5.4.

Table 5.4: Degree of entrainment at different superficial slurry velocities at 298 ± 1 K.

Location	Degree of entrainment (e_G)		
	$u_{sl} = 0.007$ m/s	$u_{sl} = 0.014$ m/s	$u_{sl} = 0.021$ m/s
Top section	0.543	0.786	0.826
Middle section	0.540	0.683	0.718
Bottom section	0.506	0.572	0.708

5.5.3. Effect of particle size on the entrainment of coal particles

The effect of size of coal particles on the entrainment at a constant slurry concentration (i.e., 5.56 kg/m^3), surfactant concentration (i.e., 100 g/m^3), superficial gas velocity (i.e., 0.063 m/s), and superficial slurry velocity (i.e., 0.021 m/s) in the presence of SDBS is shown in Fig. 5.4.

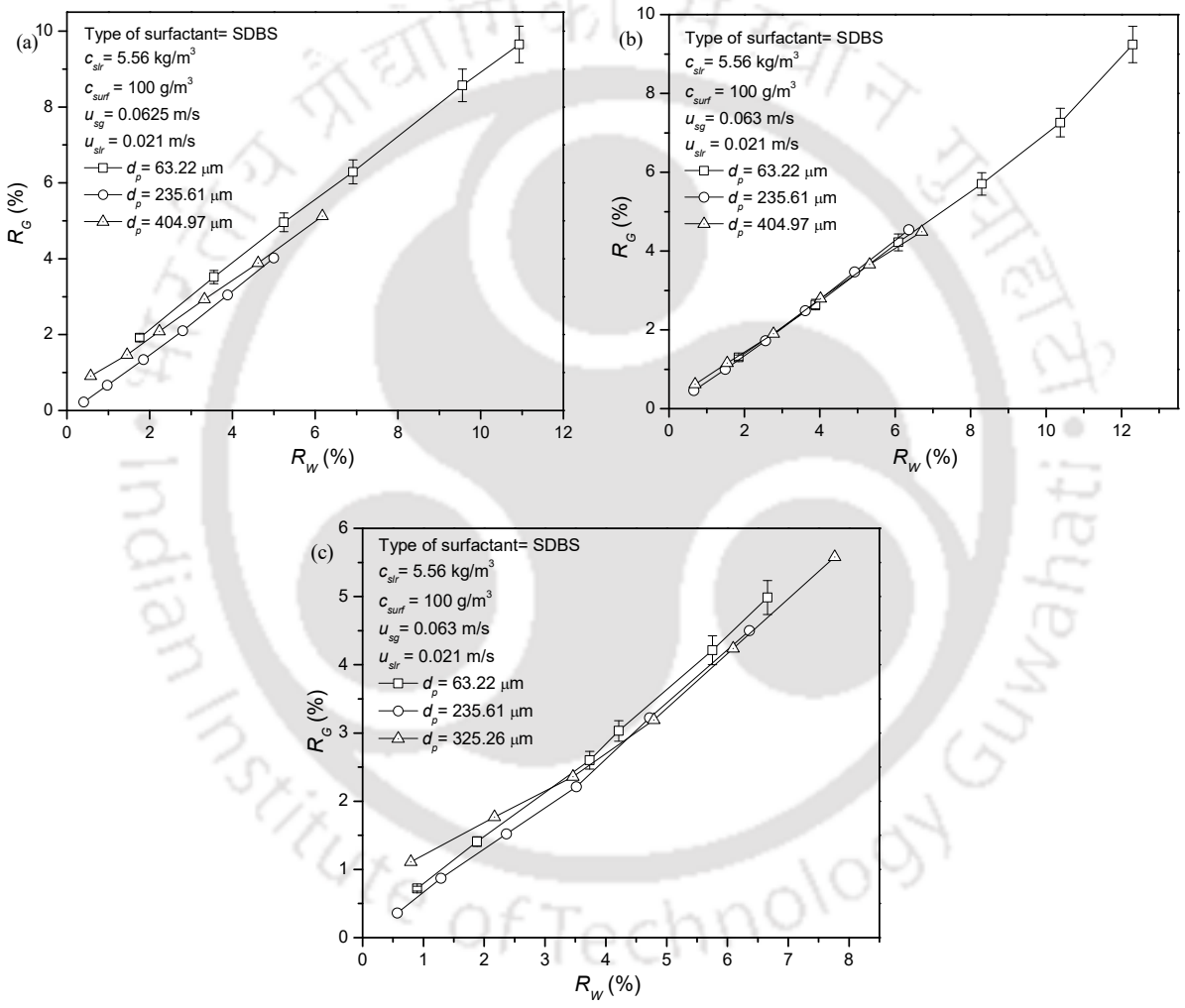

Figure 5.4: Effect of particle size on the entrainment of coal particles: (a) top, (b) middle, and (c) bottom sections.

It was observed that the degree of entrainment decreased with increasing particle size. This corroborates the results of (Runge, 2010), who showed that the entrainment increased as the particles became finer. The degree of entrainment varying with particle size is given in Table 5.5.

Table 5.5: Degree of entrainment for different particle sizes at 298 ± 1 K.

Location	Degree of entrainment (e_G)		
	d_p = 63.22 µm	d_p = 235.61 µm	d_p = 325.26 µm
Top section	0.841	0.826	0.757
Middle section	0.743	0.718	0.651
Bottom section	0.735	0.708	0.640

5.5.4. Effect of slurry concentration on the entrainment of coal particles

The effect of slurry concentration on the entrainment of coal particles at a fixed particle size (i.e., 235.61 µm), surfactant concentration (i.e., 100 g/m^3), superficial gas velocity (i.e., 0.063 m/s), and superficial slurry velocity (i.e., 0.021 m/s) in the presence of SDBS is shown in Fig. 5.5.

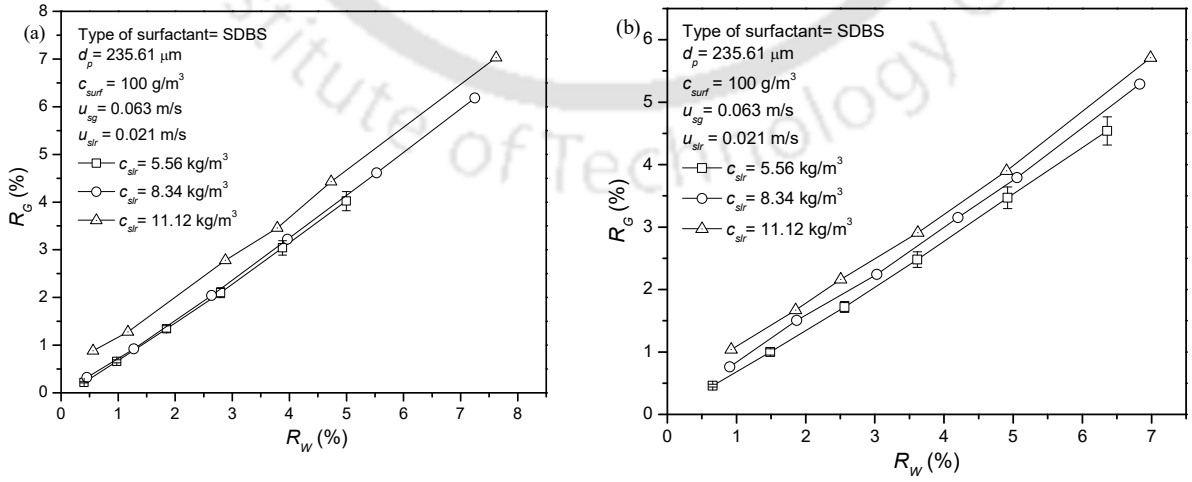

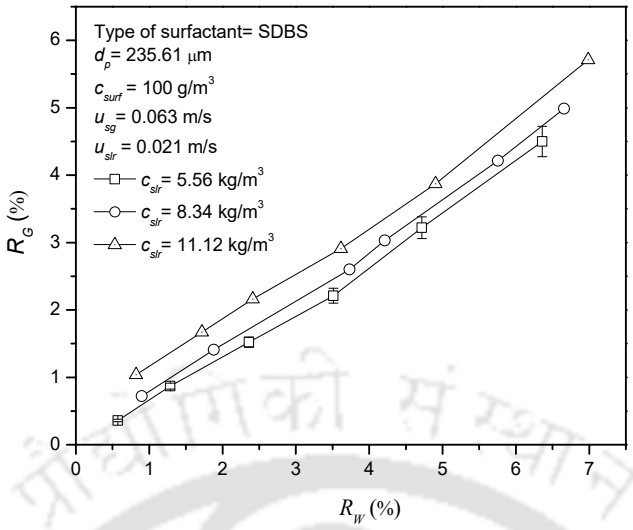

Figure 5.5: Effect of slurry concentration on the entrainment of coal particles: (a) top, (b) middle, and (c) bottom sections.

It is concluded that the degree of entrainment increased with the increasing concentration of the particles at all the sections of the column. As the concentration of particles increases, more particles are transferred to the froth. (Wang et al., 2015a) reported that the increase in particle concentration increases the number of entrained particles. An increase in the density of the pulp increases the entrainment of the particles. The degree of entrainment at different slurry concentrations is shown in Table 5.6.

Table 5.6: Degree of entrainment at different slurry concentrations at 298 ± 1 K.

Location	Degree of entrainment (e_G)		
	$c_{slr} = 5.56$ kg/m^3	$c_{slr} = 8.34$ kg/m^3	$c_{slr} = 11.12$ kg/m^3
Top section	0.826	0.867	0.877

Middle section	0.718	0.756	0.766
Bottom section	0.708	0.735	0.747

5.5.5. Effect of surfactant concentration on the entrainment of coal particles

The effect of surfactant concentration on the entrainment of coal particles at a constant slurry concentration (i.e., 5.56 kg/m^3), particle size (i.e., 235.61 μm), superficial gas velocity (i.e., 0.063 m/s), and superficial slurry velocity (i.e., 0.021 m/s) in the presence of CTAB is shown in Fig. 5.6.

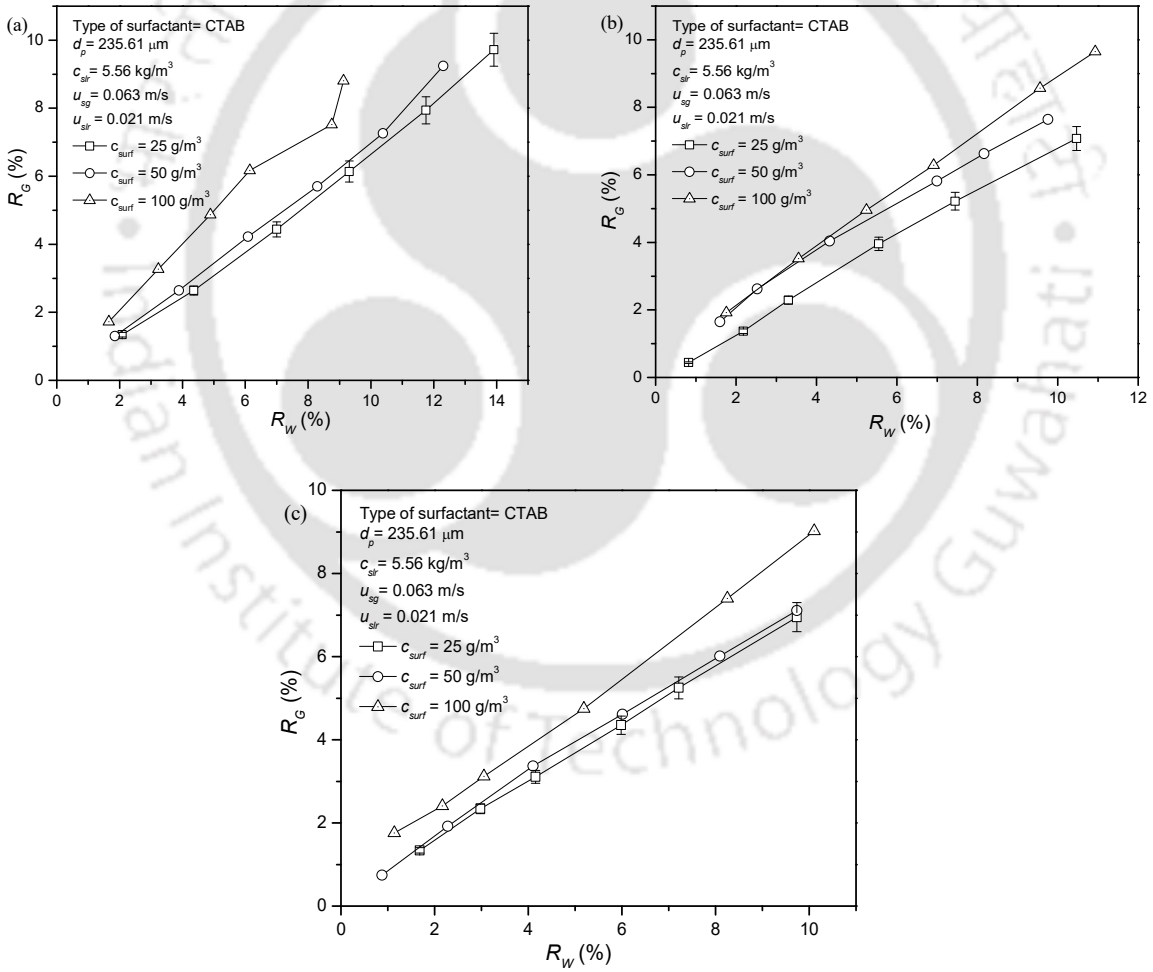

Figure 5.6: Effect of surfactant concentration on the entrainment of coal particles: (a) top, (b) middle, and (c) bottom sections.

From the experimental results, it is seen that the degree of entrainment (e_p) increased as the concentration of the surfactant was increased from 25 to 100 g/m^3. The degree of entrainment at the top, middle, and bottom sections at different surfactant concentrations are given in Table 5.7.

Table 5.7: Degree of entrainment at different surfactant concentrations at 298 ± 1 K.

Location	Degree of entrainment (e_G)		
	c_{surf} = 25 g/m^3	c_{surf} = 50 g/m^3	c_{surf} = 100 g/m^3
Top section	0.711	0.743	0.881
Middle section	0.696	0.721	0.841
Bottom section	0.693	0.711	0.816

5.5.6. Effect of the surfactant type on the entrainment of coal particles

The effect of surfactant type (i.e., SDBS and CTAB) on the entrainment of coal particles at a constant slurry concentration (i.e., 5.56 kg/m^3), particle size (i.e., 235.61 μm), surfactant concentration (i.e., 100 g/m^3), superficial gas velocity (i.e., 0.063 m/s), and superficial slurry velocity (i.e., 0.021 m/s) is shown in Fig. 5.7.

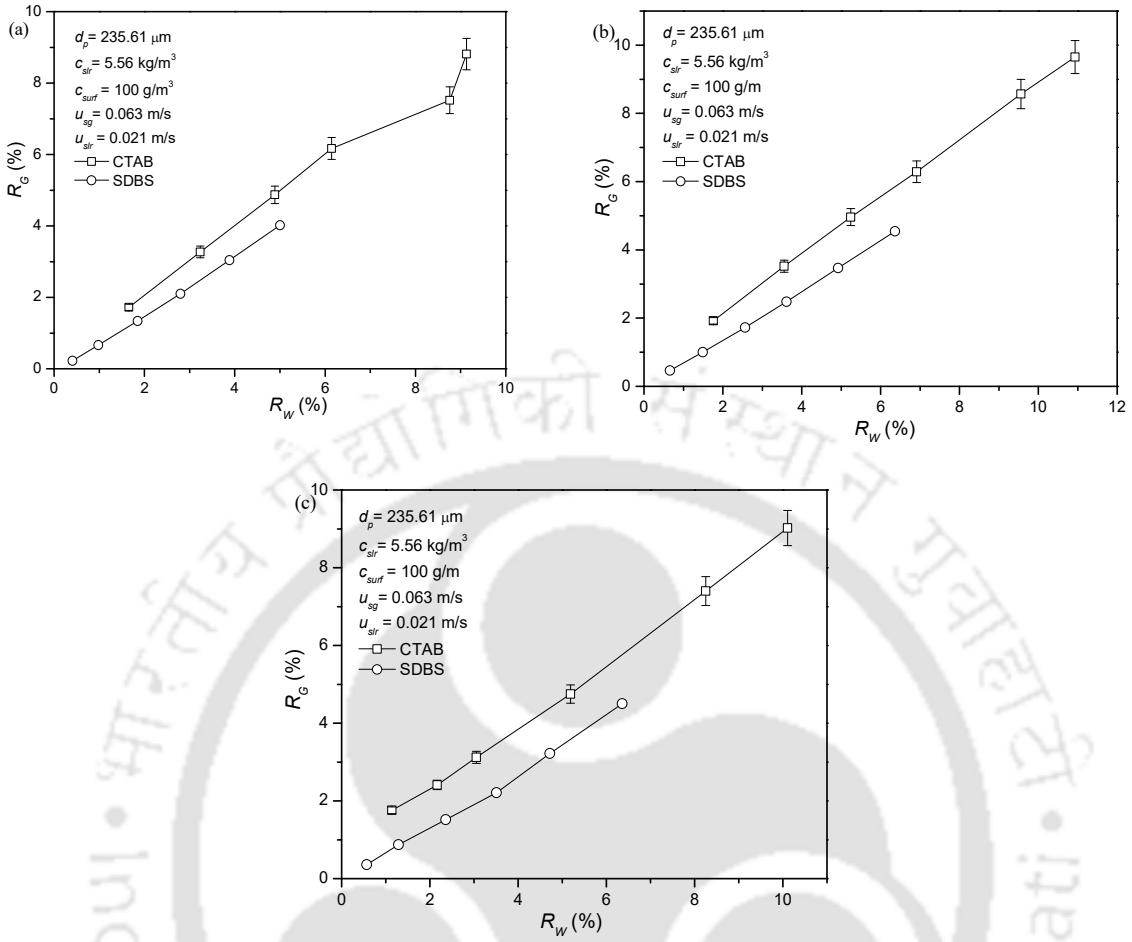

Figure 5.7: Effect of surfactant type on the entrainment of coal particles: (a) top, (b) middle, and (c) bottom sections.

From the experimental results, it was observed that the degree of entrainment of the coal particles was greater in CTAB presence than SDBS in all the sections. The degree of entrainment for the different types of surfactants is given in Table 5.8.

Table 5.8: Degree of entrainment for the different types of surfactants at 298 ± 1 K.

Location	Degree of entrainment (e_G)

	CTAB (100 g/m^3)	SDBS (100 g/m^3)
Top section	0.881	0.826
Middle section	0.841	0.718
Bottom section	0.816	0.708

5.6. Development of the general empirical correlation for entrainment of the coal particles

The degree of entrainment of the coal particles is observed to rely on superficial gas velocity $\left(u_{sg}\right)$, superficial slurry velocity $\left(u_{slr}\right)$, sauter mean diameter $\left(d_{b,32}\right)$, diameter of the particles $\left(d_p\right)$, height of the column $\left(h\right)$, diameter of the column $\left(d_c\right)$, surface tension (σ), slurry density $\left(\rho_{slr}\right)$, slurry viscosity $\left(\mu_{slr}\right)$, and the acceleration due to gravity (g). This dependence can be expressed as

$$e_G = f(u_{sg}, u_{slr}, d_{b,32}, d_p, h, d_c, \sigma, \rho_{slr}, \mu_{slr}, g) \tag{5.4}$$

The following correlation is developed for predicting the entrainment of coal particles using dimensional analysis and multiple linear regression of the experimental data.

$$e_G = 2.44\left(\frac{u_{sg}}{u_{slr}}\right)^{1.388}\left(\frac{d_b}{d_c}\right)^{-2.115}\left(\frac{h}{d_c}\right)^{0.116}\left(\frac{d_p}{d_c}\right)^{-0.063}\mathrm{We}_{slr}^{\,0.160}\,\mathrm{Re}_{slr}^{\,-0.263}\,\mathrm{Fr}_{slr}^{\,1.708} \tag{5.5}$$

where Re_{slr} is the Reynolds number $\left(\text{i.e., } d_c u_{sl}\rho_{slr}/\mu_{slr}\right)$, We_{slr} is the Weber number $\left(\text{i.e., } d_c u_{sg}^2\rho_{slr}/\sigma\right)$, and Fr_{slr} is the Froude number $\left(\text{i.e., } u_{sg}/\sqrt{gd_c}\right)$.

The standard error and correlation coefficient of equation (5.5) are 0.0477 and 0.9509, respectively. The correlation is valid within the following ranges: $1.0 \le u_{sg}/u_{slr} \le 9.0$; $4.79\times10^{-2} \le d_b/d_c \le 9.11\times10^{-2}$; $3.164 \le h/d_c \le 9.945$; $1.15\times10^{-3} \le d_p/d_c \le 7.36\times10^{-3}$; $0.128 \le \mathrm{We}_{slr} \le 1.484$; $212.51 \le \mathrm{Re}_{slr} \le 844.29$; $9.459\times10^{-3} \le \mathrm{Fr}_{slr} \le 2.838\times10^{-2}$.

A comparison between the degree of entrainment experimentally obtained and that predicted by equation (5.6) is shown in Fig. 5.8.

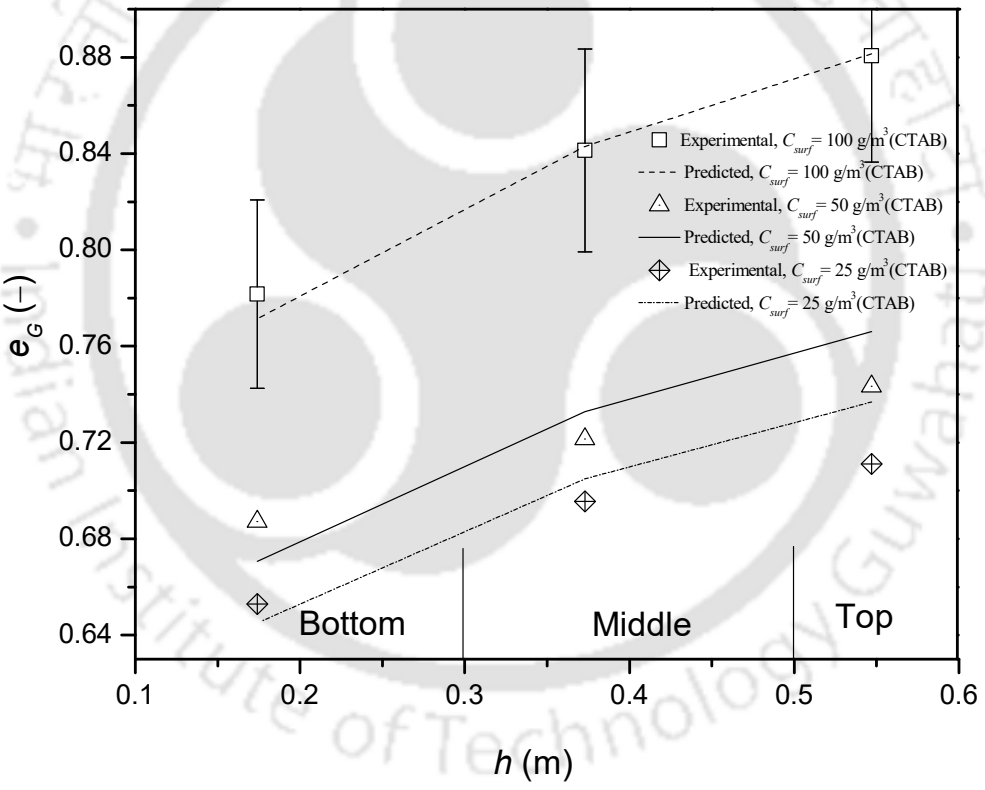

Figure 5.8: Comparison of degree of entrainment at different surfactant concentrations.

5.7. Effect of different variables on mean bubble size

The size of the bubbles was measured by a photographic method under different operating conditions. A typical snapshot of the bubble in the column is shown in Figure 5.9.

Fig. 5.9. Typical images of the bubbles in the three-phase system at different superficial gas velocity, slurry concentration, particle size, axial height, and surfactant concentration. A typical bubble size distribution is shown in Figure 5.10. (This figure is withhold because of copyright)

Figure 5.10: A typical bubble size distribution for the particle size $\left(d_p\right)$ range of 150–300 μm and 300–425 μm. (This figure is withhold because of copyright)

5.7.1. Effect of superficial gas velocity, axial height, and slurry concentration on Sauter mean diameter

The effect of axial height (0.2, 0.4, and 0.6 m), superficial gas velocity (0.007, 0.021, and 0.035 m/s), slurry concentration (0.2 and 0.8 wt %) on Sauter mean diameter at fixed particle size 235.61 μm in Figure 5.11. There are 3 different regions of the axial height of the column is used for the bubble size measurement i.e, region A (0 to 0.2 m), region B (0.2 to 0.4 m), region C (0.4 to 0.6 m).

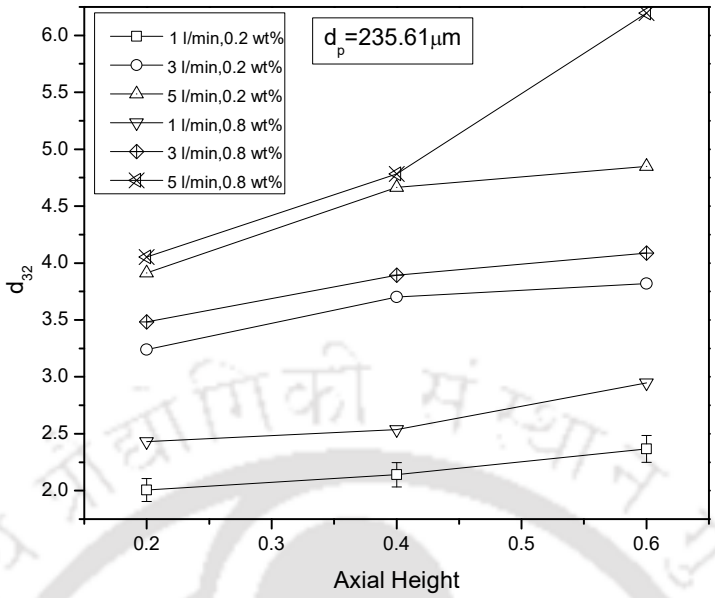

Figure 5.11: Effect of superficial gas velocity, axial height, and slurry concentration on mean bubble size.

It is noticed that the bubble size is increasing with an increase in gas flow rate and axial height. Many authors pointed out the increase in bubble size with an increase in superficial gas velocity (Passos et al., 2015; Tyagi and Buwa, 2017). The coalescence of the bubbles increases with an increase in superficial gas velocity and therefore increases the bubble size. When the bubbles travel from region A to region C, along the axial direction, it's get coalesced, and increases its size. Bubble coalescence theory describes that due to the buoyant force, the bubbles dissimilar diameter have different rise velocity, which causes collision among bubbles and coalescence (Shukla et al., 2008). It is observed that the bubble size increases with an increase in slurry concentration at all superficial gas velocities. The addition of particles increases the viscosity of the fluid. Due to increase in the viscosity of the system causes the coalescence of the gas bubbles, and therefore increases the bubble size (Götz et al., 2016; Kara et al., 1982; Kato et al., 1972; Ojima et al., 2015; Rabha et al., 2013b; Sehabiague and Morsi, 2013).

5.7.2. Effect of particle size and surfactant concentration on Sauter mean bubble diameter

The effect of Sauter mean bubble diameter on different particle sizes (235.61 and 428.55 μm) and different surface concentrations (4 and 10 g/m^3) at a fixed superficial gas velocity 0.021 m/s, fixed slurry concentration 0.2 wt % shows in Fig. 5.12.

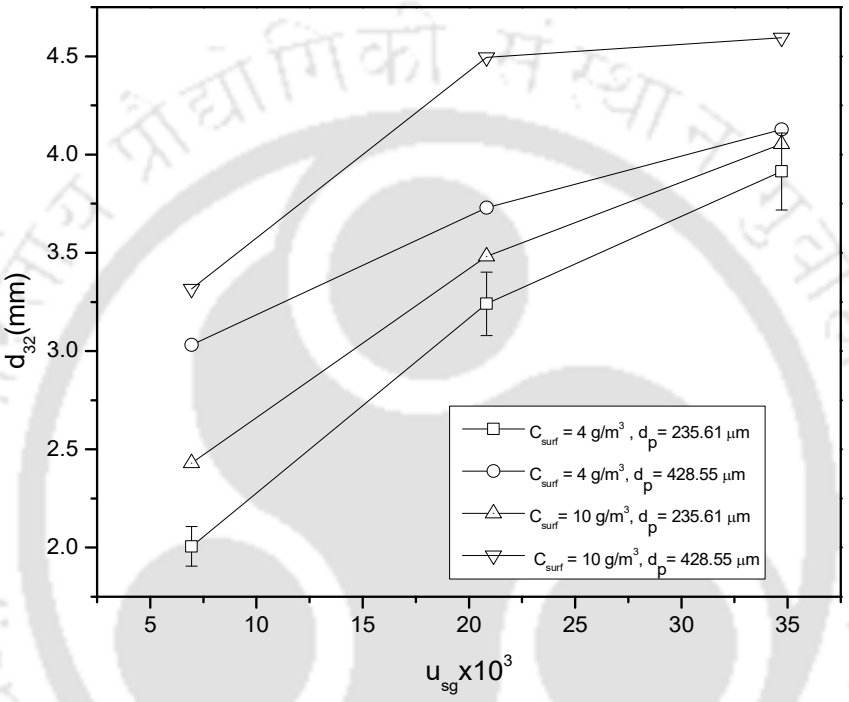

Fig 5.12: Effect of particle size and surfactant concentration on mean bubble size.

It is observed that the increase in surfactant concentration increases the bubble size. Because, when surfactant concentration increases, the surface tension reduces. So bubble size increases. It is also seen that when it increases the particle size, increases the bubble size.

Based on the present experimental data, a general correlation was developed, which was used to calculate the bubble diameter from equation (5.6). The correlation can be expressed as

$$\frac{d_{b,32}}{d_c} = 2.11\times10^{3}\left(\frac{d_p}{d_c}\right)^{0.251} \mathrm{We}_{slr}^{0.318}\ \mathrm{Re}_{slr}^{-0.324}\left(\frac{h}{d_c}\right)^{0.155} \tag{5.6}$$

which is valid within the ranges $4.284\times10^{-3} \le d_p/d_c \le 9.23\times10^{-3}$; $0.068 \le \mathrm{We}_{slr} \le 1.899$; $308.063 \le \mathrm{Re}_{slr} \le 1741.62$; $0.00946 \le \mathrm{Fr}_{slr} \le 0.0473$; $3.636 \le h/d_c \le 10.909$.

5.8. Conclusion

From the entrainment studies of coal particles carried out in a laboratory flotation column, it was observed that CTAB gave better entrainment than SDBS. The entrainment of coal particles increased with the increasing concentration of the surfactants, i.e., it is seen that the degree of entrainment (e_p) increased as the concentration of the surfactant was increased from 25 to 100 g/m^3. The degree of entrainment was proportional to the superficial gas and liquid velocities. An increase in the gas and liquid velocities significantly increased the entrainment. An increase in the particle size decreased the entrainment, whereas the increase in the particle concentration increased entrainment. An empirical correlation based on the aforementioned parameters was developed for predicting the entrainment of the coal particles, which may be useful for the scale-up of the process for industrial applications.

CHAPTER 6: KINETICS OF FLOTATION FOR FINE PARTICLE RECOVERY

In this chapter, the recovery of coal particles in a continuous flotation column was investigated at regular time intervals to determine its dependence on the type of surfactant, particle size, and gas

and slurry velocities. The kinetics of the cumulative recovery was established. The induction time and flotation rate constant were analyzed based on the recovery efficiency incorporating the stability, attachment, and collision efficiencies of the particles with the bubbles. A generalized correlation for the rate constant and the induction time was also proposed on the basis of the experiments carried out under different operating conditions. The proposed work will be useful to intensify the transport efficiency of the flotation systems during scale-up on the industrial scale.

6.1. Introduction and literature

Froth flotation separates and concentrates minerals depending on the variation in the physicochemical properties of the interfaces, e.g., the surface hydrophobicity and floatability between the mineral and gangue particles. Generally, the separation is carried out in mechanical cells in which the entrainment of the fine hydrophilic gangue particles takes place in the froth phase. Because of the intrinsic mechanics of the phenomenon, it has a damaging effect on the performance (metallurgical) of the process. A successful method to impede the entrainment of such fine gangue came forth with the advent of the column flotation cell, which utilizes a deep froth zone. To prompt a cleaning action of the froth, this zone is washed with water (termed as "wash water"). This introduction of the column has become a plus to the conventional flotation circuits (Uribe et al., 1999). A typical scheme of movement of any gangue or valuable component between the froth and pulp zones in a flotation column is shown in Fig. 6.1.

Figure 6.1: Transfer of materials between the froth zones and pulp. ((This figure is withhold because of copyright)

Regardless of the transportation mechanism employed for getting to the froth region, particles can go back to the pulp region, or at last, set off the froth region into the concentrate launder if the levels of the controlled variables permit the froth removal.

Considerable work over the past decades done on column flotation shows the increasing interest in this technology, a direct result of which is the research on many aspects of column flotation. Flotation columns perform relatively better (e.g., a better product grade is achieved) as compared to the mechanical cells (conventional) in the washing operations due to their special froth operation, which has been explained in detail by Finch and Dobby (1990). The industrial use of this technology has spread in many fields like the treatment of coal, wastewater, corn, clays, proteins, resins, dyes, rubber, glass, fats, plastics, cane sugar, and fruit juices. A considerable number of parameters involved, and the interaction between three phases (i.e., gas, liquid, and solid) makes it one of the most compound mineral processing operations. Various components related to the floated mineral can affect the efficiency of separation by flotation, such as its surface properties, degree of liberation, several operating variables (gas and liquid velocity, frother concentration, particle concentration, and size), and grade. The particle shape is also a very important factor that affects the floatability of many minerals (Allan and Woodcock, 2001; Guven et al., 2016; Hicyilmaz et al., 2006; Hiçyilmaz et al., 2004; Jordens et al., 2016; Ulusoy et al., 2004; Xia, 2017).

Many degrees of freedom in the operating variables of the flotation columns have led to significant variations in the metallurgical performance, which have provided much scope for improving their control (Jordens et al., 2016). That is why it is necessary to understand the factors affecting the process to comprehend the mechanism of flotation. Several studies have been carried out to understand the kinetics of flotation and its recovery efficiency. Most of the flotation test data from

the literature suggest the first-order rate equation under practical operating conditions (Agar et al., 1998; Cilek, 2004; Dowling et al., 1985; Jameson et al., 1977; Oliveira et al., 2001; Wills and Finch, 2015). Li et al. (2018) examined the flotation kinetics of coal with different size fractions and aeration rates and proposed a new kinetic model based on their results. Their work indicated that the efficiency of flotation relies on the size of the coal particles. Chen et al. (2018) employed an oily-bubble flotation method for optimizing the parameters that affect the recovery efficiency of a gangue particle. They achieved a better flotation efficiency and higher material recovery at a much lower dosage of the collector. For the combustible matter recovery, they proposed a quadratic model. Sarikaya and Özbayoğlu (1995) observed that the size of the particles has a significant effect on the flotation process. Cai et al. (2018) proposed a comprehensive flotation mechanism for the low-rank metamorphic oxidized coal slimes. Their analysis showed that the number of pores, the specific surface area, and the number of oxygen-containing functional groups on the surface increased after oxidation, which increased the recovery efficiency of the particles by flotation.

According to Dey et al. (2013), the oxidized coals have a negative surface charge due to the presence of the functional groups such as –COOH and –OH. Using mechanical and column flotation cells, they studied flotation at different pH and determined the pre-treatment efficiency of the coal particles. Rahman et al. (2012) studied the recovery efficiency in a laboratory-scale flotation column by changing the feed size. Abkhoshk et al. (2010) studied the effect of particle size on the flotation recovery and observed that it has a significant effect on the kinetic constants. Ofori et al. (2014) developed a kinetic model for flotation to predict the rate constants and recovery of coal particles. Szczerkowska et al. (2018) studied the kinetics of flotation of various hydrophobic platelets of different shapes in the aqueous solutions of a non-ionic frother.

Kurniawan et al. (2011) studied the effect of frother (Dowfroth 250) presence in the $MgCl_2$, NaCl, and $NaClO_3$ solutions, which can affect the efficacy of flotation of coal particles. They explained the mechanism of flotation improvement and attempted to connect the recovery of flotation with bubble size in the froth stability and froth phase. They reported that the presence of electrolytes in the system increased the flotation recovery based on its concentration and type. They came to the conclusion that the introduction of salt to a flotation system produced finer bubbles in the froth phase, which enhanced the kinetics of the coal flotation. The type and concentration of the electrolyte were found to be effective. They also reported a relationship between the flotation recovery and the stability of the froth.

Moreover, a direct correlation was established between the bubble size distribution and the flotation recovery in the froth phase. Recently, Vinnett et al. (2019a) have characterized the kinetics based on an inversion approach. Vinnett et al. (2019b) evaluated the flotation rate with a set of one-parameter models. Conventionally, rougher recovery achieved at a certain time is used for the evaluation of flotation efficiency. Since the cumulative recovery of a constituent in the concentrate is proportional to the time of flotation, it can be contemplated as a time-rate recovery (Sripriya et al., 2003; Yuan et al., 1996). So, a mathematical model, including both the recovery and rate functions, can thoroughly relate the recovery profiles. It is found that coal particles in a flotation pulp possess a variety of rate constants, which are based on floatability (Ofori et al., 2006). Several researchers have deliberated the kinetic aspects of froth flotation with a focus on the particle size (Hernáinz and Calero, 2001; Loewenberg and Davis, 1994; Polat et al., 2003; Uçurum and Bayat, 2007). However, because of the accumulation of the fine particles, a complex relationship is established between particle size and flotation rate (Al Taweel et al., 1986; Humeres and Debacher, 2002). Later, for a better knowledge of the flotation process, several models have

been developed. Dowling et al. (1985) examined 13 different models of flotation and differentiated among them based on several sets of data on time –recovery profiles of copper ore. Zhou et al. (2019) have reported the relationships between the surface properties of the meta-bituminous, and sub-bituminous coals, and their flotation properties. In addition, they investigated the usability of the flotation kinetic constants obtained from various kinetic models for the prediction of the flotation response. They analyzed the flotation data by six flotation kinetic models successfully. They reported that with increasing collector dosage, the flotation rate constants decreased while the opposite trend was observed for flotation recovery. Lynch et al. (1981) have described three sets for the flotation models (i.e., probability, empirical, and kinetic). The empirical models include a trial and error feedback method to optimization and are too specific to their environment. Moreover, model parameters from statistical techniques do not have any physical significance and do not provide any information of the flotation process. The empirical models offer little predictive capacity beyond the conditions used in their evaluation (Nguyen and Schulze, 2004). The probability models mainly evaluate the probabilities of froth stability, particle–bubble collision, and adhesion. The simple form of the probability approach is similar to the kinetic models (Sripriya et al., 2003; Yuan et al., 1996), and it has been highly useful to better understand which leads to reasonably accurate predictions (Hernáinz and Calero, 2001). This work considers a kinetic model based on the probabilities of adhesion, particle–bubble collision, and froth stability. Recovery of coal particles in a continuous flotation column has been investigated at regular time intervals to determine its dependency on the type of surfactant, particle size, gas and slurry velocities. The size of the bubble, as required for the model analysis, was experimentally estimated by a photographic method under different operating conditions. Based on the present experimental data at different operating conditions, a general correlation was developed, which was used to calculate the bubble

diameter. A generalized correlation for the rate constant and the induction time was also proposed based on the experimental data under the different operating conditions.

6.2. Experimentation

6.2.1. Experimental setup

Fig. 6.2 denotes the schematic representation of the experimental setup for the recovery of fine coal particles. The details and information about the different components of the experimental set up are already discussed in section 2.2.1 in Chapter 2.

Figure 6.2: (a) Schematic representation of the experimental setup: 1. air compressor, 2. storage tank, 3. pump, 4. spherical sparger, 5. solenoid valve, 6. flotation column, 7. control valve, 8. liquid rotameter, 9. gas rotameter, 10. collecting hood, 11. collecting beaker, and (b) spherical sparger. ((This figure is withhold because of copyright)

6.2.2. Materials and experimental procedure

The anionic surfactant sodium dodecylbenzene sulfonate (SDBS) (> 95 % purity) and cationic surfactant, N-Cetyl-N, N, N-trimethyl ammonium bromide (CTAB) (99% purity) were purchased

from Sigma Aldrich (Germany), and Loba Chemie (India) respectively. These two chemicals were used as surface-active agents. The extraction, crushing, and particle size analysis of the coal particle is already discussed in section 2.2.2.

All the experiments were carried out at standard conditions. The ranges of superficial slurry velocity and superficial gas velocity are $0.007 \le u_{slr} \le 0.021$ and $0.021 \le u_{sg} \le 0.063$ m/s, respectively. Five different surfactant concentrations (i.e., 25, 50, 75, 100, and 150 g/m^3) were used. The details of the measurement of slurry density, slurry viscosity, and surface tension already discussed in section 2.2.2. The physical properties of the materials used in the experiments are shown in Tables 6.1 and Table 6.2.

Table 6.1: Physical properties of the systems at 298 ± 1 K.

Slurry concentration (kg/m^3)	Surfactant concentration (g/m^3)	Viscosity (mPa s)		Density (kg/m^3)	
		SDBS	CTAB	SDBS	CTAB
5.56	25	1.309	1.347	1004.96	1004.94
	50	1.421	1.494	1005.25	1005.29
	75	1.516	1.639	1005.47	1005.61
	100	1.619	1.786	1005.73	1005.94
	150	1.827	2.079	1006.24	1006.61

Table 6.2: Surface tensions of aqueous surfactant solutions at 298 ± 1 K.

Surfactant concentration (g/m^3)	Surface tension (N/m)	
	SDBS	CTAB

25	0.0358	0.0312
50	0.0300	0.0290
75	0.0258	0.0212
100	0.0208	0.0162
150	0.0108	0.0062

The flotation column was thoroughly cleaned and washed with tap water. For all the experiments, tap water was used. Coal particles, along with the surfactant, were added to the solution tank. The tank was filled with 9 dm^3 of water. The slurry was introduced at a high point of 0.73 m from the base of the column. Froth generated in the column, under a particular set of operating conditions, accumulated in the collector box. At regular intervals of 120 s, the froth was collected continuously in beakers. Each set of experiments was done for 1200 s. The samples after collection were dried in an oven (make: Sonuu, India; model: Digitel) at 383 K for ~1 d. The analysis was performed for a set of constraints such as particle size, superficial liquid velocity, superficial gas velocity surfactant concentration, and surfactant type.

6.3. Model for flotation kinetics

Flotation works by three main processes, i.e., (i) aeration (ii) mixing, and (iii) separation. Various models were proposed to interpret the flotation kinetics in terms of hydrodynamics (Dai et al., 2000; Finch and Dobby, 1990; Tuteja et al., 1994). The kinetic models are focused on the interaction between the bubbles and particles. In this work, the flotation of fine coal particles by bubbling was considered as a first-order process. The kinetic equation for the rate of recovery of particles can be expressed as (Bloom and Heindel, 1997).

$$\frac{dN_p}{dt} = -KN_p = ZE_cE_aE_s \tag{6.1}$$

where K is the rate constant, and N_p is the number density of floatable mineral particles. The parameter, *Z*, is linked to the bubble–particle collision frequency. It depends on the flotation pulp hydrodynamics and size of the bubbles and particles, and E_a, E_c, and E_s are the particle–bubble adhesion, collision, and stability efficiencies, respectively. The parameter, *Z*, is expressed as (Pyke et al., 2003).

$$Z = 5N_bN_p\left(\frac{d_p + d_{b,32}}{2}\right)^2\left(\bar{V}_b^2 + \bar{V}_p^2\right)^{1/2} \tag{6.2}$$

where $\bar{V}_p$ and $\bar{V}_b$ are the average velocity of the particle and bubble relative to fluid velocity. The number density (N_b) of the bubble can be calculated from the following equation.

$$N_b = \frac{6\varepsilon_g}{\pi d_{b,32}^3} \tag{6.3}$$

where ε_g denotes the gas holdup and $d_{b,32}$ represents the Sauter mean bubble diameter. In the present work, since $d_b \gg d_p$, $\left(V_p^2\right)^{1/2}$ can be neglected. Therefore, Eq. (6.2) can be written as

$$Z = 30\left(\frac{N_p\varepsilon_g}{\pi d_{b,32}^3}\right)\left(\frac{d_{b,32} + d_p}{2}\right)^2\left(\bar{V}_b^2\right)^{1/2} \tag{6.4}$$

The root-mean-square velocity of the bubbles can be calculated as (Schubert, 1999).

$$\left(\bar{V}_b^2\right)^{1/2} = \frac{0.33\varepsilon^{4/9} d_{b,32}^{7/9}}{\nu^{1/3}} \left(\frac{\Delta\rho}{\rho_f}\right)^{2/3} \tag{6.5}$$

where $\Delta\rho$ is the difference in the densities of the fluid $\left(\rho_f\right)$ and particle $\left(\rho_p\right)$, ν is the kinematic viscosity of the fluid and ε is the energy dissipation rate per unit mass. ε can be calculated as (Wu and Patterson, 1989).

$$\varepsilon = 0.85 \left(\frac{\bar{U}_{cx}^2 + \bar{U}_{cy}^2 + \bar{U}_{cz}^2}{2}\right)^{3/2} L^{-1} \tag{6.6}$$

where L is the flow length scale and U_c is the circulation velocity of slurry. The length scale is $0.07d_c$ (Cant, 2001). Therefore Eq. (6.6) can be expressed as

$$\varepsilon = 12.143 \left(\frac{\bar{U}_{cx}^2 + \bar{U}_{cy}^2 + \bar{U}_{cz}^2}{2}\right)^{3/2} d_c^{-1} \tag{6.7}$$

Eq. (6.4) can be modified by using Eqs. (6.5) and (6.7) as

$$Z = 30 \left(\frac{N_p \varepsilon_g}{\pi d_{b,32}^3}\right) \left(\frac{d_{b,32} + d_p}{2}\right)^2 \left(\frac{d_{b,32}^{7/9}}{\nu^{1/3}}\right) \left(\frac{\Delta\rho}{\rho_f}\right)^{2/3} \left[\left(\frac{\bar{U}_{cx}^2 + \bar{U}_{cy}^2 + \bar{U}_{cz}^2}{2}\right) d_c^{-1}\right]^{4/9} \tag{6.8}$$

Substituting Z from Eq. (6.8) to Eq. (6.1), the expression of K becomes

$$K = 30 \left(\frac{\varepsilon_g}{\pi d_{b,32}^3}\right) \left(\frac{d_{b,32} + d_p}{2}\right)^2 \left(\frac{d_{b,32}^{7/9}}{\nu^{1/3}}\right) \left(\frac{\Delta\rho}{\rho_f}\right)^{2/3} \left[\left(\frac{\bar{U}_c^2}{2}\right)^{3/2} d_c^{-1}\right]^{4/9} E_c E_a E_s \tag{6.9}$$

where $\left(\bar{U}_{cx}^2 + \bar{U}_{cy}^2 + \bar{U}_{cz}^2\right)/2 = \bar{U}_c^2/2$ (6.10)

At any time, the fractional recovery of the particle $R_{c,t}$ by flotation is expressed as

$$R_{c,t} = R_{\max}\left[1-\exp\left(-Kt\right)\right] \tag{6.11}$$

The fractional recovery $\left(R_{c,t}\right)$ is the ratio of cumulative recovery of the particles at a time to the initial feed of the particles. $R_{\max}$ is the maximum (fractional) theoretical flotation recovery of the particles, t is the cumulative flotation time, and the parameter, K is called the flotation rate constant. By fitting the model to an experimental recovery–time curve $R_{\max}$ (maximum recovery) and K (first-order rate constant) are obtained. To evaluate the variables affecting the flotation process, they can be used. An assumption that the concentration of the floatable material is the only independent variable is taken for the derivation of this equation (Gupta and Yan, 2016; Labidi et al., 2007).

6.3.1. Collision efficiency

The collision efficiency is defined as the ratio of the number of particles colliding with the bubble to the number of particles swept across the projected area of the bubble per unit time (Weber and Paddock, 1983). A review of the different models for calculating the collision efficiency has been given by Dai et al. (2000). Collision efficiency for the mobile bubble surface can be predicted by the Sutherland equation (Sutherland, 1948; Weber and Paddock, 1983). The model for the collision efficiency proposed by Weber and Paddock (1983) is based on the assumption that the particles are very small, and the particle–fluid hydrodynamic interaction is insignificant. According to their model, the collision efficiency can be expressed by two components, i.e., one involving the particle settling velocity due to the gravity and the other involving the fluid velocity at the bubble surface. The former component is known as the *gravitational effect,* and the latter is termed as an *interceptional effect*. They are dependent on

the bubble Reynolds number and are obtained from the Navier–Stokes equations. The collision efficiency, expressed by Weber and Paddock (1983) is given by

$$E_c = E_{cg} + E_{ci} \tag{6.13}$$

The collision efficiency resulting because of the gravitational effect $\left(E_{cg}\right)$ is given by Weber and Paddock (1983)

$$E_{cg} = \left(\frac{U_p}{1+U_p}\right)\left[1+\left(\frac{d_p}{d_{b,32}}\right)^2\right]\sin^2\theta_c \tag{6.14}$$

Figure 6.3: A typical diagram for the collision between the bubble and the particle (This figure is withhold because of copyright).

The schematic diagram of the bubble and particle collision is shown in Fig 6.3. θ_c is the angle of tangency between the particle grazing trajectory and the bubble surface, or the collision angle above which no collision is possible, R_b is the radius of the bubble, r_p is the radius of the particle, r is the distance between the surfaces of the bubble and particle, R_c is the centre distance between particle and bubble at an angle, θ_c as shown in Fig. 6.3 and U_p is the particle velocity. The value of the maximum collision angle is governed by the bubble Reynolds number and can be given by the following equations, which were developed by the empirical curve fitting to the collision data (Woo and Sun-Wai, 1971).

$$\theta_c = 78.1 - 7.37\log\left(\mathrm{Re}_{sl}\right) \quad \text{for} \quad 20 < \mathrm{Re}_{sl} < 400 \tag{6.15}$$

$$\theta_c = 98 - 12.49\log\left(10\,\mathrm{Re}_{sl}\right) \quad \text{for} \quad 1 < \mathrm{Re}_{sl} < 20 \tag{6.16}$$

$$\theta_c = 90 - 2.5\log\left(100\,\mathrm{Re}_{sl}\right) \quad \textbf{for} \quad 0.1 < \mathrm{Re}_{sl} < 1 \tag{6.17}$$

The collision efficiency governed by interceptional effect $\left(E_{ci}\right)$ is given by Weber and Paddock (1983)

$$E_{ci} = 1.5\left[1 + \left(\frac{3}{16}\right)\left(\frac{\mathrm{Re}_{sl}}{1 + 0.249\,\mathrm{Re}_{sl}}\right)\right]\left(\frac{d_p}{d_{b,32}}\right)^2 \quad \text{for} \quad \mathrm{Re}_{sl} < 200 \tag{6.18}$$

6.3.2. Stability efficiency

Stabilization or destabilization of a bubble–particle aggregate can be assessed by the stability efficiency. Joachim (1993) proposed that the acceleration force that controls the detachment of a particle from the bubble depends on the intensity of turbulence in the flow. The attachment forces are hydrostatic and capillary while the detachment forces are due to buoyancy, gravity, and capillary pressure inside the gas bubble. According to Duan et al. (2003), the sum of these forces is zero at equilibrium. At this equilibrium condition, the stability efficiency can be expressed as

$$E_S = 1 - \exp\left[1 - \frac{6\sigma\sin\left(\omega\right)\sin\left(\omega + \theta\right)}{d_p^2\left(\Delta\rho g + \rho_p a_c\right) + 1.5 d_p\left\{\sin\left(\omega\right)\right\}^2 f\left(d_{b,32}\right)}\right] \tag{6.19}$$

where a_c is the centrifugal acceleration, and σ is the surface tension, which is dependent on the level of turbulence in the turbulent flow field in the flotation column. ω denotes the angle of a

particle at the liquid–gas interface $\left(\omega = 180^{\circ} - \theta/2\right)$ and g is the acceleration due to gravity. The function, $f\left(d_{b,32}\right)$, is defined as (Joachim, 1993)

$$f\left(d_b\right) = \left[\frac{4\sigma}{d_{b,32}} - d_{b,32}\rho_f g\right] \tag{6.20}$$

If the particle is smaller than the bubble, the centrifugal acceleration $\left(a_c\right)$ can be calculated by

$$a_c = 1.9\frac{\varepsilon^{2/3}}{d_{b,32}^{1/3}} \tag{6.21}$$

where ε is the energy dissipated per unit mass of the dispersed phases. It can be calculated as

$$\varepsilon = \frac{\Delta P\left(Q_g + Q_{sl}\right)}{\rho_{sl} V_{dis}} \tag{6.22}$$

where ΔP is the frictional pressure drop, V_{dis} is the volume of discharge, Q_g is the gas flow rate, ρ_{sl} is the slurry density, and Q_{sl} is the slurry flow rate.

6.3.3. Attachment efficiency

In mineral flotation, the attachment of a hydrophobic particle to a bubble is the major phenomenon in the particle–bubble interaction. When the contact time is more than the induction time $\left(T_i\right)$ of the particle–bubble, the particle–bubble attachment prevails. The time required for the liquid film between the bubble and the particle to thin and collapse is known as induction time. If a particle collides on the bubble surface with kinetic energy sufficient enough to result in a substantial distortion of the surface, the colliding particle bounces from the deformed surface due to the elastic

energy of the deformed portion. The portion of all colliding particles that stay on the bubble for a time greater than the induction time is termed as attachment efficiency (E_a) (Dobby and Finch, 1987). After the collision, the particle slides over the bubble, and attachment takes place when the liquid film thins and ruptures (Dobby and Finch, 1987). Thus, particles that have sliding time higher than the induction time will attach to bubbles. According to Dobby and Finch (1987) the attachment efficiency, based on the modification for the particle–bubble system, can be expressed as

$$E_a = \left[\frac{\sin(\theta_a)}{\sin(\theta_m)}\right]^2 \tag{6.23}$$

where θ_a is the adhesion angle when the particle impacts the bubble. This angle relates to the induction time and the sliding time to the attachment efficiency due to the sliding time is equal to the induction time (Dai et al., 1998). θ_m is the maximum probable collision angle of the particle on the surface of the bubble, which is given by (Dukhin, 1982)

$$\theta_m = \sin^{-1}\left[2\beta\left\{\left(1+\beta^2\right)^{1/2} - \beta\right\}\right]^{1/2} \tag{6.24}$$

where the parameter, β , is a function of the relative significance of the interceptional and inertial contributions to the collision process, which is defined as (Dai et al., 1999)

$$\beta = \frac{4E_{su}}{9K_a} \tag{6.25}$$

where E_{su} is the collision efficiency, defined by (Sutherland, 1948)

$$E_{su} = 3d_p / d_{b,32}. \tag{6.26}$$

The parameter, K_a, is defined as (Dai et al., 1998)

$$K_a = \frac{2U_c\left(\rho_p - \rho_f\right)d_p^2}{9\nu d_{b,32}} \tag{6.27}$$

Under potential flow conditions, the adhesion angle is given by (Dobby and Finch, 1987)

$$\theta_a = 2\tan^{-1}\left[\exp\left\{T_i \frac{2\left(U_{sp}+U_p\right)+U_b\left(\frac{d_p}{d_p+d_{b,32}}\right)^3}{d_p+d_{b,32}}\right\}\right] \tag{6.28}$$

In this work, the induction time $\left(T_i\right)$ is obtained by fitting Eq. (6.10) to the experimental data on the recovery under different operating conditions. The flotation rate constant was determined by this method. From the rate constant, the induction time was calculated based on Eq. (6.9) or (6.11). A typical result of the variation of recovery with time, and the determination of the rate constant by using Eq. (6.11) are shown in Fig. 6.4.

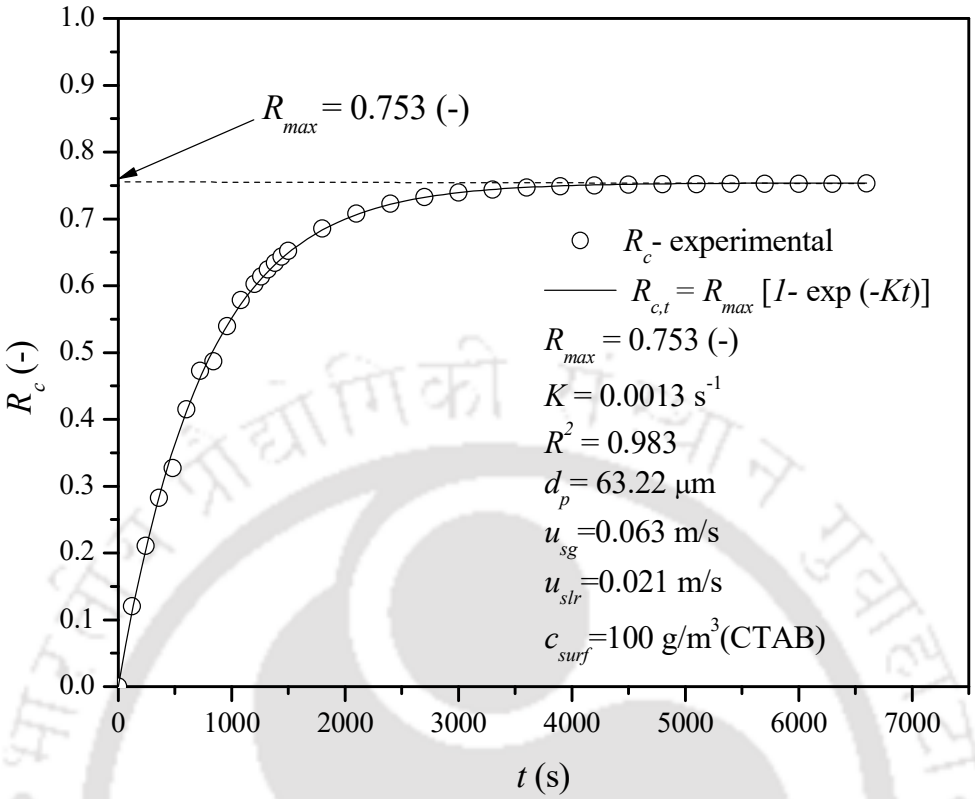

Figure 6.4: Variation of recovery with time, and determination of the rate constant.

6.4. Results and discussion

6.4.1. Effect of superficial gas velocity on the recovery of coal particles

The effect of superficial gas velocity on the recovery of coal particles at a constant slurry concentration (i.e., 5.56 kg/m^3), surfactant concentration (i.e., 100 g/m^3), superficial slurry velocity (i.e., 0.007 m/s), and particle size (i.e., 235.61 μm) in the presence of CTAB (i.e., cationic surfactant) and SDBS (i.e., anionic surfactant) is shown in Fig. 6.5. The bubbles were responsible for carrying the coal particles to the recovery plate. The recovery of the coal particles increased with the increasing volume of the froth.

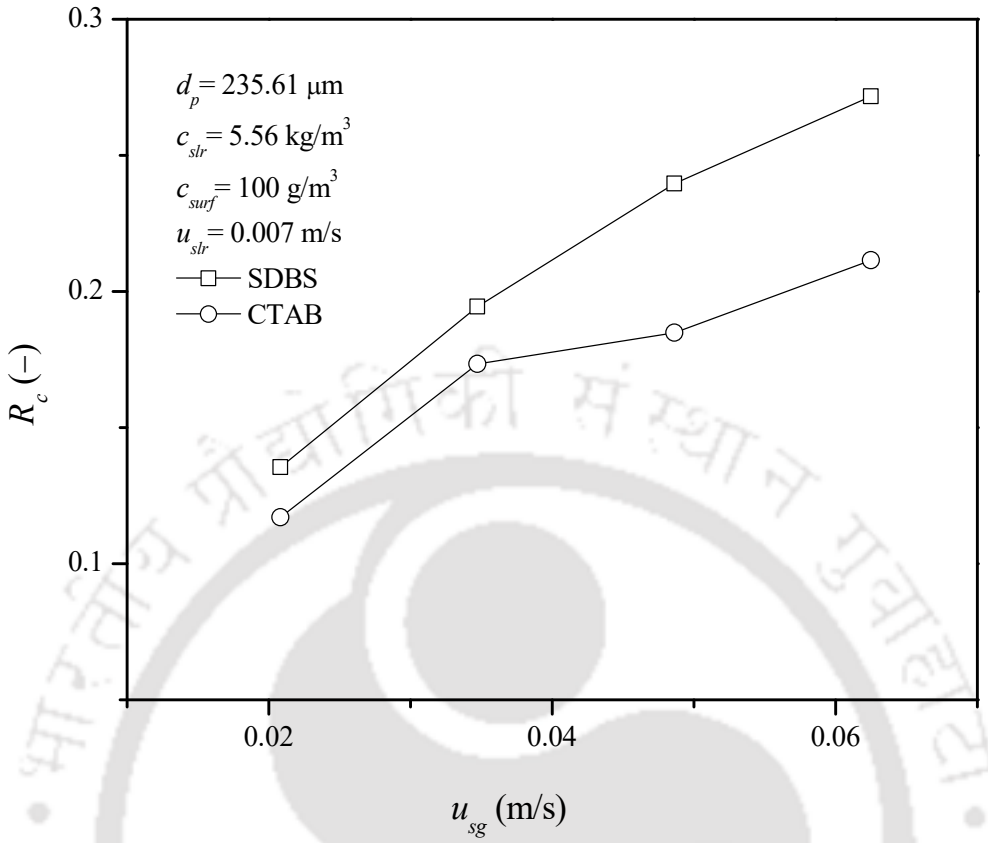

Figure 6.5: Effect of superficial gas velocity on the recovery of the coal particles.

It was found that the amount of recovery was increased with the increasing amount of the gas passing through the column. As the gas velocity was increased from 0.021 to 0.063 m/s, the percentage recovery in the presence of CTAB increased from 13 to 27%, and the same in the presence of SDBS increased from 11.5 to 20 %. The model developed by Soni (2013) predicts that the recovery of the particles by flotation would increase with the increased airflow rate. Similar results were obtained by Mackay et al. (2018). They have reported the complex effects of the superficial gas velocity and particle size on the recovery of copper.

6.4.2. Effect of superficial slurry velocity on the recovery of coal particles

The effect of superficial slurry velocity on the recovery of coal particles at a constant slurry concentration (i.e., 5.56 kg/m^3), surfactant concentration (i.e., 100 g/m^3), superficial gas velocity

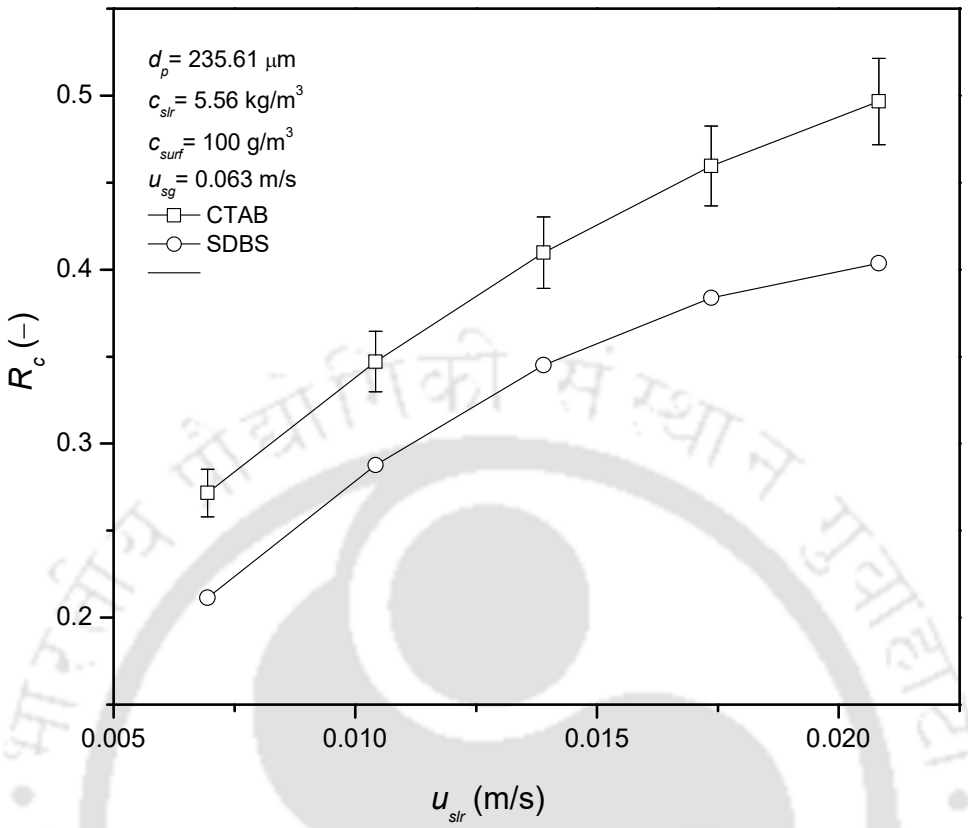

Figure 6.6: Effect of liquid velocity on the recovery of the coal particles.

(i.e., 0.063 m/s) and particles size (i.e., 235.61 μm) in the presence of CTAB (i.e., cationic surfactant) and SDBS (i.e., anionic surfactant) is shown in Fig. 6.6. It was found that the amount of recovery of the particles depended on the slurry flow rate.

When slurry velocity was increased from 0.007 to 0.021 m/s, the recovery increased from 27 to 49% in the presence of CTAB. For SDBS, the recovery increased from 23 to 39%. Due to the lower surface tension of CTAB, gets very stable small bubble. So recovery rate of coal particle is higher in presence of CTAB compared to SDBS.

6.4.3. Effect of particle size on the recovery of coal particles

The effect of particle size on the recovery of coal particles at a constant slurry concentration (i.e., 5.56 kg/m^3), superficial gas velocity (i.e., 0.063 m/s), and superficial slurry velocity (i.e., 0.021 m/s) is shown in Fig. 6.7.

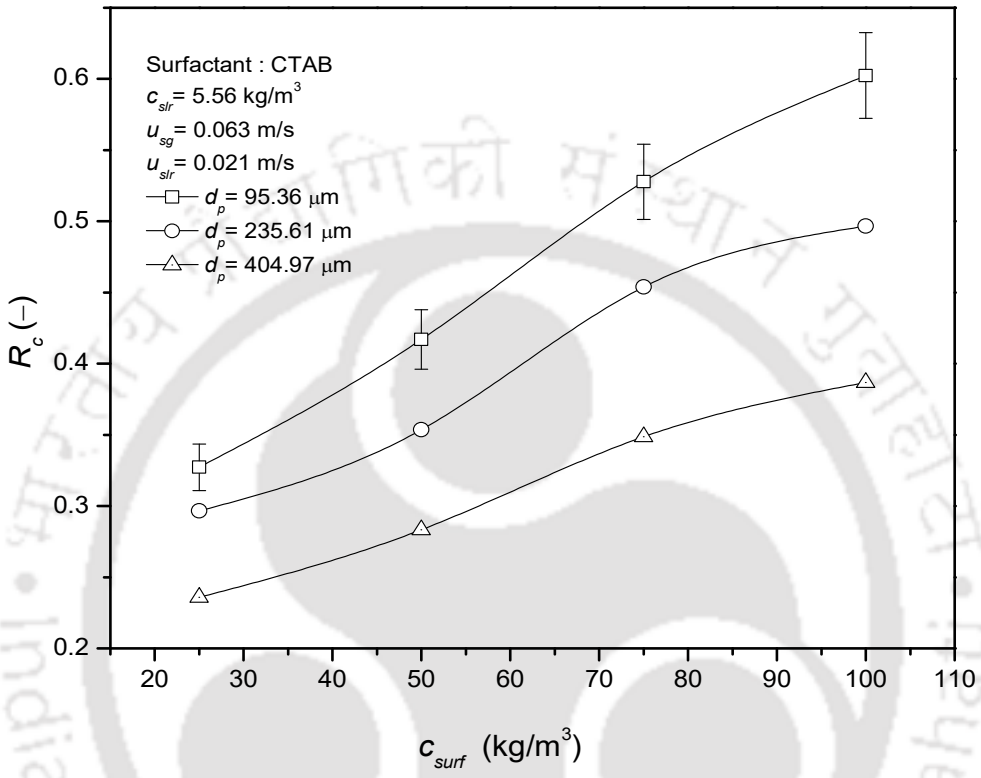

Figure 6.7: Effect of particle size on the recovery of the coal particles.

It was observed from these experiments that the amount of recovery was more for the smaller particles, which is expected because the smaller particles are easily carried with the froth. The maximum recovery was ~60% in the presence of 100 g/m^3 CTAB for the 95.36 μm particles. When the size of the particles was increased, the time required for the particles to attach to the bubble surface increased, which resulted in a decrease in recovery (Ye et al., 1989; Yoon and Yordan, 1991).

6.4.4. Effect of surfactant concentration on the recovery of coal particles

The surfactant concentration's effect on the recovery of coal particles for CTAB and SDBS is shown in Fig. 6.8.

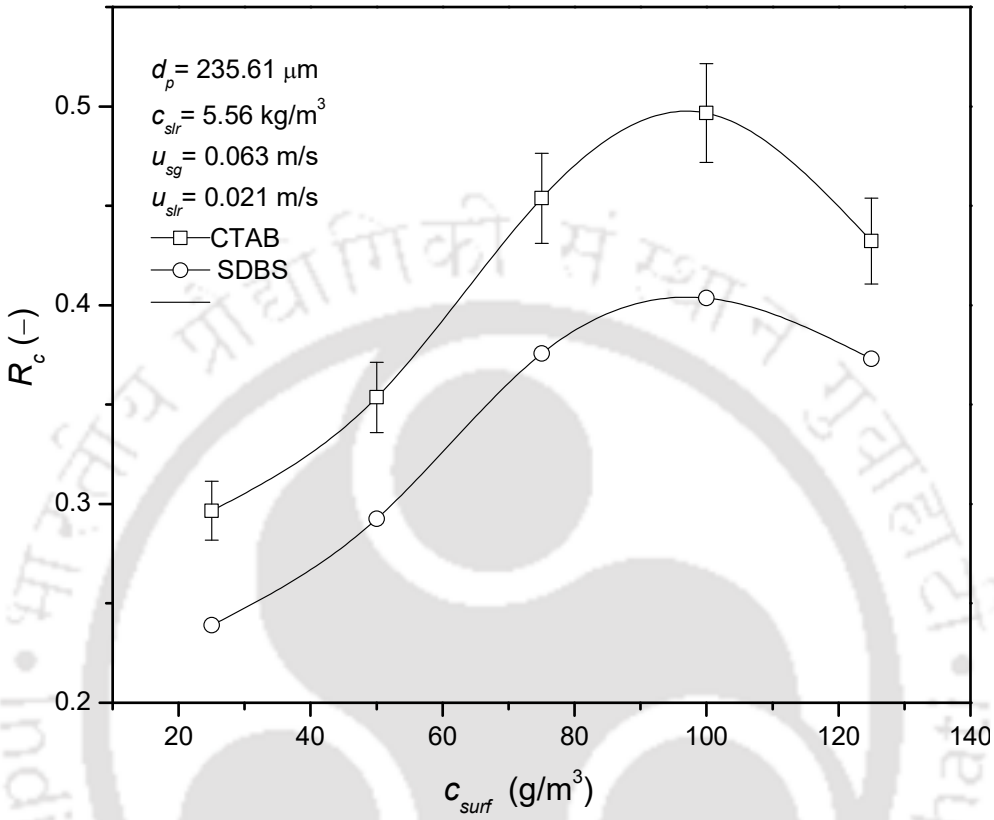

Figure 6.8: Effect of surfactant concentration on the recovery of the coal particles.

The surfactant concentration was varied from 25 to 100 g/m^3. The slurry concentration (i.e., 5.56 kg/m^3), particle size (i.e., 235.61 μm), superficial gas velocity (i.e., 0.063 m/s), and superficial slurry velocity (i.e., 0.021 m/s) were kept constant.

The surfactant concentration significantly influences the number density of the bubbles and the stability of the particles on the bubble surface. The probability of collision between a particle and the bubble is significantly affected by the surfactant concentration. The probability of collision increases with increasing particle size but decreases with increasing bubble size.

From the experimental results, it was observed that the recovery of coal particles increased with increasing surfactant concentration in the feed. However, after a certain limit, the recovery was reduced inasmuch as the amount of froth reached its maximum limit. The same phenomenon was observed for CTAB as well as SDBS. When the concentration of CTAB was increased from 25 to 100 g/m^3, the recovery increased from 29 to 49%. For the same increment in the SDBS concentration, the recovery increased from 24 to 40%. The recovery began to decrease when the surfactant concentration was increased beyond 100 g/m^3. It decreased to 43 and 37% for CTAB and SDBS, respectively, when the surfactant concentration was 125 g/m^3.

6.4.5. Variation of recovery of the particles with time

The variation of the recovery of the coal particles with time in the CTAB and SDBS surfactant's presence at a constant slurry concentration (i.e., 5.56 kg/m^3), particle size (i.e., 235.61 μm), surfactant concentration (i.e., 100 g/m^3), superficial gas velocity (i.e., 0.063 m/s), and superficial slurry velocity (i.e., 0.021 m/s) is shown in Fig. 6.9. The amount of coal recovery increased as the time elapsed because the coal particles were carried to the top along with the froth and were separated from the feed.

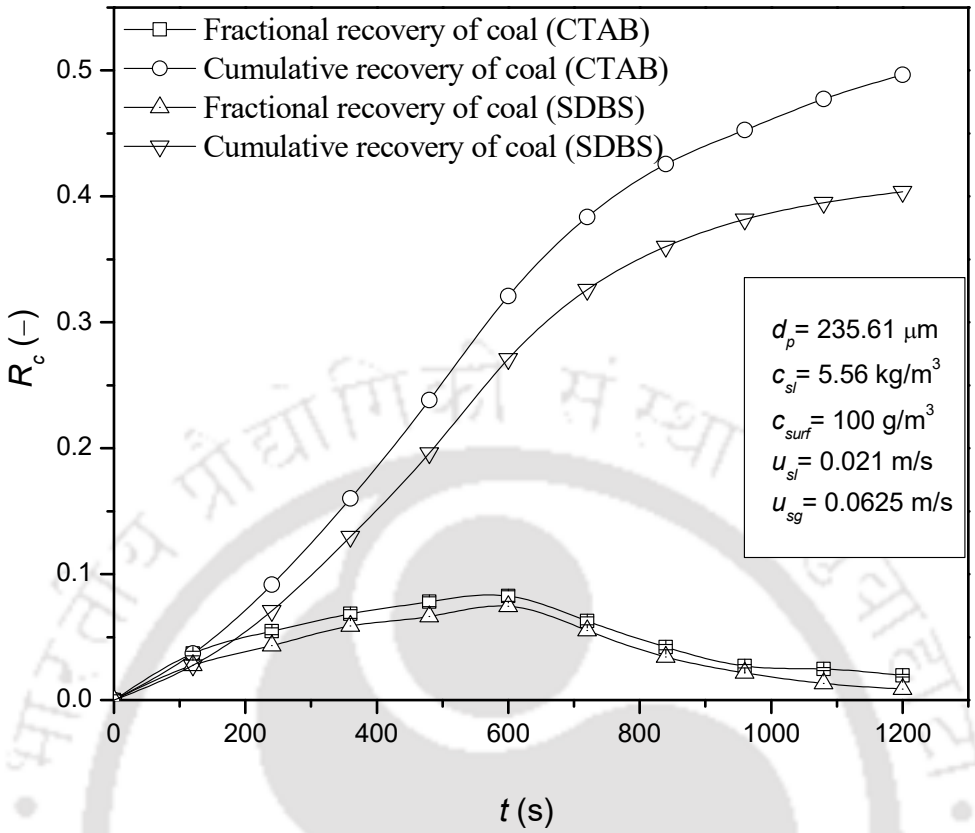

Figure 6.9: Variation of recovery of the particles with time.

From these results, it can be concluded that the fractional recovery initially increased with time, and then decreased at longer times.

6.4.6. Interpretation of induction time

Sven-Nilsson (1934) presented the concept of induction time by moving a bubble towards a flat mineral surface and then receding it away. The induction time is the minimum contact time for the successful thinning of the intervening liquid film to critical thickness, where the film ruptures. The induction time is dependent on many physical constraints (Yoon and Yordan, 1991). From the experimental results, it is observed that the induction time is a function of the concentration,

particle size, superficial gas velocity, and superficial slurry velocity. It is dependent on the type of surfactant as well.

An increase in superficial slurry velocity decreases the time for the particle–bubble adhesion and results in the reduction of the induction time. Particles having a shorter induction time can be captured with ease, and are supposed to have a higher selectivity. As shown in Fig. 6.10, the induction time increases with increasing particle size. A correlation for the induction time has been developed by dimensional analysis in terms of the operating variables. The numerical constants of the correlation were determined by the multiple regression analysis using the present experimental data. The correlation can be expressed as

$$\frac{T_i u_{sl}}{d_c} = 4.10\times10^{4}\left(\frac{u_{sg}}{u_{sl}}\right)^{-1.354}\left(\frac{d_{b,32}}{d_c}\right)^{4.255}\left(\frac{d_p}{d_c}\right)^{0.297} \mathrm{We}_{slr}^{0.191}\,\mathrm{Re}_{slr}^{-0.171}\,\mathrm{Fr}_{slr}^{-0.580} \qquad (6.29)$$

where Re_{slr} is the Reynolds number $\left(\equiv d_c u_{sl}\rho_{slr}/\mu_{slr}\right)$, We_{slr} is the Weber number $\left(\equiv d_c u_{sl}^2\rho_{slr}/\sigma\right)$, Fr_{slr} is the Froude number $\left(\equiv u_{sl}/\sqrt{g d_c}\right)$. The correlation coefficient and standard error of Eq. (6.29) are 0.9498, and 0.1181 respectively. The correlation is valid for the following ranges: $3 \le u_{sg}/u_{sl} \le 9$; $0.06 \le d_b/d_c \le 0.091$; $1.15\times10^{-3} \le d_p/d_c \le 7.36\times10^{-3}$; $0.1284 \le \mathrm{We}_{slr} \le 3.8808$; $212.51 \le \mathrm{Re}_{slr} \le 844.29$; $9.45\times10^{-3} \le \mathrm{Fr}_{slr} \le 28.36\times10^{-3}$. The percentage error of the correlation given by Eq. (6.29) is ± 18.31.

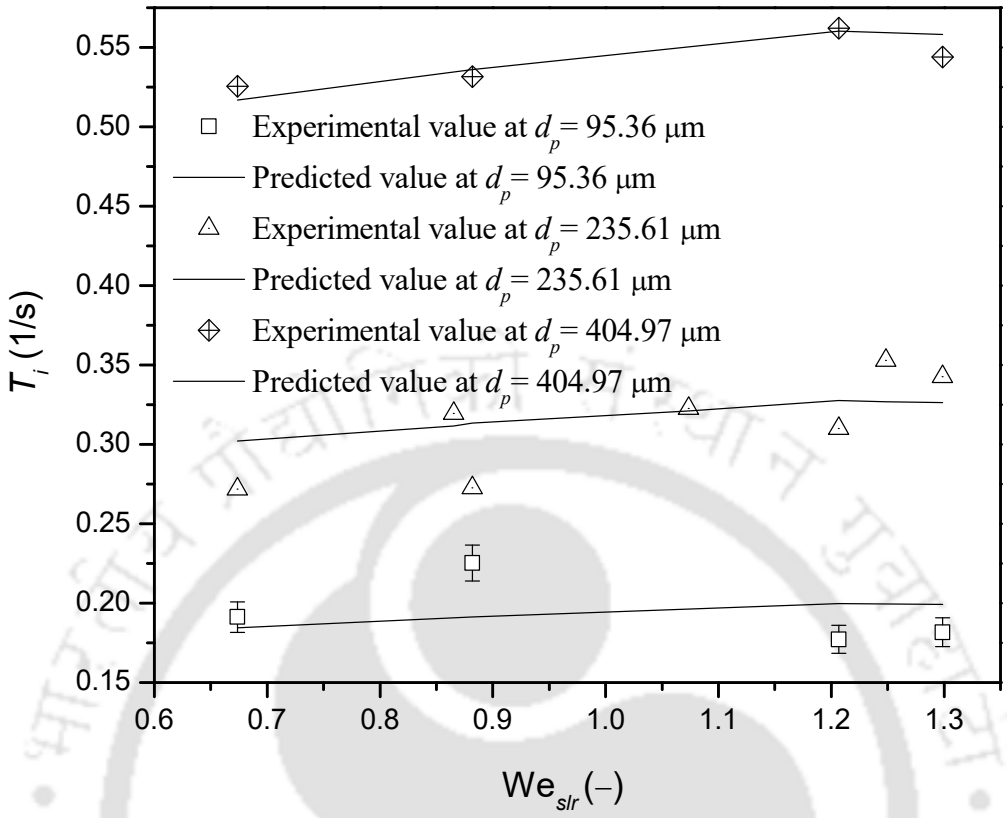

Figure 6.10: Variation of induction time with Weber number for different particle sizes.

6.4.7. Interpretation of the flotation rate constant

The flotation rate constant depends on the superficial slurry velocity, superficial gas velocity, type of surfactant, surfactant concentration, and particle size. A rise in the superficial slurry velocity significantly raises the frequency of collision. It is also seen that the surfactant concentration has an important effect on the rate constant. The presence of a surfactant enhances the rate constant in two ways. Firstly, it decreases the bubble size, which increases the particle–bubble collision. As shown in Fig. 6.11, the flotation rate constant decreases with increasing particle size. With the experimental data, a correlation has been developed to predict the flotation rate constant. This correlation is

$$\left(\frac{Kd_c}{u_{sl}}\right)=6.79\times10^{-12}\left(\frac{u_{sg}}{u_{sl}}\right)^{3.565}\left(\frac{d_{b,32}}{d_c}\right)^{-2.513}\left(\frac{d_p}{d_c}\right)^{0.238}\mathrm{We}_{slr}^{-0.282}\,\mathrm{Re}_{slr}^{1.840} \qquad (6.30)$$

The correlation coefficient and standard error of Eq. (6.30) are 0.9864, and 0.1653 respectively. The ranges of validity of these correlations are: $3.0\le u_{sg}/u_{sl}\le 9.0; 0.0694\le d_b/d_c\le 0.0911;$ $1.149\times10^{-3}\le d_p/d_c\le 7.36\times10^{-3}; 0.1284\le \mathrm{We}_{slr}\le 3.8808; 212.51\le \mathrm{Re}_{slr}\le 869.24$. The percentage error of the correlation given by Eq. (6.30) is ± 17.29.

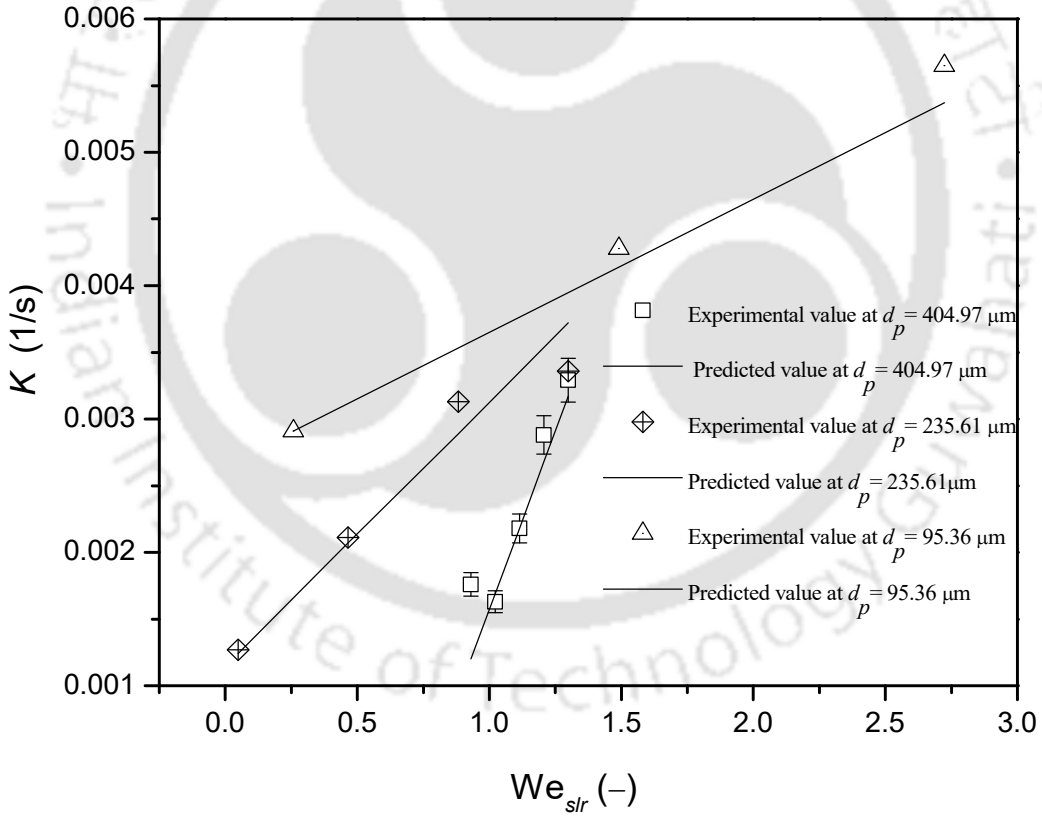

Figure 6.11: Variation of the flotation rate constant with Weber number for different particle sizes.

6.5. Conclusion

The present study was carried out to determine the effects of superficial slurry velocity, superficial gas velocity, particle size, and surfactant concentration on the recovery of fine coal particles in a counter-current flotation column. CTAB and SDBS were used as the cationic and anionic surfactants, respectively. It was found that the coal recovery increased with the superficial gas velocity. As the gas velocity was increased from 0.021 to 0.063 m/s, the recovery in the presence of CTAB increased from 13 to 27%, and the same in the presence of SDBS increased from 11.5 to 20%. Also, the recovery increased with the superficial slurry velocity. For CTAB, when the slurry velocity was increased from 0.007 to 0.021 m/s, the recovery increased from 27 to 49%. On the other hand, the recovery increased from 23 to 39% for SDBS. The recovery was more for the smaller particles. The maximum recovery was ~60% at 100 g/m^3 CTAB for the 95.36 µm particles. The recovery of the particles increased with the surfactant concentration in the feed. However, beyond a certain limit, the recovery was reduced, inasmuch as the amount of froth reached its maximum. The same trend was observed for both the surfactants. When the CTAB surfactant's concentration was increased from 25 to 100 g/m^3, the recovery increased from 29 to 49%. For the same increase in the SDBS concentration, the recovery increased from 24 to 40%. For CTAB and SDBS, the recovery decreased to 43 and 37%, respectively, when the surfactant concentration was 125 g/m^3.

CHAPTER 7 : OVERALL CONCLUSIONS AND RECOMMENDATIONS

7.1. Overall conclusions

The present study is about the hydrodynamics and efficiency of the fine coal particle recovery in a laboratory-scale flotation column under batch and continuous modes. Hydrodynamics such as gas holdup, frictional flow resistance, mixing characteristics of phases were studied and analyzed based on the effect of several operating variables in the presence of surface-active agents.

The gas holdup of the system was found increased profoundly with increasing superficial gas velocity, whereas it decreased with increasing slurry concentration. The effects of four different particle size on gas holdup were analyzed. The gas holdup of the system reduced due to the solid loading, and this reduction was more pronounced at the higher slurry concentrations. The gas holdup of the system was higher in the presence of the cationic surfactant as compared to the anionic surfactant. The addition of particles decreased the gas holdup at all gas flow rates and slurry concentrations. Solids decreased the gas holdup at all superficial gas velocities as a result of increased bubble coalescence, which increased the bubble size, and hence the bubble rise velocity. The gas holdup of the system was higher in the presence of CTAB as compared to SDBS and 1-Hexanol. Particle size did not have a significant effect on gas holdup. Nonetheless, a slight increase in gas holdup was observed in the presence of larger particles. The gas holdup of the flotation system is analyzed with the drift-flux and slip velocity model. The generalized correlation model is also proposed to interpret the gas holdup in the two and three-phase systems. All developed correlations are suited to interpret the experiments' values well within the error range of ± 20%.

Effects of slurry concentration, surfactant concentration, gas flow rate, particle size, and surfactant type on frictional pressure drop were studied. From the current study, it can be concluded that the frictional pressure drop of the system increases with an increase in the superficial gas velocity, slurry concentration, and average particle size. The highest increment in frictional pressure drop (53.66%) occurs at the superficial gas velocity of 0.035 m/s. However, the lowest increment (16.04%) is at 0.007 m/s superficial gas velocity when the particle size varies from 63.22 to 404.97 μm. The frictional pressure drop in the three-phase systems is decreasing with increases in the surfactant concentration. Frictional pressure drop reported in the present system is mainly considered to be primarily due to the liquid-wall friction and phase circulation velocity. It is concluded that the larger bubbles are responsible for higher circulation velocity, which in turn increases the slurry momentum, hence the frictional pressure drop increases. In the presence of high surfactant concentration, the bubble sizes are smaller and do not cause much circulation of slurry and, therefore, tend to reduce the frictional pressure drop. The frictional pressure drop in the presence of 1-Hexanol is higher as compared to the CTAB and SDBS surfactant, which is because of the fact that the surface tension decreasing capability of 1-Hexanol surfactant is smaller than other two surfactants. It is also concluded that the frictional pressure drop in the flotation column is smaller in the case of two-phase in comparison to the three-phase system. The addition of particles to the system led to an increase in the frictional pressure drop. The correlation model is also proposed to interpret the frictional pressure drop in the two and three-phase systems. All developed correlations are suitable to interpret the experimental values well within the error range of ± 20%.

The effects of slurry concentration, particle size, surfactant dose, and gas and slurry velocities on the mixing characteristics were studied. For the three-phase counter-current flow systems, the

characteristic factor of the velocity distribution decreased with increasing superficial gas velocity and surfactant concentration. However, it increased as the slurry concentration, and particle size increased. The dispersion coefficient of the bubble motion increased as the superficial gas velocity and surfactant concentration increased. It also increased as the slurry concentration, and particle size increased. The study shows that the dispersion number is a strong function of slurry concentration, particle size, surfactant dose, and gas and slurry velocities. The velocity distribution model was successfully applied to analyze the dispersion due to bubble motion and the velocity distribution characteristic factor. The dispersion number was found to increase with increasing gas and slurry velocities. The prime cause was increased turbulence and interaction between the phases in the column. An increase in the slurry concentration caused a little reduction in the dispersion number. It was due to an increase in the apparent viscosity of the system. The increase in the particle size significantly reduced the dispersion number. The characteristic factor of the velocity distribution decreased with increasing superficial gas velocity and surfactant concentration, while it increased as the slurry concentration and particle size increases. The dispersion coefficient of the bubble motion increased as the superficial gas velocity and surfactant concentration increased, while it decreases with an increase in slurry concentration and particle size. A correlation was developed for the prediction of dispersion number in terms of dimensionless groups, which was in good agreement with the experimental results.

From the entrainment studies of coal particles carried out in a laboratory flotation column, it was observed that CTAB gave better entrainment than SDBS. The entrainment of coal particles increased with the increasing concentration of the surfactants, i.e., the degree of entrainment $\left(e_p\right)$ increased as the concentration of the surfactant was increased from 25 to 100 g/m^3. An increase in the gas and liquid velocities significantly increased the entrainment. An increase in the particle

size decreased the entrainment, whereas the increase in the particle concentration increased entrainment. An empirical correlation based on the parameters was developed for predicting the entrainment of the coal particles, which may be useful for the scale-up of the process for industrial applications. An empirical correlation based on a wide range of operating variables was developed to predict the degree of entrainment. It was observed that the cationic surfactant gave a better degree of entrainment than its anionic counterpart. The Sauter mean bubble diameter was found to vary in the range of 2.14 –5.94 mm. Bubble size distribution was approximated by the log-logistic distribution.

The present study was also carried out to determine the effects of superficial slurry velocity, superficial gas velocity, particle size, and surfactant concentration on the recovery of fine coal particles in a counter-current flotation column in the presence of surface-active agents. It was found that the coal recovery increased with the superficial gas velocity. As the gas velocity was increased from 0.021 to 0.063 m/s, the recovery in the presence of CTAB increased from 13 to 27%, and the same in the presence of SDBS increased from 11.5 to 20%. Also, the recovery increased with the superficial slurry velocity. For CTAB, when the slurry velocity was increased from 0.007 to 0.021 m/s, the recovery increased from 27 to 49%. On the other hand, the recovery increased from 23 to 39% for SDBS. The recovery was more for the smaller particles. The maximum recovery was ~60% at 100 g/m^3 CTAB for the 95.36 μm particles. The recovery of the particles increased with the surfactant concentration in the feed. However, beyond a certain limit, the recovery was reduced, inasmuch as the amount of froth reached its maximum. The same trend was observed for both the surfactants. When the CTAB surfactant's concentration was increased from 25 to 100 g/m^3, the recovery increased from 29 to 49%. For the same increase in the SDBS

concentration, the recovery increased from 24 to 40%. For CTAB and SDBS, the recovery decreased to 43 and 37%, respectively, when the surfactant concentration was 125 g/m^3.

7.2. Recommendations for future work

Today, many chemical and biochemical industries are facing major challenges due to the complex phenomenon of gas-liquid and gas-liquid-solid in multi-phase contactors. This work focuses on hydrodynamics studies, recovery, and kinetics of coal flotation. However, more studies are required for further understanding of complex hydrodynamic behavior to asses the efficacy of the mineral beneficiation in the flotation column and its scaleup for industrial installation.

Some recommendations for further study as follows.

- The computational flow dynamics for the hydrodynamics and also for the kinetics of flotation is to be studied with real ore from different sources.
- Hydrodynamic studies with different non-Newtonian fluid and its modeling are required as the slurry system is non-Newtonian fluid in nature.
- Studies on the radial distribution of gas holdup with different surfactants, with different particles, in various sizes of the column also required for industrial application.
- In this thesis, axial mixing is studied and analyzed, but there is a lack of study in radial mixing. A CFD approach for mixing phenomenon is recommended.
- For the entrainment study, only one type of particle (coal) is used. The entrainment study with more than one particle will be useful as the real ore is of a mixture of different types of materials. Also the true flotation behavior to be studied in continuous flow operation.

- The scale-up of the recovery of coal particle and its kinetic analysis is also recommended for future study based on changing the geometry of the flotation column.
- Also recovery of more than one particle and its separation is also recommended for future study.

Nomenclature

a_c	centrifugal acceleration of the particle (m/s^2)
c_{slr}	slurry concentration (kg/m^3)
c_{surf}	surfactant concentration (g/m^3)
C	tracer concentration (g/dm^3)
C_θ	dimensionless tracer concentration, C/C_0 (–)
C_0	initial tracer concentration (g/dm^3)
C_o	distribution parameter (–)
$d_{b,32}$	Sauter mean diameter (m)
d_{bi}	individual bubble diameter (m)
d_c	column diameter (m)
d_p	diameter of particle (m)

D_b	dispersion coefficient of bubble motion (m^2/s)
D_T	molecular diffusivity at the axis of the column (m^2/s)
e_G	degree of entrainment for the coal particles (–)
E_a	attachment efficiency (–)
E_c	collision efficiency (–)
E_{cg}	collision efficiency due to gravitational effect (–)
E_{ci}	collision efficiency governed by interceptional effect
E_s	stability efficiency (–)
E_{su}	collision efficiency as defined in Eq. (6.26) (–)
E_z	axial dispersion coefficient (m^2/s)
f_{sp}	single phase Fanning friction factor (–)
f_{tp}	three-phase Fanning friction factor (–)
g	acceleration due to gravity (m/s^2)
h	height of the column (m)
h_l	slurry height before gas sparging (m)

h_m slurry height after gas sparging (m)

k characteristics factor of velocity distribution (–)

K flotation rate constant

K_a parameter defined in Eq. (6.27) (kg/m^3)

K_C conductivity (mS/m)

L flow length (m)

N total number of parameters (–)

N_b number density of the bubbles (1/m^3)

N_p number density of the particles (1/m^3)

Q_g gas flow rate (m^3/s)

Q_{sl} slurry flow rate (m^3/s)

r_p radius of the particle (m)

R_b radius of the bubble (m)

R_c cumulative mass recovery of the valuable particles (%)

$R_{c,t}$ recovery of the coal particles with time (–)

R_{max} maximum recovery (–)

R_{TF}	recovery by true flotation (%)
R_G	cumulative mass recovery of the gangue particles (%)
R_W	cumulative mass recovery of water (%)
t	time (s)
t_m	mean residence time (s)
T_i	induction time (s)
u_0	maximum velocity at the axis of the column (m/s)
u_a	actual velocity of the slurry (m/s)
u_b	bubble terminal rise velocity (m/s)
u_d	weighted average drift velocity (m/s)
u_g	actual gas velocity (m/s)
u_l	actual liquid velocity (m/s)
u_r	relative velocity (m/s)
u_s	slip velocity (m/s)
u_{sg}	superficial gas velocity (m/s)
u_{sl}	superficial liquid velocity (m/s)

u_{slr}	superficial slurry velocity (m/s)
U	the standard uncertainty of the average value (–)
U_b	bubble rise velocity (m/s)
U_c	bubble–particle circulation velocity (m/s)
U_p	particle velocity (m/s)
U_r	percentage relative uncertainties of the continual experiments (–)
U_{sp}	suspension velocity (m/s)
V_b	velocity of bubble (m/s)
$\left(\overline{V_b^2}\right)^{1/2}$	root mean square velocity of the bubbles (m/s)
$\left(\overline{V_p^2}\right)^{1/2}$	root mean square velocity of the particles (m/s)
V_{dis}	volume of discharge (m^3)
x	axial distance between the locations of tracer input and measurement (m)
$\overline{x}$	mean of the continual experiment (–)
x_i	i^{th} component of parameters (–)
z	dimensionless axial distance between the locations of tracer input and the measurement position, x/L (–)

Z	parameter in collision efficiency (–)

Greek

β	parameter defined in Eq (6.25) (kg/m^3)
$\delta(\theta)$	Dirac delta function (–)
ΔH	difference between the two pressure points (m)
ΔP	frictional pressure drop (N/m^2)
ΔP_a	pressure drop due to acceleration (Pa)
ΔP_f	frictional Pressure drop (Pa)
ΔP_h	hydrostatic pressure drop (Pa)
$\Delta P_{f,sp}$	frictional pressure drop for single phase system (Pa)
$\Delta P_{f,tp}$	frictional pressure drop for three phase system (Pa)
ΔP_T	total pressure drop (Pa)
ε	energy dissipation rate per unit mass (m^2/s^3)
ε_g	gas holdup (–)
ε_l	liquid holdup (–)

ε_s	solid holdup (–)
θ	dimensionless time, t/τ (–)
μ_g	gas viscosity (kg/m s)
μ_l	liquid viscosity (kg/m s)
μ_m	mixture viscosity (kg/m s)
μ_{slr}	apparent slurry viscosity (m Pas)
ι	kinematic viscosity (m^2/s)
$\Delta\rho$	density difference between the particle and the fluid (kg/m^3)
ρ_f	density of fluid (kg/m^3)
ρ_p	density of particle (kg/m^3)
ρ_l	liquid density (kg/m^3)
ρ_g	gas density (kg/m^3)
ρ_m	mixture density (kg/m^3)
ρ_s	solid particle density (kg/m^3)
ρ_{slr}	slurry density (kg/m^3)
ρ_{sp}	single phase density (kg/m^3)

ρ_{tp}	three-phase density (kg/m^3)
σ	surface tension (N/m)
σ^2	variance (–)
σ_θ^2	normalized variance (–)
τ	mean residence time (s)
ϕ	geometric factor of the particle (–)
ϕ_S	solid volume fraction in the slurry (–)
θ	contact angle (rad)
θ_a	adhesion angle (rad)
θ_c	collision angle above which no collision is possible (rad)
θ_m	maximum possible collision angle defined in Eq. (6.24) (rad)
X	Martinelli parameter (–)
ω	Angle of a particle at the gas–liquid interface (rad)

Abbreviations

CTAB	N-cetyl-N,N,N-trimethylammonium bromide

SDBS	Sodium dodecyl benzene sulfonate
STDEV	standard deviation

Dimensionless numbers

Eu	Euler number (–)
Fr_l	Froude number for two-phase system (–)
Fr_{slr}	Froude number for three phase system (–)
N_d	dispersion number (–)
Pe	Peclet number (–)
Re_g	Reynolds number of gas (–)
Re_l	Reynolds number of liquid (–)
Re_r	gas Reynolds number based on relative velocity of gas and slurry (–)
Re_{slr}	Reynolds number of slurry (–)
We_l	Weber number for two-phase system (–)
We_{slr}	Weber number for three-phase system (–)

References

Abkhoshk, E., Kor, M., Rezai, B., 2010. A study on the effect of particle size on coal flotation kinetics using fuzzy logic. Expert Syst. Appl. 37, 5201–5207. https://doi.org/10.1016/j.eswa.2009.12.071

Agar, G.E., Chia, J., Requis-C, L., 1998. Flotation rate measurements to optimize an operating circuit. Miner. Eng. 11, 347–360. https://doi.org/10.1016/s0892-6875(98)00013-2

Akita, K., Yoshida, F., 1973. Gas holdup and volumetric mass transfer coefficient in bubble columns. Effects of liquid properties. Ind. Eng. Chem. Process Des. Dev. 12, 76–80. https://doi.org/10.1021/i260045a015

Al-Shamrani, A.A., James, A., Xiao, H., 2002. Separation of oil from water by dissolved air flotation. Colloids Surfaces A Physicochem. Eng. Asp. 209, 15–26. https://doi.org/10.1016/S0927-7757(02)00208-X

Al Taweel, A.M., Delory, B., Wozniczek, J., Stefanski, M., Andersen, N., Hamza, H.A., 1986. Influence of the surface characteristics of coal on its flotability. Colloids and surfaces. 18, 9–18. https://doi.org/10.1016/0166-6622(86)80190-1

Allan, G.C., Woodcock, J.T., 2001. A review of the flotation of native gold and electrum. Miner. Eng. 14, 931–962. https://doi.org/10.1016/S0892-

6875(01)00103-0

Anastasiou, A.D., Passos, A.D., Mouza, A.A., 2013. Bubble columns with fine pore sparger and non-Newtonian liquid phase: Prediction of gas holdup. Chem. Eng. Sci. 98, 331–338. https://doi.org/10.1016/j.ces.2013.05.006

Aris. R., 1956. On the dispersion of a solute in a fluid flowing through a tube. Proc. R. Soc. London. Ser. A. Math. Phys. Sci. 235, 67–77. https://doi.org/10.1098/rspa.1956.0065

Ata, S., 2001. Froth phenomena in flotation. The University of Newcastle, Newcastle, Australia.

Bahadori, A., 2012. Prediction of axial dispersion in plug-flow reactors using a simple method. J. Dispers. Sci. Technol. 33, 200–205. https://doi.org/10.1080/01932691.2011.561159

Bahramian A. and Elyasi S. 2020. One-dimensional drift-flux model and a new approach to calculate drift velocity and gas holdup in bubble columns, Chemical Engineering Science, 211, 115302

Baird, M.H.I., Rice, R.G., 1975. Axial dispersion in large unbaffled columns. Chem. J. 9, 171–174.

Banisi, S., Finch, J.A., Laplante, A.R., Weber, M.E., 1995a. Effect of solid particles on gas holdup in flotation columns-II. Investigation of mechanisms of

gas holdup reduction in presence of solids. Chem. Eng. Sci. 50, 2335–2342. https://doi.org/10.1016/0009-2509(95)00076-H

Banisi, S., Finch, J.A., Laplante, A.R., Weber, M.E., 1995b. Effect of solid particles on gas holdup in flotation columns-I. Measurement. Chem. Eng. Sci. 50, 2329–2334.

Bascur, O., Herbst, J., 1982. Dynamic modelling of a Flotation cell with a view towards automatic control. Canada: Canadian inst mining metallurgy petroleum.

Behringer, H., 1952. The flow of liquid-gas mixtures in vertical tubes, in: VDI-Union of German Engineers. Amsterdam (Netherlands),. https://doi.org/10.2172/12405591

Besagni, G., Inzoli, F., 2017. The effect of liquid phase properties on bubble column fluid dynamics: Gas holdup, flow regime transition, bubble size distributions and shapes, interfacial areas and foaming phenomena. Chem. Eng. Sci. 170, 270–296. https://doi.org/10.1016/j.ces.2017.03.043

Besarati, S.M., Myers, P.D., Covey, D.C., Jamali, A., 2015. Modeling friction factor in pipeline flow using a GMDH-type neural network. Cogent Eng. 2. https://doi.org/10.1080/23311916.2015.1056929

Bhole, M.R., Joshi, J.B., 2008. Modelling gas holdup in flotation column froths.

Can. J. Chem. Eng. 85, 369–373. https://doi.org/10.1002/cjce.5450850312

Bhunia, K., Kundu, G., Mukherjee, D., 2018. Performance, mixing and kinetics study in the flotation column reactor using coal. Sep. Sci. Technol. 53, 2998–3007. https://doi.org/10.1080/01496395.2018.1490323

Bhunia, K., Kundu, G., Mukherjee, D., 2017. Gas holdup characteristics in a flotation column with different solids. Sep. Sci. Technol. 52, 1298–1309. https://doi.org/10.1080/01496395.2017.1287196

Bhunia, K., Kundu, G., Mukherjee, D., 2014. Pressure characteristics in a flotation column. Int. J. ChemTech Res. 6, 276–285.

Bińk, A.K., Duczmal, B., Machniewski, P., 2001. Hydrodynamics and ozone mass transfer in a tall bubble column. Chem. Eng. Sci. 56, 6233–6240. https://doi.org/10.1016/S0009-2509(01)00213-5

Bisshop, J.P., 1974. A study of particle entrainment in flotation froths. The University of Queensland, Brisbane, Australia.

Bloom, F., Heindel, T.J., 1997. Mathematical modelling of the flotation deinking process., IPST Technical Paper Series Number 634. Institute of Paper Science and Technology Atlanta, Georgia.

Bulatovic, S.M., 2007. Handbook of flotation reagents: Chemistry, theory and

practice flotation of sulfide ores. Elsevier. https://doi.org/10.1016/B978-0-444-53029-5.X5009-6

Cai, Y., Du, M., Wang, S., Liu, L., 2018. Flotation characteristics of oxidized coal slimes within low-rank metamorphic. Powder Technol. 340, 34–38. https://doi.org/10.1016/j.powtec.2018.09.006

Cant, S., 2001. S. B. Pope, Turbulent Flows, Cambridge University Press, Cambridge, U.K., Combustion and Flame 125. https://doi.org/10.1016/s0010-2180(01)00244-9

Cao, C., Dong, S., Geng, Q., Guo, Q., 2008. Hydrodynamics and axial dispersion in a gas-liquid-(solid) EL-ALR with different sparger designs. Ind. Eng. Chem. Res. 47, 4008–4017. https://doi.org/10.1021/ie0715254

Chakraborty, D., Guha, M., Banerjee, P.K., 2009. CFD simulation on influence of superficial gas velocity, column size, sparger arrangement, and taper angle on hydrodynamics of the column flotation cell. Chem. Eng. Commun. 196, 1102–1116. https://doi.org/10.1080/00986440902897376

Chen, S., Li, L., Qu, J., Liu, Q., Tang, L., Tao, X., Fan, H., 2018. Oily bubble flotation technology combining modeling and optimization of parameters for enhancement of flotation of low-flame coal. Powder Technol. 335, 171–185. https://doi.org/10.1016/j.powtec.2018.04.053

Cilek, E.C., 2004. Estimation of flotation kinetic parameters by considering interactions of the operating variables. Miner. Eng. 17, 81–85. https://doi.org/10.1016/j.mineng.2003.10.008

Clark, N.N., Flemmer, R.L., 1985. Predicting the holdup in two-phase bubble upflow and downflow using the Zuber and Findlay drift-flux model. AIChE J. 31, 500–503. https://doi.org/10.1002/aic.690310323

Clark, N.N., Van Egmond, J.W., Nebiolo, E.P., 1990. The drift-flux model applied to bubble columns and low velocity flows. Int. J. Multiph. Flow. 16, 261–279. https://doi.org/10.1016/0301-9322(90)90058-Q

Cruz, E.B., 1997. A comprehensive dynamic model of the column flotation unit operation. Diss. Virginia Tech, Virginia.

Dai, Z., Dukhin, S., Fornasiero, D., Ralston, J., 1998. The inertial hydrodynamic interaction of particles and rising bubbles with mobile surfaces. J. Colloid Interface Sci. 197, 275–292. https://doi.org/10.1006/jcis.1997.5280

Dai, Z., Fornasiero, D., Ralston, J., 2000. Particle-bubble collision models - A review. Adv. Colloid Interface Sci. 85, 231–256. https://doi.org/10.1016/S0001-8686(99)00030-5

Dai, Z., Fornasiero, D., Ralston, J., 1999. Particle–bubble attachment in mineral flotation. J. Colloid Interface Sci. 217, 70–76.

https://doi.org/10.1006/jcis.1999.6319

De Swart, J.W.A., Van Vliet, R.E., Krishna, R., 1996. Size, structure and dynamics of 'large' bubbles in a two-dimensional slurry bubble column. Chem. Eng. Sci. 51, 4619–4629. https://doi.org/10.1016/0009-2509(96)00265-5

Deckwer, W.D., 1992. Bubble Column Reactors, Wiley: Chichester. New York.

Deckwer, W.D., Burckhart, R., Zoll, G., 1974. Mixing and mass transfer in tall bubble columns. Chem. Eng. Sci. 29, 2177–2188. https://doi.org/10.1016/0009-2509(74)80025-4

Degaleesan, S., Dudukovic, M.P., Toseland, B.A., Bhatt, B.L., 1997. A two-compartment convective-diffusion model for slurry bubble column reactors. Ind. Eng. Chem. Res. 36, 4670–4680. https://doi.org/10.1021/ie970200s

Desouky, S.E.M., E1-Emam, N.A., 1981. Program designs for pseudoplastic fluids. Oil Gas J. 87 (51), 48–51.

Dey, S., Paul, G.M., Pani, S., 2013. Flotation behaviour of weathered coal in mechanical and column flotation cell. Powder Technol. 246, 689–694. https://doi.org/10.1016/j.powtec.2013.06.015

Dobby, G.S., Finch, J.A., 1987. Particle size dependence in flotation derived from a fundamental model of the capture process. Int. J. Miner. Process. 21, 241–

260. https://doi.org/10.1016/0301-7516(87)90057-3

Dobby, G.S., Finch, J.A., 1986. A model of particle sliding time for flotation size bubbles. J. Colloid Interface Sci. 109, 493–498. https://doi.org/10.1016/0021-9797(86)90327-9

Dobby, G.S., Yianatos, J.B., Finch, J.A., 1988. Estimation of bubble diameter in flotation columns from drift flux analysis. Can. Metall. Q. 27, 85–90. https://doi.org/10.1179/cmq.1988.27.2.85

Dowling, E.C., Klimpel, R.R., Aplan, F.F., 1985. Model discrimination in the flotation of a porphyry copper ore. Mining, Metall. Explor. 2, 87–101. https://doi.org/10.1007/bf03402602

Duan, J., Fornasiero, D., Ralston, J., 2003. Calculation of the flotation rate constant of chalcopyrite particles in an ore. Int. J. Miner. Process. 72, 227–237. https://doi.org/10.1016/S0301-7516(03)00101-7

Duangprasert, T., Sirivat, A., Siemanond, K., Wilkes, J.O., 2008. Vertical two-phase flow regimes and pressure gradients under the influence of SDS surfactant. Exp. Therm. Fluid Sci. 32, 808–817. https://doi.org/10.1016/j.expthermflusci.2007.10.005

Duerr-Auster, N., Gunde, R., Mäder, R., Windhab, E.J., 2009. Binary coalescence of gas bubbles in the presence of a non-ionic surfactant. J. Colloid Interface

Sci. 333, 579–584. https://doi.org/10.1016/j.jcis.2009.01.016

Dukhin, S.S., 1982. Role of inertial forces in flotation of small particles. Colloid J. USSR. 44(3), 388–397.

Eissa, S.H., Schugerl, K., 1975. Holdup and backmixing investigations in cocurrent and countercurrent bubble columns. Chem. Eng. Sci. 30, 1251–1256. https://doi.org/10.1016/0009-2509(75)85048-2

El-Kayar, A., Hussein, M., Zatout, A.A., Hosny, A.Y., Amer, A.A., 1993. Removal of oil from stable oil-water emulsion by induced air flotation technique. Sep. Technol. 3, 25–31. https://doi.org/10.1016/0956-9618(93)80003-A

Fahad, M.K., Prakash, R., Majumder, S.K., Ghosh, P., 2019. Gas holdup in the gas-liquid-coal slurry flow in a flotation column in presence of surface active agent. Multiph. Sci. Technol. 31, 199–214. https://doi.org/10.1615/MultScienTechn.2019029957

Fan, L.S., Hemminger, O., Yu, Z., Wang, F., 2007. Bubbles in nanofluids. Ind. Eng. Chem. Res. 46, 4341–4346. https://doi.org/10.1021/ie061532c

Fan, L.S., Yang, G.Q., Lee, D.J., Tsuchiya, K., Luo, X., 1999. Some aspects of high-pressure phenomena of bubbles in liquids and liquid-solid suspensions. Chem. Eng. Sci. 54, 4681–4709. https://doi.org/10.1016/S0009-

2509(99)00348-6

Fan, W., Sun, Y., Chen, H., 2014. Bubble volume and aspect ratio generated in non-Newtonian fluids. Chem. Eng. Technol. 37, 1566–1574. https://doi.org/10.1002/ceat.201400083

Farzanegan, A., Khorasanizadeh, N., Sheikhzadeh, G.A., Khorasanizadeh, H., 2017. Laboratory and CFD investigations of the two-phase flow behavior in flotation columns equipped with vertical baffle. Int. J. Miner. Process. 166, 79–88. https://doi.org/10.1016/j.minpro.2017.07.009

Finch, J.A., Dobby, G.S., 1990. Column flotation, first ed Pergamon Press, Oxford, England.

Fornasiero, D., Filippov, L., 2017. Innovations in the flotation of fine and coarse particles. J. Phys. Conf. Ser. Vol. 879. No. 1. IOP Publ.

Friedel, L., 1978. Pressure-drop during gas-vapor-liquid flow in pipes. Chem. Ing. Tech. 50, 167–180. https://doi.org/10.1615/MultScienTechn.2019031051

Fuerstenau, D.W., 1980. Fine particle flotation. Fine Part. Process. 1, 669–705.

Fuerstenau, D.W., 1962. Froth Flotation 50Th Anniversary Volume. American Institute of Mining, Metallurgical, and Petroleum Engineers, New York,USA.

Fuerstenau, M.C., Han, K.N., 2003. Principles of Mineral Processing. Society for

Mining, Metallurgy, and Exploration, Litteton, Colorado, USA.

Ganat, T., Hrairi, M., 2018. Gas–liquid two-phase upward flow through a vertical pipe: Influence of pressure drop on the measurement of fluid flow rate. Energies. 11, 2937. https://doi.org/10.3390/en11112937

Gandhi, B., Prakash, A., Bergougnou, M.A., 1999. Hydrodynamic behavior of slurry bubble column at high solids concentrations. Powder Technol. 103, 80–94. https://doi.org/10.1016/S0032-5910(98)00182-X

Gaudin, A.M., 1957. Flotation. McGraw-Hill.

Gaudin, A.M., Mular, A.L., O'connor, R.F., 1960. Separation of Microorganisms by Flotation: II. Flotation of Spores of Bacillus subtilis var. niger 1. Appl. Microbiol. 8, 91.

Ghajar, A.J., Bhagwat, S.M., 2013. Effect of void fraction and two-phase dynamic viscosity models on prediction of hydrostatic and frictional pressure drop in vertical upward gas–liquid two-phase flow. Heat Transf. Eng. 34, 1044–1059. https://doi.org/10.1080/01457632.2013.763541

Ghani, Z.A., Ishak, M.A.M., Ismail, K., 2011. Direct liquefaction of Mukah Balingian low-rank Malaysian coal: Optimization using response surface methodology. Asia-Pacific J. Chem. Eng. 6, 581–588. https://doi.org/10.1002/apj.442

Gharai, M., Venugopal, R., 2016. Modeling of flotation process – An overview of different approaches. Miner. Process. Extr. Metall. Rev. 37, 120–133. https://doi.org/10.1080/08827508.2015.1115991

Ghosh, P., 2004. Coalescence of air bubbles at air–water interface. Chem. Eng. Res. Des., 82(7), 849–854.

Gondo, S., Tanaka, S., Kazikuri, K., Kusunoki, K., 1973. Liquid mixing by large gas bubbles in bubble columns. Chem. Eng. Sci. 28, 1437–1445. https://doi.org/10.1016/0009-2509(73)85148-6

Götz, M., Lefebvre, J., Mörs, F., Reimert, R., Graf, F., Kolb, T., 2016. Hydrodynamics of organic and ionic liquids in a slurry bubble column reactor operated at elevated temperatures. Chem. Eng. J. 286, 348–360. https://doi.org/10.1016/j.cej.2015.10.044

Gupta, A., Yan, D.S., 2016. Mineral processing design and operations: An introduction. Elsevier.

Guven, O., Karakas, F., Kodrazi, N., Celik, M.S., 2016. Dependence of morphology on anionic flotation of Alumina. Int. J. Miner. Process. 156, 69–74. https://doi.org/10.1016/j.minpro.2016.06.006

Hassanzadeh, A., Karakas, F., 2017. Recovery improvement of coarse particles by stage addition of reagents in industrial copper flotation circuit. J. Dispers. Sci.

Technol. 38, 309–316. https://doi.org/10.1080/01932691.2016.1164061

Hemmings, C., 1981. On the significance of flotation froth liquid lamella thickness. Trans. Inst. Min. Met. 90, 96–638.

Hernáinz, F., Calero, M., 2001. Froth flotation: Kinetic models based on chemical analogy. Chem. Eng. Process. Process Intensif. 40, 269–275. https://doi.org/10.1016/S0255-2701(00)00125-2

Herrera-Urbina, R., 2003. Recent developments and advances in formulations and applications of chemical reagents used in froth flotation. Miner. Process. Extr. Metall. Rev. 24, 139–182. https://doi.org/10.1080/08827500306898

Hicyilmaz, C., Ulusoy, U., Bilgen, S., Yekeler, M., Akdogan, G., 2006. Response of rough and acute surfaces of pyrite with 3-D approach to the flotation. J. Min. Sci. 42, 393–402. https://doi.org/10.1007/s10913-006-0068-x

Hiçyilmaz, C., Ulusoy, U., Yekeler, M., 2004. Effects of the shape properties of talc and quartz particles on the wettability based separation processes. Appl. Surf. Sci. 233, 204–212. https://doi.org/10.1016/j.apsusc.2004.03.209

Hikita, H., Kikukawa, H., 1974. Liquid-phase mixing in bubble columns: Effect of liquid properties. Chem. Eng. J. 8, 191–197. https://doi.org/10.1016/0300-9467(74)85024-0

Honaker, R.Q., Mohanty, M.K., 1996. Enhanced column flotation performance for fine coal cleaning. Miner. Eng. 9, 931–945. https://doi.org/10.1016/0892-6875(96)00085-4

Hughmark, G.A., Pressburg, B.S., 1961. Holdup and pressure drop with gas-liquid flow in a vertical pipe. AIChE J. 7, 677–682. https://doi.org/10.1002/aic.690070429

Humeres, E., Debacher, N.A., 2002. Kinetics and mechanism of coal flotation. Colloid Polym. Sci. 280, 365–371. https://doi.org/10.1007/s00396-001-0618-3

Ishkintana, L.K., Bennington, C.P.J., 2010. Gas holdup in pulp fibre suspensions: Gas voidage profiles in a batch-operated sparged tower. Chem. Eng. Sci. 65, 2569–2578. https://doi.org/10.1016/j.ces.2009.12.040

Jameson, G.J., Nam, S., Young, M.M., 1977. Physical factors affecting recovery rates in flotation. Miner. Sci. Eng. 9, 103–118.

Jamialahmadi, M., Müller-Steinhagen, H., 1991. Effect of solid particles on gas hold-up in bubble columns. Can. J. Chem. Eng. 69, 390–393. https://doi.org/10.1002/cjce.5450690149

Jena, M.S., Biswal, S.K., Das, S.P., Reddy, P.S.R., 2008. Comparative study of the performance of conventional and column flotation when treating coking coal fines. Fuel Process. Technol. 89, 1409–1415.

https://doi.org/10.1016/j.fuproc.2008.06.012

Jianping, W., Shonglin, X., 1998. Local hydrodynamics in a gas-liquid-solid three-phase bubble column reactor. Chem. Eng. J. 70(1), 81–84.

Jin, H., Yang, S., He, G., Wang, M., Williams, R.A., 2010. The effect of gas-liquid counter-current operation on gas hold-up in bubble columns using electrical resistance tomography. J. Chem. Technol. Biotechnol. 85, 1278–1283. https://doi.org/10.1002/jctb.2428

Joachim, H., 1993. Flotation as a heterocoagulation process: Possibilities of calculating the probability of flotation. Coagul. Flocculation Theory Appl. 126, 321.

Johnson, N.W., 1972. The Flotation behaviour of some chalcopyrite ores. The University of Queensland, Brisbane, Australia.

Jordens, A., Marion, C., Grammatikopoulos, T., Waters, K.E., 2016. Understanding the effect of mineralogy on muscovite flotation using QEMSCAN. Int. J. Miner. Process. 155, 6–12. https://doi.org/10.1016/j.minpro.2016.08.003

Joshi, J.B., 1980. Axial mixing in multiphase contactors - A unified correlation. Chem. Eng. Res. Des. 58A, 155–165.

Joshi, J.B., Parasu Veera, U., Prasad, C. V., Phanikumar, D. V., Deshphande, N.S., Thakre, S.S., Thorat, B.N., 1998. Gas hold-up structure in bubble column reactors. Pinsa. 64, 441–567.

Joshi, J.B., Sharma, M., 1979. A circulation cell model for bubble columns. Chem. Eng. Res. Des. 57A, 244–251.

Jowett, A., 1966. Flotation kinetics. Gangue mineral contamination of froth. Brit Chem Eng. 11(5), 330–333.

Kang, Y., Kim, S.D., 1986. Radial dispersion characteristics of two- and three-phase fluidized beds. Ind. Eng. Chem. Process Des. Dev. 25, 717–722. https://doi.org/10.1021/i200034a020

Kantarci, N., Borak, F., Ulgen, K.O., 2005. Bubble column reactors. Process Biochem. 40(7), 2263–2283. https://doi.org/10.1016/j.procbio.2004.10.004

Kara, S., Kelkar, B.G., Shah, Y.T., Carr, N.L., 1982. Hydrodynamics and axial mixing in a three-phase bubble column. Ind. Eng. Chem. Process Des. Dev. 21, 584–594. https://doi.org/10.1021/i200019a009

Karagüzel, C., 2010. Selective separation of fine albite from feldspathic slime containing colored minerals (Fe-Min) by batch scale dissolved air flotation (DAF). Miner. Eng. 23, 17–24. https://doi.org/10.1016/j.mineng.2009.09.002

Kato, Y., 1972. Longitudinal dispersion coefficient of a liquid in a bubble column. Int Chem. Eng 12, 182–187.

Kato, Y., Morooka, S., Koyama, M., Kago, T., Yang, S.-Z., 1985. Longitudinal dispersion coefficient of liquid in three-phase fluidized bed for gas-liquid-solid systems. J. Chem. Eng. Japan. 18, 313–318. https://doi.org/10.1252/jcej.18.313

Kato, Y., Nishiwaki, A., 1971. Longitudinal dispersion coefficient of liquid in bubble column. Kagaku Kogaku Ronbunshu. 35, 912–916. https://doi.org/10.1252/kakoronbunshu1953.35.912

Kato, Y., Nishiwaki, A., Fukuda, T., Tanaka, S., 1972. The behavior of suspended solid particles and liquid in bubble columns. J. Chem. Eng. Japan. 5, 112–118. https://doi.org/10.1252/jcej.5.112

Kawase, Y., Moo-Young, M., 1986. Liquid phase mixing in bubble columns with Newtonian and non-Newtonian fluids. Chem. Eng. Sci. 41, 1969–1977. https://doi.org/10.1016/0009-2509(86)87113-5

Kawatra, S.K., Eisele, T.C., 1988. Rheological effects in grinding circuits. Int. J. Miner. Process. 22, 251–259. https://doi.org/10.1016/0301-7516(88)90067-1

Kelkar, B.G., Shah, Y.T., Carr, N.L., 1984. Hydrodynamics and axial mixing in a three-phase bubble column. Effects of slurry properties. Ind. Eng. Chem.

Process Des. Dev. 23, 308–313. https://doi.org/10.1021/i200025a021

Khare, A.S., Joshi, J.B., 1990. Effect of fine particles on gas hold-up in three-phase sparged reactors. Chem. Eng. J. 44, 11–25. https://doi.org/10.1016/0300-9467(90)80050-M

Khuntia, S., Majumder, S.K., Ghosh, P., 2012. Microbubble-aided water and wastewater purification: A review. Rev. Chem. Eng. 28, 191–221. https://doi.org/10.1515/revce-2012-0007

Kim, S.-J., Choi, J., Jeon, Y.-T., Lee, I., Won, C.-H., Chung, J., 2015. Microbubble-inducing characteristics depending on various nozzle and pressure in dissolved air flotation process. Ksce J. Civ. Eng. 19, 558–563. https://doi.org/10.1007/s12205-013-0514-7

Kim, S.D., Kim, C.H., 1983. Axial dispersion characteristics of three phase fluidized beds. J. Chem. Eng. Japan 16, 172–178. https://doi.org/10.1252/jcej.16.172

Kim, S.D., Kim, H.S., Han, J.H., 1992. Axial dispersion characteristics in three-phase fluidized beds. Chem. Eng. Sci. 47, 3419–3426. https://doi.org/10.1016/0009-2509(92)85053-E

Kirjavainen, V.M., 1996. Review and analysis of factors controlling the mechanical flotation of gangue minerals. Int. J. Miner. Process. 46, 21–34.

https://doi.org/10.1016/0301-7516(95)00057-7

Koide, K., Takazawa, A., Komura, M., Matsunaga, H., 1984. Gas holdup and volumetric liquid-phase mass transfer coefficient in solid-suspended bubble columns. J. Chem. Eng. Japan 17, 459–466. https://doi.org/10.1252/jcej.17.459

Krishna, R., Urseanu, M.I., Van Baten, J.M., Ellenberger, J., 2000. Liquid phase dispersion in bubble columns operating in the churn-turbulent flow regime. Chem. Eng. J. 78, 43–51. https://doi.org/10.1016/S1385-8947(99)00167-9

Kumar, S., Srinivasulu, N., Munshi, P., Khanna, A., 2013. Flow regime transition identification in three phase co-current bubble columns. Can. J. Chem. Eng. 91, 516–523. https://doi.org/10.1002/cjce.21688

Kunii, D., Levenspiel, O., 1991. Fluidization Engineering, 2nd ed. Butterworth-Heinemann, Stoneham. Massachusetts, USA.

Kurniawan, A.U., Ozdemir, O., Nguyen, A. V., Ofori, P., Firth, B., 2011. Flotation of coal particles in MgCl2, NaCl, and NaClO3 solutions in the absence and presence of Dowfroth 250. Int. J. Miner. Process. 98, 137–144. https://doi.org/10.1016/j.minpro.2010.11.003

Kursun, H., 2017. The influence of frother types and concentrations on fine particles' entrainment using column flotation. Sep. Sci. Technol. 52, 722–731. https://doi.org/10.1080/01496395.2016.1267215

Labidi, J., Pèlach, M.À., Turon, X., Mutjé, P., 2007. Predicting flotation efficiency using neural networks. Chem. Eng. Process. Process Intensif. 46, 314–322. https://doi.org/10.1016/j.cep.2006.06.011

Lapidus, L., Elgin, J.C., 1957. Mechanics of vertical-moving fluidized systems. AIChE J. 3, 63–68. https://doi.org/10.1002/aic.690030112

Laplante, A.R., Kaya, M., Smith, H.W., 1989. The effect of froth on flotation kinetics- A mass transfer approach. Miner. Process. Extr. Metall. Rev. 5, 147–168. https://doi.org/10.1080/08827508908952648

Lazaridis, N.K., Matis, K.A., Stalidis, G.A., Mavros, P., 1992. Dissolved-air flotation of metal ions. Sep. Sci. Technol. 27, 1743–1758. https://doi.org/10.1080/01496399208019444

Lee, J.E., Lee, J.K., 2002. Effect of microbubbles and particle size on the particle collection in the column flotation. Korean J. Chem. Eng. 19, 703–710. https://doi.org/10.1007/BF02699321

Lelinski, D., Allen, J., Redden, L., Weber, A., 2002. Analysis of the residence time distribution in large flotation machines. Miner. Eng. 15, 499–505. https://doi.org/10.1016/S0892-6875(02)00070-5

Leonard, C., Ferrasse, J.H., Boutin, O., Lefevre, S., Viand, A., 2015. Bubble column reactors for high pressures and high temperatures operation. Chem.

Eng. Res. Des. https://doi.org/10.1016/j.cherd.2015.05.013

Levenspiel, O., 1972. Chemical Reaction Engineering. John Wiley & Sons, New York.

Li, N., Li, Y., Fu, X., Gao, F., Zhang, C., Xia, W., Liang, L., 2018. Flotation kinetics of coal in the Inflatable Cyclonic Flotation Column. Powder Technol. 335, 204–210. https://doi.org/10.1016/j.powtec.2018.05.028

Li, X., Xu, H., Liu, J., Zhang, J., Li, J., Gui, Z., 2016. Cyclonic state micro-bubble flotation column in oil-in-water emulsion separation. Sep. Purif. Technol. 165, 101–106. https://doi.org/10.1016/j.seppur.2016.01.021

Liang, W., Jin, Y., Yu, Z., Wang, Z., Zhu, J., Chen, J., 1996. Flow characteristics and mixing properties in a high velocity liquid-solid loop reactor. Chem. Eng. J. Biochem. Eng. J. 63, 181–188. https://doi.org/10.1016/S0923-0467(96)03098-9

Lim, H.O., Jae Seo, M., Kang, Y., Won Jun, K., 2011. Particle fluctuations and dispersion in three-phase fluidized beds with viscous and low surface tension media. Chem. Eng. Sci. 66, 3234–3242. https://doi.org/10.1016/j.ces.2011.02.027

Loewenberg, M., Davis, R.H., 1994. Flotation rates of fine, spherical particles and droplets. Chem. Eng. Sci. 49, 3923–3941. https://doi.org/10.1016/0009-

2509(94)00200-2

Lu, W.J., Hwang, S.J., Chang, C.M., 1995. Liquid velocity and gas holdup in three-phase internal loop airlift reactors with low-density particles. Chem. Eng. Sci. 50, 1301–1310. https://doi.org/10.1016/0009-2509(95)98842-3

Lynch, A.J., Johnson, N.W., Manlapig, E. V., Thorne, C.G., 1981. Mineral and coal flotation circuits: Their simulation and control. Elsevier Science Ltd, Amsterdam.

Mackay, I., Mendez, E., Molina, I., Videla, A.R., Cilliers, J.J., Brito-Parada, P.R., 2018. Dynamic froth stability of copper flotation tailings. Miner. Eng. 124, 103–107. https://doi.org/10.1016/j.mineng.2018.05.005

Majumder, 2016. Hydrodynamics and transport processes of inverse bubbly flow. Elsevier, Amsterdam. Netherlands. https://doi.org/10.1016/B978-0-12-803287-9.00007-2

Majumder, S.K., 2019. Hydrodynamics and mass transfer in downflow slurry bubble columns. Apple Academic Press, New York, USA. https://doi.org/10.1201/9781351249867

Majumder, S.K., Ghosh, S., Kundu, G., Mitra, A.K., 2011. Frictional pressure drop of gas-Newtonian and gas-non Newtonian slug flow in vertical pipe. Int. J. Chem. React. Eng. 9. https://doi.org/10.2202/1542-6580.2847

Mandal, A., Kundu, G., Mukherjee, D., 2004. Studies on frictional pressure drop of gas-non-Newtonian two-phase flow in a cocurrent downflow bubble column. Chem. Eng. Sci. 59, 3807–3815. https://doi.org/10.1016/j.ces.2004.03.037

Manish, P., Majumder, S.K., 2009. Quality of mixing in a downflow bubble column based on information entropy theory. Chem. Eng. Sci. 64, 1798–1805. https://doi.org/10.1016/j.ces.2009.01.008

Manjrekar, O.N., Dudukovic, M.P., 2015. Application of a 4-point optical probe to a Slurry Bubble Column Reactor. Chem. Eng. Sci. 131, 313–322. https://doi.org/10.1016/j.ces.2015.03.027

Mankosa, M.J., Yoon, R.H., Luttrell, G.H., Adel, G.T., 1992. The application of Microcel™ column flotation to fine coal cleaning. Coal Prep. 10, 177–188. https://doi.org/10.1080/07349349208905201

Massinaei, M., Jahedsaravani, A., Taheri, E., Khalilpour, J., 2019. Machine vision based monitoring and analysis of a coal column flotation circuit. Powder Technol. 343, 330–341. https://doi.org/10.1016/j.powtec.2018.11.056

Massinaei, M., Kolahdoozan, M., Noaparast, M., Oliazadeh, M., Sahafipour, M., Finch, J.A., 2007. Mixing characteristics of industrial columns in rougher circuit. Miner. Eng. 20, 1360–1367. https://doi.org/10.1016/j.mineng.2007.08.016

Matis, K.A, 1994. Flotation sciences and engineering, CRC Press. New York, USA.

Matis, K.A., Gallios, G.P., Kydros, K.A., 1993. Separation of fines by flotation techniques. Sep. Technol. 3(2), 76–90. https://doi.org/10.1016/0956-9618(93)80007-E

Matis, K.A., Mavros, P., 1991. Recovery of metals by ion flotation from dilute aqueous solutions. Sep. Purif. Rev. 20, 1–48. https://doi.org/10.1080/03602549108021407

Melo, F., Laskowski, J.S., 2007. Effect of frothers and solid particles on the rate of water transfer to froth. Int. J. Miner. Process. 84, 33–40. https://doi.org/10.1016/j.minpro.2007.04.003

Mena, P.C., Ruzicka, M.C., Rocha, F.A., Teixeira, J.A., Drahoš, J., 2005. Effect of solids on homogeneous-heterogeneous flow regime transition in bubble columns. Chem. Eng. Sci. 60, 6013–6026. https://doi.org/10.1016/j.ces.2005.04.020

Mills, P.J.T., Yianatos, J.B., O'Connor, C.T., 1992. The mixing characteristics of solid and liquid phases in a flotation column. Miner. Eng. 5, 1195–1205. https://doi.org/10.1016/0892-6875(92)90159-7

Mohammed, A.A., 2007. Removal of emulsified paraffine from water: Effect of

bubble size and particle size on kinetic of flotation. J. Chem. Pet. Eng. 8, 1–5.

Mota, D.O.D.I., Castro, D.J.A., Casqueira, D.G.R., Junior, D.O.A.G., 2015. Study of electroflotation method for treatment of wastewater from washing soil contaminated by heavy metals. J. Mater. Res. Technol. 4, 109–113. https://doi.org/10.1016/j.jmrt.2014.11.004

Moys, M.H., 1978. A study of a plug-flow model for flotation froth behaviour. Int. J. Miner. Process. 5, 21–38. https://doi.org/10.1016/0301-7516(78)90003-0

Muhsin, H.A.A.K., 2008. Experimental study of liquid dispersion in bubble column. Diyala J. Eng. Sci. 1(1), 56–85. https://doi.org/10.24237/djes.2017.10413

Muroyama, K., Hashimoto, K., Kawabata, T., Ronbunshu, M.S., 1978. Axial liquid mixing in three-phase fluidized beds. Kagaku Kogaku Ronbunshu. 4(6), 622.

Neethling, S.J., Cilliers, J.J., 2002. The entrainment of gangue into a flotation froth. Int. J. Miner. Process. 64, 123–134. https://doi.org/10.1016/S0301-7516(01)00067-9

Nguyen, A., Schulze, H., 2004. Colloidal science of flotation, Marcel Dekker. New York, USA.

Nouri, N.M., Yekani Motlagh, S., Navidbakhsh, M., Dalilhaghi, M., Moltani, A.A.,

2013. Bubble effect on pressure drop reduction in upward pipe flow. Exp. Therm. Fluid Sci. 44, 592–598. https://doi.org/10.1016/j.expthermflusci.2012.08.022

Ofori, P., O'Brien, G., Firth, B., Jenkins, B., 2006. Flotation process diagnostics and modelling by coal grain analysis. Miner. Eng. 19, 633–640. https://doi.org/10.1016/j.mineng.2005.09.036

Ofori, P., O'Brien, G., Hapugoda, P., Firth, B., 2014. Distributed flotation kinetics models - A new implementation approach for coal flotation. Miner. Eng. 66, 77–83. https://doi.org/10.1016/j.mineng.2014.07.013

Ohki, Y., Inoue, H., 1970. Longitudinal mixing of the liquid phase in bubble columns. Chem. Eng. Sci. 25, 1–16. https://doi.org/10.1016/0009-2509(70)85016-3

Ojima, S., Sasaki, S., Hayashi, K., Tomiyama, A., 2015. Effects of particle diameter on bubble coalescence in a slurry bubble column. J. Chem. Eng. Japan. 48, 181–189. https://doi.org/10.1252/jcej.14we248

Oliveira, J.F., Saraiva, S.M., Pimenta, J.S., Oliveira, A.P.A.A., 2001. Kinetics of pyrochlore flotation from Araxa mineral deposits. Miner. Eng. 14, 99–105. https://doi.org/10.1016/S0892-6875(00)00163-1

Otake, T., Tone, S., Shinohara, K., 1981. Gas holdup in the bubble column with

cocurrent and countercurrent gas-liquid flow. J. Chem. Eng. Japan . 14(4), 338–340.

Pal, S.S., Mitra, A.K., Roy, A.N., 1980. Pressure drop and holdup in vertical two-phase cocurrent flow with improved gas-liquid mixing. Ind. Eng. Chem. Process Des. Dev. 19, 67–75. https://doi.org/10.1021/i260073a012

Parmar, R., Majumder, S.K., 2016. Mineral beneficiation by ionic microbubble in continuous plant prototype: Efficiency and its analysis by kinetic model. Chem. Eng. Sci. 142, 42–54. https://doi.org/10.1016/j.ces.2015.12.001

Parmar, R., Majumder, S.K., 2015. Dispersion characteristics of ionic microbubble suspension in continuous plant prototype developed for mineral beneficiation. Chem. Eng. Process. Process Intensif. 95, 43–53. https://doi.org/10.1016/j.cep.2015.05.011

Parmar, R., Majumder, S.K., 2014. Hydrodynamics of microbubble suspension flow in pipes. Ind. Eng. Chem. Res. 53, 3689–3701. https://doi.org/10.1021/ie402815v

Passos, A.D., Voulgaropoulos, V.P., Paras, S. V., Mouza, A.A., 2015. The effect of surfactant addition on the performance of a bubble column containing a non-Newtonian liquid. Chem. Eng. Res. Des. 95, 93–104. https://doi.org/10.1016/j.cherd.2015.01.008

Polat, M., Polat, H., Chander, S., 2003. Physical and chemical interactions in coal flotation. Int. J. Miner. Process. 72, 199–213. https://doi.org/10.1016/S0301-7516(03)00099-1

Polli, M., Stanislao, M. Di, Bagatin, R., Bakr, E.A., Masi, M., 2002. Bubble size distribution in the sparger region of bubble columns. Chem. Eng. Sci. 57, 197–205. https://doi.org/10.1016/S0009-2509(01)00301-3

Pouplin, A., Masbernat, O., Décarre, S., Liné, A., 2011. Wall friction and effective viscosity of a homogeneous dispersed liquid-liquid flow in a horizontal pipe. AIChE J. 57, 1119–1131. https://doi.org/10.1002/aic.12334

Prakash, R., Kumar Majumder, S., Singh, A., 2018a. Gas holdup and frictional pressure drop contributions in microstructured two-and three-phase bubbling bed with Newtonian and non-Newtonian liquids: Effect of coarse and fine particles with surface active agent. Chem. Eng. Process. - Process Intensif. 133, 40–57. https://doi.org/10.1016/j.cep.2018.09.020

Prakash, R., Majumder, S.K., 2017. Analysis of particle recovery in flotation column based on information entropy theory. Trans. Indian Inst. Met. 70, 403–410. https://doi.org/10.1007/s12666-016-0994-5

Prakash, R., Majumder, S.K., Singh, A., 2019. Particle-laden bubble size and its distribution in microstructured bubbling bed in the presence and absence of a

surface active agent. Ind. Eng. Chem. Res. 58, 3499–3522. https://doi.org/10.1021/acs.iecr.8b05625

Prakash, R., Majumder, S.K., Singh, A., 2018b. Flotation technique: Its mechanisms and design parameters. Chem. Eng. Process. - Process Intensif. 127, 249–270. https://doi.org/10.1016/j.cep.2018.03.029

Pyke, B., Fornasiero, D., Ralston, J., 2003. Bubble particle heterocoagulation under turbulent conditions. J. Colloid Interface Sci. 265, 141–151. https://doi.org/10.1016/S0021-9797(03)00345-X

Qi, B.C., Aldrich, C., 2002. Effect of ultrasonic treatment on zinc removal from hydroxide precipitates by dissolved air flotation. Miner. Eng. 15, 1105–1111. https://doi.org/10.1016/S0892-6875(02)00261-3

Rabha, S., Schubert, M., Hampel, U., 2013a. Intrinsic flow behavior in a slurry bubble column: A study on the effect of particle size. Chem. Eng. Sci. 93, 401–411. https://doi.org/10.1016/j.ces.2013.02.034

Rabha, S., Schubert, M., Wagner, M., Lucas, D., Hampel, U., 2013b. Bubble size and radial gas hold-up distributions in a slurry bubble column using ultrafast electron beam X-ray tomography. AIChE J. 59, 1709–1722. https://doi.org/10.1002/aic.13920

Rahman, R.M., Ata, S., Jameson, G.J., 2012. The effect of flotation variables on

the recovery of different particle size fractions in the froth and the pulp. Int. J. Miner. Process. 106, 70–77. https://doi.org/10.1016/j.minpro.2012.03.001

Reese, J., Jiang, P., Fan, L.S., 1996. Bubble characteristics in three-phase systems used for pulp and paper processing. Chem. Eng. Sci. 51, 2501–2510. https://doi.org/10.1016/0009-2509(96)00108-X

Reith, T., Renken, S., Israël, B.A., 1968. Gas hold-up and axial mixing in the fluid phase of bubble columns. Chem. Eng. Sci. 23, 619–629. https://doi.org/10.1016/0009-2509(68)89007-4

Rice, R.G., Tupperainen, J.M.I., Hedge, R.M., 1981. Dispersion and hold-up in bubble columns - comparison of rigid and flexible spargers. Can. J. Chem. Eng. 59, 677–687. https://doi.org/10.1002/cjce.5450590605

Rollbusch, P., Becker, M., Ludwig, M., Bieberle, A., Grünewald, M., Hampel, U., Franke, R., 2015. Experimental investigation of the influence of column scale, gas density and liquid properties on gas holdup in bubble columns. Int. J. Multiph. Flow 75, 88–106. https://doi.org/10.1016/j.ijmultiphaseflow.2015.05.009

Rousseau, R.W., 1987. Handbook of separation process technology. Wiley-Interscience, NewYork, USA.

Rubinstein, J., 1994. Column flotation: Processes, designs and practices. Process

engineering for the chemical, metals and minerals industry. USA.

Rubio, F.C., Mirón, A.S., García, M.C.C., Camacho, F.G., Grima, E.M., Chisti, Y., 2004. Mixing in bubble columns: A new approach for characterizing dispersion coefficients. Chem. Eng. Sci. 59, 4369–4376. https://doi.org/10.1016/j.ces.2004.06.037

Rubio, J., Souza, M.L., Smith, R.W., 2002. Overview of flotation as a wastewater treatment technique. Miner. Eng. 15, 139–155. https://doi.org/10.1016/S0892-6875(01)00216-3

Runge, K., 2010. Laboratory flotation testing - An essential tool for ore characterisation. Spectr. Ser., 16, 155–173.

Sada, E., Kumazawa, H., Iguchl, T., Lee, C., 1986. Gas holdup and mass-transfer characteristics in a three-phase bubble column. Ind. Eng. Chem. Process Des. Dev. 25, 472–476. https://doi.org/10.1021/i200033a020

Sarhan, A.R., Homadi, A.M., Naser, J., 2020. Modelling detachment rates of hydrophobic particles from bubbles in a froth phase. Sep. Purif. Technol. 235, 116–200. https://doi.org/10.1016/j.seppur.2019.116200

Sarhan, A.R., Naser, J., Brooks, G., 2018a. CFD modeling of bubble column: Influence of physico-chemical properties of the gas/liquid phases properties on bubble formation. Sep. Purif. Technol. 201, 130–138.

https://doi.org/10.1016/j.seppur.2018.02.037

Sarhan, A.R., Naser, J., Brooks, G., 2018b. CFD model simulation of bubble surface area flux in flotation column reactor in presence of minerals. Int. J. Min. Sci. Technol. 28, 999–1007. https://doi.org/10.1016/j.ijmst.2018.05.004

Sarhan, A.R., Naser, J., Brooks, G., 2018c. Bubbly flow with particle attachment and detachment–A multi-phase CFD study. Sep. Sci. Technol. 53, 181–197. https://doi.org/10.1080/01496395.2017.1375525

Sarhan, A.R., Naser, J., Brooks, G., 2018d. Effects of particle size and concentration on bubble coalescence and froth formation in a slurry bubble column. Particuology. 36, 82–95. https://doi.org/10.1016/j.partic.2017.04.011

Sarhan, A.R., Naser, J., Brooks, G., 2017a. CFD analysis of solid particles properties effect in three-phase flotation column. Sep. Purif. Technol. 185, 1–9. https://doi.org/10.1016/j.seppur.2017.04.042

Sarhan, A.R., Naser, J., Brooks, G., 2017b. Numerical simulation of froth formation in aerated slurry coupled with population balance modelling. Can. Metall. Q. 56, 45–57. https://doi.org/10.1080/00084433.2016.1268771

Sarhan, A.R., Naser, J., Brooks, G., 2016. CFD simulation on influence of suspended solid particles on bubbles' coalescence rate in flotation cell. Int. J. Miner. Process. 146, 54–64. https://doi.org/10.1016/j.minpro.2015.11.014

Sarikaya, M., Özbayoğlu, G., 1995. Flotation characteristics of oxidized coal. Fuel 74, 291–294. https://doi.org/10.1016/0016-2361(95)92668-V

Schubert, H., 1999. On the turbulence-controlled microprocesses in flotation machines. Int. J. Miner. Process. 56, 257–276. https://doi.org/10.1016/S0301-7516(98)00048-9

Sehabiague, L., Morsi, B.I., 2013. Hydrodynamic and mass transfer characteristics in a large-scale slurry bubble column reactor for gas mixtures in actual Fischer-Tropsch cuts. Int. J. Chem. React. Eng. 11(1), 83–102. https://doi.org/10.1515/ijcre-2012-0042

Senapati, P.K., Panda, D., Parida, A., 2009. Predicting viscosity of limestone-water slurry. J. Miner. Mater. Charact. Eng. 08, 203–221. https://doi.org/10.4236/jmmce.2009.83018

Shabalala, N.Z.P., Harris, M., Leal Filho, L.S., Deglon, D.A., 2011. Effect of slurry rheology on gas dispersion in a pilot-scale mechanical flotation cell. Miner. Eng. 24, 1448–1453. https://doi.org/10.1016/j.mineng.2011.07.004

Shah, Y.T., Kelkar, B.G., Godbole, S.P., Deckwer, W. -D, 1982. Design parameters estimations for bubble column reactors. AIChE J. https://doi.org/10.1002/aic.690280302

Shawaqfeh, A.T., 2003. Gas holdup and liquid axial dispersion under slug flow

conditions in gas-liquid bubble column. Chem. Eng. Process. Process Intensif. 42, 767–775. https://doi.org/10.1016/s0255-2701(02)00082-x

Shukla, S.C., Kukade, S., Mandal, S.K., Kundu, G., 2008. Coal-oil-water multiphase fuel: Rheological behavior and prediction of optimum particle size. Fuel. 87, 3428–3432. https://doi.org/10.1016/j.fuel.2008.05.027

Shukla, S.C., Kundu, G., Mukherjee, D., 2010. Study of gas holdup and pressure characteristics in a column flotation cell using coal. Miner. Eng. 23, 636–642. https://doi.org/10.1016/j.mineng.2010.03.005

Sivaiah, M., Majumder, S.K., 2013a. Dispersion characteristics of liquid in a modified gas-liquid-solid three-phase downflow bubble column. Part. Sci. Technol. 31, 210–220. https://doi.org/10.1080/02726351.2012.694400

Sivaiah, M., Majumder, S.K., 2013b. Hydrodynamics and mixing characteristics in an ejector-induced downflow slurry bubble column (EIDSBC). Chem. Eng. J. 225, 720–733. https://doi.org/10.1016/j.cej.2013.04.023

Smith, C.A., 1984. Dynamic simulation of sulphide flotation circuits, Ph.D. Thesis. The University of Queensland, Brisbane, Australia,.

Smith, P.G., Warren, L.J., 1989. Entrainment of particles into flotation froths. Miner. Process. Extr. Metall. Rev. 5, 123–145. https://doi.org/10.1080/08827508908952647

Soni, G., 2013. Development and validation of a simulator based on a first-principle flotation model. Virginia Tech.

Sripriya, R., Rao, P.V.T.T., Choudhury, B.R., 2003. Optimisation of operating variables of fine coal flotation using a combination of modified flotation parameters and statistical techniques. Int. J. Miner. Process. 68, 109–127. https://doi.org/10.1016/S0301-7516(02)00063-7

Sutherland, K.L., 1948. Physical chemistry of flotation. XI. Kinetics of the flotation process. J. Phys. Chem. 52, 394–425. https://doi.org/10.1021/j150458a013

Sven-Nilsson, I., 1934. Effect of contact time between mineral and air bubbles on flotation. Kol loid, 230.

Szatkowski, M., 1987. Factors influencing behaviour of flotation froth. Inst. Min. Metall. Trans. 96, 115–122.

Szczerkowska, S., Wiertel-Pochopien, A., Zawala, J., Larsen, E., Kowalczuk, P.B., 2018. Kinetics of froth flotation of naturally hydrophobic solids with different shapes. Miner. Eng. 121, 90–99. https://doi.org/10.1016/j.mineng.2018.03.006

Tao, D., 2004. Role of bubble size in flotation of coarse and fine particles - A review. Sep. Sci. Technol. 39, 741–760. https://doi.org/10.1081/ss-120028444

Tassel, F., Rubio, J., Misra, M., Jena, B.C., 1997. Removal of mercury from gold cyanide solution by dissolved air flotation. Miner. Eng. 10, 803–811. https://doi.org/10.1016/s0892-6875(97)00058-7

Tavera, F.J., Escudero, R., Finch, J.A., 2001. Gas holdup in flotation columns: Laboratory measurements. Int. J. Miner. Process. 61, 23–40. https://doi.org/10.1016/S0301-7516(00)00026-0

Taylor, G.I., 1953. Dispersion of soluble matter in solvent flowing slowly through a tube. Math. Phys. Sci. 219, 186–203. https://doi.org/10.1098/rspa.1953.0139

Tessele, F., Misra, M., Rubio, J., 1998. Removal of Hg, As and Se ions from gold cyanide leach solutions by dissolved air flotation. Miner. Eng. 11, 535–543.

Tian, Y., Azhin, M., Luan, X., Liu, F., Dubljevic, S., 2018. Three-phases dynamic modelling of column flotation process. IFAC-PapersOnLine. 51(21), 99–104. https://doi.org/10.1016/j.ifacol.2018.09.399

Tokoro, C., Okano, Y., 2001. Boundary conditions for column flotation - A study by transfer function representation of an axial diffusion model. Miner. Eng. 14, 49–64. https://doi.org/10.1016/S0892-6875(00)00159-X

Towell, G.D., 1972. Axial mixing of liquid and gas in larger bubble reactors, in: Proc. 5th Europ. and 2nd Int. Symp. Chem. Reac. Eng. B3-1. Elsevier.

Tuteja, R.K., Spottiswood, D.J., Misra, V.N., 1994. Mathematical models of the column flotation process a review. Miner. Eng. 7, 1459–1472. https://doi.org/10.1016/0892-6875(94)90038-8

Tyagi, P., Buwa, V. V., 2017. Dense gas–liquid–solid flow in a slurry bubble column: Measurements of dynamic characteristics, gas volume fraction and bubble size distribution. Chem. Eng. Sci. 173, 346–362. https://doi.org/10.1016/j.ces.2017.07.042

Uçurum, M., Bayat, O., 2007. Effects of operating variables on modified flotation parameters in the mineral separation. Sep. Purif. Technol. 55, 173–181. https://doi.org/10.1016/j.seppur.2006.11.019

Ulusoy, U., Hiçylmaz, C., Yekeler, M., 2004. Role of shape properties of calcite and barite particles on apparent hydrophobicity. Chem. Eng. Process. Process Intensif. 43, 1047–1053. https://doi.org/10.1016/j.cep.2003.10.003

Uribe-Salas, A., Perez-Garibay, R., Nava-Alonso, F., 2008. Dynamic and geometrical models to estimate the density of fully-loaded bubbles in the column flotation of silica sand. Open Miner. Process. J. 1, 1–5. https://doi.org/10.2174/1874841400801010001

Uribe, S.A., Vázquez, V.D., Pérez, G.R., Nava, A.F., 1999. A statistical model for the concentrate water in flotation columns. Miner. Eng. 12, 937–948.

Vadlakonda, B., Mangadoddy, N., 2018. Hydrodynamic study of three-phase flow in column flotation using electrical resistance tomography coupled with pressure transducers. Sep. Purif. Technol. 203, 274–288. https://doi.org/10.1016/j.seppur.2018.04.039

Vail, Y.K., Manakov, N.K., Manshili, V. V., 1968. Turbulent mixing in a 3-phase fluidized bed. Int. Chem. Eng. 8 (2), 293.

Vashisth, S., Bennington, C.P.J., Grace, J.R., Kerekes, R.J., 2011. Column flotation deinking: State-of-the-art and opportunities. Resour. Conserv. Recycl. 55, 1154–1177. https://doi.org/10.1016/j.resconrec.2011.06.013

Vinnett, L., Navarra, A., Waters, K.E., 2019a. An inversion approach to characterize batch flotation kinetics. Miner. Eng. 143, 105944. https://doi.org/10.1016/j.mineng.2019.105944

Vinnett, L., Navarra, A., Waters, K.E., 2019b. Comparison of different methodologies to estimate the flotation rate distribution. Miner. Eng. 130, 67–75. https://doi.org/10.1016/j.mineng.2018.10.011

Voigt, J., Hecht, V., Schügerl, K., 1980. Absorption of oxygen in countercurrent multistage bubble columns-II. Aqueous solutions with high viscosity. Chem. Eng. Sci. 35, 1317–1323. https://doi.org/10.1016/0009-2509(80)85124-4

Wang, L., Peng, Y., Runge, K., 2015a. Entrainment in froth flotation: The degree

of entrainment and its contributing factors. Powder Technol. 288, 202–211. https://doi.org/10.1016/j.powtec.2015.10.049

Wang, L., Peng, Y., Runge, K., Bradshaw, D., 2015b. A review of entrainment: Mechanisms, contributing factors and modelling in flotation. Miner. Eng. 70, 77–91. https://doi.org/10.1016/j.mineng.2014.09.003

Warren, L.J., 1985. Determination of the contributions of true flotation and entrainment in batch flotation tests. Int. J. Miner. Process. 14, 33–44. https://doi.org/10.1016/0301-7516(85)90012-2

Weber, M.E., Paddock, D., 1983. Interceptional and gravitational collision efficiencies for single collectors at intermediate Reynolds numbers. J. Colloid Interface Sci. 94, 328–335. https://doi.org/10.1016/0021-9797(83)90270-9

Wilkinson, P.M., Haringa, H., Stokman, F.P.A., Van Dierendonck, L.L., 1993. Liquid mixing in a bubble column under pressure. Chem. Eng. Sci. 48, 1785–1791. https://doi.org/10.1016/0009-2509(93)80348-T

Wills, B.A., 2006. Will's mineral processing technology: An introduction to the practical aspects of ore treatment and mineral recovery, 7th ed. Butterworth-Heinemann, Oxford, UK.

Wills, B.A., Finch, J., 2015. Wills' mineral processing technology: An introduction to the practical aspects of ore treatment and mineral recovery. Butterworth-

Heinemann, Oxford, UK.

Woo, Sun-Wai, 1971. Simultaneous free and forced covection around submerged cylinders and spheres.

Wu, H., Patterson, G.K., 1989. Laser-Doppler measurements of turbulent-flow parameters in a stirred mixer. Chem. Eng. Sci. 44, 2207–2221. https://doi.org/10.1016/0009-2509(89)85155-3

Xia, W., 2017. Role of particle shape in the floatability of mineral particle: An overview of recent advances. Powder Technol. 317, 104–116. https://doi.org/10.1016/j.powtec.2017.04.050

Xia, W., Niu, C., Ren, C., 2017a. Enhancement in floatability of sub-bituminous coal by low-temperature pyrolysis and its potential application in coal cleaning. J. Clean. Prod. 168, 1032–1038. https://doi.org/10.1016/j.jclepro.2017.09.119

Xia, W., Zhou, C., Peng, Y., 2017b. Enhancing flotation cleaning of intruded coal dry-ground with heavy oil. J. Clean. Prod. 161, 591–597. https://doi.org/10.1016/j.jclepro.2017.05.193

Xing, Y., Gui, X., Cao, Y., Wang, Y., Xu, M., Wang, D., Li, C., 2017. Effect of compound collector and blending frother on froth stability and flotation performance of oxidized coal. Powder Technol. 305, 166–173.

https://doi.org/10.1016/j.powtec.2016.10.003

Xing, Y., Xu, M., Gui, X., Cao, Y., Babel, B., Rudolph, M., Weber, S., Kappl, M., Butt, H.J., 2018. The application of atomic force microscopy in mineral flotation. Adv. Colloid Interface Sci. 256, 373–392. https://doi.org/10.1016/j.cis.2018.01.004

Xu, M., Finch, J.A., Laplante, A.R., 1991. Numerical solution to axial dispersion model in flotation column studies. Can. Metall. Q. 30, 71–77. https://doi.org/10.1179/cmq.1991.30.2.71

Xu, Y., Fang, X., Su, X., Zhou, Z., Chen, W., 2012. Evaluation of frictional pressure drop correlations for two-phase flow in pipes. Nucl. Eng. Des. 253, 86–97. https://doi.org/10.1016/j.nucengdes.2012.08.007

Yang, G.Q., Fan, L.S., 2003. Axial liquid mixing in high-pressure bubble columns. AIChE J. 49, 1995–2008. https://doi.org/10.1002/aic.690490810

Yang, Y.M., Maa, J.R., 1984. Bubble coalescence in dilute surfactant solutions. J. Colloid Interface Sci. 98, 120–125. https://doi.org/10.1016/0021-9797(84)90484-3

Ye, Y., Khandrika, S.M., Miller, J.D., 1989. Induction-time measurements at a particle bed. Int. J. Miner. Process. 25, 221–240. https://doi.org/10.1016/0301-7516(89)90019-7

Yianatos, J., Bergh, L., Vinnett, L., Panire, I., Díaz, F., 2015. Modelling of residence time distribution of liquid and solid in mechanical flotation cells. Miner. Eng. 78, 69–73. https://doi.org/10.1016/j.mineng.2015.04.011

Yianatos, J., Contreras, F., Díaz, F., Villanueva, A., 2009. Direct measurement of entrainment in large flotation cells. Powder Technol. 189, 42–47. https://doi.org/10.1016/j.powtec.2008.05.013

Yianatos, J.B., Bergh, L.G., 1992. RTD studies in an industrial flotation column: Use of the radioactive tracer technique. Int. J. Miner. Process. 36, 81–91. https://doi.org/10.1016/0301-7516(92)90065-5

Yianatos, J.B., Bergh, L.G., Díaz, F., Rodríguez, J., 2005. Mixing characteristics of industrial flotation equipment. Chem. Eng. Sci. 60, 2273–2282. https://doi.org/10.1016/j.ces.2004.10.039

Yianatos, J.B., Finch, J.A., Laplante, A.R., 1988. Selectivity in column flotation froths. Int. J. Miner. Process. 23, 279–292. https://doi.org/10.1016/0301-7516(88)90021-X

Yoon, R.H., 1993. Microbubble flotation. Miner. Eng. 6, 619–630. https://doi.org/10.1016/0892-6875(93)90116-5

Yoon, R.H., Luttrell, G.H., 1989. The Effect of Bubble Size on Fine Particle Flotation. Miner. Process. Extr. Metall. Rev. 5, 101–122.

https://doi.org/10.1080/08827508908952646

Yoon, R.H., Yordan, J.L., 1991. Induction time measurements for the quartz-amine flotation system. J. Colloid Interface Sci. 141, 374–383. https://doi.org/10.1016/0021-9797(91)90333-4

Yoshida, Y., Katsumoto, T., Taniguchi, S., Shimosaka, A., Shirakawa, Y., Hidaka, J., 2013. Prediction of viscosity of slurry suspended fine particles using coupled DEM-DNS simulation. Chem. Eng. Trans. 32, 2089–2094. https://doi.org/10.3303/CET1332349

Yuan, X.M., Pålsson, B.I., Forssberg, K.S.E., 1996. Statistical interpretation of flotation kinetics for a complex sulphide ore. Miner. Eng. 9, 429–442. https://doi.org/10.1016/0892-6875(96)00028-3

Zheng, X., Johnson, N.W., Franzidis, J.P., 2006. Modelling of entrainment in industrial flotation cells: Water recovery and degree of entrainment. Miner. Eng. 19, 1191–1203. https://doi.org/10.1016/j.mineng.2005.11.005

Zhou, Y., Albijanic, B., Tadesse, B., Wang, Y., Yang, J., Li, G., Zhu, X., 2019. Surface hydrophobicity of sub-bituminous and meta-bituminous coal and their flotation kinetics. Fuel. 242, 416–424. https://doi.org/10.1016/j.fuel.2019.01.051

Zhou, Z.A., Plitt, L.R., Egiebor, N.O., 1993. The effects of solids and reagents on

the characteristics of coal flotation in columns. Miner. Eng. 6, 291–306. https://doi.org/10.1016/0892-6875(93)90037-N

Zuber, N., Findlay, J.A., 1965. Average volumetric concentration in two-phase flow systems. J. Heat Transfer 87, 453–468. https://doi.org/10.1115/1.3689137